ENDOTHELIAL REGULATION OF VALVE INTERSTITIAL CELLS IN CALCIFIC AORTIC VALVE DISEASE

A Dissertation

Presented to the Faculty of the Graduate School

of Cornell University

In Partial Fulfillment of the Requirements for the Degree of

Doctor of Philosophy

by

Jennifer Marie Richards

May 2015

ENDOTHELIAL REGULATION OF VALVE INTERSTITIAL CELLS IN CALCIFIC AORTIC VALVE DISEASE

Jennifer Marie Richards, Ph.D.

Cornell University 2015

Calcified aortic valve disease (CAVD) is an increasingly prevalent pathology that often manifests in the degenerative calcification of the valve tissue. Currently, the only treatment for aortic valve calcification is surgical intervention, and a clinically useful molecular signature of CAVD progression has not yet been found. Recent clinical trials testing lipid-lowering therapies were ineffective against aortic stenosis progression, which emphasizes that CAVD may undergo a distinctly different pathogenesis from that of atherosclerosis. While CAVD is no longer believed to be a passive degenerative process, the cellular mechanisms by which the valve calcifies are not wholly understood. There remains a need to understand cellular mechanisms of valve pathogenesis, as well as an in-depth analysis of the altogether unique calcified lesions that form as a result of the disease.

The focus of this dissertation was the development of a 3D construct in which the interplay between valve endothelial (VEC) and valve interstitial cells (VIC) could be illuminated in various calcification-prone environments. The completion of this work yielded insights into cellular responses to osteogenic, mineralized, and altered mechanical environments, which could be used to identify potential therapeutic targets or early diagnosis strategies in the future. A 3D hydrogel construct was first developed for the co-culture of interstitial and endothelial cells, which is more

physiologically relevant than current 2D models. Under osteogenic conditions, endothelial cells were found to have a protective effect against VIC activation and calcification (Chapter 2). Next, the mineralized lesions and surrounding organic tissue in calcified valves were characterized and found to have a heterogeneous composition of apatite and calcium phosphate mineral crystals (Chapter 3). These findings prompted the use of synthetically derived hydroxyapatite nanoparticles of two different maturation states in order to better evaluate cellular response to a highly mineralized matrix, characteristic of later stages of valve disease (Chapter 4). Finally, the effects of an altered mechanical environment, as is typical in valve disease, were examined by increasing mechanical tension in 3D hydrogel constructs and applying cyclic mechanical strain (Chapter 5).

Overall, this body of work has made significant advancements in understanding individual and incorporative cellular responses to osteogenic, mineralized and mechanical 3D environments. This work has contributed to the emerging appreciation that 3-dimensional multi-cellular co-cultures are vital to mechanistic understanding of valve pathogenesis. Our 3D platform shows great promise for future studies, and could enable direct screening of molecular mechanisms of calcification and testing of potential molecular inhibitors.

BIOGRAPHICAL SKETCH

Jen graduated with highest honors in 2009 from Worcester Polytechnic Institute with a B.S. in Biomedical Engineering. During her undergraduate studies, Jen was a member of the Tau Beta Pi Engineering Honors Society, as well as Alpha Eta Mu Beta, the National Biomedical Engineering Honors Society due to academic achievement. Jen spent the first of two summers volunteering at the University of New Hampshire Climate Change Research Center, examining the emission of carbon dioxide and methane from local wetland regions. Her second summer internship was at Dartmouth-Hitchcock Medical Center, investigating the role of glypican-1 in pancreatic cancer. In her senior year, she developed an orthopedic device and accompanying surgical instrumentation for correction of coxofemoral luxation in canines, for which she received the Provost's Award for Best Major Qualifying Project. Outside of academics, Jen was a 4-year varsity softball player, serving her last two years as captain and was awarded a place on the Academic All-American Second Team in her senior year.

Jen studied as a Ph.D. candidate in Biomedical Engineering at Cornell University under the direction of Dr. Jonathan Butcher. During her tenure at Cornell, she was awarded the GAANN and Morgan Family Fellowships, as well as a 2-year NSF STEM (Science, Technology, Engineering, and Math) GK-12 fellowship to design and teach science curriculum in the classroom. Jen has mentored multiple students and has worked on 4 first-author papers, as well as contributing to several others. She has presented her work at seven conferences across the country and one internationally. Her research focuses on understanding the interplay between valve endothelial and interstitial cells during calcific aortic valve disease.

For my family

ACKNOWLEDGMENTS

Above all, I would like to acknowledge and thank both my mother and father. Without their constant support, guidance and love, I would not be the person I am today. To Christina, my sister, I would like to thank for continuing to inspire me to push the boundaries of my comfort and experiences, because you will always regret what you never try. Although she will never read this, I would like to acknowledge my dog, Molly, who has brought me joy and comfort in some of the most difficult times during my graduate career, when I needed them the most.

I would like to thank my advisor Dr. Jonathan Butcher for his guidance and support during the completion of this degree. Not only was he a research mentor, but he opened his home and family to his students and always made us feel welcome. I also appreciated that his wife, Christine, was always very kind and welcoming to me, and without whom our lab outings would not have been possible. I would like to express my gratitude to the members of my committee, Drs. Cindy Reinhart-King, Lara Estroff and Adele Boskey for their advice and encouragement during my graduate studies.

I must acknowledge the countless people who I have had the privilege and pleasure of working with over the years. First and foremost is my lab family, both past and present, that made doing research so enjoyable day to day. Thank you to Phil Buskohl, Gretchen Mahler, Russ Gould, Emily Farrar, Stephanie Lindsey and Chelsea Gregg. To my undergraduate mentee, Alexa Wnorowski, without whom this work would not have been complete, I say a special thank you and note that I am truly proud of all of your well-deserved achievements. I would like to acknowledge several individuals in collaborating labs, Dr. Debra Lin, Dr. Amy Blakeley, Jennie

Russ and David Diaz. Thank you for spending so much time helping with the materials science portion of this thesis – I could not have done it without you. Thank you to people outside of the lab who have offered support and true friendship over the years, especially Jenny Puetzer, Shawn and Teri Carey, and Katie and Alex Melville. A special thank you goes to Shawn who put in a ridiculous amount of time setting up a thesis template that made formatting this document so much easier. To my roommate and lab-mate Laura Hockaday, I would like to extend a special thank you for your warm and cheerful personality as well as always being there for me. I will miss our cathartic TV marathons.

Finally, I would like to thank my entire family for always supporting me and encouraging me to follow my dreams and to be the best I can be.

Funding for this work was provided by the GAANN (Graduate Assistance in Areas of National Need) Fellowship, the Morgan Family Fellowship, and the NSF (National Science Foundation) GK-12 program: DGE 0841291. Additional funding was provided by the AHA (American Heart Association) and the NIH (National Institute of Health).

TABLE OF CONTENTS

LIST OF FIGURES

Chapter 1

Chapter 2

Chapter 3

Chapter 4

Chapter 5

Chapter 7

LIST OF ABBREVIATIONS

2D	Two dimensional
3D	Three dimensional
αSMA	Alpha smooth muscle actin
ANOVA	Analysis of variance
ARS	Alizarin red S
CAVD	Calcific aortic valve disease
cGMP	Cyclic guanosine monophosphate
CLIMB	Cornell Learning Initiative in Medicine and Bioengineering
CO_2	Carbon dioxide gas
Ctrl	Control
DETA-NO	Diethylenetriamine nitric oxide
EDS	Energy dispersive spectroscopy
EtOH	Ethanol
eNOS	Endothelial nitric oxide synthase
FBS	Fetal bovine serum
FTIR	Fourier transform infrared spectroscopy
GADDS	General area detector diffraction system
HA	Hydroxyapatite
HCl	Hydrochloric acid
iNOS	Inducible nitric oxide synthase
KBr	Potassium bromide
L-NAME	N-nitro-L-arginine methyl ester
NaOH	Sodium hydroxide
nNOS	Neuronal nitric oxide synthase
NO	Nitric oxide
OCN	Osteocalcin
OGM	Osteogenic media
OPN	Osteopontin
PAVEC	Porcine aortic valve endothelial cell
PAVIC	Porcine aortic valve interstitial cell
PBS	Phosphate-buffered saline

PDMS	Polydimethylsiloxane
PECAM	Platelet endothelial cell adhesion molecule
PFA	Paraformaldehyde
PMMA	Poly(methyl methacrylate)
ROCK	Rho-associated protein kinase
RT-PCR	Reverse transcriptase polymerase chain reaction
Runx2	Runt-related transcription factor 2
SEM	Standard error of the mean
SEM-EDS	Scanning electron microscopy - energy dispersive X-ray spectrometry
sGC	Soluble guanylyl cyclase
TEM	Transmission electron microscopy
XRD	X-ray diffraction

CHAPTER 1

INTRODUCTION

1.1 The Aortic Valve

Heart Valve Anatomy

The aortic heart valve is one of four valves found in the heart whose function is to facilitate and maintain unidirectional blood flow. This valve is located between the base of the aorta and the top of the left ventricle, and is subjected to highly pressurized blood flow. The valve is a uniquely constructed tissue, comprised of three leaflets that attach at their base to the aortic root, with their free edges coapting to prevent regurgitation of blood when the valve is closed[1]. Each leaflet is composed of a highly organized ECM structure that is compartmentalized into three layers, the fibrosa, spongiosa and ventricularis[2]. The fibrosa, situated closest to the aorta, is comprised of mostly collagen that provides tensile stiffness[3,4], while the ventricularis is composed of elastin that enables tissue motion[5,6]. The middle spongiosa layer is made up of collagen fibers and various glycosaminoglycans[6]. While valve thickness varies, the leaflets are normally no more than 1mm, but are still able to withstand a vast mechanical load during coaptation[7]. The heart beats more than 100,000 times per day, which means the aortic valve must be strong and robust over a lifetime of nearly 3 billion heart beats[8].

Cells of the Aortic Valve

The cellular elements of the aortic valve include valvular interstitial cells (VIC), which are the most abundant cell type and are distributed throughout the entirety of

the valve, and valvular endothelial cells (VEC), which line the surface of the valve and are phenotypically unique from endothelial cells found elsewhere in the vascular system[9,10]. VIC synthesize and are strongly attached to ECM, and have the ability to remodel collagen and other matrix components[11]. Although mostly fibroblast-like (~95%), VIC are a heterogeneous population (~5% myofibroblasts, smooth muscle cells and progenitor cells)[12–15] whose phenotype is largely regulated by surrounding environmental conditions[16]. The endothelium provides a protective lining for the underlying tissue by regulating permeability, mediating inflammation, and preventing thrombosis[17]. VEC are mechanically sensitive, and are vitally important for valve homeostasis and ECM remodeling through the regulation of hemodynamic signals to underlying interstitial cells[17,18]. Interestingly, VEC from opposite sides of the valve leaflets have been shown to have differential transcriptional profiles and respond differently to pathological levels of shear stress conditions[19]; it has been hypothesized that these differences may contribute to the vulnerability of the fibrosa to develop calcification during several valve diseases, including calcific aortic valve disease and bicuspid aortic valve disease[20].

1.2 Heart Valve Pathology

Prevalence and Manifestation of Valve Disease

Calcified aortic valve disease (CAVD) is an increasingly prevalent pathology that often manifests in the degenerative calcification of the valve tissue. The normally thin, fibrous tissue of the valve leaflet stiffens and becomes heavily calcified over time (Figure 1.1). Present in up to 2.5% of the total population, CAVD becomes increasingly prevalent with age, appearing in about 13% of those over the age of 75[21]. CAVD is currently diagnosed via echocardiography[22], but a clinically useful molecular

signature of CAVD progression has not yet been found[23]. Recent clinical trials testing lipid metabolism agents (e.g. statins) in CAVD have been disappointing, but underscore that CAVD pathogenesis is an active process with distinctly different features from atherosclerosis[24–26]. In particular, large occlusive mineralized lesions develop on the aortic valve cusps, while vascular calcifications are often significantly smaller[27]. These lesions exhibit evidence of both dystrophic calcification (calcium-containing crystal nucleation within apoptotic bodies) and osteogenic calcification (via osteoblast-like deposition of mineralized matrix)[28]. There remains a need to clarify a mechanistic reason for the initiation of valve pathogenesis, as well as an in-depth analysis of the unique calcified lesions that form as a result of the disease.

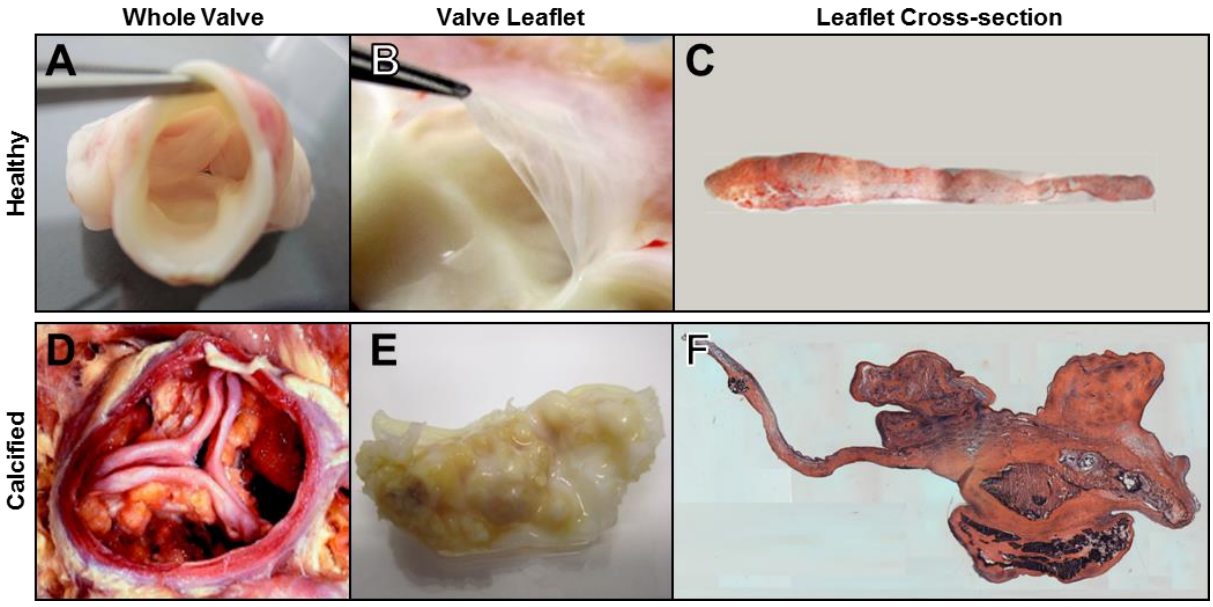

Figure 1.1: Gross morphology of healthy and calcified aortic valves. A) Whole explanted human aortic valve and B) one healthy valve leaflet. C) Cross-section of healthy valve leaflet, stained with hematoxylin & eosin (H&E). D) Whole calcified human aortic valve and E) one heavily calcified valve leaflet. F) Cross-section of diseased valve leaflet, stained with hematoxylin & eosin (H&E).

Cellular Dysfunction in Valve Disease

Early aortic valve stenosis is characterized by systemic endothelial dysfunction[29], and aortic-sided VEC express fewer inhibitors to calcification. This directly corresponds to the tendency of calcified nodule formation on the aortic side of the valve[20]. Subsets of VEC have been shown to undergo EMT in vitro in response to inflammatory stimuli[30], which could potentially contribute to activated VIC populations responsible for calcification of the ECM. When the aortic valve becomes diseased, the normally quiescent VIC become activated, increasing in proliferation and matrix remodeling, as well as becoming more myofibroblastic in phenotype[15]. Myofibroblastic activation is a key factor in eventual calcification, as the inhibition of αSMA or RhoA activity inhibits calcific nodule formation in vitro[31]. Populations of activated VIC also have been shown to differentiate into osteoblast-like cells responsible for bone formation[32]. Calcification of aortic valves occurs due to a combination of active mineralization by transformed osteoblast-like cells and apoptosis-driven dystrophic calcification. There is evidence that calcified valves contain a minority of apoptotic and necrotic cells localized in regions of calcification[33].

There are several projected contributors to valve calcification and cellular activation during valve disease. Studies in both mouse and human valves established that a small percentage of VIC are mesenchymal stem cells[34]. While subsets of these progenitor cells behave like valve myofibroblasts, expressing αSMA and collagen, others could be differentiated into osteoblast-like cells[35]. Specific mechanisms for aortic valve calcification remain elusive; however, there are several potential mediators that have been identified. Nitric oxide (NO) is a potent vasodilator secreted primarily by endothelial cells and confers many cardiovascular benefits through its action on smooth muscle[36], but its role in aortic valve function is unclear.

Serum levels of endothelial nitric oxide synthase (eNOS) inhibitors correlate with aortic valve stenosis in patients with CAVD. A large percentage of eNOS deficient mice develop bicuspid aortic valves[37], and increasing NO in 2D cultured VIC inhibits the formation of calcified nodules[38]. These results suggest that endothelial derived NO may modulate VIC calcification, but to what ends and mechanism is unclear. Another potential antagonist to valve calcification is NOTCH1. NOTCH1 inhibits Runx2 transcription[39], and NOTCH1 deficient humans are at significant risk of aortic valve calcification[40,41]. Further work is still needed to identify strategic targets for modulating aortic valve remodeling and preventing calcification.

1.3 Mineralization of Heart Valves

Soft Tissue Mineralization

Soft tissue calcification mainly refers to calcium salts that are deposited and grows within the tissue[42]. Calcification of soft tissue differs from bone formation in that it commonly occurs in response to an injury or an imbalance of ions within the bloodstream[43]. Hydroxyapatite (HA, $Ca_{10}(PO_4)_6(OH)_2$) crystals are deposited within the extracellular matrix and align with collagen fibers, while osteocalcin produced by osteoblasts attach to the crystals and may promote growth[44]. Studies have also demonstrated that hydroxyapatite taken up by cells can induce necrosis, which provides the crystals with nucleation sites from which growth can occur[44]. While mechanistically different, bone formation and soft tissue mineralization in the cardiovascular system share many factors, including an increase of bone morphogenic protein-2 (BMP-2), Wnt-signaling, and bone matrix protein (osteocalcin and osteopontin) expression[43,45]. *In vitro* studies revealed that valve cells could be induced to calcify when exposed to osteogenic environments; in these studies, cells

acquired a transformed phenotype that closely resemble osteoblasts[32]. Several groups identified the calcific deposits within diseased valves to have a range of morphologies and structural features[46–48].

Biomineral Characterization of Valve Disease

There are several techniques that have been employed to analyze the structure, chemical composition and crystallinity of the mineral that constitutes calcific nodules in valve disease, including X-ray diffraction (XRD), Fourier transform infrared spectroscopy (FTIR), Raman spectroscopy, and scanning electron microscopy with energy dispersive X-ray spectrometry (SEM-EDS)[49–53]. Morphologies of crystals can vary within mineralized lesions, with features ranging from round or sphere-like to flat, rod-like shapes[48,52]. Electron microscopy determined that the mineral salts within calcified valves are a combination of several calcium phosphate phases, including hydroxyapatite (HA) and octacalcium phosphate (OCP), which is potentially a precursor phase to HA[49]. Several studies document a variability of calcium (Ca) and phosphorus (P) within valve mineral deposits, but with similar elemental composition to that of bone[46,54]. FTIR and XRD analysis of valve calcification reveal that the structure is again a variation of poorly crystalline apatite and more highly crystalline hydroxyapatite[47,55,56]. One recent study incorporated nano-analytical electron microscopy techniques to identify spherical mineral particles within not only calcified lesions, but also non-calcified regions of the valve tissue. Interestingly, these spherical particles, as well as other studies, revealed an internal structure more crystalline than that of bone, while the dense calcium phosphate material that often surrounded the particles was thought to be poorly crystalline apatite[57,58]. The variability and heterogeneity of structure, shape and composition of mineral found

within valve calcification suggest a progressive maturation process within the mineral as the tissue composition continually changes throughout the lifespan of the disease.

1.4 Mechanics in Valve Disease

Valve Hemodynamics and Mechanical Stresses

Heart valves are located in a mechanically complex and demanding environment. With over 3 billion cardiac cycles in an average lifetime[2], the aortic valve undergoes a combination of normal, tensile, compressive, bending, and shear stresses[59], as shown in Figure 1.2. Endothelial cells sense vastly different shear patterns depending

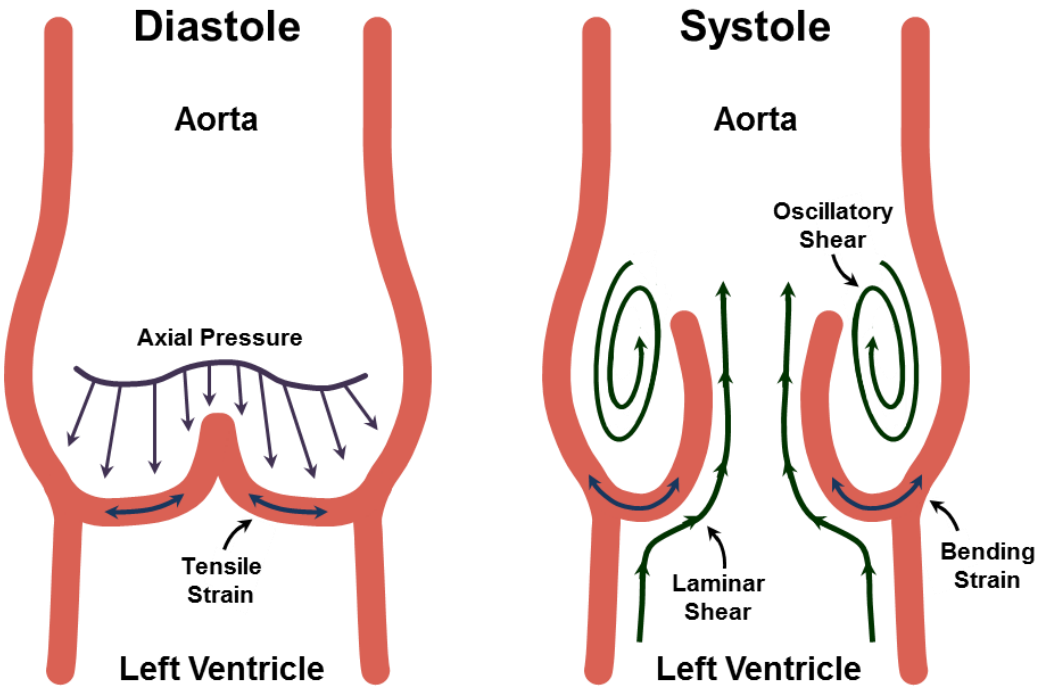

Figure 1.2: Illustration of diastolic and systolic mechanical forces in the aortic valve.

on the their location on the valve; during systole, the aortic-sided *fibrosa* experiences oscillatory shear stress, while the ventricular-sided *ventricularis* is exposed to laminar shear stress[60]. It has been demonstrated that endothelial cells from opposite sides of

the valve have different transcriptional profiles[20], perhaps accounting for the one-sided preference of the emergence of calcific nodules during valve disease. Interstitial cells within the valve tissue respond to various mechanical cues, regulating their phenotype and facilitating matrix remodeling[11,12].

During valve pathogenesis, the mechanical environment changes due to altered shape and continued mineral growth within the tissue. While VIC are normally quiescent and fibroblast-like, they become activated (α-smooth muscle actin (αSMA) positive) in diseased conditions[13]. Valve endothelial cells are extremely mechanosensitive, experiencing different mechanical environments on the outflow and inflow sides of the valve[61], which may explain the side-specific differences in gene expression of these unique cells. Phenotypic changes in cells result from responses to mechanical cues, which could lead to pathogenesis. Only recently have we begun to understand the unique behaviors of these cells, for which *in vitro* experimentation has played a key role. It is important to combine mechanical stimulation with biochemical signaling when studying the pathogenesis of these valve cells.

Cellular Models and Behavior In Vitro

Because of the unique pathology involving the calcification of valve tissue, there has been much interest in the behavior of valve cells to osteogenic and mechanical stimuli. It is well established that interstitial cells are induced to calcify on 2D substrates with a source of phosphate salts introduced in cell culture medium[62], and the addition of growth factors such as TGFβ can accelerate the calcification time[63]. Interstitial cells grown on matrices are sensitive to changes in stiffness[64–66]. Similarly, endothelial cells are mechanosensitive, in that they will align perpendicular to flow[9],

and they can be induced to undergo an EMT-like transformation under mechanical stresses[67] or exposure to inflammatory cytokines, such as TNFα[30]. While there have been many studies examining the individual contributions of interstitial or endothelial cells, there have been surprisingly few studies that investigate cellular interactions and phenotypic changes in co-culture[68]. Valve homeostasis is characterized by complex interactions and signaling between the two cell types, which are then disrupted during disease; this maintains the need for a model to examine both VIC and VEC in tandem for a better mechanistic understanding of valve disease. There have been a few co-cultures reported, including one that forms hypercellular constructs via magnetic levitation[69], and others whereby endothelial cells are separated from VIC via a transwell membrane[70]. However, the current methods used to study cellular changes due to osteogenic or mechanical environments are limited in their ability to examine interactions between the cell types, and potential signaling that may occur in response to changes in microenvironment.

1.5 Research Objectives

The overall goal of this dissertation is to elucidate the interplay between valve endothelial (VEC) and valve interstitial cells (VIC) in calcification-prone environments, and how mechanical strain affects these interactions. To accomplish this, I developed and utilized a 3D collagen hydrogel culture system that recapitulates VIC-induced matrix calcification to examine a possible mechanistic role of VEC in valve calcification. Specifically, I investigated endothelial-derived nitric oxide (NO) as a mechanism by which VEC regulate VIC phenotype in earlier stages of valve pathogenesis. To determine cell phenotype and behavior in the mineral-rich environment of the later stage of the disease, I examined the chemical composition

and structure of calcific nodules in diseased valve tissue, and incorporated synthesized mineral nanoparticles with the *in vitro* model used previously. In addition, I used a custom bioreactor to apply equibiaxial strain to the collagen hydrogels in order to examine the mechanical role in valve calcification, as well as the alteration of cell interactions in this mechanical environment. The overriding hypotheses were that 1) endothelial cells are inherently protective against valve calcification and this protective behavior is disrupted due to both 2) mineral imbalance and 3) changes in strain. I implemented methods for both *in vitro* and *ex vivo* experiments to address the following aims:

Aim 1 (Chapter 2)

The specific aim of this chapter was to identify how valve endothelial dysfunction modulates endothelial nitric oxide (eNOS) signaling to promote pathological interstitial activation and valve matrix remodeling. The overriding hypothesis was that valve endothelial cells have a protective effect against interstitial-driven valve calcification, and that a disruption of the endothelial-driven nitric oxide signaling occurs during valve pathogenesis. In this study, we determined how aortic valve endothelial cells (VEC) regulate aortic valve interstitial cell (VIC) phenotype and matrix calcification through nitric oxide. This study was divided into two main parts. First, we used an anchored *in vitro* collagen hydrogel culture system and we demonstrated that 3D-cultured porcine VIC do not calcify in osteogenic media unless under mechanical stress. However, co-culture with porcine VEC significantly attenuated VIC calcification through inhibition of myofibroblastic activation, osteogenic differentiation, and calcium deposition. Incubation with the nitric oxide (NO) donor DETA-NO inhibited VIC osteogenic differentiation and matrix calcification, while incubation with

the NO blocker L-NAME augmented calcification even in 3D VIC-VEC co-culture. The second part of this study examined explanted human and porcine leaflets to evaluate nitric oxide signaling and calcification potential. We found that aortic VEC, but not VIC, expressed endothelial nitric oxide synthase (eNOS) in both porcine and human valves, which was reduced in osteogenic media. eNOS expression was reduced in calcified human aortic valves in a side specific manner. Porcine leaflets exposed to soluble guanylyl cyclase inhibitor ODQ increased osteocalcin and αSMA expression. Finally, side-specific shear stress applied to porcine aortic valve leaflet endothelial surfaces increased cyclic GMP (cGMP) production in VEC. Valve endothelial-derived nitric oxide is a natural inhibitor of early phases of valve calcification, and therefore may be an important regulator of valve homeostasis and pathology.

Aim 2 (Chapters 3 and 4)

The specific aim of these chapters was to evaluate the mineral composition of calcified valves in order to mimic a mineral-rich 3D environment with which to evaluate valve cell phenotype and matrix calcification.

The working hypothesis for chapter 3 was that matrix mineralization and mature calcific nodule formation have varied mineral composition and crystallinity. This study paired traditional characterization methods to analyze calcification structure and crystallinity with FTIR imaging to compare compositional parameters between valves with varying degrees of mineralization. We demonstrate that the valve has activated cellular profiles of both myofibroblastic and osteoblast-like phenotypes that are spatially diverse throughout the valve. We also confirmed that the mineralized tissue was a heterogeneous mix of crystalline apatite material and poorly crystalline

hydroxyapatite. Acidity and crystallinity values were higher in areas of lower mineralization, indicating new mineral formation in a manner that may be distinct from bone. Within calcified regions of close proximity, there were compact mineral deposits with a mineralized tissue content higher than that of bone adjacent to areas with lower mineral:matrix ratios. Through this study we were able to highlight the heterogeneity of the calcified valves, both in areas of highly mineralized lesions as well as in areas of surrounding valve tissue.

In chapter 4, it was postulated that mineral imbalances in the collagen matrix will disrupt normal interactions and signaling between valve endothelial and interstitial cells. Using the information gathered in chapter 3 regarding the variability of mineral crystallinity and morphology in different areas of the valve, we used synthetically prepared HA particles of varying crystallinities and sizes to evaluate how a mineral-rich collagen matrix regulates interstitial and endothelial interactions and phenotypes. HA particles were successfully distributed within collagen constructs, and demonstrate that differences in crystallinity of particles drive different myofibroblastic and osteoblastic responses in valve cells. Additionally, calcium deposition within collagen gels depended on particle crystallinity, and this difference was not entirely apoptosis-driven. Altogether, we demonstrate that mineral-rich hydrogel models provide a 3D platform to evaluate valve cell responses to a later stage of valve disease, which is characterized by mineralized valve tissue.

Aim 3 (Chapter 5)

The goal of this chapter was to investigate how mechanical strain mediates interstitial and endothelial cell phenotype and regulates matrix remodeling and calcification. While previous chapters evaluate various osteogenic environments in

order to evaluate VIC-VEC interactions, they were done so in static culture, which does not take into account the role of the changing mechanical environment experienced by cells. In this chapter, we determined how mechanical tension and cyclic strain regulate interstitial and endothelial interactions and phenotypes in 3D osteogenic environments. We seeded collagen hydrogels into stainless steel compression springs so there was equal constraint around the circumference of the gel. Then, using a modified version of a previously reported novel bioreactor system[71], we applied cyclic strain over a period of 7 days and demonstrated that VIC+VEC co-cultures in osteogenic environments develop calcific nodules in both static and strained cultures. Differences between nodules arose between static and strained conditions, and matrix fiber reorganization was apparent around nodule areas. Cyclic strain enhanced apoptosis in co-cultures while decreasing proliferation, suggesting an active remodeling of the collagen hydrogels in strained conditions. Co-culture gels cultured statically in OGM increased myofibroblastic activation, which was then decreased when cyclically strained. However, cyclic strain increased expression of osteogenic genes in co-culture gels, suggesting osteoblastic differentiation is enhanced in part by a dynamically strained environment. Finally, blocking cell contractility through a ROCK inhibitor demonstrated the need for cellular tension for calcification, nodule formation and myofibroblastic activation. The results presented in this chapter strongly advocate for a 3D platform that incorporates VEC and VIC interactions while undergoing a changing mechanical environment, which is necessary to understand how progressively increasing mechanical tension during CAVD affect the pathology of both endothelial and interstitial cells.

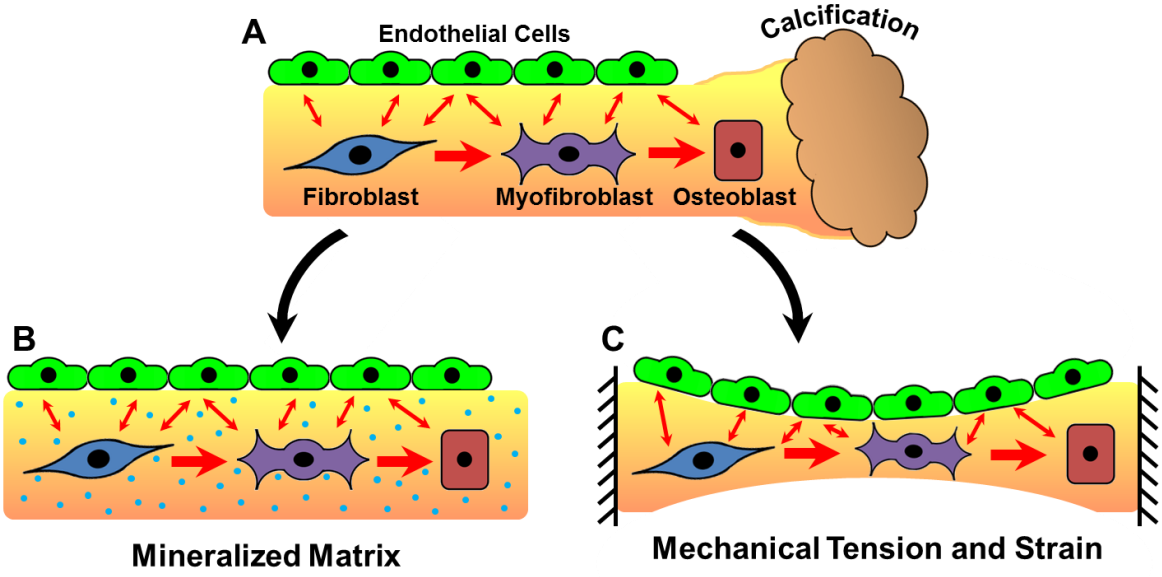

Figure 1.3: Illustration of overall aims of this dissertation. A) I developed a 3D co-culture hydrogel model that recapitulates VIC-induced matrix calcification and the myofibroblastic/osteoblastic shift of VIC in osteogenic environments to examine mechanistic role of VEC in valve calcification. B) Using synthetic HA nanoparticles incorporated into the hydrogel model, I investigated cell phenotype and interactions when in a mineral-containing environment, which is a better representation of later disease stages. C) The final aim of this thesis investigated how cell interactions and phenotypes change with mechanical strain.

Summary

Using a 3D model of valve calcification is a powerful tool for examining the interaction of interstitial and endothelial cells in different environments. Figure 1.3 illustrates the use of a 3D hydrogel model to investigate cellular interactions under various environments. Together, the work presented in this dissertation gives mechanistic insight to pathological cellular signaling and matrix remodeling in static osteogenic and mineral-rich environments, as well as static and dynamics mechanical environments. Because mechanisms that regulate VEC-VIC interactions in valve pathogenesis have not been fully explored, it is my hope that these studies may contribute to the development of future therapeutic targets or diagnostic techniques that will help prevent or treat calcific aortic valve disease.

REFERENCES

1. Chen J-H, Simmons C a. Cell-matrix interactions in the pathobiology of calcific aortic valve disease: critical roles for matricellular, matricrine, and matrix mechanics cues. *Circulation research*. 2011;108(12):1510–24.

2. Hinton RB, Yutzey KE. Heart valve structure and function in development and disease. *Annual review of physiology*. 2011;73:29–46.

3. Kershaw J, Misfeld M, Sievers H, Yacoub M, Chester A. Specific regional and directional contractile responses of aortic cusp tissue. *Journal of Heart Valve Disease*. 2004;13(5):798–803.

4. Sacks MS, Yoganathan AP. Heart valve function: a biomechanical perspective. *Philosophical transactions of the Royal Society of London. Series B, Biological sciences*. 2007;362(1484):1369–91.

5. Schoen FJ. Aortic valve structure-function correlations: role of elastic fibers no longer a stretch of the imagination. *Journal of Heart Valve Disease*. 1997;6(1):1–6.

6. Scott, Michael and Vesely I. Aortic valve cusp microscructure: The role of elastin. *The Annals of Thoracic Surgery*. 1995;60(Supplement 2):S391–S394.

7. Otto CM, Kuusisto J, Reichenbach DD, Gown a M, O'Brien KD. Characterization of the early lesion of "degenerative" valvular aortic stenosis. Histological and immunohistochemical studies. *Circulation*. 1994;90:844–853.

8. Levine HJ. Rest heart rate and life expectancy. *Journal of the American College of Cardiology*. 1997;30(4):1104–6.

9. Butcher JT, Penrod AM, García AJ, Nerem RM. Unique morphology and focal adhesion development of valvular endothelial cells in static and fluid flow environments. *Arteriosclerosis, thrombosis, and vascular biology*. 2004;24(8):1429–34.

10. Butcher JT, Tressel S, Johnson T, Turner D, Sorescu G, Jo H, Nerem RM. Transcriptional profiles of valvular and vascular endothelial cells reveal phenotypic differences: influence of shear stress. *Arteriosclerosis, thrombosis, and vascular biology*. 2006;26(1):69–77.

11. Taylor PM, Batten P, Brand NJ, Thomas PS, Yacoub MH. The cardiac valve interstitial cell. *The international journal of biochemistry & cell biology*. 2003;35(2):113–8.

12. Taylor PM, Allen SP, Yacoub MH. Phenotypic and functional characterization of interstitial cells from human heart valves, pericardium and skin. *The Journal of heart valve disease*. 2000;9(1):150–158.

13. Rabkin-Aikawa E, Farber M, Aikawa M, Schoen FJ. Dynamic and reversible changes of interstitial cell phenotype during remodeling of cardiac valves. *The Journal of heart valve disease*. 2004;13(5):841–7.

14. Bairati A, DeBiasi S. Presence of a smooth muscle system in aortic valve leaflets. *Anatomy and embryology*. 1981;161:329–340.

15. Liu AC, Joag VR, Gotlieb AI. The emerging role of valve interstitial cell phenotypes in regulating heart valve pathobiology. *The American journal of pathology*. 2007;171(5):1407–18.

16. Mulholland DL, Gotlieb AI. Cell biology of valvular interstitial cells. *The Canadian journal of cardiology*. 1996;12(3):231–236.

17. Butcher JT, Nerem RM. Valvular endothelial cells and the mechanoregulation of valvular pathology. *Philosophical transactions of the Royal Society of London. Series B, Biological sciences*. 2007;362(1484):1445–57.

18. Rabkin E, Aikawa M, Stone JR, Fukumoto Y, Libby P, Schoen FJ. Activated interstitial myofibroblasts express catabolic enzymes and mediate matrix remodeling in myxomatous heart valves. *Circulation*. 2001;104:2525–2532.

19. Hoehn D, Sun L, Sucosky P. Role of Pathologic Shear Stress Alterations in Aortic Valve Endothelial Activation. *Cardiovascular Engineering and Technology*. 2010;1(2):165–178.

20. Simmons CA, Grant GR, Manduchi E, Davies PF. Spatial heterogeneity of endothelial phenotypes correlates with side-specific vulnerability to calcification in normal porcine aortic valves. *Circulation research*. 2005;96(7):792–9.

21. Go AS, Mozaffarian D, Roger VL, Benjamin EJ, Berry JD, Borden WB, Bravata DM, Dai S, Ford ES, Fox CS, Franco S, Fullerton HJ, Gillespie C, Hailpern SM, Heit J a., et al. Heart Disease and Stroke Statistics--2013 Update A Report From the American Heart Association. *Circulation*. 2012.

22. Baumgartner H, Hung J, Bermejo J, Chambers JB, Evangelista A, Griffin BP, Iung B, Otto CM, Pellikka P a, Quiñones M. Echocardiographic assessment of valve stenosis: EAE/ASE recommendations for clinical practice. *European journal of echocardiography : the journal of the Working Group on Echocardiography of the European Society of Cardiology*. 2009;10(1):1–25.

23. Beckmann E, Grau JB, Sainger R, Poggio P, Ferrari G. Insights into the Use of Biomarkers in Calcific Aortic Valve Disease. *Journal of Heart Valve Disease*. 2010;19(4):441–452.

24. Cowell SJ, Newby DE, Prescott RJ, Bloomfield P, Reid J, Northridge DB, Boon N a. A randomized trial of intensive lipid-lowering therapy in calcific aortic stenosis. *The New England Journal of Medicine*. 2005;352(23):2389–97.

25. Farmer J a. Intensive lipid lowering with simvastatin and ezetimibe in aortic stenosis (the SEAS trial). *Current atherosclerosis reports*. 2009;11:82–83.

26. Yutzey KE, Demer LL, Body SC, Huggins GS, Towler D a., Giachelli CM, Hofmann-Bowman M a., Mortlock DP, Rogers MB, Sadeghi MM, Aikawa E. Calcific Aortic Valve Disease: A Consensus Summary From the Alliance of Investigators on Calcific Aortic Valve Disease. *Arteriosclerosis, Thrombosis, and Vascular Biology*. 2014;34:2387–2393.

27. Roijers RB, Dutta RK, Cleutjens JPM, Mutsaers PH a, de Goeij JJM, van der Vusse GJ. Early calcifications in human coronary arteries as determined with a proton microprobe. *Analytical Chemistry*. 2008;80(1):55–61.

28. Mohler ER, Gannon F, Reynolds C, Zimmerman R, Keane MG, Kaplan FS. Bone Formation and Inflammation in Cardiac Valves. *Circulation*. 2001;103(11):1522–1528.

29. Poggianti E, Venneri L, Chubuchny V, Jambrik Z, Baroncini LA, Picano E. Aortic valve sclerosis is associated with systemic endothelial dysfunction. *Journal of the American College of Cardiology*. 2003;41(1):136–41.

30. Farrar EJ, Butcher JT. Heterogeneous susceptibility of valve endothelial cells to mesenchymal transformation in response to TNFα. *Annals of biomedical engineering*. 2014;42(1):149–61.

31. Monzack EL, Gu X, Masters KS. Efficacy of simvastatin treatment of valvular interstitial cells varies with the extracellular environment. *Arteriosclerosis, Thrombosis, and Vascular Biology*. 2009;29:246–253.

32. Rajamannan NM, Subramaniam M, Rickard D, Stock SR, Donovan J, Springett M, Orszulak T, Fullerton D a, Tajik a J, Bonow RO, Spelsberg T. Human aortic valve calcification is associated with an osteoblast phenotype. *Circulation*. 2003;107(17):2181–4.

33. Jian B, Narula N, Li Q, Mohler E, Levy R. Progression of aortic valve stenosis: TGF-{beta}1 is present in calcified aortic valve cusps and promotes aortic valve interstitial cell calcification via apoptosis. *Annals of Thoracic Surgery*. 2003;75(2):456–466.

34. Deb A, Wang S, Skelding K, Miller D, Simper D, Caplice N. Bone marrow-derived myofibroblasts are present in adult human heart valves. *Journal of Heart Valve Disease*. 2005;14(5):674–678.

35. Monzack EL, Masters KS. Can valvular interstitial cells become true osteoblasts? A side-by-side comparison. *The Journal of heart valve disease*. 2011;20(4):449–63.

36. Behrendt D, Ganz P. Endothelial function. From vascular biology to clinical applications. *The American journal of cardiology*. 2002;90(10C):40L–48L.

37. Lee TC, Zhao YD, Courtman DW, Stewart DJ. Abnormal Aortic Valve Development in Mice Lacking Endothelial Nitric Oxide Synthase. *Circulation*. 2000;101(20):2345–2348.

38. Kennedy J a, Hua X, Mishra K, Murphy G a, Rosenkranz AC, Horowitz JD. Inhibition of calcifying nodule formation in cultured porcine aortic valve cells by nitric oxide donors. *European journal of pharmacology*. 2009;602(1):28–35.

39. Hilton MJ, Tu X, Wu X, Bai S, Zhao H, Kobayashi T, Kronenberg HM, Teitelbaum SL, Ross FP, Kopan R, Long F. Notch signaling maintains bone marrow mesenchymal progenitors by suppressing osteoblast differentiation. *Nature medicine*. 2008;14(3):306–314.

40. Garg V, Muth AN, Ransom JF, Schluterman MK, Barnes R, King IN, Grossfeld PD, Srivastava D. Mutations in NOTCH1 cause aortic valve disease. *Nature*. 2005;437(7056):270–4.

41. Nigam V, Srivastava D. Notch1 represses osteogenic pathways in aortic valve cells. *Journal of molecular and cellular cardiology*. 2009;47(6):828–34.

42. Giachelli CM. Ectopic calcification: new concepts in cellular regulation. *Zeitschrift für Kardiologie*. 2001;90 Suppl 3:31–7.

43. Steitz S a, Speer MY, McKee MD, Liaw L, Almeida M, Yang H, Giachelli CM. Osteopontin inhibits mineral deposition and promotes regression of ectopic calcification. *The American journal of pathology*. 2002;161(6):2035–46.

44. Giachelli CM. Ectopic Calcification: gathering the hard facts about soft tissue mineralization. *American Journal of Pathology*. 1999;154(3):671–675.

45. Towler D a. Molecular and cellular aspects of calcific aortic valve disease. *Circulation Research*. 2013;113:198–208.

46. Tomazic BB, Edwards WD, Schoen FJ. Physicochemical characterization of natural and bioprosthetic heart valve calcific deposits: Implications for prevention. *The Annals of Thoracic Surgery*. 1995;60(95):S322–S327.

47. Prieto RM. Study on the structure and composition of aortic valve calcific deposits. etiological aspects. *Journal of Biophysical Chemistry*. 2011;02(01):19–25.

48. Gilinskaya LG, Rudina NA, Okuneva GN, Vlasov YA. Pathogenic Mineralization on Human Heart Valves. III. Electron Microscopy. *Journal of Structural Chemistry*. 2003;44(6):1038–1045.

49. Mikroulis D, Mavrilas D, Kapolos J, Koutsoukos PG, Lolas C. Physicochemical and microscopical study of calcific deposits from natural and bioprosthetic heart valves. Comparison and implications for mineralization mechanism. *Journal of materials science. Materials in medicine*. 2002;13(9):885–9.

50. Pilarczyk M, Czamara K, Baranska M, Natorska J, Kapusta P, Undas A, Kaczor A. Calcification of aortic human valves studied in situ by Raman microimaging: Following mineralization from small grains to big deposits. *Journal of Raman Spectroscopy*. 2013;44(April):1222–1229.

51. Mangialardo S, Cottignoli V, Cavarretta E, Salvador L, Postorino P, Maras A. Pathological biominerals: Raman and infrared studies of bioapatite deposits in human heart valves. *Applied Spectroscopy*. 2012;66(10):1121–1127.

52. Bazin D, Daudon M, Combes C, Rey C. Characterization and some physicochemical aspects of pathological microcalcifications. *Chemical reviews*. 2012;112(10):5092–120.

53. Weska RF, Aimoli CG, Nogueira GM, Leirner A a., Maizato MJS, Higa OZ, Polakievicz B, Pitombo RNM, Beppu MM. Natural and prosthetic heart valve calcification: Morphology and chemical composition characterization. *Artificial Organs*. 2010;34(4):311–318.

54. Cottignoli V, Cavarretta E, Salvador L, Valfré C, Maras A. Morphological and Chemical Study of Pathological Deposits in Human Aortic and Mitral Valve Stenosis: A Biomineralogical Contribution. *Pathology Research International*. 2015;2015:1–14.

55. Tomazic BB. Physicochemical principles of cardiovascular calcification. *Zeitschrift für Kardiologie*. 2001;80:68–80.

56. Dritsa V, Pissaridi K, Koutoulakis E, Mamarelis I, Kotoulas C, Anastassopoulou J. An infrared spectroscopic study of aortic valve. A possible mechanism of calcification and the role of magnesium salts. *In vivo*. 2014;28:91–8.

57. Bertazzo S, Gentleman E, Cloyd KL, Chester AH, Yacoub MH, Stevens MM. Nano-analytical electron microscopy reveals fundamental insights into human cardiovascular tissue calcification. *Nature materials*. 2013;12(6):576–83.

58. Pachman L, Morgan G, McCarthy P, Huskin A, Malaisrie S, Spevak L, Boskey A. The Composition And Structure Of Calcifications In Juvenile Dermatomyositis Differs From Calcified Aortic Valves Removed From Adults Without JDM [abstract]. *Arthritis Rheumatism*. 2013;65(Suppl 10):228.

59. Arjunon S, Rathan S, Jo H, Yoganathan AP. Aortic valve: mechanical environment and mechanobiology. *Annals of biomedical engineering*. 2013;41(7):1331–46.

60. Balachandran K, Sucosky P, Yoganathan AP. Hemodynamics and mechanobiology of aortic valve inflammation and calcification. *International journal of inflammation*. 2011;2011:263870.

61. Schoen FJ. Evolving concepts of cardiac valve dynamics: the continuum of development, functional structure, pathobiology, and tissue engineering. *Circulation*. 2008;118(18):1864–80.

62. Cloyd KL, El-Hamamsy I, Boonrungsiman S, Hedegaard M, Gentleman E, Sarathchandra P, Colazzo F, Gentleman MM, Yacoub MH, Chester AH, Stevens MM. Characterization of Porcine Aortic Valvular Interstitial Cell "Calcified" Nodules. Aikawa E, ed. *PLoS ONE*. 2012;7(10):e48154.

63. Benton J a, Kern HB, Leinwand L a, Mariner PD, Anseth KS. Statins block calcific nodule formation of valvular interstitial cells by inhibiting alpha-smooth muscle actin expression. *Arteriosclerosis, thrombosis, and vascular biology*. 2009;29(11):1950–7.

64. Yip CYY, Chen J-H, Zhao R, Simmons C a. Calcification by valve interstitial cells is regulated by the stiffness of the extracellular matrix. *Arteriosclerosis, thrombosis, and vascular biology*. 2009;29(6):936–42.

65. Chen JH, Chen WLK, Sider KL, Yip CYY, Simmons C a. β-Catenin Mediates Mechanically Regulated, Transforming Growth Factor-β1-Induced Myofibroblast Differentiation of Aortic Valve Interstitial Cells. *Arteriosclerosis, Thrombosis, and Vascular Biology*. 2011;31:590–597.

66. Benton J a, Kern HB, Anseth KS. Substrate properties influence calcification in valvular interstitial cell culture. *The Journal of heart valve disease*. 2008;17(6):689–699.

67. Balachandran K, Alford PW, Wylie-Sears J, Goss J a, Grosberg A, Bischoff J, Aikawa E, Levine R a, Parker KK. Cyclic strain induces dual-mode endothelial-mesenchymal transformation of the cardiac valve. *Proceedings of the National Academy of Sciences of the United States of America*. 2011;108(50):19943–8.

68. Butcher JT, Nerem RM. Valvular Endothelial Cells Regulate the Phenotype of Interstitial Cells in Co-culture : Effects of Steady Shear Stress. *Tissue Engineering*. 2006;12(4):905–915.

69. Tseng H, Balaoing LR, Grigoryan B, Raphael RM, Killian TC, Souza GR, Grande-Allen KJ. A three-dimensional co-culture model of the aortic valve using magnetic levitation. *Acta Biomaterialia*. 2014;10(1):173–182.

70. Gould ST, Matherly EE, Smith JN, Heistad DD, Anseth KS. The role of valvular endothelial cell paracrine signaling and matrix elasticity on valvular interstitial cell activation. *Biomaterials*. 2014;35(11):3596–606.

71. Gould RA, Chin K, Santisakultarm TP, Dropkin A, Richards JM, Schaffer CB, Butcher JT. Cyclic strain anisotropy regulates valvular interstitial cell phenotype and tissue remodeling in three-dimensional culture. *Acta biomaterialia*. 2012;8(5):1710–9.

CHAPTER 2

SIDE-SPECIFIC ENDOTHELIAL-DEPENDENT REGULATION OF AORTIC VALVE CALCIFICATION: INTERPLAY OF HEMODYNAMICS AND NITRIC OXIDE SIGNALING

Published in American Journal of Pathology*

2.1 Abstract

Arterial endothelial cells maintain vascular homeostasis and vessel tone in part through the secretion of nitric oxide. In this study, we determine how aortic valve endothelial cells (VEC) regulate aortic valve interstitial cell (VIC) phenotype and matrix calcification through nitric oxide. Using an anchored *in vitro* collagen hydrogel culture system, we demonstrate that 3D-cultured porcine VIC do not calcify in osteogenic media unless under mechanical stress. Co-culture with porcine VEC however significantly attenuated VIC calcification through inhibition of myofibroblastic activation, osteogenic differentiation, and calcium deposition. Incubation with the nitric oxide (NO) donor DETA-NO inhibited VIC osteogenic differentiation and matrix calcification, while incubation with the NO blocker L-NAME augmented calcification even in 3D VIC-VEC co-culture. Aortic VEC, but not VIC, expressed endothelial nitric oxide synthase (eNOS) in both porcine and human, which was reduced in osteogenic media. eNOS expression was reduced in calcified human aortic valves in a side specific manner. Porcine leaflets exposed to soluble guanylyl cyclase inhibitor ODQ increased osteocalcin and αSMA expression. Finally, side-specific shear stress

*Richards JM, El-Hamamsy I, Chen S, Sarang Z, Sarathchandra P, Yacoub MH, Chester, AH, Butcher JT. "Side-Specific Endothelial-Dependent Regulation of Aortic Valve Calcification: Interplay of Hemodynamics and Nitric Oxide Signaling" Am J Pathol. 2013;182(5):1922-31.

applied to porcine aortic valve leaflet endothelial surfaces increased cyclic GMP (cGMP) production in VEC. Valve endothelial-derived nitric oxide is a natural inhibitor of early phases of valve calcification, and therefore may be an important regulator of valve homeostasis and pathology.

2.2 Introduction

Calcific aortic valve disease (CAVD) is a serious and increasingly prevalent clinical problem. CAVD involves the development and growth of calcific deposits on the surface and within the flexible leaflets of the valve, progressively occluding the orifice and impairing ventricular function. Aortic valve stenosis is present in up to 25% of Americans over the age of 65[1]. Even moderately functioning valves seriously increase the risks for cardiomyopathy, atherosclerosis, and stroke[2]. CAVD is diagnosed hemodynamically via echocardiography[3], but a clinically useful molecular signature of CAVD progression remains elusive[4]. Recent clinical trials testing lipid metabolism agents (e.g. statins) in CAVD have been disappointing, but underscore that CAVD pathogenesis is an active process with distinctly different features from atherosclerosis[5]. In particular, large occlusive mineralized lesions develop on the aortic valve cusps, while vascular calcifications are often significantly smaller[6]. These lesions exhibit evidence of both dystrophic calcification (calcium crystal nucleation within apoptotic bodies) and osteogenic calcification (via osteoblast-like deposition of mineralized matrix)[7]. Valve interstitial cells (VIC) near calcifications express osteoblast specific proteins such as runx-2 and osteocalcin, which is replicated in 2D cell culture when exposed to osteogenic differentiation media[8, 9]. Prior to calcification, normally fibroblastic VIC transition to activated myofibroblasts, exhibiting elevated proliferation, expressing contractile proteins such as alpha smooth muscle actin

(αSMA), and enhanced matrix turnover[10-12]. The vast majority of studies investigating the molecular mechanisms of VIC phenotypic transitions test these cells in artificial 2D culture conditions and in isolation from their neighboring endothelium.

Heart valve cusps are lined with endothelium that is critically important for transducing hemodynamic signals and delivering nutrients to the underlying VIC. Little is known about the function of valve endothelial cells (VEC) in tissue homeostasis and disease pathogenesis. In 3D co-culture, aortic VEC help maintain VIC quiescence by inhibiting proliferation and myofibroblastic activation in a shear stress dependent manner[13]. Early aortic valve stenosis is characterized by systemic endothelial dysfunction[14]. In situ gene expression profiles show that aortic-sided VEC normally express fewer inhibitors of calcification, directly corresponding to the aortic-sided preference for calcific nodule formation in CAVD[15]. Similarly, VEC express an anti-calcific gene expression profile when cultured under unidirectional shear flow[13], but the molecular mechanisms by which VEC regulate VIC phenotype remain elusive.

Nitric oxide (NO) is a potent vasodilator secreted primarily by endothelial cells and confers many cardiovascular benefits through its action on smooth muscle[16], but its role in aortic valve function is unclear. Serum levels of endothelial nitric oxide synthase (eNOS) inhibitors correlate with aortic valve stenosis in patients with CAVD. A large percentage of eNOS deficient mice develop bicuspid aortic valves[17]. Aortic valve inflammation is associated with decreased NO availability and increased oxidative stress[18]. Increasing NO or intracellular cGMP in 2D cultured VIC inhibits the formation of calcified nodules[19]. Conversely, endothelial NO in diseased aortic valves can become decoupled from antioxidant signaling, leading to an increased risk of calcification[20]. These results suggest that endothelial derived NO may modulate VIC calcification, but to what ends and mechanism is unclear.

The objective of this study therefore was to determine how VEC modulate VIC fate and tissue homeostasis in calcification prone environments. We establish that VEC naturally suppress VIC calcification by reducing myofibroblastic activation, osteogenic differentiation, and matrix calcification of VIC *in vitro* and *ex vivo*. We then determined that endothelial-secreted nitric-oxide (NO) antagonizes calcification pathogenesis in aortic valves *ex vivo* and *in vitro*. We additionally show that eNOS derived NO signaling through sGC binding and intracellular cGMP activation is shear stress driven in aortic valves in a side-specific manner. Finally, we show that calcified human aortic valves exhibit reduced eNOS expression in a side specific manner.

2.3 Materials and Methods

Valve Cell Isolation and Culture

Porcine heart valves were kindly donated by Shirk Meats of Dundee, NY, and Cheal Meats of Essex, UK. Porcine aortic valve endothelial cells (PAVEC) and aortic valve interstitial cells (PAVIC) were isolated using collagenase digestion as described elsewhere[21-23], and cultured in cultured in Dulbecco's Modified Eagle's Medium (DMEM, Invitrogen) supplemented with 10% fetal bovine serum (FBS, Gibco) and 1% penicillin-streptomycin (Gibco) at 37°C and 5% CO_2. PAVEC culture media was further supplemented with 50 units/mL Heparin (Sigma). For experiments, PAVIC were used between passage 3 and 8, whereas PAVEC were used between passage 3 and 5. To confirm the phenotype of cells used in cell cultures, particularly valve endothelial cells, a panel of immunofluorescent stains were conducted (Figure 2.1). Results show positive αSMA expression (Draq5 nuclear counterstain) in PAVIC cultures and strong von Willebrand factor expression (Draq5 nuclear counterstain) in

PAVEC cultures, which led us to the conclusion that our isolated PAVEC are in fact true endothelial EC.

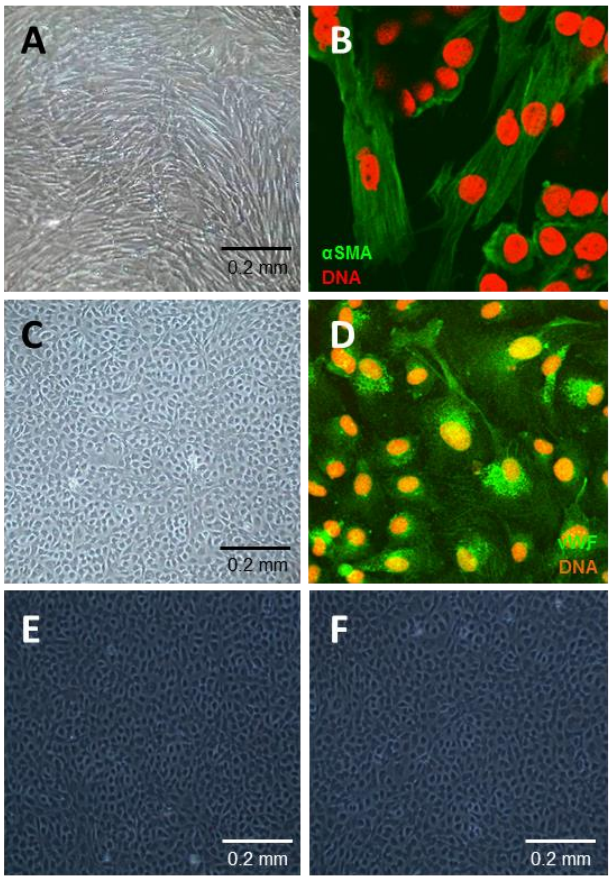

Figure 2.1: Confirmation of PAVIC and PAVEC phenotype. A,B) Porcine aortic valve interstitial cells (PAVIC) in primary culture. C,D) Porcine aortic valve endothelial cells (PAVEC) in primary culture 2D PAVEC monolayers cultured in E) normal (control) culture medium, and F) osteogenic medium. No calcific nodules form in PAVEC in either condition.

3D In Vitro Valve Calcification Models

Three-dimensional (3D) collagen hydrogels were created in 3X DMEM with 10% FBS, 2 mg/mL type I collagen, and adequate 0.1M NaOH to neutralize the solution (Figure 2.2 and previously described[13, 22]). Collagen hydrogels were created with either: 1) PAVIC ($1x10^6$ cells/ml) embedded within the gel alone, 2) a monolayer of PAVEC ($5x10^5$ cells/cm^2) seeded on top of the gel, or 3) the combination

PAVIC/PAVEC seeding (Figure 2.2). The edge of each well of a 24-well plate was ringed with a hydrophobic pen, and then exposed to UV sterilization for 1 hour prior to gel seeding to ensure gels remained in the center of the well (Appendix B for full protocol). Gels were allowed to polymerize for one hour in 37°C at 5% CO_2 prior to PAVEC monolayer seeding on top (if applicable). A subset of gels were released after 12 hours from the bottom of the well plate, allowing them to float freely within the culture media, while the rest remained geometrically constrained through adhesion to the substrate. Gels were cultured with either control or osteogenic medium (control medium supplemented with 10 mM β-glycerophosphate, 50 µg/ml ascorbic acid and 10nM dexamathesone, OGM) for up to 14 days with media changed every 48 hours.

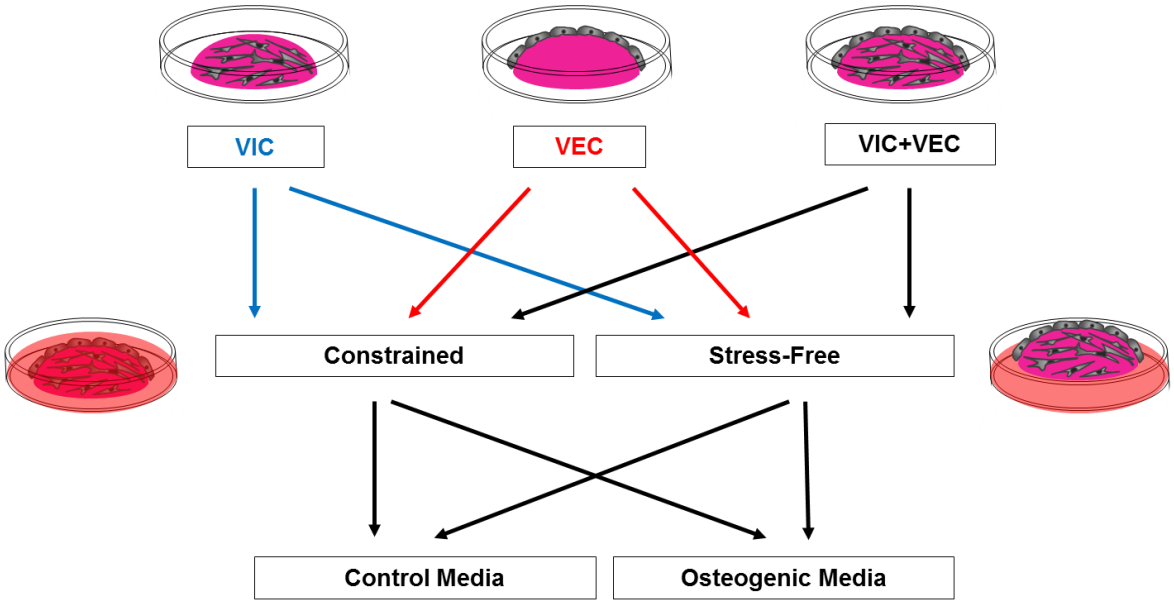

Figure 2.2: Schematic of 3D collagen hydrogen model. Three combinations for modeling: PAVIC alone embedded within collagen gel; PAVEC monolayer seeded atop collagen gel; co-culture of PAVIC embedded and monolayer of PAVEC on collagen gel. Each gel type was split into two mechanical groups: constrained and stress-free. Constrained gels were left adhered to the bottom of the well, while stress-free gels were released after 12 hours and left to float freely within the culture media. These groups, in turn were split into a further culturing division, either cultured in normal control media, or fed with media supplemented with osteogenic differentiation factors.

Compaction and Calcification Analyses

Compaction of free floating gels (stress-free) under different experimental conditions was measured from tracings of digital images and compared as a percentage of the original area of the gel. To quantify calcified matrix developed in different experimental conditions, an Alizarin Red absorbance assay was implemented. Gels were fixed with paraformaldehyde and then incubated with 40 nM Alizarin red S (ARS) dye. This dye binds to calcium crystals in cells or matrix fibers, revealing a red color[24]. Unbound solution was washed out overnight under gentle rocking. Bound ARS dye was then released from the gels using 10% acetic acid, followed by neutralization with 10% ammonium hydroxide. The concentration of dye in solution was then quantified using absorbance spectroscopy at 405 nm wavelength.

Quantitative Real-Time RT-PCR

Extraction of total RNA from homogenized hydrogels was performed using the RNeasy Mini Kit (QIAGEN), which was then reverse transcribed into complementary cDNA using the SuperScript III kit (Invitrogen), according to the manufacturer's instructions. RT- PCR was performed on all samples using SYBR Green PCR master mix (Applied Biosystems, Foster City, CA) and a MiniOpticon Real-Time PCR Detection System (BioRad, Hercules, CA).

Histological and Immunofluorescence Analyses

Collagen gels were fixed overnight in 4% paraformaldehyde and placed in 70% ethanol. Gels were then paraffin embedded and sectioned at 6 μm. Slides were deparaffinized and stained with hematoxylin and eosin (Harleco) to depict matrix and

cellular architecture. Slides were rinsed and coverslipped with permount. Slides were viewed using a Zeiss microscope and several representative pictures were taken from each gel.

For immunofluorescence, gels or coverslips with cells were fixed in 4% paraformaldehyde (PFA), permeabilized with 0.2% Triton-X 100, and blocked with 1% BSA overnight as previously described[22]. Gels were incubated at 4°C with rabbit anti-human α-SMA 1:100 or rabbit-anti human von Willebrand factor 1:100 (Invitrogen). Goat anti-rabbit secondary antibody at 1:100 was incubated for 2 hours at room temperature. The nuclear counterstain Draq5 was incubated for 30 minutes. Specimens were imaged using laser confocal microscopy, and the images processed using ImageJ as previously described[22].

Additionally, calcified human aortic valves were obtained from adults undergoing planned, non-elective valve replacement surgery. Grossly normal, non-calcified human aortic valves were obtained from valve donors from non-cardiac deaths. Human tissue procurement was conducted with the Institutional Review Board approved protocols at the Harefield Hospital. Specimens were assessed for eNOS expressing using the above methods.

Proliferation and Apoptosis Assays

Anti-bromodeoxyuridine (Invitrogen) immunohistochemistry was used to identify proliferating cells, and a terminal deoxyribonucleotidyl transferase-mediated dUTP nick end labeling (TUNEL) assay kit (Invitrogen) was used to visualize cells undergoing apoptosis. For cell proliferation analysis, BrdU was added at a 1:100 concentration to the media for the last 12 hours of the experiment. Gels were imaged and analyzed in ImageJ. Proliferation was measured via the percentage of BrdU

positive cells compared to total cell nuclei, while apoptosis assessed TUNEL-positive cells as a percentage of total cell number. Both proliferation and apoptosis were normalized to control conditions. Draq5 was used as a nuclear counterstain for proliferation and apoptosis assays.

Nitric Oxide Regulation of Aortic Valve Calcification In Vitro

PAVIC-only gels were cultured in control and osteogenic medium as described above, but in the presence of 1μM diethylenetriamine nitric oxide adduct (DETA-NO, Sigma) as a nitric oxide donor. Fresh DETA-NO was added daily. In the loss-of-function assay, PAVIC+PAVEC gels were treated with two concentrations (500μM and 2mM) of N-nitro-L-arginine methyl ester (L-Name, Sigma), which was added every other day to either control or OGM. Matrix calcification and gene expression were quantified as before.

Ex Vivo Assay for Side-Specific Aortic Valve Endothelium Regulation of Leaflet Calcification

We previously published a concentric plate system for selective exposure of aortic or ventricular surfaces aortic valve cusps in culture[25]. Porcine aortic valve leaflets were placed with either fibrosa or ventricularis surface endothelium exposed to either control or osteogenic medium conditions for a period of up to 21 days. Calcified lesion location, number, and size were determined using Alizarin Red and von Kossa staining, either *en face* or in thin sections of paraffin embedded samples. Number of nodules, nodule size, and overall distribution were quantitatively compared across culture medium and exposed leaflet surface. Identical ex-vivo leaflet culture experiments were conducted in control and osteogenic medium, but in the presence

of L-NAME (100 μM) as a specific inhibitor of nitric oxide synthase. Fresh L-NAME was added with each medium exchange. Nodule formation and characteristics were quantified as before (n=4).

Hemodynamic Regulation of Nitric oxide Signaling Ex Vivo

The fibrosa and ventricular endothelial surfaces of the aortic valve are exposed do different shear stress patterns in vivo. As nitric oxide production is regulated by shear stress, we implemented a previously published cone-and-plate system to expose either the fibrosa or ventricularis side of the cusps to their physiological waveforms (12). We used cyclic guanosine monophosphate (cGMP) as a surrogate for nitric oxide (NO) production as supported by many studies[26-28]. Aortic valve cusps were mounted in a custom housing that ensured cusps were oriented perpendicular to the direction of flow (radially) as in vivo[23, 29]. The side specific VEC were then exposed to their physiological flow patterns then analyzed at 2 time points: 30 minutes or 4 hours. Experiments were performed in the presence of isobutylmethylxanthine (IBMX), a non-specific inhibitor of phosphodiesterase (PDE), to prevent degradation of cGMP in the tissue. After experiments, all tissues were excised, flash frozen, crushed in liquid nitrogen, and then homogenized in 0.1M HCl. After centrifugation, the supernatant was collected and stored at -80°C until the cGMP analysis. cGMP measurements were performed using a commercially available kit (K372-100, BioVision, UK). As per the manufacturer's instructions, the supernatant was acetylated to increase the sensitivity of cGMP detection, and the finished Protein G Coated Plate was read in an optical spectrometer at 450nm. Differentiation of cGMP-mediated effects of NO from cGMP-indpendent effects was achieved by selectively

exposing leaflets to soluble guanylyl cyclase inhibitor ODQ and activator BAY in OGM for up to 21 days.

Statistical Analysis

All data are expressed as mean ± standard error, with at least 3 independent experiments per treatment. Data was analyzed statistically with JMP for Windows. Analysis of variance with Tukey's post-hoc test was used to compare differences between means (differences between means were considered significant at $P \leq 0.05$).

2.4 Results

VIC calcification in 3D culture occurs only when mechanically stressed

Porcine valve interstitial cells (PAVIC) and porcine valve endothelial cells (PAVEC) were isolated and phenotype confirmed via morphology and immunohistochemistry. Maintenance of spatial integrity of PAVEC and PAVIC in 3D cultures over 14 days was confirmed via histology (Figure 2.3). 3D cultured PAVIC in

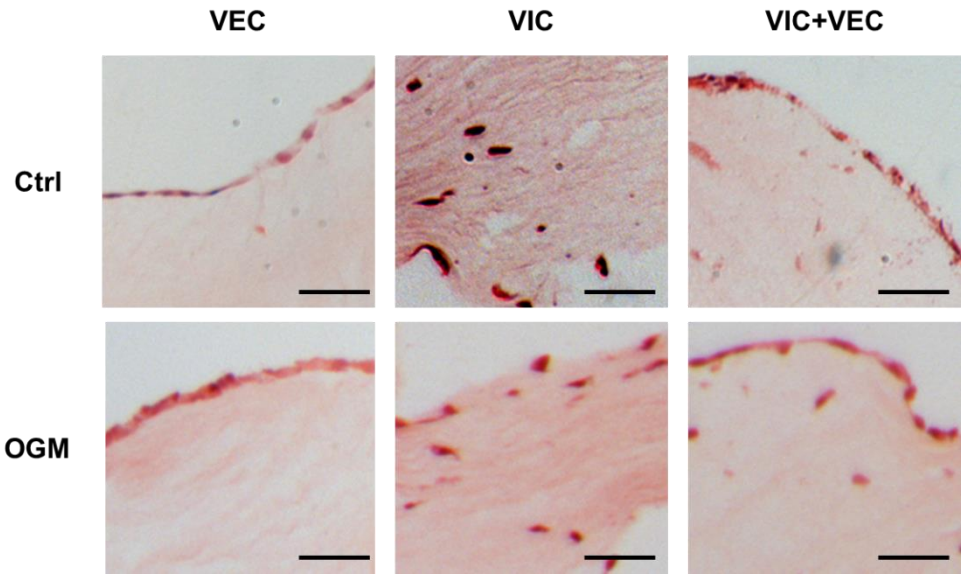

Figure 2.3: Collagen hydrogel histology. Representative images of hematoxylin and eosin stained constrained 3D gels after 14 days of culture. Scale bar = 50μm

stress-free environments compacted significantly more in OGM than in control media (5.6% ± 0.53 vs. 8.3% ± 0.38 of original area, P<0.05) over a 7 day period (Figure 2.4A). Stress-free 3D cultured PAVIC did not exhibit any calcium deposition (via Alizarin red staining) in control or OGM conditions over 14 days (Figure 2.4B). However, PAVIC cultured within anchored (mechanically stressed) 3D gels for 14 days developed significant calcium deposition when cultured in OGM, but not in control media (2.2 ± 0.08 vs. 0.88 ± 0.08 relative Alizarin red dye absorbance, P<0.05). Interestingly, collagen gels with PAVEC surface monolayers did not compact or have any detectable calcium deposition, regardless of culture medium.

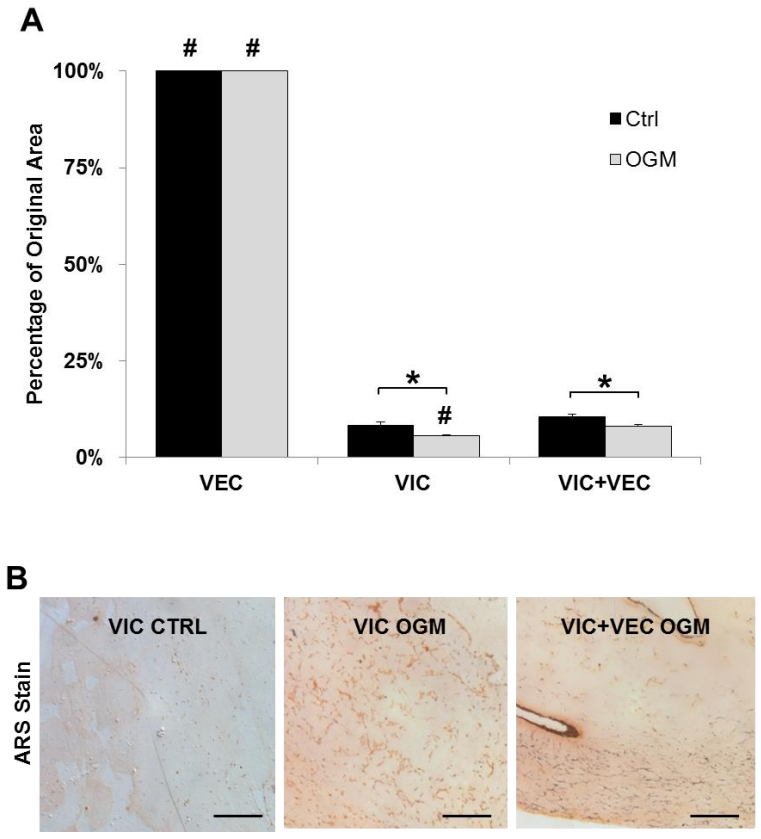

Figure 2.4: Compaction and calcification of stress-free gels. A) Stress-free 3D hydrogel compaction as a percent of original area in normal control and osteogenic culture conditions, n=6 *P<0.05 within groups (effect of media), #P<0.05 between treatment groups (effect of cell type). B) Alizarin Red staining shows no calcification in stress-free 3D PAVIC and PAVIC+PAVEC gels, scale bar=200 μm.

Mechanically stressed PAVEC-only 3D cultures also did not calcify, yielding lower relative dye absorbance that VIC controls (0.13 ± 0.01 in PAVEC control and 0.15 ± 0.03 in PAVEC OGM, Figure 2.5A, B). These results suggest that PAVIC, but not PAVEC, calcify in response to osteogenic media conditions, and in 3D culture this process requires mechanical stress.

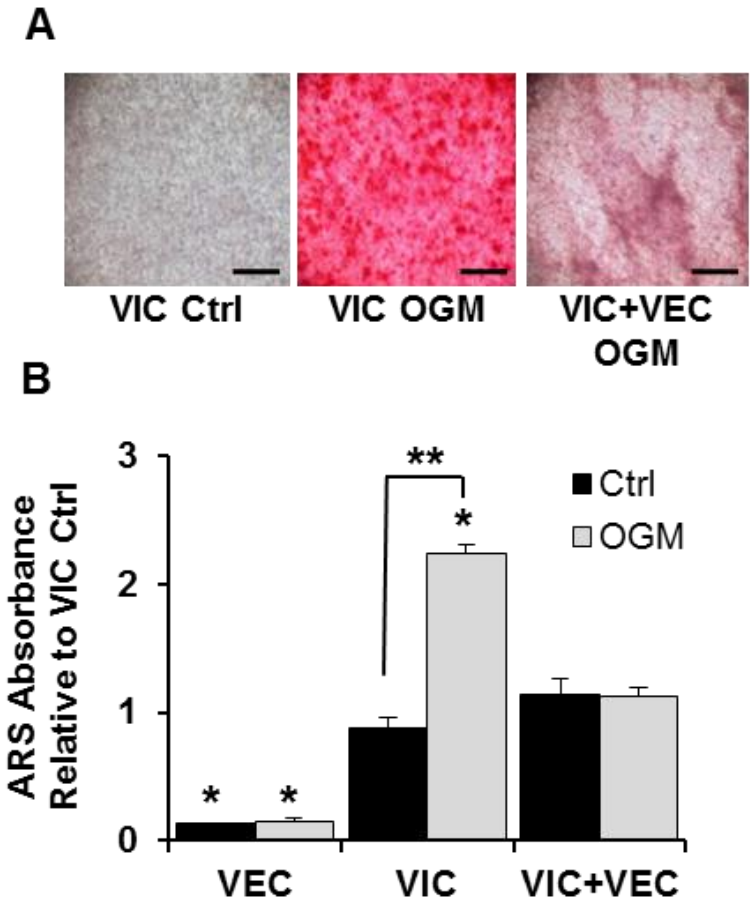

Figure 2.5: Calcification of mechanically stressed hydrogels. A) Representative Alizarin Red S (ARS) stained hydrogels in control (Ctrl), osteogenic (OGM) and co-culture (VIC+VEC) conditions, scale bar=200µm. B) Quantification of calcium deposition via ARS absorbance in 3D hydrogel VIC/VEC co-culture, n=6. Each measurement is relative to VIC control. Values expressed as relative dye absorbance and are means±SEM. **P<0.05 within groups (effect of media), *P<0.05 between treatment groups (effect of cell type).

Valvular endothelial cells inhibit interstitial calcification in 3D culture

Addition of PAVEC monolayers to 3D cultured PAVIC in stress-free, control medium conditions resulted in no changes in calcium deposition (none detected) or matrix compaction. In stress-free OGM conditions, PAVEC co-culture reduced PAVIC matrix compaction (8.0% ± 0.55% vs. 5.6% ± 0.33% of original area, respectively, $P<0.05$), but still exhibited no detectable calcium deposition. In mechanically stressed gels, there was no discernible calcium deposition in either PAVIC or PAVIC+PAVEC co-culture in control conditions. All measurements are relative to PAVIC control. Interestingly, PAVEC monolayers co-cultured with PAVIC in mechanically stressed 3D cultures resulted in significantly reduced matrix calcification (1.12 ± 0.07 vs. 2.24 ± 0.08 Alizarin Red absorbance in PAVIC only, $P<0.05$, Figure 2.5B). These findings indicate that PAVEC inhibit the PAVIC calcification occurring in mechanically stressed 3D culture. Therefore, the remainder of our studies focused on mechanically stressed 3D culture conditions.

Valvular endothelial cells inhibit myofibroblastic and osteoblastic differentiation in vitro

We next examined whether OGM modulated 3D cultured PAVIC proliferation or apoptosis via BrdU and TUNEL staining, respectively (Figure 2.6). Proliferation analysis via anti-BrdU immunostaining revealed no significant difference in cell proliferation due to culture in OGM in any cell type relative to controls (All $P>0.05$, Figure 2.6A). Additionally, apoptosis was not significantly affected by culture in OGM over 14 days (All $P<0.05$, Figure 2.6B).

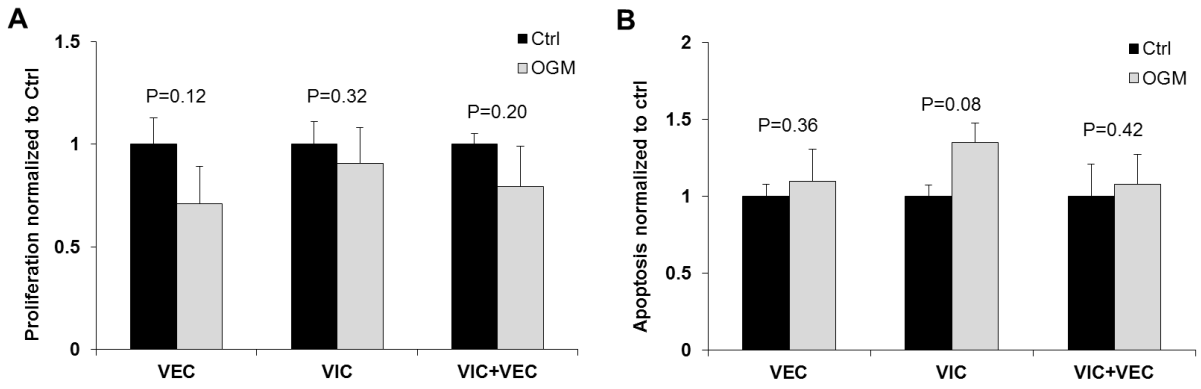

Figure 2.6: Proliferation and apoptosis of collagen gels. A) Proliferation of cells (BrdU-positive nuclei) in co-culture hydrogels with and without OGM, normalized to each cell control, n=6. B) Apoptosis (TUNEL-positive cells) of cells in co-culture hydrogels with and without OGM, normalized to each cell control (n=6)

Immunohistochemistry revealed that PAVIC 3D cultured in OGM increased αSMA protein expression relative to controls, which was reduced with PAVEC co-culture (Figure 2.7A). Similar results were found with quantitative real-time PCR, which revealed a 3.25 ± 0.31 fold increase of αSMA expression in 3D cultured PAVIC in OGM compared with controls ($P<0.05$). Co-culture with PAVEC reduced this expression to 0.63 ± 0.01 fold in OGM, which was in fact less than in control conditions. PAVEC gels in both control media and OGM expressed virtually undetectable αSMA (0.0003 ± 0.0001 fold in PAVEC control and 0.006 ± 0.006 fold in PAVEC OGM, $P<0.05$) compared to PAVIC controls (Figure 2.7B). Stressed 3D cultures of PAVIC exposed to OGM also markedly upregulated genes involved in osteogenic differentiation, including osteocalcin and Runx-2 (Figure 2.7B). 3D co-culture of PAVIC with PAVEC reverted expression of Runx-2 and osteocalcin to control levels (PAVIC osteocalcin 3.33 ± 0.44 and Runx-2 5.31 ± 0.57 vs. PAVIC+PAVEC osteocalcin 1.40 ± 0.29 and Runx-2 1.50 ± 0.34 in OGM, $P<0.05$, Figures 2.7B). Collectively, these results suggest that calcification of 3D PAVIC in

this system involves myofibroblastic activation and osteoblastic differentiation, but not apoptosis. Furthermore, PAVEC mitigates tissue calcification through inhibition of PAVIC differentiation.

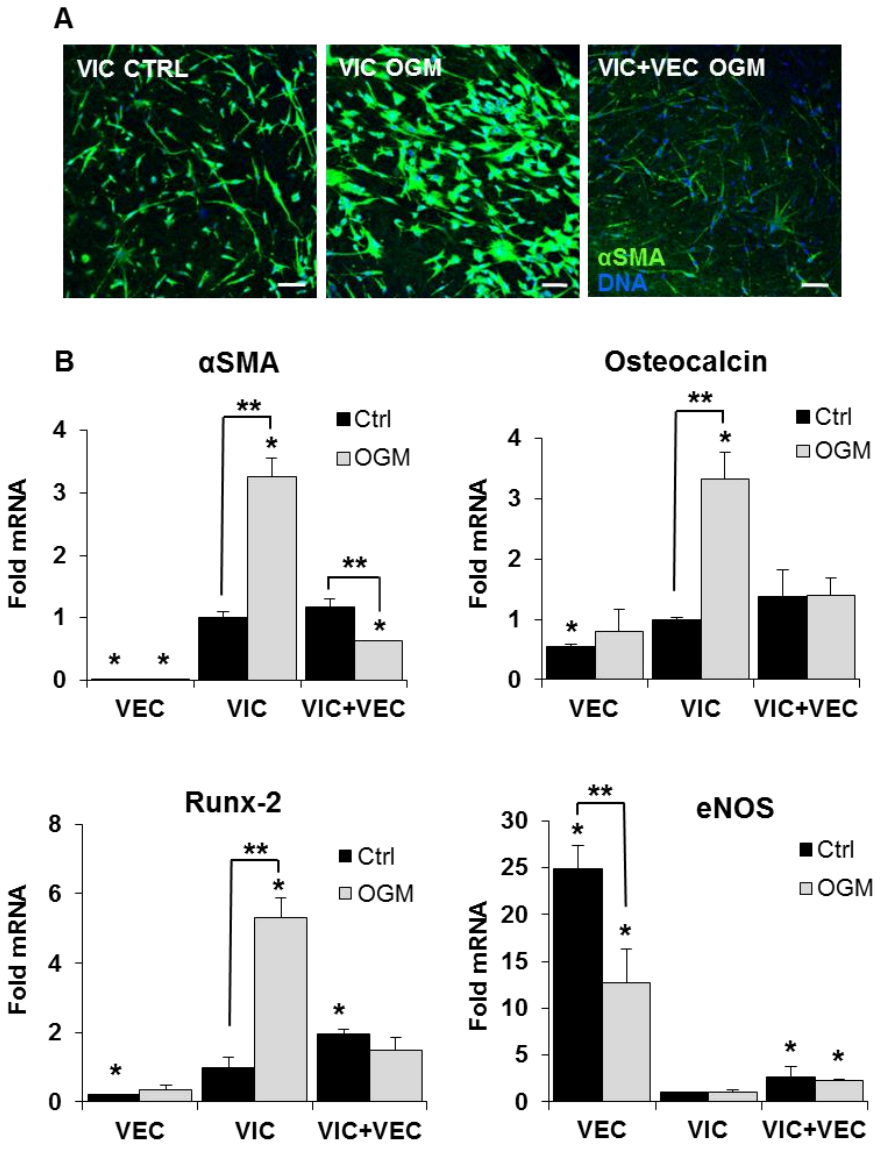

Figure 2.7: Myofibroblastic activation and osteogenic differentiation of valve cells. A) Immunohistochemistry of α-SMA (green) expression in 3D PAVIC and PAVIC+PAVEC gels, scale bar = 50 μm. B) Real-time PCR shows the effect of OGM on the expression of αSMA, osteocalcin, Runx-2 and eNOS in constrained 3D PAVIC and PAVIC+PAVEC gels, n=6. Values are expressed as fold expression changes and are means±SEM. **P<0.05 within groups (effect of media), *P<0.05 between treatment groups (effect of cell type).

Nitric oxide secretion by valvular endothelial cells inhibits osteoblastic differentiation and matrix calcification

We confirmed maintenance of PAVEC monolayers for the full culture period via histology and PECAM1 gene expression (Figure 2.8A). Endothelial nitric oxide synthase (eNOS) gene expression was 24.93 ± 2.48 fold greater in PAVEC than PAVIC in control media ($P<0.05$, Figure 2.7B). Culture with OGM significantly reduced PAVEC eNOS expression, but still remained 12.76 ± 3.56 fold greater than that of PAVIC ($P<0.05$). PAVIC-specific expression of eNOS was uniformly low and not affected by culture medium.

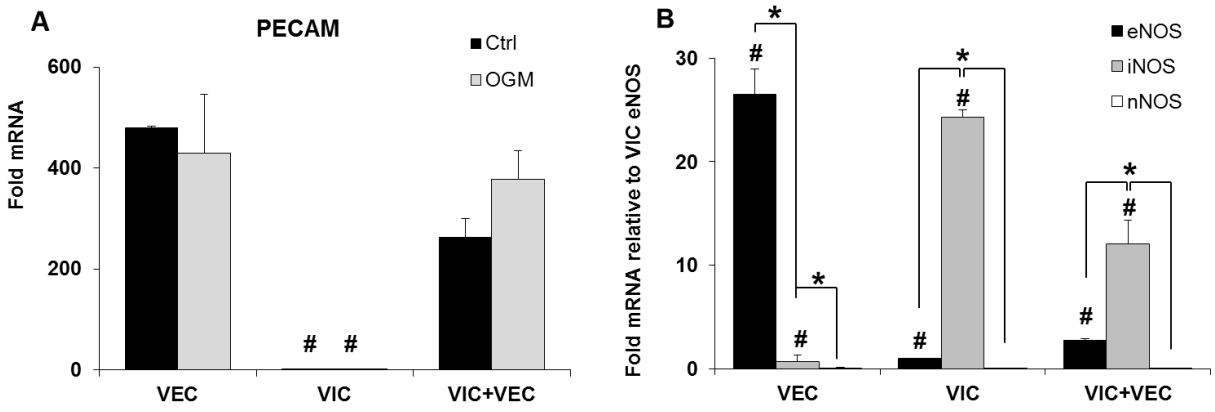

Figure 2.8: Endothelial markers in collagen gels. A) Real time qPCR of A) PECAM1 and B) all three NOS isoforms (eNOS, iNOS, nNOS) expression in ctrl and OGM experimental conditions , n=6. Values are expressed as fold expression changes and are means±SEM. *P<0.05 within groups (effect of media), #P<0.05 between treatment groups (effect of cell type).

When placed in co-culture with OGM, eNOS expression remained significantly elevated over PAVIC controls (2.27 ± 0.18 fold, $P<0.05$), but markedly reduced in comparison to PAVEC alone (Figure 2.7B). This was expected due to the relative amounts of the two cell types in the co-culture samples. Comparison of eNOS gene

expression with those of the two other NO synthases, iNOS and nNOS, suggested that PAVEC only express eNOS while PAVIC express iNOS (Figure 2.8B).

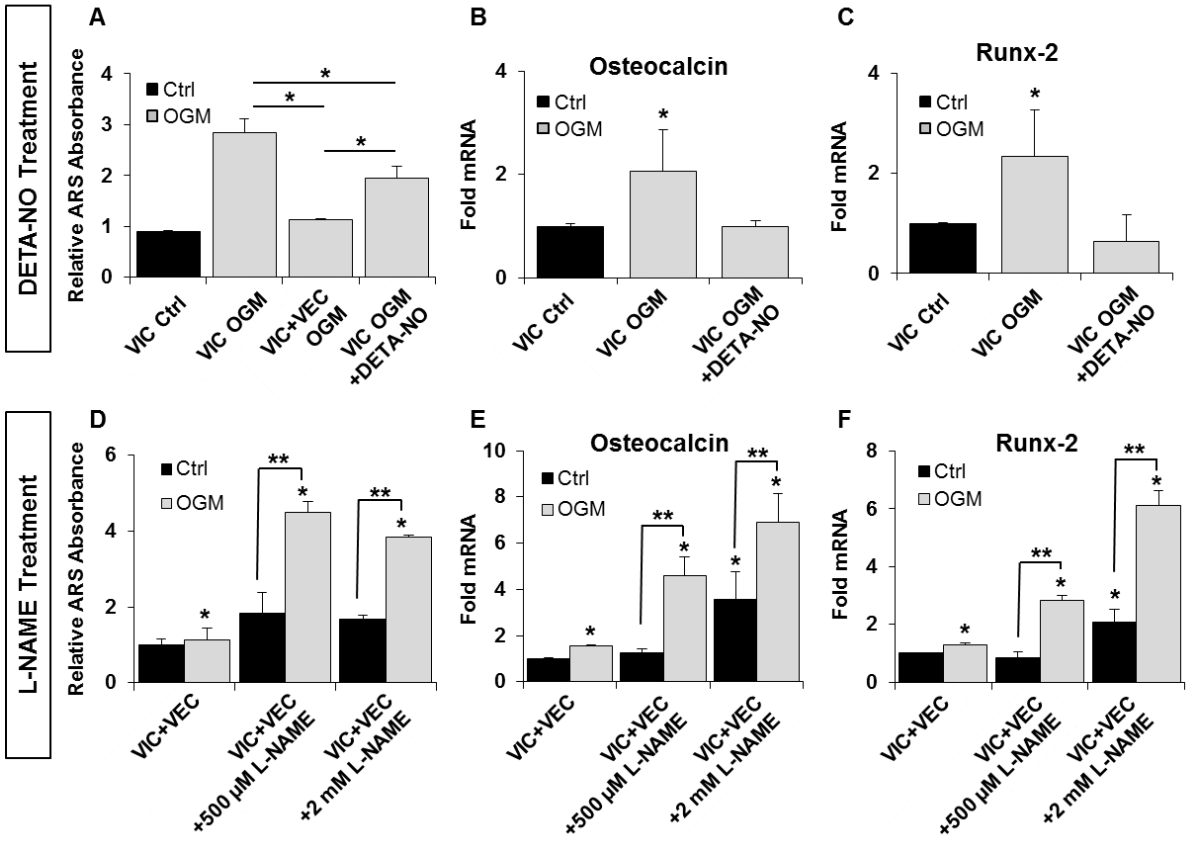

Figure 2.9: Nitric oxide and calcification. A) Quantitative tissue calcification via relative absorbance of ARS in constrained 3D PAVIC gels in control and OGM, as well as OGM treated with 1μM DETA-NO *P<0.05. B) Osteocalcin and C) Runx-2 expression in constrained 3D PAVIC gels treated with OGM and 1μM DETA-NO. D) Comparison of the effect of different concentrations of L-NAME on the on calcium deposition within co-culture gels via ARS staining. E) Osteocalcin and F) Runx-2 expression in constrained 3D co-culture gels treated with OGM and L-NAME. **P<0.05 within groups (effect of media), *P<0.05 between treatment groups (effect of cell type).

When exogenous NO (1 μM diethylenetriamine nitric oxide, DETA-NO) was administered to PAVIC in 3D OGM culture, the same anti-calcific response as from PAVEC co-culture occurred. DETA-NO supplementation decreased calcium

deposition by PAVIC by over 30% (2.8 ± 0.3 vs. 1.9 ± 0.2 relative absorbance of Alizarin Red, $P<0.05$, Figure 2.9A), combined with similar decreases in osteogenic genes osteocalcin and Runx-2 (Figure 2.9B,C). Conversely, when PAVIC+PAVEC co-cultures were treated with the NO inhibitor N-nitro-L-arginine methyl ester (L-Name, 500μM and 2mM), the anti-calcific effects of PAVEC were prevented. Calcium deposition increased 2-fold in co-culture (Figure 2.9D) with OGM and L-NAME, with no effect of concentration. This was combined with significant increases in osteocalcin and Runx-2 gene expression in co-cultures with OGM and L-NAME (Figures 2.9E,F). As the anti-calcific effects of NO were only mimicked when PAVEC were added to PAVIC cultures, we are confident that the source of NO production in this system is endothelial. Therefore, endothelial secreted nitric oxide inhibits osteogenic differentiation and matrix calcification by PAVIC.

Calcification occurs preferentially in the fibrosa of aortic valves ex vivo

Complementing our *in vitro* findings, we cultured porcine aortic valve leaflets with either the ventricular or fibrosa surface exposed to OGM or control medium. No calcified nodule formation was observed in either fibrosa or ventricularis tissue layers in cusps at fresh (baseline) or after 10 days culture in control medium. Ventricularis sided culture in OGM produced a negligible amount of nodules compared to control medium (0.5 ± 0.5 nodules in OGM vs. 0.25 ± 0.25 nodules in baseline and control, Figure 2.10). In contrast, fibrosa sided culture in OGM developed a significant number of calcific (Alizarin-red positive) deposits after 10 days (9.5 ± 3.5 vs. 0.5 ± 0.5 nodules/hpf in the ventricularis, respectively, $P<0.05$).

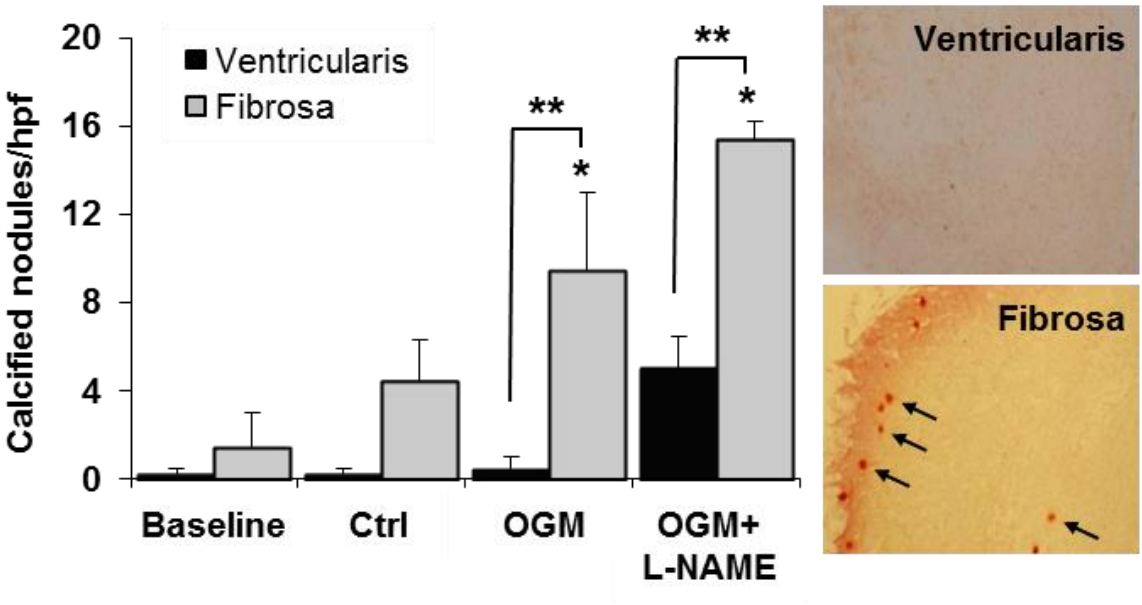

Figure 2.10: Side-specific calcification in ex vivo aortic valve leaflets. Comparison of Alizarin Red-positive nodules per high powered field (hfp) formed on the ventricular and aortic sides of intact valve cusps before (Baseline) and after 3 weeks of incubation in control media (Ctrl), osteogenic media (OGM) or OGM supplemented with 100μM L-NAME, n=4, *P<0.05 within groups (effect of media), **P<0.05 between treatment groups (effect of cell side). Images within the graph are representative histological sections of ARS-positive nodules on aortic valve cusps placed in OGM.

L-NAME (100μM) supplemented OGM culture significantly increased the number of calcified lesions in organ culture compared to OGM alone (15.4 ± 0.8 vs. 9.5 ± 3.5 nodules, P<0.05). As expected, more calcified lesions formed in the fibrosa compared to the ventricularis when NO was blocked by L-NAME (15.4 ± 0.8 vs. 5.0 ± 1.4, P<0.05). Collectively, these results confirm and extend our *in vitro* findings by demonstrating a fibrosa sided preference for calcium nodule formation in osteogenic conditions, with calcification exacerbated by inhibition of nitric oxide.

Valvular endothelial nitric oxide signaling is side specific and regulated by fluid shear stress

We previously reported that eNOS protein expression was greater in the ventricularis than fibrosa endothelium on healthy porcine aortic valves[13], which might explain the side specific propensity for calcification. We therefore investigated the side-specific nature of eNOS expression in non-diseased and calcified human aortic valves (Figure 2.11A). Almost 5-fold more eNOS protein was expressed on the ventricularis side (2.46 ± 0.50 vs. 0.49 ± 0.11, P<0.05, Figure 2.11B) in non-calcified aortic valves.

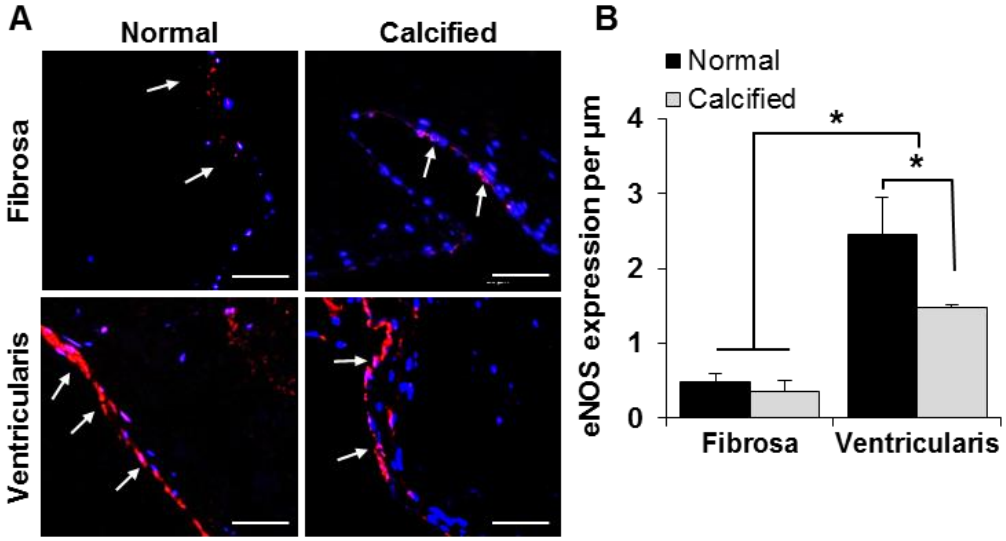

Figure 2.11: eNOS expression in human aortic valves. A) Immunofluorescent staining for endothelial nitric oxide synthase (eNOS) (red) on the ventricular and aortic side of normal and calcified human valves, arrows indicate eNOS expression bars=20 µm B) Quantitative measure of eNOS expression on the ventricular and aortic side of normal and calcified human valves (measured area of expression per length) *P<0.05.

eNOS expression was significantly reduced overall in calcified valves compared to non-diseased valves, but ventricularis sided endothelial eNOS expression remained markedly higher than fibrosa-sided expression (2.46 ± 0.50 vs. 1.48 ± 0.03 in calcified

valves, P<0.05). Interestingly, the lower basal-level fibrosa sided eNOS expression remained statistically unchanged with calcification (P=0.19). Together these results support that eNOS expression is side-specific and correlates inversely with propensity for calcification in aortic valves.

As eNOS signaling is shear stress sensitive in blood vessels[30], we hypothesized that hemodynamics may potentiate side-specific eNOS signaling. We used cGMP as a quantitative readout of NO signaling[26-28]. *En face* immunostaining demonstrated that ventricularis PAVEC had elevated intrinsic cGMP expression compared to fibrosa PAVEC (Figure 2.12A).

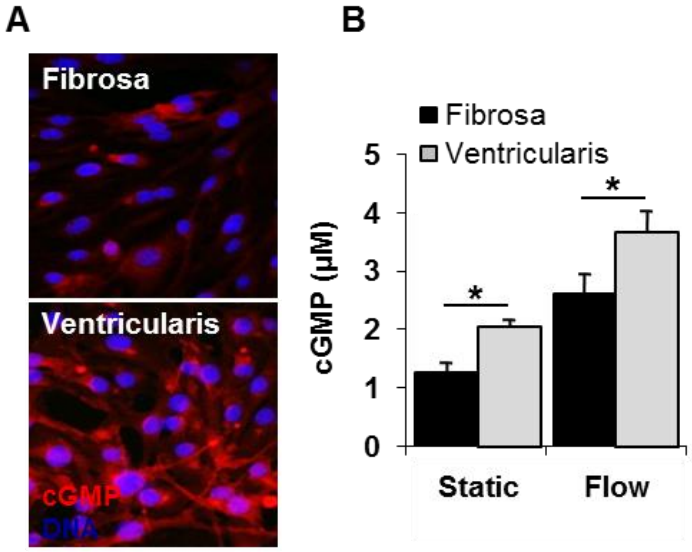

Figure 2.12: cGMP on valve cusps with physiological flow conditions. A) Immunohistochemistry cGMP (red) on healthy porcine aortic valves on both fibrosa and ventricularis sides of the valve cusps. B) Accumulation of cGMP in valve cusps following exposure of the aortic or ventricular sides of the aortic valve to their respective patterns of flow *P<0.05.

Ventricular and fibrosa surfaces were then selectively exposed to their side-specific physiological ventricular or aortic flow waveforms in a cone in plate apparatus[31]. Side-specific fluid shear stress induced marked increase in cGMP

production by both endothelial surfaces in comparison to static controls (2.71 ± 0.26 μM on aortic and 3.75 ± 0.31 μM on ventricular side in flow vs. 1.08 ± 0.25 μM on aortic and 2.09 ± 0.12 μM on ventricular side in static culture, $P<0.05$, Figure 2.12B). The pulsatile unidirectional ventricularis flow patterned shear stress stimulated significantly more cGMP production than the oscillatory-like fibrosa-sided shear stress patterns (3.75 ± 0.31 μM vs. 2.71 ± 0.26 μM, $P<0.05$, Figure 2.12B).

To determine if the increase in cGMP expression was due to NO signaling, porcine leaflets were selectively exposed to soluble guanylyl cyclase inhibitor ODQ and activator BAY for 21 days. Immunohistochemistry reveals higher osteocalcin on the fibrosa side in OGM and OGM+ODQ conditions (Figure 2.13A). αSMA expression was higher on both sides of the valve in OGM, with higher expression on the ventricularis in both OGM+ODQ and OGM+BAY conditions (Figure 2.13A). Quantification of ARS-positive nodules formed on the leaflets in these conditions revealed a significant increase in OGM and OGM+ODQ, with an inhibition of nodule formation with OGM+BAY (Figure 2.13B). Taken together, these results indicate that side-specific hemodynamic forces regulate local endothelial nitric oxide signaling to modulate the risk of calcification in aortic valve leaflets.

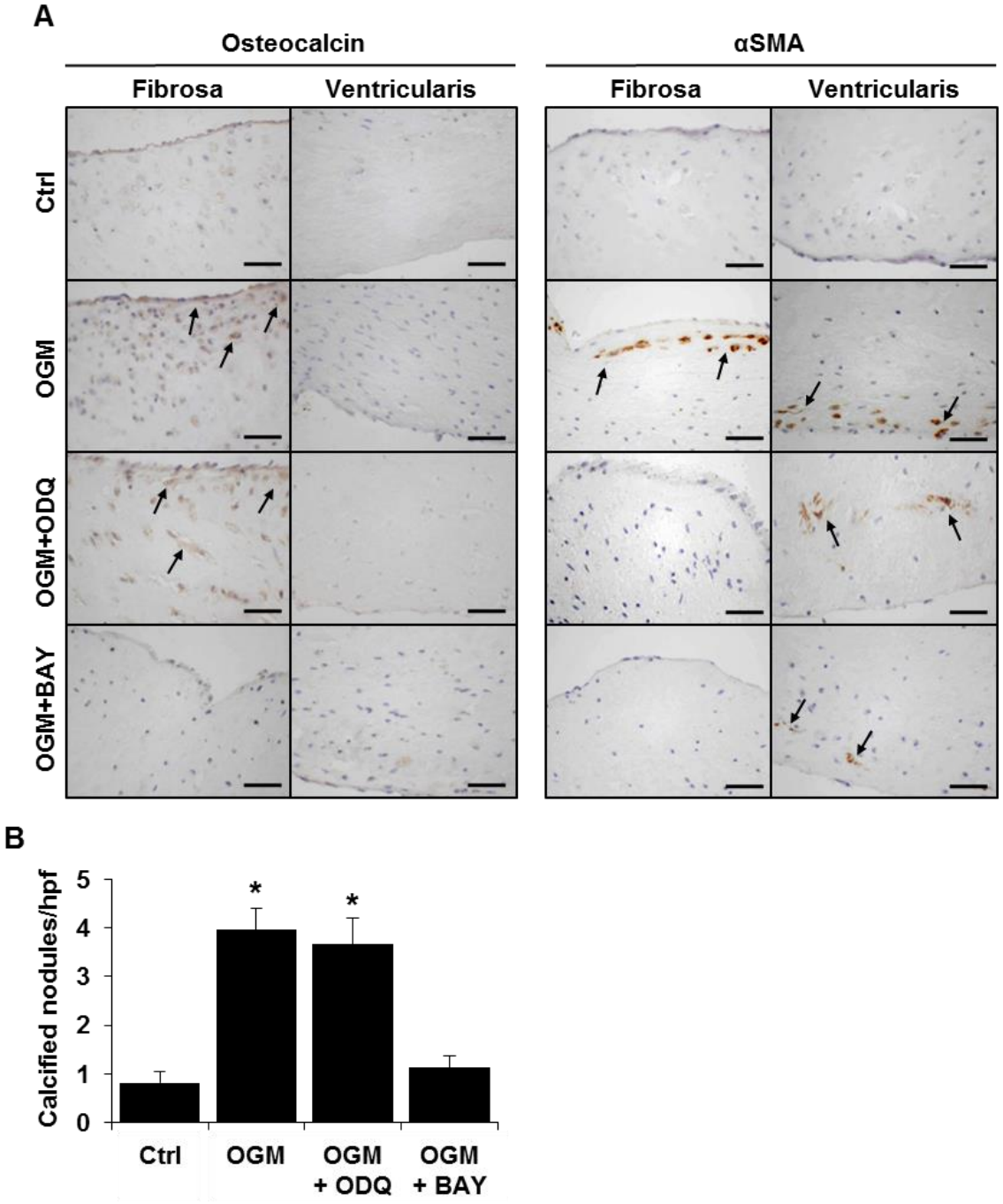

Figure 2.13: Nitric oxide and nodule formation on valve leaflets. A) Immuno-histochemistry for osteocalcin and αSMA on porcine leaflets exposed to OGM with sGC inhibitor (ODQ) and sGC activator (BAY). B) Quantification of ARS-positive nodules formed with OGM supplemented with ODQ and BAY *P<0.05

2.5 Discussion

Calcific aortic valve disease is a significant clinical problem for which basic pathobiological mechanisms are poorly understood. That CAVD progression occurs differently than atherosclerosis was further underscored with the recent disappointing results of cholesterol metabolism (statin) drug therapy for aortic valve disease[32]. There is therefore a significant need to identify functional mechanisms of aortic valve calcification and their molecular interactions so as to develop valve specific diagnostic and therapeutic treatments. In this study, we implemented an anchored 3D hydrogel culture system that showed that mechanical stress was critically important for developing calcium deposition in a physiological matrix environment. The findings of our study identify a multifaceted mechanism of aortic valve calcific pathogenesis that integrates microenvironmental hemodynamics, endothelial function and interstitial cell differentiation. We identify valve endothelial-secreted nitric oxide (NO) as a natural antagonist of multiple aspects of calcific aortic valve pathogenesis. NO decreases myofibroblastic activation, osteoblastic differentiation, and matrix calcification by valvular interstitial cells. In a complementary study, we recently demonstrated that aortic valve endothelium can decrease valve matrix stiffness in an NO dependent manner[33]. Maintenance of cusp compliance is critically important for efficient valve function. Substrate stiffness can alter cellular function[34], and was recently shown to potentiate aortic valve interstitial cell myofibroblastic differentiation and calcified aggregate formation in 2D culture with osteogenic medium[35]. In the native valve, the fibrosa is stiffer than the ventricularis, which therefore supports its enhanced risk of calcification[36, 37]. While anchored 3D gels are likely mechanically stiffer than the free-floating controls[38], our data supports PAVIC calcification via osteoblastic differentiation rather than apoptosis in response to OGM, which occurs

on compliant substrates as indicated by Yip et al[35]. Therefore, apoptosis based calcification may occur preferentially near locally rigid, calcium-containing deposits rather than within the initial lesion in aortic valves. Taken together, these findings suggest that eNOS mitigates the risk of calcification through maintaining quiescent fibroblastic interstitial cell phenotype, which may in turn keep mechanical stress at a "healthy" basal level[39]. It seems therefore that disturbance to this balance, whether via local mechanical, hemodynamic, and/or eNOS signaling, can cause a vicious cycle of decreased nitric oxide and increased tissue stiffness, both exacerbating the risk of osteogenic differentiation and matrix calcification.

Calcified nodules in diseased human aortic valves occur almost exclusively on the aortic surface. We found in this study that fibrosa-sided VEC express less eNOS protein and cGMP than ventricularis-sided VEC, both at baseline and under physiological flow conditions. We here further confirmed these eNOS protein expression trends in normal and calcific human aortic valves. Previous cDNA microarray analyses by Simmons et al identified 20% elevated eNOS gene expression in normal pig valves, but no protein or functional analyses of nitric oxide signaling was reported[15, 40]. In agreement with their more recent study in hypercholesteremic pigs, we found no significant difference in fibrosa sided eNOS gene expression in calcification prone conditions[45]. Supporting this NO mechanism, a recent study by Kennedy et al found that valve interstitial cell calcific nodule formation in 2D culture was blocked by both soluble NO donors or selectively raising intracellular cGMP concentrations[19]. C-type natriuretic peptide (CNP), which also stimulates cGMP-dependent kinases, has also been reported to regulate valve interstitial cell phenotype and to have a possible role in regulating the calcification process[41]. CNP is known to increase cGMP via activation of a particulate isoform of

guanylate cyclase (GC-B), while nitric oxide stimulates the soluble isoforms of the enzyme (sGC)[42]. In our study, cGMP production and eNOS protein expression were co-localized specifically to valve endothelium, stimulated by side-dependent hemodynamics, and correlated directly with anti-calcific effects in both pig and human valves. Therefore, we believe that endothelial nitric oxide is the biological entity that mediates the effects on PAVEC on PAVIC in 3D co-culture, but further study is warranted to assess the potential of agents to regulate the valvular interstitial calcification process that signal via cGMP-dependent kinases and their potential interactions with NO.

Our results show that ventricularis-sided endothelium was the main source of nitric oxide for the aortic valve, likely due to its hemodynamic environment. Natural inhibition of fibrosa calcification may be maintained via diffusion of NO from the ventricularis surface, which would be impaired with leaflet thickening and/or fibrosis that precedes calcification[43]. Collectively, these findings motivate consideration of potential therapeutic strategies for mitigating or preventing aortic valve calcification through targeted valve NO supplementation, such as with L-arginine or tetrahydrobiopterin (BH4). Our results also highlight the need for NO secreting endothelium in tissue engineered heart valves.

It is important to note that the beneficial effects of NO in valves may be more complexly regulated, as Miller et al identified a paradoxical uncoupling of NO in valve tissue sections that may drive an increase in oxidative stress, which they localized to calcified valve lesions[44]. Protective NO effects may therefore be dose dependent. While our study focused on eNOS, there are likely other important mechanisms contributing to valvular calcification, including side-specific heterogeneity. The fibrosa is particularly rich in collagen, whereas the ventricularis contains a high amount of

elastin. Recent work by Masters et al. shows that ECM proteins can independently modulate osteoblastic differentiation of interstitial cells[45]. Indeed, this cross-communication regulates many of the functions of interstitial cells in health and disease and helps explain the pathophysiology of calcific vasculopathies in subjects with mutations in collagen or elastin[46]. Recent studies have highlighted the re-emergence of many genes found in embryonic valve development in diseased valves, including NOTCH1, periostin, and chondromodulin[47-49]. In conclusion, our results strongly advocate for the incorporation of endothelial signaling to fully understand the biological and pathobiological regulation of aortic valve function. This platform enables direct screening of molecular mechanisms of calcification and testing putative molecular inhibitors.

REFERENCES

1. Towler DA: Oxidation, Inflammation, and Aortic Valve Calcification: Peroxide Paves an Osteogenic Path, Journal of the American College of Cardiology 2008, 52:851-854

2. Otto CM, Lind BK, Kitzman DW, Gersh BJ, Siscovick DS: Association of Aortic-Valve Sclerosis with Cardiovascular Mortality and Morbidity in the Elderly, New England Journal of Medicine 1999, 341:142-147

3. Baumgartner H, Hung J, Bermejo J, Chambers JB, Evangelista A, Griffin BP, Iung B, Otto CM, Pellikka PA, Quiñones M: Echocardiographic assessment of valve stenosis: EAE/ASE recommendations for clinical practice, European Journal of Echocardiography 2009, 10:1-25

4. Beckmann E, Grau JB, Sainger R, Poggio P, Ferrari G: Insights into the Use of Biomarkers in Calcific Aortic Valve Disease, J Heart Valve Dis 2010, 19:441-452

5. Cowell SJ, Newby DE, Prescott RJ, Bloomfield P, Reid J, Northridge DB, Boon NA: A Randomized Trial of Intensive Lipid-Lowering Therapy in Calcific Aortic Stenosis, New England Journal of Medicine 2005, 352:2389-2397

6. Roijers RB, Dutta RK, Cleutjens JPM, Mutsaers PHA, de Goeij JJM, van der Vusse GJ: Early Calcifications in Human Coronary Arteries As Determined with a Proton Microprobe, Analytical Chemistry 2007, 80:55-61

7. Mohler ER, Gannon F, Reynolds C, Zimmerman R, Keane MG, Kaplan FS: Bone Formation and Inflammation in Cardiac Valves, Circulation 2001, 103:1522-1528

8. Rajamannan NM, Subramaniam M, Rickard D, Stock SR, Donovan J, Springett M, Orszulak T, Fullerton DA, Tajik AJ, Bonow RO, Spelsberg T: Human Aortic Valve Calcification Is Associated With an Osteoblast Phenotype, Circulation 2003, 107:2181-2184

9. Chen J-H, Yip CYY, Sone ED, Simmons CA: Indentification and Characterization of Aortic Valve Mesenchymal Progenitor Cells with Robust Osteogenic Calcification Potential, Am J Pathol 2009, 174:1109-1119

10. Walker GA, Masters KS, Shah DN, Anseth KS, Leinwand LA: Valvular Myofibroblast Activation by Transforming Growth Factor-β, Circulation Research 2004, 95:253-260

11. Liu AC, Gotlieb AI: Transforming Growth Factor-β Regulates *in Vitro* Heart Valve Repair by Activated Valve Interstitial Cells, Am J Pathol 2008, 173:1275-1285

12. Cushing MC, Liao J-T, Anseth KS: Activation of valvular interstitial cells is mediated by transforming growth factor-β1 interactions with matrix molecules, Matrix Biology 2005, 24:428-437

13. Butcher JT, Nerem RM: Valvular endothelial cells regulate the phenotype of interstitial cells in co-culture: effects of steady shear stress, Tissue Eng 2006, 12:905-915

14. Poggianti E, Venneri L, Chubuchny V, Jambrik Z, Baroncini LA, Picano E: Aortic valve sclerosis is associatedwith systemic endothelial dysfunction, Journal of the American College of Cardiology 2003, 41:136-141

15. Simmons CA, Grant GR, Manduchi E, Davies PF: Spatial Heterogeneity of Endothelial Phenotypes Correlates With Side-Specific Vulnerability to Calcification in Normal Porcine Aortic Valves, Circ Res 2005, 96:792-799

16. Behrendt D, Ganz P: Endothelial Function: From Vascular Biology to Clinical Applications, Am J Cardiol 2002, 90:40L-48L

17. Lee TC, Zhao YD, Courtman DW, Stewart DJ: Abnormal Aortic Valve Development in Mice Lacking Endothelial Nitric Oxide Synthase, Circulation 2000, 101:2345-2348

18. Clapp BR, Hingorani AD, Kharbanda RK, Mohamed-Ali V, Stephens JW, Vallance P, MacAllister RJ: Inflammation-induced endothelial dysfunction involves reduced nitric oxide bioavailability and increased oxidant stress, Cardiovascular Research 2004, 64:172-178

19. Kennedy JA, Hua X, Mishra K, Murphy GA, Rosenkranz AC, Horowitz JD: Inhibition of calcifying nodule formation in cultured porcine aortic valve cells by nitric oxide donors, European Journal of Pharmacology 2009, 602:28-35

20. Miller JD, Chu Y, Brooks RM, Richenbacher WE, Pena-Silva R, Heistad DD: Dysregulation of Antioxidant Mechanisms Contributes to Increased Oxidative Stress in Calcific Aortic Valvular Stenosis in Humans, J Am Coll Cardiol 2008, 52:843-850

21. Gould RA, Butcher JT: Isolation of Valvular Endothelial Cells, J Vis Exp 2010, e2158

22. Butcher JT, Nerem RM: Porcine aortic valve interstitial cells in three-dimensional culture: comparison of phenotype with aortic smooth muscle cells, J Heart Valve Dis 2004, 13:478-485; discussion 485-476

23. Butcher JT, Penrod AM, Garcia AJ, Nerem RM: Unique Morphology and Focal Adhesion Development of Valvular Endothelial Cells in Static and Fluid Flow Environments, Arterioscler Thromb Vasc Biol 2004, 24:1429-1434

24. Puchtler H, Meloan SN, Terry MS: On The History And Mechanism of Alizarin and Alizarin Red S Stains for Calcium, Journal of Histochemistry & Cytochemistry 1969, 17:110-124

25. Sucosky P, Padala M, Elhammali A, Balachandran K, Jo H, Yoganathan AP: Design of an Ex Vivo Culture System to Investigate the Effects of Shear Stress on Cardiovascular Tissue, Journal of Biomechanical Engineering 2008, 130:035001

26. Moncada S, Palmer RM, Higgs EA: Nitric oxide: physiology, pathophysiology, and pharmacology, Pharmacological Reviews 1991, 43:109-142

27. Jaimes EA, Sweeney C, Raij L: Effects of the Reactive Oxygen Species Hydrogen Peroxide and Hypochlorite on Endothelial Nitric Oxide Production, Hypertension 2001, 38:877-883

28. Fournet-Bourguignon M-P, Castedo-Delrieu M, Bidouard J-P, Leonce S, Saboureau D, Delescluse I, Vilaine J-P, Vanhoutte PM: Phenotypic and Functional Changes in Regenerated Porcine Coronary Endothelial Cells : Increased Uptake of Modified LDL and Reduced Production of NO, Circ Res 2000, 86:854-861

29. Deck JD: Endothelial cell orientation on aortic valve leaflets, Cardiovascular Research 1986, 20:760-767

30. Harrison DG: Cellular and molecular mechanisms of endothelial cell dysfunction, The Journal of Clinical Investigation 1997, 100:2153-2157

31. Sucosky P, Balachandran K, Elhammali A, Jo H, Yoganathan AP: Altered Shear Stress Stimulates Upregulation of Endothelial VCAM-1 and ICAM-1 in a BMP-4- and TGF-{beta}1-Dependent Pathway, Arterioscler Thromb Vasc Biol 2009, 29:254-260

32. Loomba RS, Arora R: Statin Therapy and Aortic Stenosis: A Systematic Review of the Effects of Statin Therapy on Aortic Stenosis, American Journal of Therapeutics 2010, 17:e110-e114110.1097/MJT.1090b1013e3181a1092b1091a1096

33. El-Hamamsy I, Balachandran K, Yacoub MH, Stevens LM, Sarathchandra P, Taylor PM, Yoganathan AP, Chester AH: Endothelium-Dependent Regulation of the Mechanical Properties of Aortic Valve Cusps, Journal of the American College of Cardiology 2009, 53:1448-1455

34. Kloxin AM, Kasko AM, Salinas CN, Anseth KS: Photodegradable Hydrogels for Dynamic Tuning of Physical and Chemical Properties, Science 2009, 324:59-63

35. Yip CYY, Chen J-H, Zhao R, Simmons CA: Calcification by Valve Interstitial Cells Is Regulated by the Stiffness of the Extracellular Matrix, Arterioscler Thromb Vasc Biol 2009, 29:936-942

36. Stella JA, Sacks MS: On the Biaxial Mechanical Properties of the Layers of the Aortic Valve Leaflet, Journal of Biomechanical Engineering 2007, 129:757-766

37. Vesely I, Noseworthy R: Micromechanics of the fibrosa and the ventricularis in aortic valve leaflets, Journal of Biomechanics 1992, 25:101-109, 111-113

38. Long JL, Tranquillo RT: Elastic fiber production in cardiovascular tissue-equivalents, Matrix Biology 2003, 22:339-350

39. Thubrikar MJ, Nolan SP, Aouad J, Deck JD: Stress Sharing Between the Sinus and Leaflets of Canine Aortic Valve, The Annals of Thoracic Surgery 1986, 42:434-440

40. Guerraty MA, Grant GR, Karanian JW, Chiesa OA, Pritchard WF, Davies PF: Hypercholesterolemia Induces Side-Specific Phenotypic Changes and Peroxisome Proliferator-Activated Receptor-{gamma} Pathway Activation in Swine Aortic Valve Endothelium, Arterioscler Thromb Vasc Biol 2010, 30:225-231

41. Yip CYY, Blaser MC, Mirzaei Z, Zhong X, Simmons CA: Inhibition of Pathological Differentiation of Valvular Interstitial Cells by C-Type Natriuretic Peptide, Arteriosclerosis, Thrombosis, and Vascular Biology 2011, 31:1881-1889

42. Potter LR: Guanylyl cyclase structure, function and regulation, Cellular Signalling 2011, 23:1921-1926

43. Otto C, Kuusisto J, Reichenbach D, Gown A, O'Brien K: Characterization of the early lesion of 'degenerative' valvular aortic stenosis. Histological and immunohistochemical studies, Circulation 1994, 90:844-853

44. Miller JD, Chu Y, Brooks RM, Richenbacher WE, Peña-Silva R, Heistad DD: Dysregulation of Antioxidant Mechanisms Contributes to Increased Oxidative Stress in Calcific Aortic Valvular Stenosis in Humans, Journal of the American College of Cardiology 2008, 52:843-850

45. Rodriguez KJ, Masters KS: Regulation of valvular interstitial cell calcification by components of the extracellular matrix, Journal of Biomedical Materials Research Part A 2009, 90A:1043-1053

46. El-Hamamsy I, Yacoub M: A measured approach to managing the aortic root in patients with bicuspid aortic valve disease, Current Cardiology Reports 2009, 11:94-100

47. Yoshioka M, Yuasa S, Matsumura K, Kimura K, Shiomi T, Kimura N, Shukunami C, Okada Y, Mukai M, Shin H, Yozu R, Sata M, Ogawa S, Hiraki Y, Fukuda K: Chondromodulin-I maintains cardiac valvular function by preventing angiogenesis, Nat Med 2006, 12:1151-1159

48. Hakuno D, Kimura N, Yoshioka M, Mukai M, Kimura T, Okada Y, Yozu R, Shukunami C, Hiraki Y, Kudo A, Ogawa S, Fukuda K: Periostin advances atherosclerotic and rheumatic cardiac valve degeneration by inducing angiogenesis and MMP production in humans and rodents, The Journal of Clinical Investigation 2010, 120:2292-2306

48. Garg V, Muth AN, Ransom JF, Schluterman MK, Barnes R, King IN, Grossfeld PD, Srivastava D: Mutations in NOTCH1 cause aortic valve disease, Nature 2005, 437:270-274

CHAPTER 3

SPATIAL ANALYSIS OF MINERAL DEPOSITION AND MATURATION IN CALCIFIED AORTIC VALVES

3.1 Abstract

Aortic valve stenosis is an increasingly prevalent pathology and is most commonly caused by progressive calcification of the valve leaflets. CAVD is characterized by large mineralized lesions that erupt from the valve matrix, but few studies have investigated the spatial heterogeneity of the calcific deposits, and there is a need for quantifiable means to assess the mineral composition. In this study, we paired traditional characterization methods to analyze calcification structure and crystallinity with FTIR imaging to quantitatively compare mineral compositional features between valves with varying degrees of mineralization. We show that the valve has activated cellular profiles of both myofibroblastic and osteoblast-like phenotypes that are spatially diverse throughout the valve. We confirmed that the mineralized tissue was a heterogeneous mix of crystalline apatite material and poorly crystalline hydroxyapatite. Acid phosphate substitutions and crystallinity values were higher in areas of lower mineralization, indicating new mineral formation in a manner that may be distinct from bone. Within calcified regions of close proximity, there were compact mineral deposits with mineral:matrix ratios higher than that of bone adjacent to areas with lower mineral:matrix ratios. These results describe the heterogeneity of the calcified valves, both in areas of highly mineralized lesions as well as in areas of surrounding valve tissue. Applying techniques that can elucidate structural and

compositional differences in pathological mineral may give new insights into the progression of valve calcification.

3.2 Introduction

Present in up to 25% of Americans over the age of 65, aortic valve stenosis is most commonly caused by progressive calcification of the valve leaflets[1,2]. Calcific aortic valve disease (CAVD) is increasingly prevalent due to the aging population and the increased diagnostic ability by echocardiography[1]. There is currently no treatment for aortic valve calcification other than though surgical intervention. Recent clinical trials testing lipid-lowering therapies were ineffective against aortic stenosis progression[3,4], which emphasizes that CAVD may undergo a distinctly different pathogenesis from that of atherosclerosis. CAVD is characterized by large mineralized lesions that erupt from the valve matrix, resulting in the valve's inability to either open fully during systole or coapt during diastole[5–7]. These lesions exhibit evidence of both dystrophic calcification (cell death-associated mineral deposition) and osteogenic calcification (via osteoblast-like deposition of mineralized matrix)[8]. The active osteogenic calcification process is thought to be a combination of early endothelial dysfunction[9] and later interstitial cell activation and differentiation[10,11]. Indeed, studies have shown that valve interstitial cells (VIC) from diseased aortic valves can have osteoblast-like phenotypes, expressing osteoblast specific proteins such as Runx2 and osteocalcin[12,13], which leads to the question of whether the mineral within calcified regions of diseased valves are similar in composition to bone.

Several studies have identified that calcified nodules within diseased valves have a similar elemental composition to that of bone, and that these deposits are highly heterogeneous in shape and composition, suggestive of a progressive maturation

process[14–16]. Several techniques have been used to analyze the structure, chemical composition and crystallinity of the mineral that constitutes calcific nodules, including X-ray diffraction, Fourier transform infrared spectroscopy (FTIR), Raman spectroscopy, and SEM-EDS. Although these studies provide great insight, they primarily focused on bulk minerals properties or Ca/P ratios[17–19], while less is known about the spatial differences of mineral composition throughout the valve. However, Bertazzo et al. recently used nano-analytical electron microscopy techniques to identify spherical hydroxyapatite particles within not only calcified lesions, but also non-calcified regions of the valve tissue[20]. Interestingly, these spherical particles revealed an internal structure more crystalline than the apatite crystals in bone, while the dense calcium phosphate material that often surrounded the particles was thought to be poorly crystalline apatite[20]. These results speak to not only the heterogeneity of the mineral throughout the calcified valve, but that it may also be formed through a biomineralization process that is not wholly bone-like (plate-like structures of poorly crystalline apatite growing along and within collagen fibers[21,22]). Despite the recent insights into the mineral composition of calcific lesions in valve disease, there has been very little quantitative analysis of mineral both in calcific nodules and within the macroscopically non-mineralized surrounding valve tissue. FTIR microscopy has the ability to not only show distributions of various FTIR peaks, but also utilizes validated parameters that can quantitatively describe HA-containing tissues[23–25]. While this technique has been used to great effect on bone, it has not yet been used for analyzing mineralized lesions in calcified valves.

The objective of this study was to characterize the spatial composition, structure and distribution of calcified lesions within valve leaflets through the progression of CAVD. We applied scanning electron microscopy with energy dispersive X-ray

spectrometry (SEM-EDS) to acquire maps of the chemical elements within the tissue, and used X-ray diffraction and FTIR to further characterize the chemical structure of the mineral. Finally, we applied FTIR imaging to map the spatial mineral and surrounding organic tissue composition and distribution of the calcific nodules, as well as quantifying compositional parameters that further define the character of the mineralized tissue.

3.3 Materials and Methods

Valve Preparation

Human diseased aortic valves were obtained from adults undergoing planned, nonelective valve replacement surgery by Dr. Sanjay Samy at the Robert Packer Hospital (Sayer, PA). All procedures were approved by Institutional Review Boards at Cornell University and the Guthrie Clinic. Valve leaflets were photographed and visually inspected for calcific severity, and split into groups that ranged from heavily calcified to little to no visual calcification, based on the area ratio of calcification. In addition, each region of individual valve leaflets was categorized as “heavily calcified”, “moderately calcified” or “non-mineralized tissue”. Leaflets from the same valves were used for both mineral and histological analysis.

Histological and Immunofluorescence Analyses

Human valve leaflets were fixed within two hours of harvesting in 4% paraformaldehyde overnight and placed in 70% ethanol. Leaflets were decalcified by immersion in a sodium citrate/formic acid solution overnight, followed by a thorough rinse in deionized water. The valve tissue was then paraffin embedded and sectioned at 6 μm, used for both histological and immunofluorescent analysis. Slides

were deparaffinized and stained with Movat's pentachrome stain to depict tissue architecture. Myofibroblastic activation and osteogenic differentiation was analyzed through IHC staining of alpha-smooth muscle actin (αSMA) and osteocalcin (OCN), respectively. Valve leaflets were stained with primary αSMA polyclonal rabbit antibody (1:100, Abcam) or primary OCN monoclonal mouse antibody (1:100, Abcam) followed by either an Alexa Fluor 568 or 488 secondary antibody (1:100, Invitrogen) and cell nuclei counterstain Draq5 (1:1000, BioStatus). Leaflets were imaged using a Zeiss 710 (Thornwood, NY) laser scanning confocal microscope, and images were processed using ImageJ.

SEM and EDS Analyses

Human valve leaflets were fixed within two hours of harvesting in 4% PFA overnight, followed by a serial dehydration with graded alcohol solutions, and then air-dried for 24 hours. Dry valve leaflets were mounted on aluminum SEM stubs with carbon tape and sputter coated with 5 nm carbon. Samples were imaged using a Field-Emission SEM (Zeiss Leo 1550), operated at 12 kV. EDS was used to examine the chemical compositions of the mineral found within the valve leaflets.

Valve Mineral Characterization

Calcified regions of human valve samples were excised and serially dehydrated with increasingly concentrated ethanol solutions, before being frozen and lyophilized. Samples were ground with mortar and pestle until a fine powder. Valve mineral crystallinity was examined by powder x-ray diffraction (pXRD) (Scintag Inc. PAD-X theta-theta X-ray Diffractometer, CuKα 1.54 Å, accelerating voltage 45 kV, current 40 mA, continuous scan, 2.0 deg/min). Phase information of valve mineral was achieved

through Fourier transform infrared (FTIR) spectroscopy (Mattson Instruments 2020 Galaxy Series FT-IR). Valve mineral was combined with KBr and pressed into pellets to obtain FTIR spectra (res 4.0 cm^{-1}, 64 scans).

GADDS

To spatially compare calcified regions of valve leaflets, we used a general area detector diffraction system (GADDS, Bruker). Valve leaflets were fixed overnight in 4% PFA and serially dehydrated with graded alcohol solutions, followed by an overnight air-drying for complete dehydration. We collected 2-D XRD patterns covering 2-70 °2θ from twelve different detector positions; the exposure time was 100 seconds per detector location and the patterns was chi-integrated to generate the conventional 2θ against intensity diffractogram. Identification and semi-quantitative estimation of the minerals were achieved by comparison of the XRD pattern with the Materials data (MDI) mineral database using JADE software (MDI).

FTIR Imaging and Mineral Parameter Analysis

Five valve leaflets of increasing calcific severity were fixed in 4% PFA overnight, followed by a serial dehydration with graded alcohol solutions and embedded in poly(methyl methacrylate) (PMMA) or Spurr's Resin. Undecalcified 2μm thick sections were cut in the frontal plane to facilitate analysis of the full thickness of the valve. For each section, 3 to 7 locations were chosen to span the mineralized and tissue portions of the valve. FTIR images were collected at a spectral resolution of 4 cm^{-1} over the spectral range 750 to 2000 cm^{-1} and a spatial resolution of 6.25μm or 25μm using an infrared imaging system (Spotlight 100, PerkinElmer Instruments, Waltham, MA). Infrared images were analyzed using ISYS chemical imaging

software (Malvern Instruments, Worcestershire, UK). The infrared spectrum at each pixel was analyzed to determine the following parameters[26]: the mineral:matrix ratio (area ratio of the phosphate v_1 (900-1200 cm^{-1}) and amide I (1585-1720 cm^{-1}) peaks)[24], which characterizes tissue mineral content; the carbonate:phosphate ratio (area ratio of the carbonate (860-890 cm^{-1}) and the phosphate v_1 (900-1200 cm^{-1}) peaks)[24], which characterizes the extent of carbonate substitution into the mineral lattice; the mineral crystallinity (XST, intensity ratio of 1030 cm^{-1} and 1020 cm^{-1} bands), which is related to crystal size and perfection assessed by x-ray diffraction[27]; and the acid phosphate substitution (intensity ratio of 1127 cm^{-1} and 1096 cm^{-1} bands)[28].

The FTIR parameters calculated at each pixel within each image yielded a distribution of values for each parameter. The distributions were characterized by the mean of the distribution in order to assess average composition and the full width at half maximum (FWHM) of the Gaussian curve to the distribution to assess compositional heterogeneity. FTIR parameter means and FWHM means were compared with analysis of variance (ANOVA) with Tukey's post-hoc test (differences between means were considered significant at $P \leq 0.05$).

3.4 Results

Histology and Immunohistochemistry

Calcified valves are clearly thickened from the base of the leaflet and contain regions of calcific nodules of varying size (Figure 3.1A). The heterogeneity of the calcified regions mirror the range in activated protein expression found throughout the valve. Alpha-smooth muscle actin (αSMA), a marker for myofibroblastic activation, is highly expressed on the outer edges of calcific nodules; additionally, αSMA is only

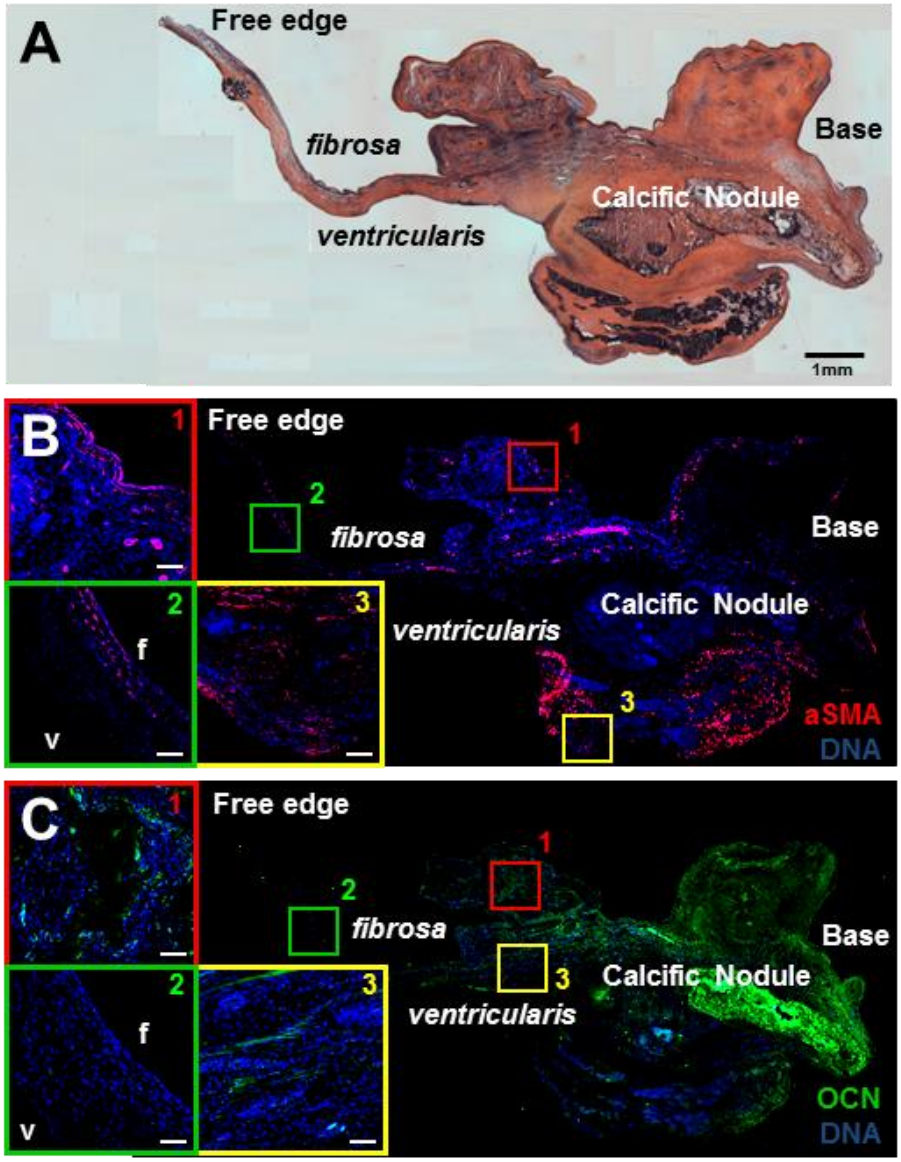

Figure 3.1: Cross-sections of human calcified aortic valve leaflet. A) Movat staining shows architecture of ECM and calcification within the diseased valve. Immunohistochemistry for B) αSMA exhibits myofibroblastic activation in interstitial cells, which a diffuse staining for C) osteocalcin indicates the presence of osteoblast-like cells around the nodule. Scale bar on inset images = 100μm.

expressed on the aortic side of the free edge of the leaflet, which is the preferential side of calcification (Figure 3.1B). Osteocalcin, a protein associated with bone formation, and often used as a marker for osteogenic differentiation, is highly

expressed throughout regions of the valve with calcifications. Osteocalcin is also dispersed through the valve, even in areas with no obvious macroscopic signs of calcification (Figure 3.1C). These results speak to the heterogeneity of activated cellular activity and deposition of calcifications throughout the valve.

Elemental analysis of valve mineral

SEM images revealed material erupting from disrupted or completely denuded areas of the endothelium (Figure 3.2A, B). A chemical analysis of the material erupting from the valve matrix using SEM equipped with EDS revealed calcium and phosphorous, with small amounts of magnesium (Figure 3.2C-G), similar to the elemental composition of bone and previously reported mineral found in calcified

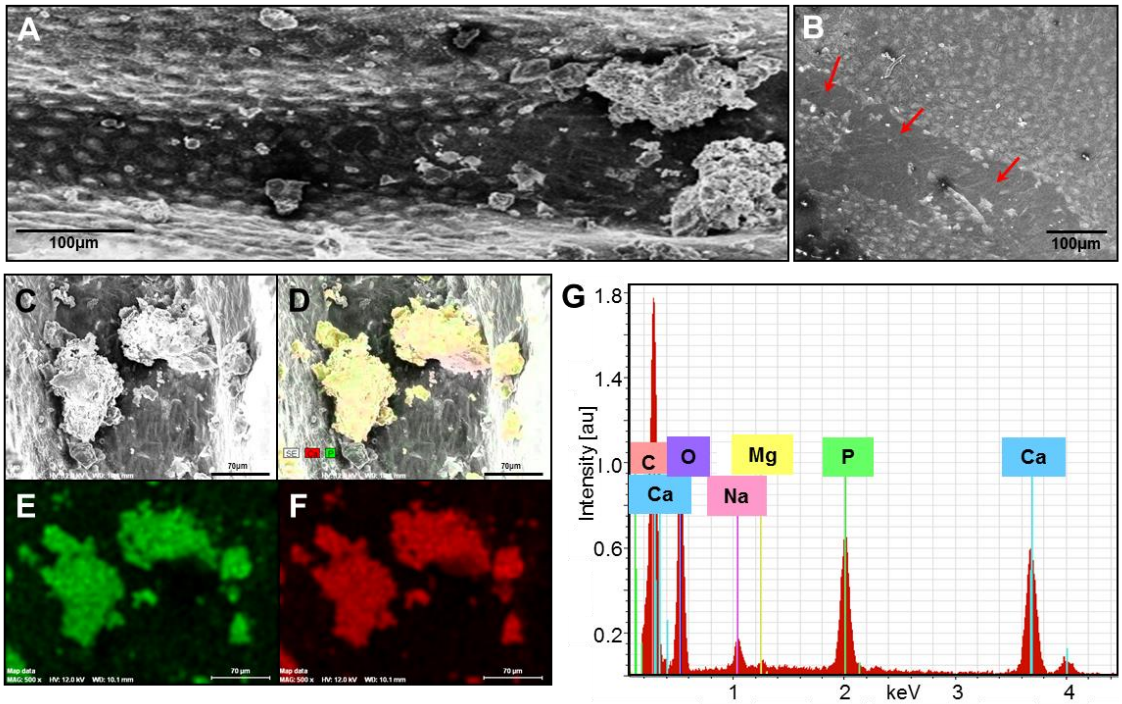

Figure 3.2: SEM images and elemental analysis of valve mineral. A) Representative SEM images of valve surface with mineral particles and disrupted endothelium and B) areas with denuded endothelial layer. C) SEM image of mineral with D) combination of E) phosphorus and F) calcium maps. G) Elemental analysis of typical valve mineral.

heart valves[14,20,29]. The Ca/P molar ratio of the mineral deposits was 1.73 ± 0.10, which is close to the Ca/P ratio found in apatite mineral in bone and stoichiometric hydroxyapatite (1.67).

Structure and crystallinity of valve mineral

FTIR probes molecular vibrations and can be used to obtain information about the local environments of specific functional groups. Each peak position represents different organic and inorganic compounds within valve samples. In the case of hydroxyapatite, the v_4 phosphate vibrational modes at 602 and 563 can be used as a metric for crystallinity. Powder x-ray diffraction was used to obtain information about the crystal lattice of apatite. Each peak can be related to a specific diffraction plane within a crystal, caused by the constructive interference of scattered x-rays at specific angles. Poor peak definition is thought to be qualitatively related to lower crystallinity. FTIR and XRD (Figure 3.3A, B) confirm the mineral phase present in the calcified valves is apatite, in agreement with previous reports[19,30–32]. Both sets of spectra show that the heavy and moderate valve calcification regions differ in their mineral character. The moderate calcifications appear less crystalline or composed of smaller

particles or perhaps both, as evidenced by the minimal splitting of the phosphate peak in FTIR spectrum and the poorer peak definition in the XRD pattern compared to the heavy calcification. Spatial comparisons of calcified valve regions via GADDS reveal apatite mineral in heavily calcified locations (Figure 3.3C), whereas valve tissue with no visible calcification had diffraction patterns containing weak peaks that did not match any known apatite structure (Figure 3.3D).

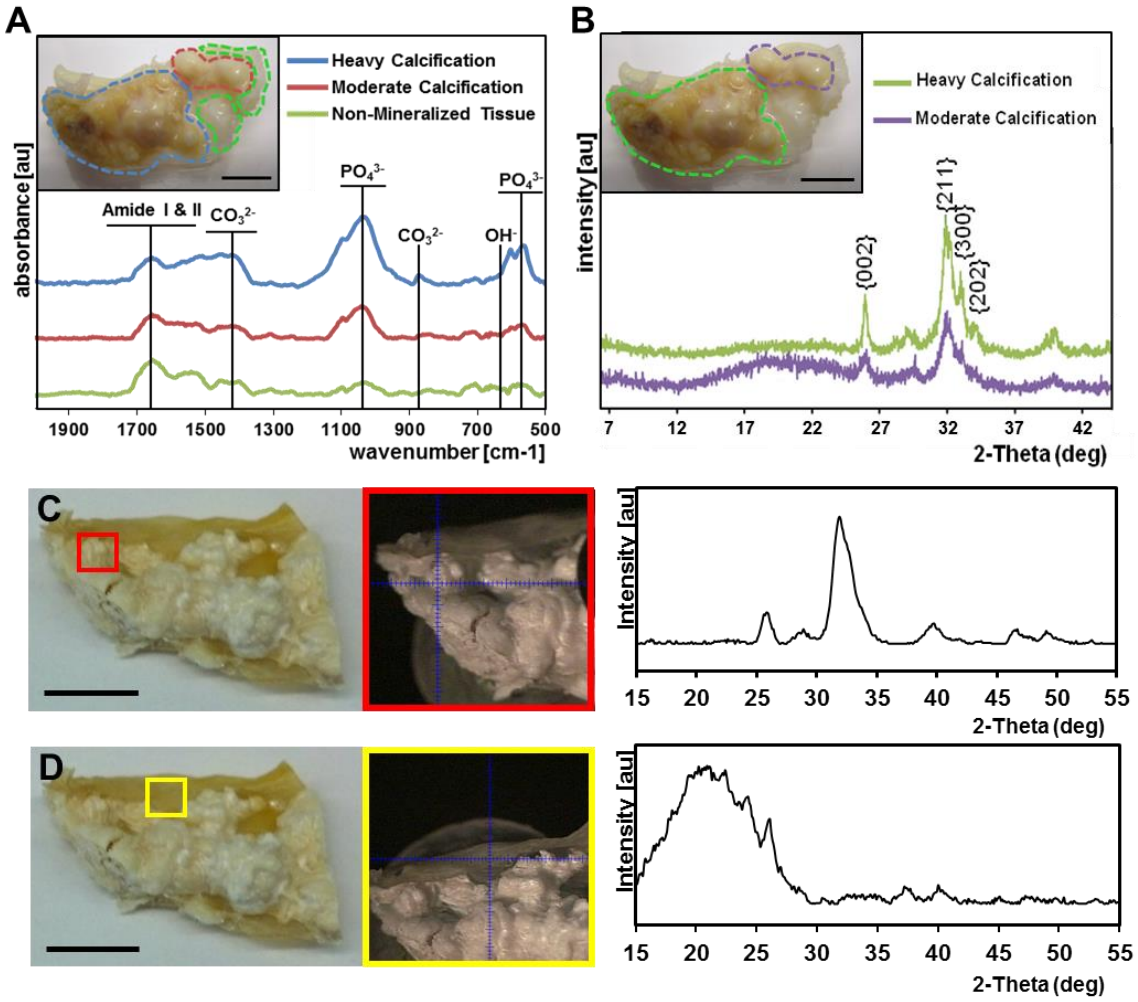

Figure 3.3: Mineral phase and crystallinity of calcified valves. A) Infrared adsorption spectra of calcified aortic valve leaflets separated into regions of heavy calcification, lesser calcification, and visibly non-mineralized tissue. Representative regions of interest are shown in the inset image. B) Powder X-ray diffraction patterns of calcified aortic valve leaflets separated into regions of heavy calcification and lesser calcification. Representative regions of interest are shown in the inset image. C) X-ray diffraction patterns of heavily mineralized and B) visually non-mineralized portions of calcified aortic valve leaflets. Scale bars = 5 mm.

Spatial analysis of mineral and quantification of composition parameters

Five valves with calcification of increasing severity were analyzed to evaluate differences in mineralized tissue composition between earlier, more immature forms

of calcification and the more mature mineralization found in later stages of the disease (Figure 3.4).

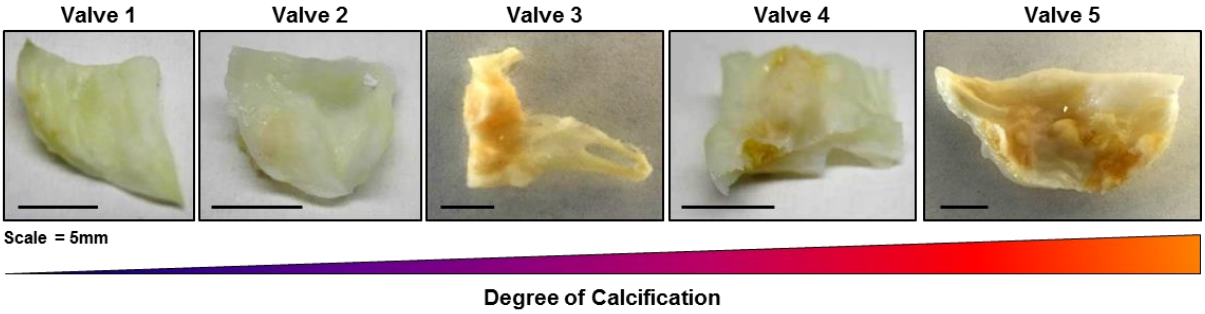

Figure 3.4: Human aortic valves with increasing severity of calcification.

Differences were apparent between valves of varying calcific severity. Both the mean values and the distribution widths of the mineral:matrix parameter increased with valves that were visibly more calcified (Figure 3.5A). While carbonate:phosphate distribution means remained similar across valves, the distribution widths tended to be larger in valves with lesser calcification (Figure 3.5B). Distribution means and widths of crystallinity differed minimally (Figure 3.5C), while the both distribution means and widths of the acid phosphate parameter was generally increased in the moderately calcified valves (Figure 3.5D). Further characterization of the mineral composition within the least calcified valve was not possible due to the low amounts of mineral present, as seen in the mineral:matrix image. Quantification of area ratio of calcification ranked each valve in order of severity and was used for further quantification of FTIR parameters (Figure 3.6A). Distribution means were quite varied across valves, but there was an upward trend of mineral:matrix ratio with increasing severity, with significance between the least and most calcified valves (0.77 ± 0.11 vs.

6.91 ± 1.66, respectively). Carbonate:phosphate, crystallinity, and acid phosphate distribution means were generally similar, with one exception in the moderately

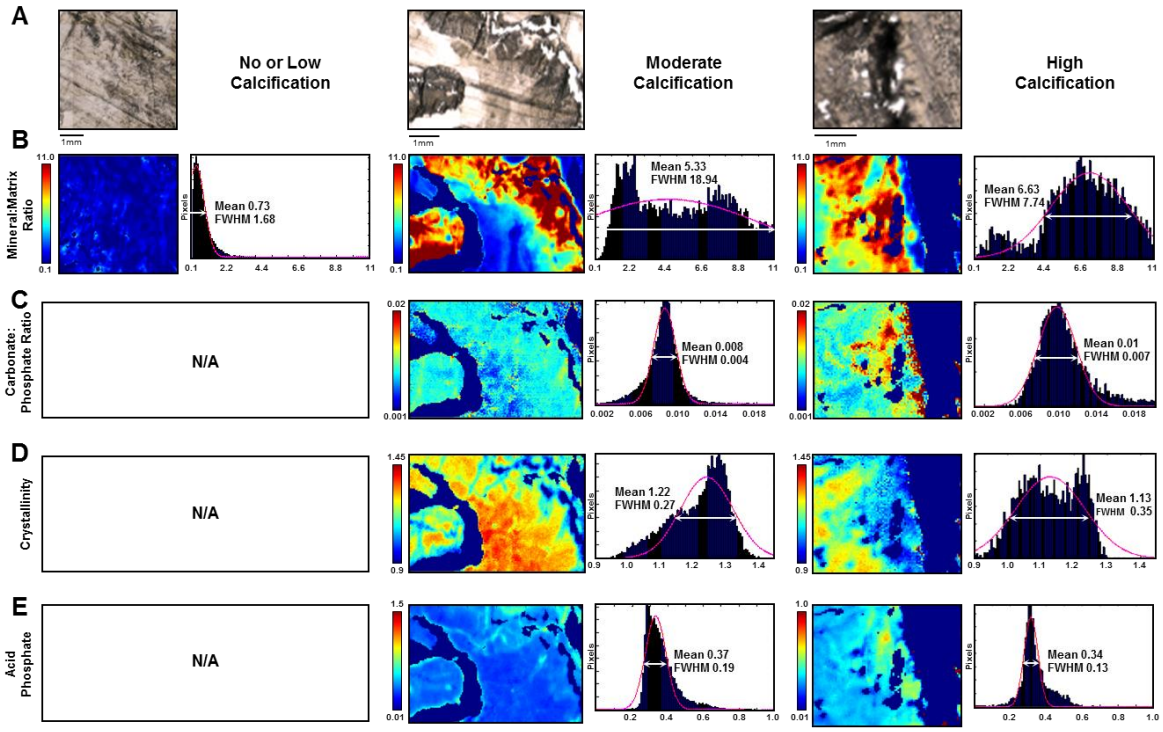

Figure 3.5: Spatial mineral composition analysis of calcified valves. A) White light images of regions within valves of low, moderate and high calcification. Representative FTIR images and associated pixel histograms with Gaussian fits of (A) mineral:matrix ratio, (B) carbonate:phosphate ratio, (C) crystallinity and (D) acid phosphate for valve leaflets with low, moderate and high area fractions of calcification. The mean and full width at half maximum (FWHM) values of the Gaussian curves are indicated on each histogram. Due to the very low mineral:matrix ratio of the low calcified samples (first column), it was not feasible to further characterize the mineral components for these valves.

calcified valve, which had significantly higher crystallinity (1.20 ± 0.006) (Figure 3.6A). The distribution widths, reflecting the heterogeneity of the sample within each FTIR parameter, were unchanged between valves in mineral:matrix and, although there was a slight upward trend of mineral:matrix distribution widths. Although there was a downward trend in carbonate:phosphate and acidity distribution widths with increasing calcific severity, these differences were not significant (Figure 3.6B).

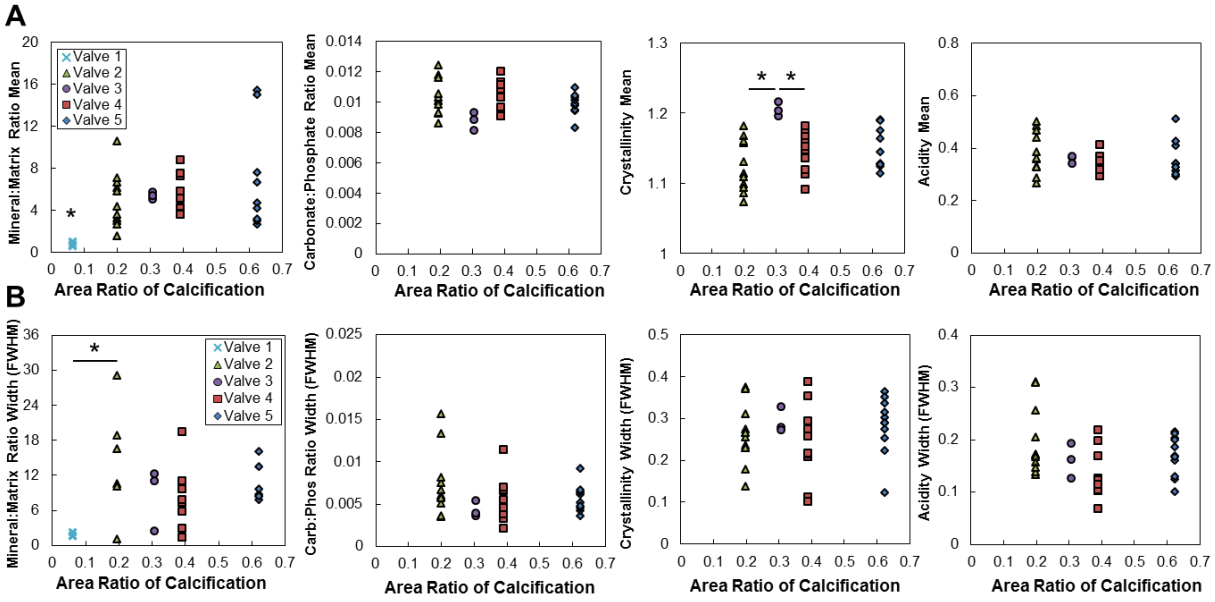

Figure 3.6: FTIR properties of human valve leaflets reported as image pixel distribution A) means and B) full widths at half maximum (FWHM) and plotted according to increasing area ratio of calcification. *P<0.05

Further investigation of the mineral:matrix distributions revealed clearly defined bi-modal peaks indicating two separate means and distribution widths within the same image (Figure 3.7A, B). Compact mineral regions in the more severely calcified valves reported means in the range of 20-25 for the higher peak distribution, which indicates a very highly mineralized sample region in direct proximity to a lesser mineralized region (Figure 3.7B). Although the mineral:matrix and crystallinity parameters in some samples displayed bi-modal distributions, the carbonate:phosphate and acid phosphate parameters did not (Figure 3.7C-E). Taken together, these results indicate that valves with macroscopically larger, more mature calcified regions tend to have higher mineralized tissue, with more compact regions having a mineral:matrix ratio higher than that of bone. It is also clear that mineralized

valve tissue is extremely heterogeneous, with varying amounts of mineralized tissue in very close proximity.

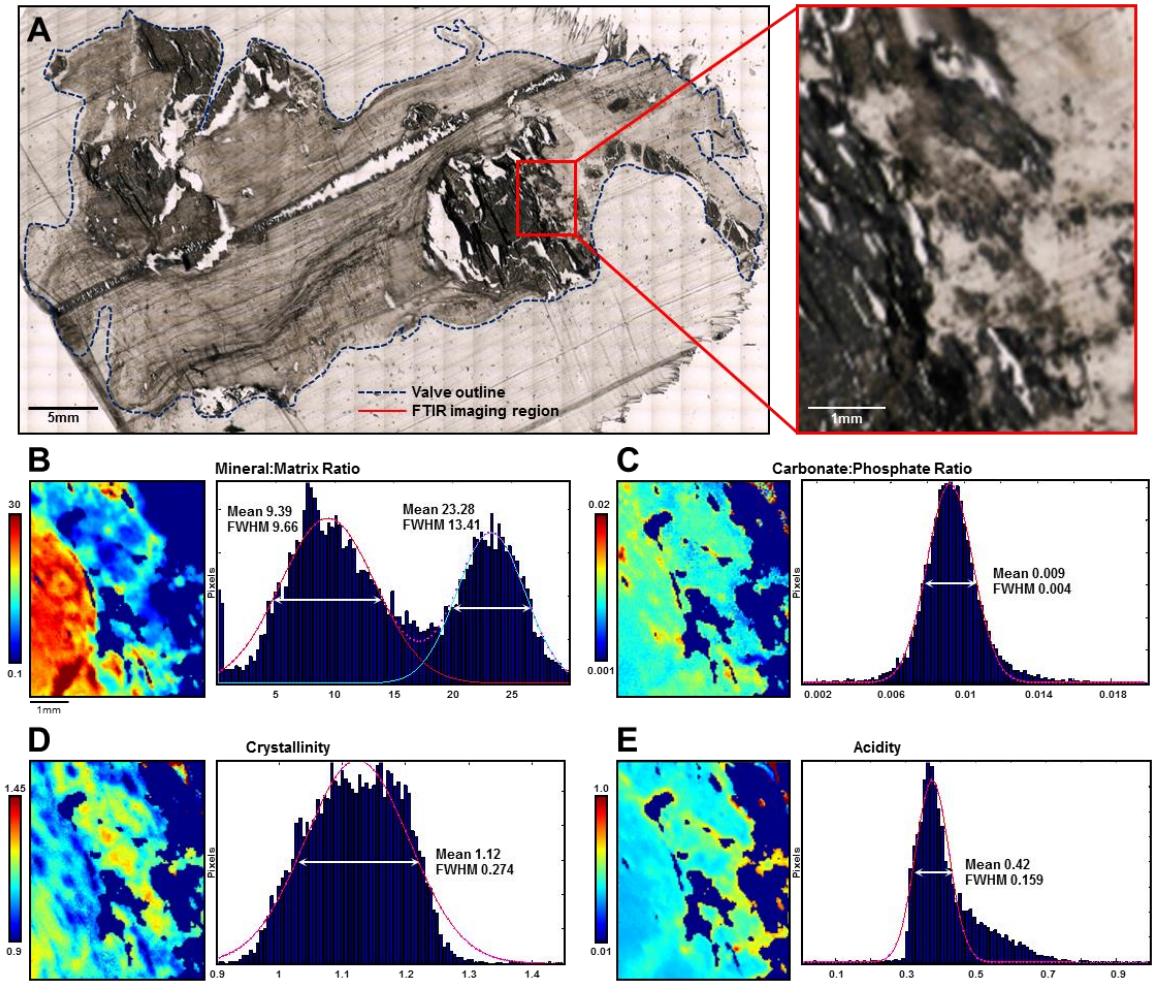

Figure 3.7: Heterogeneity of mineral composition. A) White light image of valve cross section with region of interest enlarged (right, bordered in red). FTIR images and associated pixel histograms with Gaussian fits of B) bimodal mineral:matrix ratio, C) carbonate:phosphate ratio, D) crystallinity and E) acidity for valve leaflets with low, moderate and high area fractions of calcification. The mean and full width at half maximum (FWHM) values of the Gaussian curves are indicated on each histogram.

3.5 Discussion

Aortic valve calcification is a serious pathology that presents a significant financial burden[33]. CAVD is characterized by the progressive degeneration of valve function due to the active deposition of mineral lesions within the valve leaflet tissue[34]. It has recently been established that the calcified lesions formed in valves is different in incidence from that of vascular calcification[3,35], but further investigation is needed to determine if their compositions are similar. This study uses materials science techniques to analyze the structure and composition of large calcific nodules as well as the surrounding tissue that is macroscopically non-mineralized.

We confirm through immunohistochemistry that valve cells express both myofibroblastic and osteoblast-like phenotypes, as has been reported previously[12,36]. We, however, highlight the regional variability of cell activation, noting that cells show transformed phenotypes not only at sites of highly mineralized nodule formation, but also throughout the leaflet tissue. It is also generally understood that endothelial dysfunction is one of the earliest signs of valve disease[9,37–39], and our SEM images confirm that mineralized particles also appear at sites of what appears to be endothelial injury or complete denudation of the endothelial monolayer. Elemental analysis of the mineral particles within the valve tissue revealed the presence of calcium and phosphorous, as well as small amounts of magnesium. This data agrees with complimentary studies identifying the elemental composition of valve mineralized lesions to be similar to that of bone, with Ca/P ratios similar to that of hydroxyapatite[15,31,40]. There is evidence that suggest that calcifying matrix vesicles may be in part responsible for the progression of valve calcification, but further analysis of our samples is necessary to determine whether they are present in our diseased valves[41,42]. Our results demonstrate that mineral properties are different

between calcific nodules from more severely calcified regions and lesser mineralized regions of the valves. While our analysis confirms previous studies that report a mineral phase of apatite[30,31], we also identify that the tissue surrounding large calcific nodules is in fact mineralized, characteristic of poorly crystalline hydroxyapatite. Interestingly, a recent study identified spherical mineral particles within not only calcified lesions, but also non-calcified regions of the valve tissue[20]. These results were mainly qualitative in nature, although the measured Ca/P ratio from SEM-EDS revealed that the mineral found in valves differed from that in bone.

In order to quantitatively characterize the mineral within mature calcific nodules as well as surrounding valve tissue, we utilized an imaging technique that has been used to understand mineral composition of bone in development and disease. FTIR imaging has the ability to not only show distributions of various FTIR peaks, but also utilizes validated parameters that can quantitatively describe HA-containing tissues[23–25]. While this technique has been used to great effect on bone, as well as soft tissue such as cartilage[43–45], lung[46], colon[47] and connective tissue[48], it has not yet been used for analyzing mineralized lesions in calcified valves. Mineralized material in less calcified valves displayed lower mineral:matrix ratios than valves with higher ratio areas of calcification, while exhibiting broad distributions. These results demonstrate that while less severely calcified valves have lower mineralized tissue, the degree of mineralization is very heterogeneous throughout the tissue. While there is evidence of mineral in the least severely calcified valves, further investigation is needed to analyze the mineral composition in these valves, because the mineralized tissue content was so low. Acid phosphate content was higher in lesser mineralized areas, suggesting new mineral formation in tissue surrounding mature calcific nodules. We further identified compact regions of mineralization that had higher mineral:matrix

ratios than that of bone, as well as higher crystallinity in intermediate areas. This effect may have been due to the two peaks commonly seen in the mineral:matrix and crystallinity ratios; the second of the two peaks often had a higher mineral:matrix mean than that of bone. These results suggest that although they are similar in structure and composition, valve calcification may follow a mechanistically different path than that of bone mineralization. Although we recognize that the small sample size of valves is a limitation in this particular study, we believe that we demonstrate an accurate representation of the heterogeneity of the mineral composition within the valve tissue. This study highlights the need for quantitative measurement of mineral composition, structure and heterogeneity for a better understanding of valve pathogenesis. Additional work is needed to identify unique mechanisms for valve calcification based on mineral composition, such that potential therapeutic targets could be identified in the future.

REFERENCES

1. Mozaffarian D, Benjamin EJ, Go a. S, Arnett DK, Blaha MJ, Cushman M, de Ferranti S, Despres J-P, Fullerton HJ, Howard VJ, Huffman MD, Judd SE, Kissela BM, Lackland DT, Lichtman JH, et al. Heart Disease and Stroke Statistics--2015 Update: A Report From the American Heart Association. *Circulation*. 2014;131:e29–e322.

2. Towler DA. Oxidation, Inflammation, and Aortic Valve Calcification: Peroxide Paves An Osteogenic Path. *Journal of the American College of CardiologyAmerican Coll*. 20008;52(10):851–854.

3. Teo KK, Corsi DJ, Tam JW, Dumesnil JG, Chan KL. Lipid Lowering on Progression of Mild to Moderate Aortic Stenosis: Meta-analysis of the Randomized Placebo-Controlled Clinical Trials on 2344 Patients. *Canadian Journal of Cardiology*. 2011;27(6):800–808.

4. Yutzey KE, Demer LL, Body SC, Huggins GS, Towler D a., Giachelli CM, Hofmann-Bowman M a., Mortlock DP, Rogers MB, Sadeghi MM, Aikawa E. Calcific Aortic Valve Disease: A Consensus Summary From the Alliance of Investigators on Calcific Aortic Valve Disease. *Arteriosclerosis, Thrombosis, and Vascular Biology*. 2014;34:2387–2393.

5. Butcher JT, Mahler GJ, Hockaday L a. Aortic valve disease and treatment: the need for naturally engineered solutions. *Advanced drug delivery reviews*. 2011;63(4-5):242–68.

6. O'Brien KD. Pathogenesis of calcific aortic valve disease: a disease process comes of age (and a good deal more). *Arteriosclerosis, thrombosis, and vascular biology*. 2006;26(8):1721–8.

7. Mathieu P, Boulanger M-C. Basic Mechanisms of Calcific Aortic Valve Disease. *Canadian Journal of Cardiology*. 2014;30:982–993.

8. Mohler ER, Gannon F, Reynolds C, Zimmerman R, Keane MG, Kaplan FS. Bone Formation and Inflammation in Cardiac Valves. *Circulation*. 2001;103(11):1522–1528.

9. Poggianti E, Venneri L, Chubuchny V, Jambrik Z, Baroncini LA, Picano E. Aortic valve sclerosis is associated with systemic endothelial dysfunction. *Journal of the American College of Cardiology*. 2003;41(1):136–41.

10. Liu AC, Joag VR, Gotlieb AI. The emerging role of valve interstitial cell phenotypes in regulating heart valve pathobiology. *The American journal of pathology*. 2007;171(5):1407–18.

11. Rajamannan NM, Evans FJ, Aikawa E, Grande-Allen KJ, Demer LL, Heistad DD, Simmons C a, Masters KS, Mathieu P, O'Brien KD, Schoen FJ, Towler D a, Yoganathan AP, Otto CM. Calcific aortic valve disease: not simply a degenerative process: A review and agenda for research from the National Heart and Lung and Blood Institute Aortic Stenosis Working Group. Executive summary: Calcific aortic valve disease-2011 update. *Circulation*. 2011;124(16):1783–91.

12. Rajamannan NM, Subramaniam M, Rickard D, Stock SR, Donovan J, Springett M, Orszulak T, Fullerton D a, Tajik a J, Bonow RO, Spelsberg T. Human aortic valve calcification is associated with an osteoblast phenotype. *Circulation*. 2003;107(17):2181–4.

13. Monzack, Elyssa L. and Masters KS. Can valvular interstitial cells become true osteoblasts?: A side-by-side comparison. *Journal of Heart Valve Disease*. 2011;20(4):449–463.

14. Cottignoli V, Cavarretta E, Salvador L, Valfré C, Maras A. Morphological and Chemical Study of Pathological Deposits in Human Aortic and Mitral Valve Stenosis: A Biomineralogical Contribution. *Pathology Research International*. 2015;2015:1–14.

15. Weska RF, Aimoli CG, Nogueira GM, Leirner A a., Maizato MJS, Higa OZ, Polakievicz B, Pitombo RNM, Beppu MM. Natural and prosthetic heart valve calcification: Morphology and chemical composition characterization. *Artificial Organs*. 2010;34(4):311–318.

16. Bazin D, Daudon M, Combes C, Rey C. Characterization and some physicochemical aspects of pathological microcalcifications. *Chemical reviews*. 2012;112(10):5092–120.

17. Gilinskaya LG, Grigorieva TN, Okuneva GN, Vlasov Y a. Investigation of Pathogenic Mineralization on Human Heart Valves. 1. Chemical and Phase Composition. *Journal of Structural Chemistry*. 2003;44(4):622–631.

18. Tomazic BB, Edwards WD, Schoen FJ. Physicochemical characterization of natural and bioprosthetic heart valve calcific deposits: Implications for prevention. *The Annals of Thoracic Surgery*. 1995;60(95):S322–S327.

19. Mikroulis D, Mavrilas D, Kapolos J, Koutsoukos PG, Lolas C. Physicochemical and microscopical study of calcific deposits from natural and bioprosthetic heart valves. Comparison and implications for mineralization mechanism. *Journal of materials science. Materials in medicine*. 2002;13(9):885–9.

20. Bertazzo S, Gentleman E, Cloyd KL, Chester AH, Yacoub MH, Stevens MM. Nano-analytical electron microscopy reveals fundamental insights into human cardiovascular tissue calcification. *Nature materials*. 2013;12(6):576–83.

21. Landis W, Hodgens K, Arena J, Song M, McEwen B. Structural relations between collagen and mineral in bone as determined by high voltage electron microscopic tomography. *Microscopy research and technique*. 1996;33(2):192–202.

22. Nudelman F, Pieterse L, George A, Bomans PHH, Friedrich H, Brylka LJ, Hilbers P a J, With G De, Sommerdijk N a JM. The role of collagen in bone apatite formation in the presence of hydroxyapatite nucleation inhibitors. *Nature materials*. 2011;9(12):1004–1009.

23. Boskey AL, Mendelsohn R. Infrared spectroscopic characterization of mineralized tissues. *Vibrational Spectroscopy*. 2005;38(1-2):107–114.

24. Boskey AL, Goldberg M, Kulkarni A, Gomez S. Infrared imaging microscopy of bone: illustrations from a mouse model of Fabry disease. *Biochimica et biophysica acta*. 2006;1758(7):942–7.

25. Donnelly E, Meredith DS, Nguyen JT, Gladnick BP, Rebolledo BJ, Shaffer AD, Lorich DG, Lane JM, Boskey AL. Reduced cortical bone compositional heterogeneity with bisphosphonate treatment in postmenopausal women with intertrochanteric and subtrochanteric fractures. *Journal of Bone and Mineral Research*. 2012;27(3):672–678.

26. Boskey A, Mendelsohn R. Infrared analysis of bone in health and disease. *Journal of Biomedical Optics*. 2005;10(June):031102.

27. Pleshko N, Boskey A, Mendelsohn R. Novel infrared spectroscopic method for the determination of crystallinity of hydroxyapatite minerals. *Biophysical journal*. 1991;60(October):786–793.

28. Spevak L, Flach CR, Hunter T, Mendelsohn R, Boskey A. Fourier transform infrared spectroscopic imaging parameters describing acid phosphate substitution in biologic hydroxyapatite. *Calcified Tissue International*. 2013;92:418–428.

29. Rey C, Combes C, Drouet1 C, Glimcher MJ. Bone mineral: update on chemical composition and structure C. *Osteoporosis international*. 2010;20(June 2008):1013–1021.

30. Prieto RM. Study on the structure and composition of aortic valve calcific deposits. etiological aspects. *Journal of Biophysical Chemistry*. 2011;02(01):19–25.

31. Tomazic BB. Physicochemical principles of cardiovascular calcification. *Zeitschrift für Kardiologie*. 2001;80:68–80.

32. Mangialardo S, Cottignoli V, Cavarretta E, Salvador L, Postorino P, Maras A. Pathological biominerals: Raman and infrared studies of bioapatite deposits in human heart valves. *Applied Spectroscopy*. 2012;66(10):1121–1127.

33. Go AS, Mozaffarian D, Roger VL, Benjamin EJ, Berry JD, Borden WB, Bravata DM, Dai S, Ford ES, Fox CS, Franco S, Fullerton HJ, Gillespie C, Hailpern SM, Heit J a., et al. Heart Disease and Stroke Statistics--2013 Update A Report From the American Heart Association. *Circulation*. 2012.

34. Dweck MR, Boon N a, Newby DE. Calcific aortic stenosis: a disease of the valve and the myocardium. *Journal of the American College of Cardiology*. 2012;60(19):1854–63.

35. Roger VL, Go AS, Lloyd-Jones DM, Adams RJ, Berry JD, Brown TM, Carnethon MR, Dai S, de Simone G, Ford ES, Fox CS, Fullerton HJ, Gillespie C, Greenlund KJ, Hailpern SM, et al. Heart disease and stroke statistics--2011 update: a report from the American Heart Association. *Circulation*. 2011;123(4):e18–e209.

36. Kaden JJ, Kiliç R, Sarikoç A, Hagl S, Lang S, Hoffmann U, Brueckmann M, Borggrefe M. Tumor necrosis factor alpha promotes an osteoblast-like phenotype in human aortic valve myofibroblasts: A potential regulatory mechanism of valvular calcification. *International Journal of Molectular Medicine*. 2005;16(5):869–872.

37. Gould ST, Srigunapalan S, Simmons C a., Anseth KS. Hemodynamic and cellular response feedback in calcific aortic valve disease. *Circulation Research*. 2013;113:186–197.

38. Leask RL, Jain N, Butany J. Endothelium and valvular diseases of the heart. *Microscopy research and technique*. 2003;60(2):129–37.

39. Butcher JT, Nerem RM. Valvular endothelial cells and the mechanoregulation of valvular pathology. *Philosophical transactions of the Royal Society of London. Series B, Biological sciences*. 2007;362(1484):1445–57.

40. Dritsa V, Pissaridi K, Koutoulakis E, Mamarelis I, Kotoulas C, Anastassopoulou J. An infrared spectroscopic study of aortic valve. A possible mechanism of calcification and the role of magnesium salts. *In vivo*. 2014;28:91–8.

41. Kim K. Calcification of matrix vesicles in human aortic valve and aortic media. *Federation Proceedings*. 1976;35(2):156–162.

42. New SEP, Aikawa E. Role of extracellular vesicles in de novo mineralization: An additional novel mechanism of cardiovascular calcification. *Arteriosclerosis, Thrombosis, and Vascular Biology*. 2013;33:1753–1758.

43. Khanarian NT, Boushell MK, Spalazzi JP, Pleshko N, Boskey AL, Lu HH. FTIR-I Compositional Mapping of the Cartilage-to-Bone Interface as a Function of Tissue Region and Age. *Journal of bone and mineral research : the official journal of the American Society for Bone and Mineral Research*. 2014;29(12):1–26.

44. Boskey A, Pleshko Camacho N. FT-IR imaging of native and tissue-engineered bone and cartilage. *Biomaterials*. 2007;28:2465–2478.

45. Bi X, Yang X, Bostrom MPG, Camacho NP. Fourier transform infrared imaging spectroscopy investigations in the pathogenesis and repair of cartilage. *Biochimica et Biophysica Acta - Biomembranes*. 2006;1758:934–941.

46. Krafft C, Codrich D, Pelizzo G, Sergo V. Raman mapping and FTIR imaging of lung tissue: congenital cystic adenomatoid malformation. *The Analyst*. 2008;133:361–371.

47. Krafft C, Codrich D, Pelizzo G, Sergo V. Raman and FTIR microscopic imaging of colon tissue: A comparative study. *Journal of Biophotonics*. 2008;1(2):154–169.

48. Petibois C, Gouspillou G, Wehbe K, Delage J-P, Déléris G. Analysis of type I and IV collagens by FT-IR spectroscopy and imaging for a molecular investigation of skeletal muscle connective tissue. *Analytical and bioanalytical chemistry*. 2006;386:1961–1966.

CHAPTER 4

CRYSTALLINITY OF HA NANOPARTICLES DRIVES MYOFIBROBLASTIC ACTIVATION AND CALCIFICATION IN HYDROXYAPATITE-RICH COLLAGEN MATRICES

4.1 Abstract

Calcific aortic valve disease (CAVD) is a degenerative pathology characterized by the progressive calcification of the valve leaflets. Hydroxyapatite (HA), while largely known as the predominant component of bone, has also been found in pathological mineral deposits found in valve calcification. There is evidence that the mineral formed in calcific valve leaflets have varying mineral properties, including crystallinity. It is unclear, however, how differences in mineral crystallinity affects cellular behavior during disease. This study used synthetic HA particles to evaluate how a mineral-rich collagen matrix regulates interstitial and endothelial interactions and phenotypes. HA nanoparticles of two different sizes and crystallinities were distributed within collagen constructs, which drove different myofibroblastic and osteoblastic responses in valve cells. Additionally, calcium deposition within collagen gels depended on particle size and/or crystallinity, and this difference was not entirely apoptosis-driven. Altogether, mineral-containing hydrogel models provide a 3D platform to evaluate valve cell responses to a later stage of valve disease, which is characterized by mineralized valve tissue.

4.2 Introduction

Calcific aortic valve disease (CAVD) is a degenerative pathology characterized by the progressive calcification of the valve leaflets. Present in up to 2.5% of Americans each year, this disease requires up to 250,000 surgical interventions worldwide, signifying a considerable annual financial burden[1]. Physicochemical studies have identified calcific nodules within diseased valve leaflets to be comprised of various phases of calcium phosphate crystals, ranging from amorphous calcium phosphate particles to highly crystalline hydroxyapatite[2–5]. While in normal bone development and growth, mineralization is highly regulated, diseases such as CAVD are characterized by pathological mineralized matrix deposits.

No longer thought to be a passive disease, it is now accepted that CAVD is an actively degenerative process that is characterized by early endothelial injury or dysfunction[6,7] and the activation and potential differentiation of valve interstitial cells[8]. There is evidence of both dystrophic calcification[9], caused primarily by apoptosis or necrosis, as well as active mineralization of the leaflet matrix. It has been shown that valve endothelial cells (VEC) will undergo an EMT-like transformation under inflammatory stimuli[10], and it has been postulated that activated forms of VEC may contribute to calcification. Additionally, it is well documented the population of valve interstitial cells (VIC) shift to a more myofibroblastic phenotype[11,12], and that valve cells in CAVD are associated with an osteoblast-like phenotype[13]. However, no studies currently exist that examine if direct interaction with HA particles, commonly found in the mineralized matrix of diseased valves contribute to the activation of both valve cell types.

Hydroxyapatite (HA), while largely known as the predominant component of bone, has also been found in various pathological mineral deposits, such as kidney

stones[14,15], microcalcification associated with breast cancer tumors[16,17], and calcified heart valves[18]. HA is a bioactive material that can regulate both normal and transformed cells. Previous studies have investigated the use of synthetically derived HA particles in various tissue engineering applications, in both models of disease and to induce normal mineralization, and found that the presence of HA could drive apoptosis and osteogenic expression[19–22]. The size, shape and crystallinity of synthetic HA can be controlled by the reaction conditions[23]. Although there is evidence of naturally occurring HA within valve leaflet ECM and that interstitial cells play a distinct role in the active calcification of valves[24], there is little understanding of the direct cellular consequences of HA particle proximity to valve cells. Use of synthetic HA particles could be a powerful tool to study how HA particles might drive activation of valve cells and further progress this degenerative disease.

Our objective, therefore, was to test how synthetically prepared HA particles regulate interstitial and endothelial interactions and phenotypes in a 3D environment. We utilized HA nanoparticles of varying sizes and crystallinities and incorporated them into our previously reported 3D collagen gel co-culture model[25]. After confirming successful distribution of particles within the collagen hydrogel, we found size/crystallinity-dependent differences in cellular uptake of HA nanoparticles. HA-driven apoptosis was also affected by size/crystallinity, and we discovered that smaller, less crystalline HA drove higher matrix calcium deposition, as well as increased myofibroblastic and osteoblastic responses in valve cells.

4.3 Materials and Methods

Heart Valve Preparation

Human diseased aortic valves were obtained from adults undergoing planned, nonelective valve replacement surgery by Dr. Sanjay Samy at the Guthrie Clinic

(Sayer, PA). All procedures were approved by Institutional Review Boards at Cornell University and the Guthrie Clinic. Valve leaflets were photographed and visually inspected for regions of heavy, moderate or very little calcified tissue.

HA Preparation

Hydroxyapatite nanoparticles were provided by the Estroff Lab in Materials Science and Engineering at Cornell University (Ithaca, NY), and were adapted from a previously reported method[23]. Ammonium phosphate dibasic (10mM) was added dropwise at a rate of 10 ml/min to a solution of calcium nitrate tetrahydrate (10mM) under rapid stirring in an ice bath (4°C). The reaction continued stirring for three days at 20°C. The resultant opaque suspension was concentrated 4 times by decanting the solution after allowing the solution to settle for 30 minutes, and transferred to a DI-H_2O hydrated dialysis bag (Cellu®SepT1 Part 5030-46, MWCO 3,500). The precipitate was dialyzed in 0.1M NaOH over 5 days with NaOH solutions replaced every other day.

Valve Mineral and HA Nanoparticle Characterization

As described in Chapter 3, calcified regions of human valve samples were excised and serially dehydrated with increasingly concentrated ethanol solutions, before being frozen and lyophilized. Samples were ground with mortar and pestle to a fine powder. HA particle and valve mineral crystallinity was examined by powder x-ray diffraction (pXRD) (Scintag Inc. PAD-X theta-theta X-ray Diffractometer, CuKα (1.54 Å), accelerating voltage 45 kV, current 40 mA, continuous scan, 2.0 deg/min). Phase information of valve mineral and HA particles was achieved through Fourier transform infrared (FTIR) spectroscopy (Mattson Instruments 2020 Galaxy Series FT-

IR). Dried particles and valve mineral were combined with KBr and pressed into pellets to obtain FTIR spectra (res 4.0 cm-1, 64 scans). Transmission electron microscopy (TEM) was used for HA particle shape and morphology characterization. Particles were combined with ethanol and dripped onto carbon-coated copper grids (Electron Microscopy Sciences) and examined with brightfield TEM (FEI Tecnai T-12 Spirit, 120 kV).

Preparation of HA Collagen Gels

Porcine aortic valve interstitial cells (PAVIC) and endothelial cells (PAVEC) were isolated as described previously[26] from valves donated by Shirk Meats (Dundee, NY). PAVEC were cultured in flasks coated with 50 µg/ml rat-tail collagen I (BD Biosciences) at 37°C and 5% CO_2 in DMEM (Invitrogen) supplemented with 10% FBS (Gemini Bio-Products), 1% penicillin-streptomycin (Invitrogen), and 50 U/ml heparin (Sigma-Aldrich, St Louis, MO). PAVIC were cultured identically, but without the heparin supplement and the collagen flask coating. Purity of endothelial population was monitored via quantitative real-time PCR and immunofluorescent assessment. Only cultures with consistent CD31 and VE-cadherin expression, cobblestone morphology, and non-detectable αSMA expression were used. PAVEC and PAVIC cultures were used between passage four and six.

Collagen hydrogel constructs were adapted from a procedure previously described[25,27]. The edge of each well of a 24-well plate was ringed with a hydrophobic pen, and then exposed to UV sterilization for 1 hour prior to gel seeding to ensure gels remained in the center of the well (Appendix B for full protocol). Porcine aortic valve interstitial cells (PAVIC) were suspended at 400,000 cells/ml in 3X DMEM with 10% FBS (Gemini Bioproducts), type I collagen (BD Biosciences) and

0.1M NaOH for a final gel concentration of 2 mg/ml. The collagen constructs were allowed to gel for 1 hour at 37°C before a subsequent seeding of a porcine aortic valve endothelial cell (PAVEC) monolayer at 50,000cells/gel. Collagen gels were either 1) PAVIC alone, 2) PAVEC alone (seeded on a PAVIC-free gel) or 3) a PAVIC+PAVEC co-culture. HA nanoparticle-incorporated gels were achieved by adding HA dialyzed in 0.1M NaOH to the collagen gel solution, for a final concentration of 0.25mg/ml. Particles were well mixed within the collagen solution via pipetting for complete incorporation of HA into collagen gels. VEC were added as previously stated (Figure 4.1). After 1 hour, gels were cultured with DMEM (10% FBS, 1% penicillin-streptomycin) for up to 7 days.

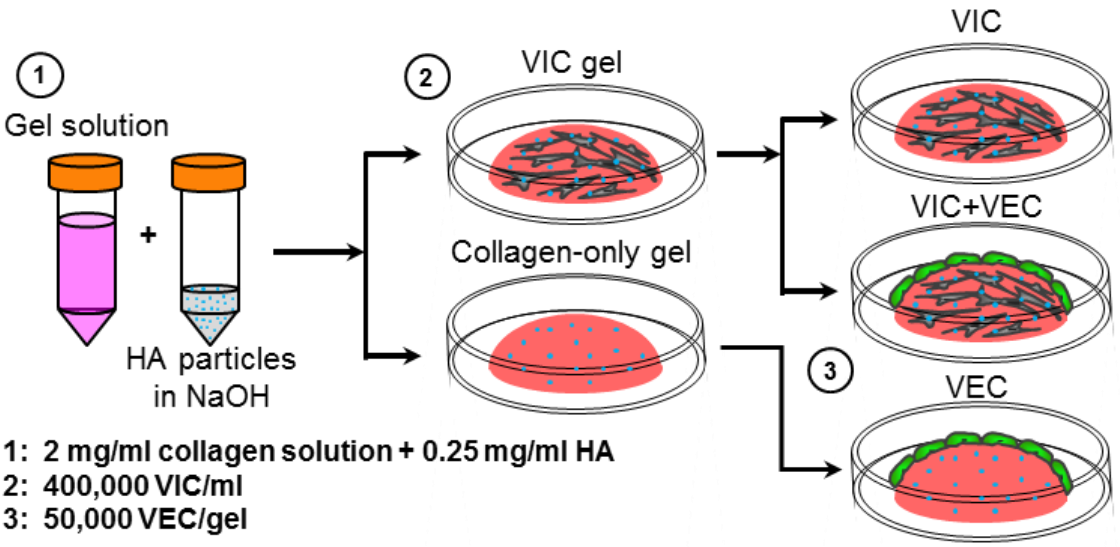

Figure 4.1: HA incorporation into collagen gels. Conceptual flowchart showing the (1) dialyzed HA and gel solution components, (2) incorporation of HA into VIC-only and blank collagen gels, and (3) addition of VEC onto specific gels for VEC-only and VIC+VEC co-cultures.

Confocal Reflectance and Particle Distribution

Particle distribution within the collagen gels was assessed with a Zeiss LSM700 confocal microscope, with a water-immersion 40X Zeiss objective and operated by

ZEN software (Carl Zeiss MicroImaging GmbH). For confocal reflectance microscopy, a solid state 405 nm laser illuminated the gel and backscattered light from the collagen fibers and aggregates of HA particles. Images were taken at 4 different depths within each gel, with each depth having 4 separate scans across the gel. Particles were counted via ImageJ (NIH) and organized in a histogram based on number of particles per scanned image.

Particle Uptake

To assess the uptake of HA particles into VIC, HA-incorporated gels were cultured for 24 hours, followed by a collagenase type-II (Worthington) digestion. Cells were re-plated and allowed to grow to confluence before being used in VIC gels with no additional HA added to the matrix. Pre- and post-collagenase digested gels were fixed with 4% PFA overnight and stained with phalloidin (f-actin, 1:40) and Draq5 (DNA, 1:1000). Fluorescence and reflectance confocal imaging was performed to visualize cellular uptake of HA nanoparticles.

Cytotoxicity and Apoptosis

Viability of cells within collagen hydrogels was determined via a live/dead cell viability assay (Invitrogen), whereby percentage of live (green) cells were compared to dead (red) cells in ImageJ. Measurements were normalized to control conditions with no HA particles. To visualize cells undergoing apoptosis, gels were fixed with 4% PFA and stained with a terminal deoxyribonucleotidyl transferase-mediated dUTP nick end labeling (TUNEL) assay kit (Invitrogen). Following a 2-hour incubation, gels were counterstained with an anti-BrdU fluorescent antibody, phalloidin (f-actin), and

Draq5 (DNA). Apoptosis was measured via the percentage of TUNEL-positive cells compared to total cell nuclei, and normalized to control conditions.

Quantitative Real-time RT-PCR

Total RNA was extracted from homogenized hydrogels using the RNeasy Mini Kit (Qiagen), which was then reverse transcribed into complementary cDNA using the iScript cDNA snythesis kit (Bio-Rad), according to the manufacturer's instructions. Quantitative real-time PCR was performed on all samples using SsoAdvanced SYBR green super mix (Bio-Rad) and a CFX96 or MiniOpticon Real-Time PCR Detection System (BioRad).

Calcium Deposition

Gels were fixed in 4% paraformaldehyde overnight and washed 3X with PBS. Gels were then incubated with 40 nM Alizarin red S (ARS) dye for 20 minutes at room temperature. Unbound solution was washed out overnight with gentle agitation. Bound ARS dye was released from the gels with 10% acetic acid, followed by neutralization with 10% ammonium hydroxide. ARS was quantified using absorbance spectroscopy at 405 nm wavelength. Blank gels with HA nanoparticles were used as controls to account for baseline levels of calcium.

Statistical Analysis

All data are expressed as means ± standard error, with at least 3 independent experiments per treatment. Data was analyzed statistically with JMP for Windows. Analysis of variance with Tukey's post-hoc test was used to compare differences between means (differences between means were considered significant at $P<0.05$).

4.4 Results

HA nanoparticles mimic native valve mineral

The size of HA particles were determined by TEM, which demonstrated smaller HA1 particles compared to HA2 particles (Figure 4.2A, B). As discussed in Chapter 3, XRD and FTIR (Figure 4.2C, D) confirm the mineral phase present in the calcified valves is apatite, in agreement with previous reports[2,28–30]. Both sets of spectra show that the heavy and moderate valve calcification regions differ in their mineral character. The moderate calcifications appear less crystalline or composed of smaller particles or perhaps both, as evidenced by the minimal splitting of the phosphate peak in FTIR spectrum and the poorer peak definition in the XRD pattern compared to the heavy calcification. We sought to synthesize apatite particles that, once seeded in a collagen scaffold, could strategically mimic this disparity of crystallinities in the two calcified regions. The XRD and FTIR spectra for the smaller, less crystalline (HA1) and larger, more crystalline (HA2) synthetic hydroxyapatite confirm a similar trend to the valves: the hydrothermally treated particles (HA2) show an increased peak definition in XRD and more splitting of the phosphate band in FTIR, demonstrating that these particles are a suitable model of mineral for the experiment.

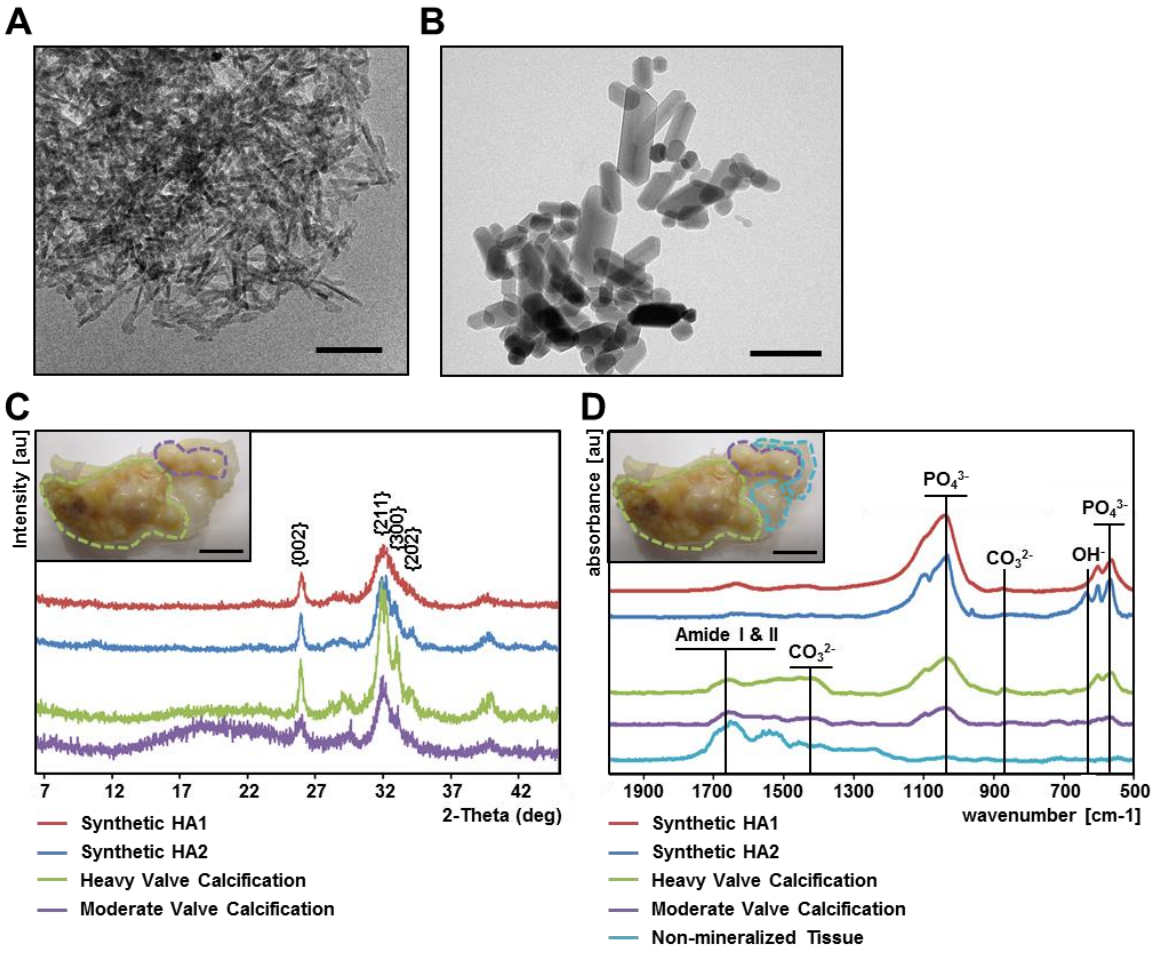

Figure 4.2: Comparison of valve mineral and HA particles. TEM of A) smaller, less crystalline HA1 and B) larger, more crystalline HA2 hydroxyapatite nanoparticles, scale bar = 100nm. C) Powder X-ray diffraction patterns of 1) HA1 and HA2 nanoparticles and 2) calcified aortic valve leaflets separated into regions of heavy calcification and lesser calcification. Representative regions of interest are shown in the inset image (scale bar = 5 mm). B) Infrared adsorption spectra of 1) HA1 and HA2 nanoparticles and 2) calcified aortic valve leaflets separated into regions of heavy calcification, lesser calcification, and visibly non-mineralized tissue. Representative regions of interest are shown in the inset image (scale bar = 5 mm)

Crystallinity and size alter particle distribution within collagen gels

Confocal reflectance microscopy revealed nanoparticle aggregates distributed throughout the collagen matrix. Particles were incorporated into collagen gels at two concentrations (0.1mg/ml and 0.25mg/ml). The smaller, less crystalline HA1 particles

had much smaller aggregates than the HA2 particles, but both particle types were well dispersed through the entire thickness of the gels (Figure 2A, B). HA1 particles had fairly normal distributions throughout the full thickness of the gel, and as expected, the 0.25mg/ml HA gel had an increased presence of particles per image (mean 16.6 ± 0.63 particles in 0.1mg/ml vs. 42.9 ± 1.38 particles in 0.25mg/ml gels) (Figure 2C). While the more crystalline/larger HA2 particles had similar increases in particle number with concentration (mean 22.67 ± 0.84 particles in 0.1mg/ml vs. 46.83 ± 1.98 particles in 0.25mg/ml gels), the HA2 particles were not as homogenously distributed throughout the gel (Figure 2C). Preliminary data revealed similar cellular responses to both concentrations of HA particles within the gels; therefore, the remainder of this paper will focus on the 0.25mg/ml concentration of HA within the collagen hydrogels.

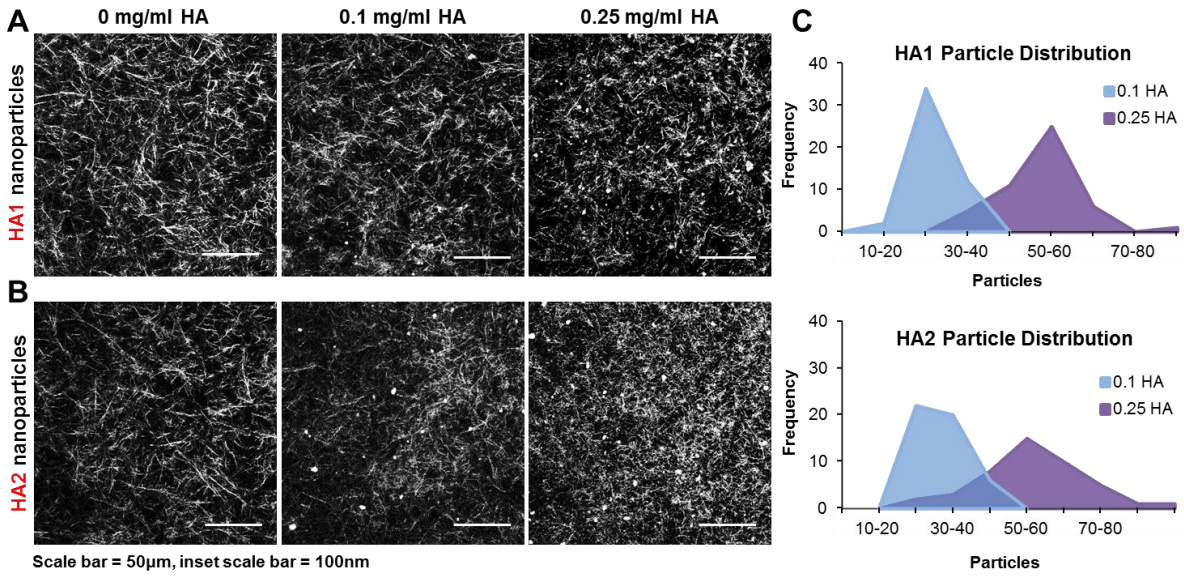

Figure 4.3: Distribution of HA nanoparticles in collagen gels. A) Distribution of smaller, less crystalline HA1 particles within collagen gels, visualized via reflectance imagine. Scale bar = 50μm. B) Distribution of larger, more crystalline HA2 particles within collagen gels, visualized via reflectance imagine. Scale bar = 50μm. C) Distribution histograms of 0.1mg/ml and 0.25mg/ml HA within collagen gels.

Cellular uptake of HA particles

After 24 hours of culture, both HA1 and HA2 particle aggregates are clearly visible throughout the collagen matrix. In addition, a combination of fluorescent and reflectance imaging reveal particles within the interstitial cells (Figure 4.4A). To ensure that HA particles were dispersed within the VIC, gels were digested using type-II collagenase, and VIC were harvested via centrifugation. When VIC were seeded within new collagen gels, free of HA particles, they were re-examined and found to still have particles within the cytoplasm (Figure 4.4B). The smaller, less crystalline HA1 particles had significantly higher uptake within the cells as compared to the larger, more crystalline HA2 particles (38.4 ± 3.46 vs. 26.3 ± 2.96 particles, respectively) (Figure 4.4C).

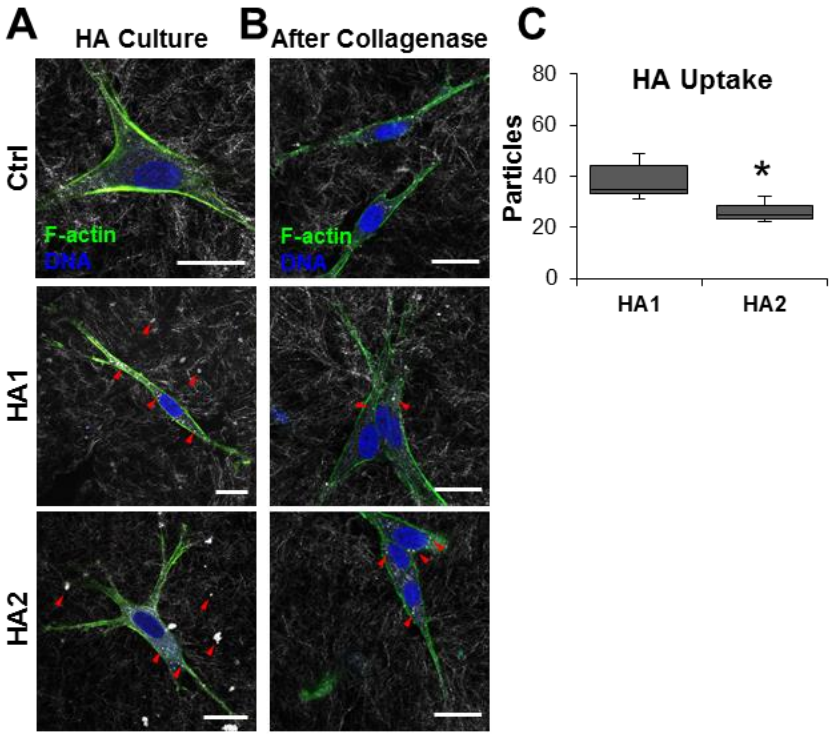

Figure 4.4: VIC uptake of HA nanoparticles. A) HA nanoparticle aggregates in an and around VIC seeded within an HA-rich gel. B) HA nanoparticle aggregates within VIC after collagen digestion and centrifugation, followed by re-seeding in HA-free collagen gels. Scale bars = 20μm. C) VIC uptake of HA particles is greater in smaller, less crystalline HA gels. Values are expressed as means ± SEM, *P<0.05.

HA particle crystallinity/size regulates apoptosis

To verify that the cells tolerated the presence of 0.25mg/ml HA particles, we performed a live/dead (green/red) assay, as well as a cellular apoptosis (TUNEL) assay on the hydrogels. Cell viability was not significantly affected due to culture with HA nanoparticles; indeed, all conditions remained over 90% alive, with the exception of VIC gels with larger, more crystalline HA2 particles (82% viable) (Figure 4.5A-C).

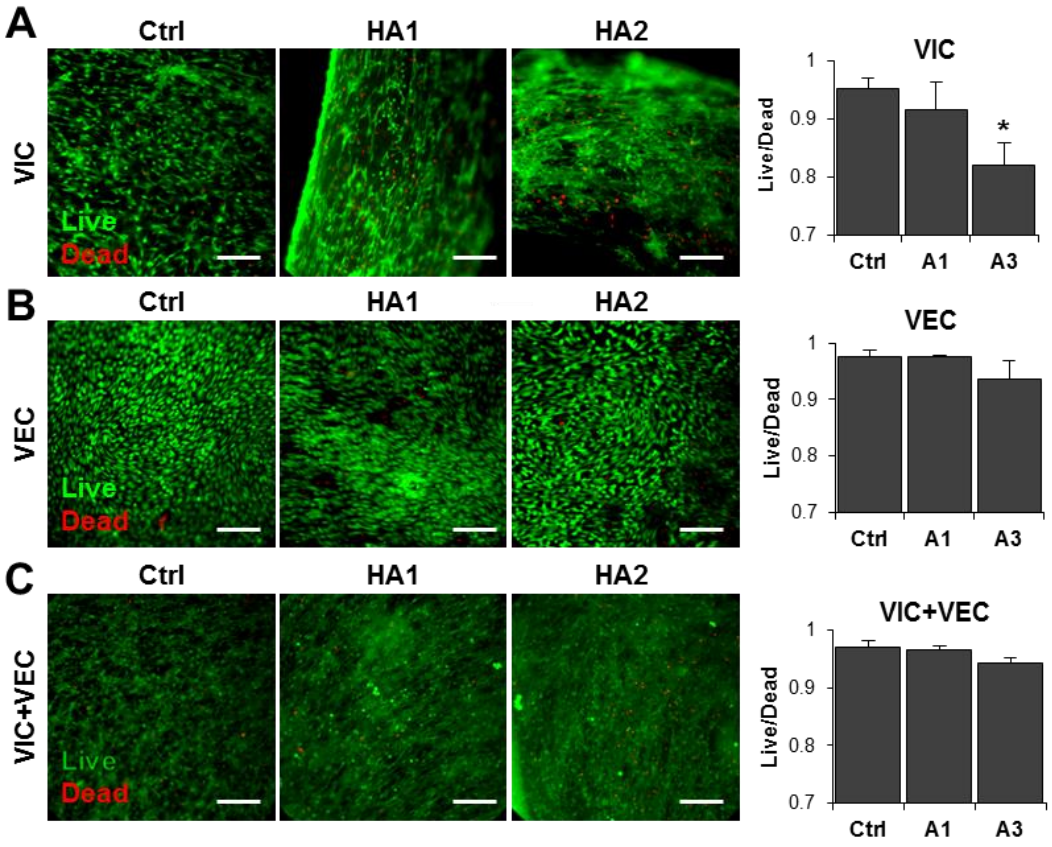

Figure 4.5: Viability of HA nanoparticle-incorporated collagen gels. Live/Dead staining of A) VIC-only, B) VEC-only and C) VIC+VEC co-cultures with or without HA nanoparticles. Viability is shown with Live/Dead and expressed as a ratio of live or dead cells over total cells. Scale bar = 200 μm. Values are expressed as means ± SEM, *P<0.05.

We next examined whether cell death was due to apoptosis, as regulated by particle crystallinity and/or size. After 7 days of culture, the number of apoptotic

(green) cells in VIC gels cultured with HA1 particles were significantly higher than those in control conditions (10.0% ± 1.4% vs. 2.9% ± 0.3%, respectively). HA2 particles did not induce an apoptotic response significantly relative to control (Figure 4.6A). Although there was a detectably higher amount of TUNEL-positive VEC when cultured with HA1 particles, the increase was not significantly different from control conditions (Figure 4.6B). VIC+VEC co-cultures had similar apoptotic responses to HA1 and HA2 particles to the VIC-only cultures, in that only the HA1 VIC+VEC gels had significantly higher apoptosis as compared to control conditions (10.9% ± 2.9% vs. 6.3% ± 0.4%, respectively) (Figure 4.6C).

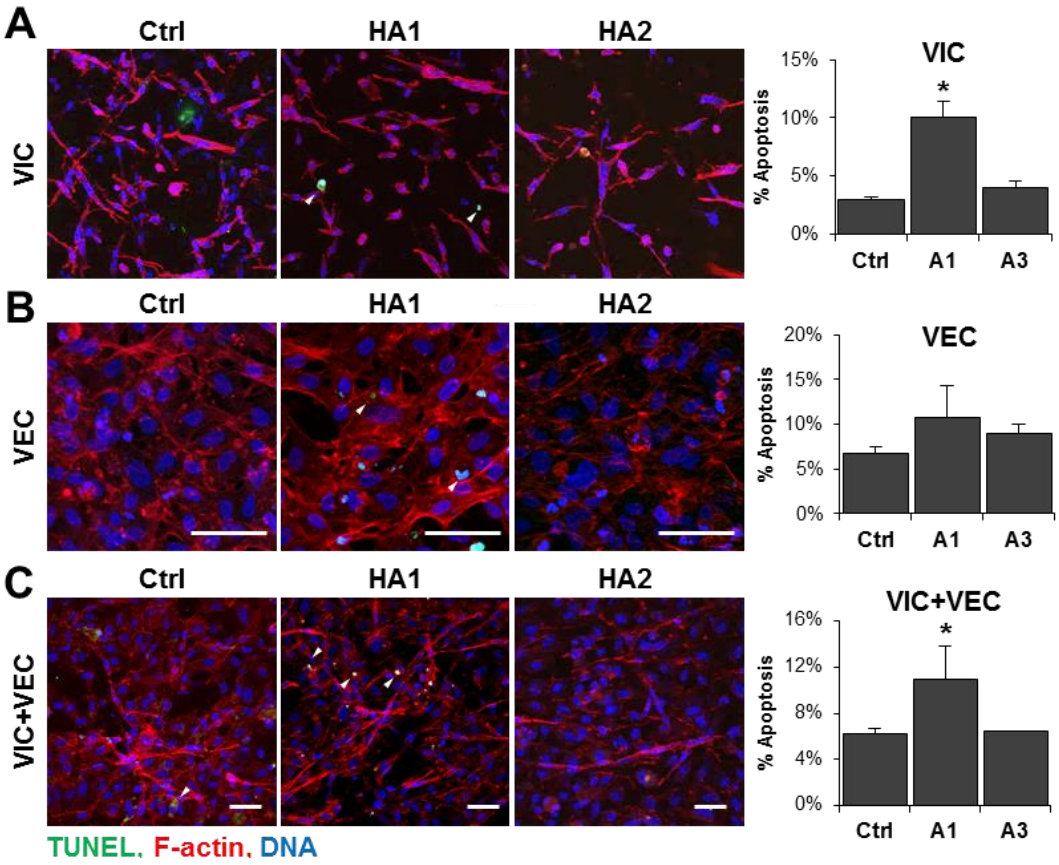

Figure 4.6: Apoptosis of HA nanoparticle-incorporated collagen gels. TUNEL staining of A) VIC-only, B) VEC-only and C) VIC+VEC co-cultures with or without HA nanoparticles. % Apoptosis is shown with TUNEL and expressed as a ratio of TUNEL-positive cells over total cells. Scale bars = 50 μm. Values are expressed as means ± SEM, *P<0.05.

Crystallinity/size regulates myofibroblastic activation and osteoblastic differentiation

Myofibroblastic activation was measured via expression of αSMA. VIC-only gels cultured for 7 days with HA1 particles expressed significantly higher αSMA (3.07 ± 0.25 fold), vs. HA-free controls. However, HA2 VIC-only gels, while higher than controls (2.11 ± 0.16 fold), expressed less αSMA than those gels cultured with the smaller, less crystalline HA1 particles (Figure 4.7A). This trend continued with VEC-only gels, with HA1 incorporated gels expressing significantly higher αSMA (6.87 ± 2.87 fold) vs. control, and HA2 gels, while higher (1.78 ± 0.27 fold), was brought back significantly closer to control levels (Figure 4.7A). VIC+VEC co-cultures combined with HA1 particles additionally expressed higher αSMA levels (4.32 ± 0.25), while culture with HA2 particles were not statistically different from that of control levels (Figure 4.7A). This data makes a strong case for the smaller, less crystalline particles, rather than the highly crystalline particles, driving myofibroblastic activation in both VIC and VEC cultures.

Similarly, 7-day culture with HA particles drive an osteoblastic response in VIC and VIC+VEC cultures. In VEC-only gels, culture with both HA1 and HA2 particles did not significantly affect expression of either Runx2 or osteopontin (OPN), except for Runx2 expression in VEC with HA1 particles (0.12 ± 0.01 fold) vs. controls (Figure 4.7B, C). Runx2 expression, while not statistically significant, was upregulated in VIC-only gels with HA1 particles (1.46 ± 0.54 fold) vs. control, while culture with HA2 particles did not increase Runx2 at all (Figure 4.7B). However, in VIC+VEC co-cultures, Runx2 was significantly increased when cultured with HA1 particles (4.44 ± 1.02 fold vs. controls), and to a much lesser degree when cultured with HA2 particles (1.82 ± 0.13 fold vs. controls) (Figure 4.7B). OPN levels were similarly increased in

VIC-only gels cultured with HA1 particles (2.55 ± 0.30 fold vs. controls), and to a lesser degree also increased when cultured with HA2 particles (1.69 ± 0.11 fold vs. controls) (Figure 4.7C). In VIC+VEC co-cultures, only culture with HA1 particles yielded a significant increase in OPN expression (2.67 ± 0.35 vs. controls) (Figure 4.7C). Collectively, this data reveals that smaller, less crystalline HA has a robust effect on myofibroblastic activation in VIC and VEC, and osteoblastic differentiation in VIC. While crystalline particles also drive VIC activation, it is to a much lesser degree.

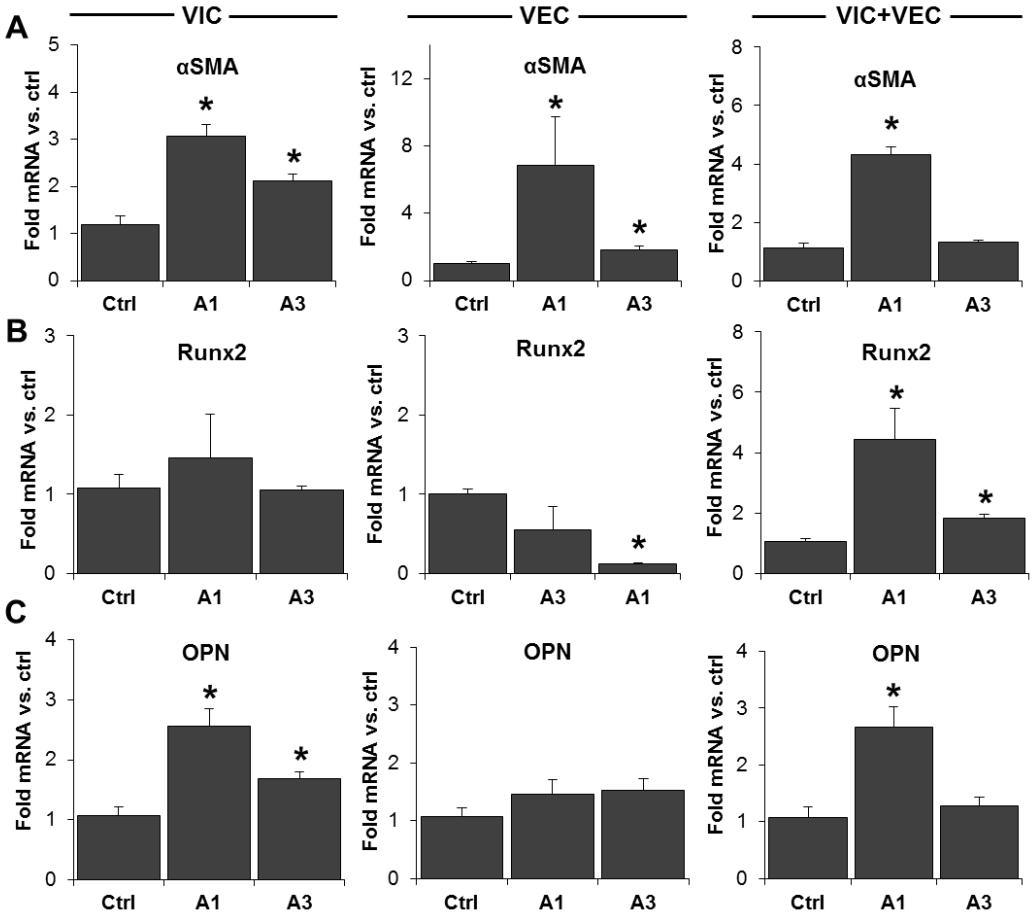

Figure 4.7: Gene expression of HA collagen gels. Real-time PCR shows effect of immature (A1) and mature (A3) HA nanoparticles on the expression of A) αSMA (Acta2), B) Runx2, and C) osteopontin in VIC-only, VEC-only and VIC+VEC co-culture gels (n=4). Values are expressed as fold changes and are means ± SEM, *P<0.05.

VIC+VEC cultures were examined for endothelial activity to determine the loss of protection against VIC activation and differentiation. VCAM1 expression was significantly higher in the smaller, less crystalline HA gels (2.35 ± 0.27 fold vs. controls) (Figure 4.8A), which indicates a potential inflammatory response by the VEC to the HA particles. Interestingly, eNOS expression was also increased in the less crystalline particles (3.02 ± 0.68 fold vs. controls) (Figure 4.8B). In addition, nitric oxide secretion into the co-culture media was analyzed, and found that there was increased nitric oxide in the less crystalline HA gels (1.06 ± 0.075 relative to controls), although this increase was not statistically significant (Figure 4.8C).

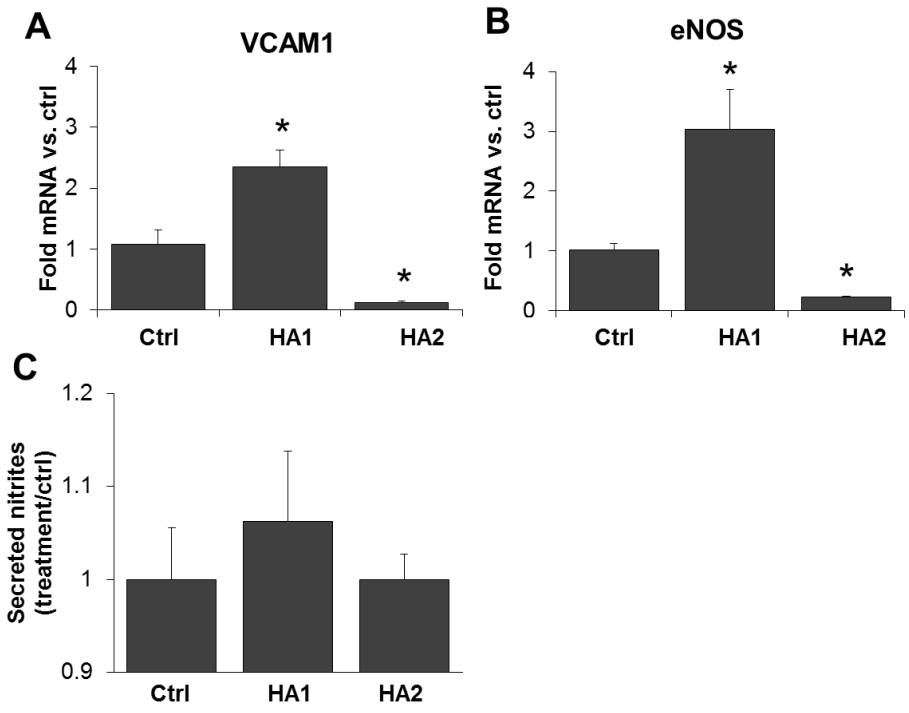

Figure 4.8: VEC activity in co-cultures with HA nanoparticles. Real-time PCR shows effect of smaller, less crystalline HA1 and larger, more crystalline HA2 nanoparticles on the expression of A) eNOS and B) VCAM1. C) Nitric oxide secretion had increased trends in smaller, less crystalline HA1 particles, although differences were not statistically significant. Values are expressed as fold changes and are means ± SEM, *P<0.05.

Crystallinity/size of HA particles drive calcium deposition

An Alizarin Red S (ARS) assay was used to determine if cells cultured in 3D with HA nanoparticles would induce a calcific response. All gels were normalized to cell-free HA-incorporated gels to account for baseline measurements of calcium, and then compared to their respective cell controls. Calcium deposition in gels with all cell types revealed a similar trend, in that gels with smaller, less crystalline HA1 particles had significantly increased calcium content when compared to controls (Figure 4.9A). VIC-only gels measured 2.73 ± 0.488 ARS absorbance, VEC-only gels measured 2.32 ± 0.06 and VIC+VEC co-cultures measured 3.08 ± 0.41, relative to their HA-free controls (Figure 4.9B). Interestingly, after 7 days of culture with the more crystalline HA2 particles, VEC-only and VIC+VEC co-cultures were no more calcified than the controls (1.54 ± 0.73 and 1.16 ± 0.03, respectively). While the HA2 VIC-only gels were statistically higher than the control level (1.24 ± 0.02), this level of calcium deposition remained drastically lower than that of its HA1 counterpart (Figure 4.9B). One interesting note is that the presence of smaller, less crystalline HA within the collagen matrix has mitigated the ability of VEC to reduce VIC calcification, as was previously found in our VEC+VEC co-cultures (in the presence of osteogenic media)[25]. These findings suggest that the smaller, less crystalline HA within the collagen hydrogels drive calcium deposition to a far greater degree than large particles with a higher crystallinity. The surface to volume ratio for smaller, less crystalline particles is much higher, which could account for this difference in cell response; these nanoparticles, due to their shape, could have a greater availability for binding and activation of the cells.

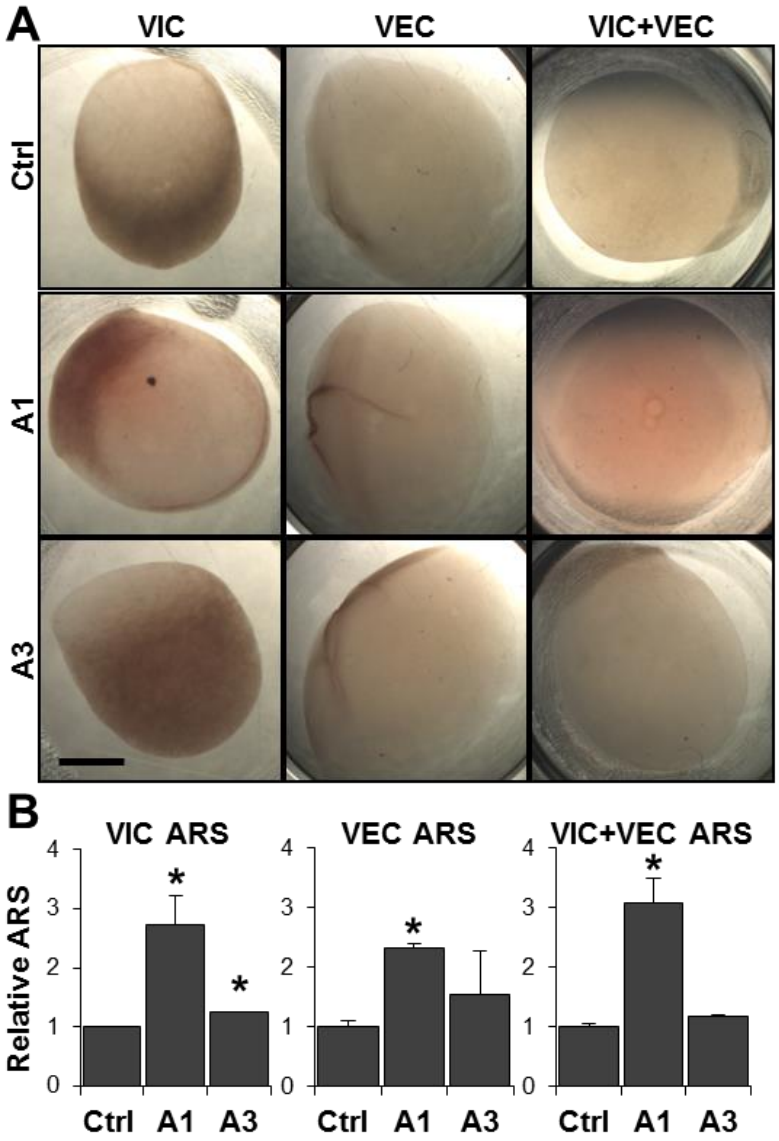

Figure 4.9: Calcium deposition in HA-incorporated gels. (A) Representative images of VIC, VEC, and VIC+VEC gels stained with Alizarin Red S (ARS) with immature (A1) and mature (A3) HA nanoparticles. (B) Quantification of calcium deposition via ARS analysis in VIC, VEC, and VIC+VEC HA-incorporated gels (n=4). Scale bar = 3mm. Values are expressed as means ± SEM, *P<0.05.

4.5 Discussion

Calcific aortic valve disease is a pathology defined by mineralized matrix deposits that range in size and crystallinity. While it is reported that calcified valves contain

regions of mineralized matrix consisting of material ranging from amorphous calcium phosphate to highly crystalline apatite[4,18], it remains unclear how these particles affect cellular phenotype and behavior. While cellular behavior in response to osteogenic stimuli in the form of phosphate salts[31–33], matrix stiffness changes[34] and growth factor exposure[35,36], there are no current models to investigate cell-mineral interactions in response to HA nanoparticle characteristics. In this study, we used synthetic hydroxyapatite particles with differing size and crystallinities in conjunction with our previously reported 3D hydrogel culture system[25] to elucidate direct effects of apatite particles on cellular behavior. We were able to incorporate and equally distribute dialyzed nanoparticles into a collagen gel, which ensured maximum contact with valve interstitial and endothelial cells.

It has been shown that cell behavior is affected by mineral characteristics. Bone marrow MSCs proliferate less and have lower differentiation potential when seeded on films made of amorphous calcium phosphate compared to crystalline hydroxyapatite[37]. Our study shows that both interstitial and endothelial cells were activated in the presence of smaller, less crystalline particles, while the larger, more crystalline particles had little to no effect on the myofibroblastic nature of the cells. Interestingly, the presence of VEC did not mitigate VIC activation, as we previously reported when cultured in osteogenic medium. This could be in part due to an inflammatory response, as indicated by the increased VCAM1 expression, or an inability of the VIC to respond to secreted nitric oxide. Similarly, culture with smaller, less crystalline HA caused osteoblastic differentiation in VIC, which was again not reduced by the presence of VEC in the co-culture. These results demonstrate that the presence of HA particles within the collagen hydrogel mitigate the protective effects that VEC have on VIC in 3D culture. Again, calcium deposition within the

collagen matrix was driven by crystallinity or particle size, as it was the smaller, less crystalline HA particle-embedded gels that calcified, while there was little to no calcium deposition within the gels incorporated with larger, more crystalline HA particles.

Dystrophic calcification is associated with necrotic and apoptosis-driven calcium deposition by cells. While apoptosis is present in regions of calcified valve leaflets, there are also regions with active pathological ectopic calcification[38,39]. Some 2D studies have shown that nodules form in response to osteogenic stimuli that have apoptotic cores[31,40]. While our study demonstrates that the smaller, less crystalline particles have a greater effect on cellular apoptosis, it should be noticed that the highest difference of apoptosis generated compared to controls was only 5%. Taken together, our 3D study reveals that not only are the particles not cytotoxic, there was very little apoptosis-driven calcification of the collagen gels, indicating a different mechanism by which calcification was occurring.

As is common with particles of this size[41,42], there was higher uptake of smaller, less crystalline HA particles within interstitial cells, which may contribute to the active calcium deposition seen by the cells in the case of the smaller particles. However, other studies have postulated that interactions of cells with surfaces of HA particles are mediated by integrins on cell membranes[43]. Additionally, it has been postulated that crystals of a differing size can affect cellular response[19]. While the insights provided by our system regarding cellular response to HA with different crystallinities, future studies could give more mechanistic insight into why these changes are occurring. It has been suggested that crystal size may be a factor in cellular differentiation, and alterations to the size of the particles in the future could be used to investigate size differences as related to changes in cell phenotype. Altogether,

mineral-containing hydrogel models provide a 3D platform to evaluate valve cell responses to a later-stage of valve disease, characterized by highly mineralized valve tissue. Furthermore, these models provide insight into the disruptive effect that HA particles has on endothelial regulation of interstitial activation and calcification.

REFERENCES

1. Mozaffarian D, Benjamin EJ, Go a. S, Arnett DK, Blaha MJ, Cushman M, de Ferranti S, Despres J-P, Fullerton HJ, Howard VJ, Huffman MD, Judd SE, Kissela BM, Lackland DT, Lichtman JH, et al. Heart Disease and Stroke Statistics--2015 Update: A Report From the American Heart Association. *Circulation*. 2014;131:e29–e322.

2. Prieto RM. Study on the structure and composition of aortic valve calcific deposits. etiological aspects. *Journal of Biophysical Chemistry*. 2011;02(01):19–25.

3. Tomazic BB, Edwards WD, Schoen FJ. Physicochemical characterization of natural and bioprosthetic heart valve calcific deposits: Implications for prevention. *The Annals of Thoracic Surgery*. 1995;60(95):S322–S327.

4. Cottignoli V, Cavarretta E, Salvador L, Valfré C, Maras A. Morphological and Chemical Study of Pathological Deposits in Human Aortic and Mitral Valve Stenosis: A Biomineralogical Contribution. *Pathology Research International*. 2015;2015:1–14.

5. Pilarczyk M, Czamara K, Baranska M, Natorska J, Kapusta P, Undas A, Kaczor A. Calcification of aortic human valves studied in situ by Raman microimaging: Following mineralization from small grains to big deposits. *Journal of Raman Spectroscopy*. 2013;44(April):1222–1229.

6. Poggianti E, Venneri L, Chubuchny V, Jambrik Z, Baroncini LA, Picano E. Aortic valve sclerosis is associated with systemic endothelial dysfunction. *Journal of the American College of Cardiology*. 2003;41(1):136–41.

7. Butcher JT, Nerem RM. Valvular endothelial cells and the mechanoregulation of valvular pathology. *Philosophical transactions of the Royal Society of London. Series B, Biological sciences*. 2007;362(1484):1445–57.

8. Rajamannan NM, Evans FJ, Aikawa E, Grande-Allen KJ, Demer LL, Heistad DD, Simmons C a, Masters KS, Mathieu P, O'Brien KD, Schoen FJ, Towler D a, Yoganathan AP, Otto CM. Calcific aortic valve disease: not simply a degenerative process: A review and agenda for research from the National Heart and Lung and Blood Institute Aortic Stenosis Working Group. Executive summary: Calcific aortic valve disease-2011 update. *Circulation*. 2011;124(16):1783–91.

9. Mohler ER, Gannon F, Reynolds C, Zimmerman R, Keane MG, Kaplan FS. Bone Formation and Inflammation in Cardiac Valves. *Circulation*. 2001;103(11):1522–1528.

10. Farrar EJ, Butcher JT. Heterogeneous susceptibility of valve endothelial cells to mesenchymal transformation in response to TNFα. *Annals of biomedical engineering*. 2014;42(1):149–61.

11. Gu X, Masters KS. Role of the Rho pathway in regulating valvular interstitial cell phenotype and nodule formation. *American journal of physiology. Heart and circulatory physiology*. 2011;300(24):H448–H458.

12. Merryman WD, Lukoff HD, Long R a, Engelmayr GC, Hopkins R a, Sacks MS. Synergistic effects of cyclic tension and transforming growth factor-beta1 on the aortic valve myofibroblast. *Cardiovascular pathology : the official journal of the Society for Cardiovascular Pathology*. 2007;16(5):268–76.

13. Rajamannan NM, Subramaniam M, Rickard D, Stock SR, Donovan J, Springett M, Orszulak T, Fullerton D a, Tajik a J, Bonow RO, Spelsberg T. Human aortic valve calcification is associated with an osteoblast phenotype. *Circulation*. 2003;107(17):2181–4.

14. Kodati VR, Tomasi GE, Turumin JL, Tu AT. Raman Spectroscopic Identification of Phosphate-Type Kidney Stones. *Applied Spectroscopy*. 1991;45(4):581–583.

15. Coe FL, Parks JH, Asplin JR. The Pathogenesis and Treatment of Kidney Stones. *The New England Journal of Medicine*. 1992;327:1141–1152.

16. Shafer-Peltier KE, Haka AS, Fitzmaurice M, Crowe J, Myles J, Dasari RR, Feld MS. Raman microspectroscopic model of human breast tissue: Implications for breast cancer diagnosis in vivo. *Journal of Raman Spectroscopy*. 2002;33:552–563.

17. Fandos-Morera A, Prats-Esteve M, Tura-Soteras J, Traveria-Cros A. Breast tumors: composition of microcalcifications. *Radiology*. 1988;169(2):325–327.

18. Bertazzo S, Gentleman E, Cloyd KL, Chester AH, Yacoub MH, Stevens MM. Nano-analytical electron microscopy reveals fundamental insights into human cardiovascular tissue calcification. *Nature materials*. 2013;12(6):576–83.

19. Shi Z, Huang X, Cai Y, Tang R, Yang D. Size effect of hydroxyapatite nanoparticles on proliferation and apoptosis of osteoblast-like cells. *Acta Biomaterialia*. 2009;5(1):338–345.

20. Liu ZS, Tang SL, Ai ZL. Effects of hydroxyapatite nanoparticles on proliferation and apoptosis of human hepatoma BEL-7402 cells. *World Journal of Gastroenterology*. 2003;9(9):1968–1971.

21. Balasundaram G, Sato M, Webster TJ. Using hydroxyapatite nanoparticles and decreased crystallinity to promote osteoblast adhesion similar to functionalizing with RGD. *Biomaterials*. 2006;27:2798–2805.

22. Kim K, Dean D, Lu A, Mikos AG, Fisher JP. Early osteogenic signal expression of rat bone marrow stromal cells is influenced by both hydroxyapatite nanoparticle content and initial cell seeding density in biodegradable nanocomposite scaffolds. *Acta biomaterialia*. 2011;7(3):1249–64.

23. Pathi SP, Lin DDW, Dorvee JR, Estroff LA, Fischbach C. Hydroxyapatite nanoparticle-containing scaffolds for the study of breast cancer bone metastasis. *Biomaterials*. 2011;32(22):5112–22.

24. Liu AC, Joag VR, Gotlieb AI. The emerging role of valve interstitial cell phenotypes in regulating heart valve pathobiology. *The American journal of pathology*. 2007;171(5):1407–18.

25. Richards J, El-Hamamsy I, Chen S, Sarang Z, Sarathchandra P, Yacoub MH, Chester AH, Butcher JT. Side-specific endothelial-dependent regulation of aortic valve calcification: interplay of hemodynamics and nitric oxide signaling. *The American journal of pathology*. 2013;182(5):1922–31.

26. Gould RA, Butcher JT. Isolation of valvular endothelial cells. *Journal of visualized experiments : JoVE*. 2010;(46):1–6.

27. Butcher JT, Nerem RM. Valvular endothelial cells regulate the phenotype of interstitial cells in co-culture: effects of steady shear stress. *Tissue engineering*. 2006;12(4):905–15.

28. Mikroulis D, Mavrilas D, Kapolos J, Koutsoukos PG, Lolas C. Physicochemical and microscopical study of calcific deposits from natural and bioprosthetic heart valves. Comparison and implications for mineralization mechanism. *Journal of materials science. Materials in medicine*. 2002;13(9):885–9.

29. Tomazic BB. Physicochemical principles of cardiovascular calcification. *Zeitschrift für Kardiologie*. 2001;80:68–80.

30. Mangialardo S, Cottignoli V, Cavarretta E, Salvador L, Postorino P, Maras A. Pathological biominerals: Raman and infrared studies of bioapatite deposits in human heart valves. *Applied Spectroscopy*. 2012;66(10):1121–1127.

31. Chen J, Peacock JR, Branch J, David Merryman W. Biophysical analysis of dystrophic and osteogenic models of valvular calcification. *Journal of biomechanical engineering*. 2015;137(2):1–6.

32. Monzack, Elyssa L. and Masters KS. Can valvular interstitial cells become true osteoblasts?: A side-by-side comparison. *Journal of Heart Valve Disease*. 2011;20(4):449–463.

33. Kennedy J a, Hua X, Mishra K, Murphy G a, Rosenkranz AC, Horowitz JD. Inhibition of calcifying nodule formation in cultured porcine aortic valve cells by nitric oxide donors. *European journal of pharmacology*. 2009;602(1):28–35.

34. Yip CYY, Chen J-H, Zhao R, Simmons C a. Calcification by valve interstitial cells is regulated by the stiffness of the extracellular matrix. *Arteriosclerosis, thrombosis, and vascular biology*. 2009;29(6):936–42.

35. Jian B, Narula N, Li Q, Iii ERM, Levy RJ. Progression of Aortic Valve Stenosis : TGF-b1 is Present in Calcified Aortic Valve Cusps and promotes aortic valve interstitial cell calcification via apoptosis. *The Annals of Thoracic Surgery*. 2003;75(2):457–465.

36. Cloyd KL, El-Hamamsy I, Boonrungsiman S, Hedegaard M, Gentleman E, Sarathchandra P, Colazzo F, Gentleman MM, Yacoub MH, Chester AH, Stevens MM. Characterization of Porcine Aortic Valvular Interstitial Cell "Calcified" Nodules. Aikawa E, ed. *PLoS ONE*. 2012;7(10):e48154.

37. Hu Q, Tan Z, Liu Y, Tao J, Cai Y, Zhang M, Pan H, Xu X, Tang R. Effect of crystallinity of calcium phosphate nanoparticles on adhesion, proliferation, and differentiation of bone marrow mesenchymal stem cells. *Journal of Materials Chemistry*. 2007;17:4690–4698.

38. Jian B, Narula N, Li Q, Mohler E, Levy R. Progression of aortic valve stenosis: TGF-beta1 is present in calcified aortic valve cusps and promotes aortic valve interstitial cell calcification via apoptosis. *The Annals of Thoracic Surgery*. 2003;72(2):457–465.

39. Mohler ER. Mechanisms of aortic valve calcification. *The American journal of cardiology*. 2004;94(11):1396–402, A6.

40. Fisher CI, Chen J, Merryman WD. Calcific nodule morphogenesis by heart valve interstitial cells is strain dependent. *Biomechanics and modeling in mechanobiology*. 2012;1.

41. Chen L, Mccrate JM, Lee JC-M, Li H. The role of surface charge on the uptake and biocompatibility of hydroxyapatite nanoparticles with osteoblast cells. *Nanotechnology*. 2011;22:105708.

42. Yuan Y, Liu C, Qian J, Wang J, Zhang Y. Size-mediated cytotoxicity and apoptosis of hydroxyapatite nanoparticles in human hepatoma HepG2 cells. *Biomaterials*. 2010;31(4):730–740.

43. Xu JL, Khor K a., Sui JJ, Zhang JH, Chen WN. Protein expression profiles in osteoblasts in response to differentially shaped hydroxyapatite nanoparticles. *Biomaterials*. 2009;30(29):5385–5391.

CHAPTER 5

CALCIFIC NODULE FORMATION IN 3D CO-CULTURE: EFFECTS OF INCREASED MECHANICAL TENSION AND CYCLIC STRAIN

5.1 Abstract

Calcific aortic valve disease (CAVD) is characterized by compromised endothelial integrity and an activated or differentiated interstitial population. Heart valve progressively become thickened and calcified during CAVD, resulting in increased mechanical stresses. In this study, we determine how mechanical tension and cyclic strain regulate interstitial and endothelial interactions and phenotypes in 3D osteogenic environments. We seeded collagen hydrogels into stainless steel compression springs so there was equal constraint around the circumference of the gel. Then, using a custom cyclic stretch bioreactor system, we applied cyclic strain over a period of 7 days and demonstrated that VIC+VEC co-cultures in osteogenic environments develop calcific nodules in both static and strained cultures. Cyclic strain enhanced apoptosis in co-cultures while decreasing proliferation, suggesting an active remodeling of the collagen hydrogels in strained conditions. Overall calcium deposition was unchanged between static and stretched conditions, but the size and morphology of nodules were different between these conditions. Co-culture gels cultured statically in OGM increased myofibroblastic activation, which was then decreased when cyclically strained. However, cyclic strain increased expression of osteogenic genes in co-culture gels, suggesting osteoblastic differentiation is enhanced in part by a dynamically strained environment. Differences were present in VEC shape and area on and off calcific nodules, as well as in collagen fiber

organization within the gel. Finally, blocking cell contractility through a ROCK inhibitor demonstrated the need for cellular tension for calcification, nodule formation and myofibroblastic activation. Our results strongly advocate for a 3D platform that incorporates VEC and VIC interactions while undergoing a changing mechanical environment, which is necessary to understand how progressively increasing mechanical tension during CAVD affect the pathology of both endothelial and interstitial cells.

5.2 Introduction

The aortic valve facilitates unidirectional blood flow between the left ventricle and the aorta and is exposed to a highly complex mechanical environment[1,2]. Valve leaflets are composed of a mixed population of mainly fibroblast-like interstitial cells that are responsible for extracellular matrix maintenance and turnover[3]. Lining the valve leaflet cusps are monolayers of endothelial cells that are arranged in a cobblestone-like morphology, and are responsible for mediating signaling from the bloodstream, as well as regulating metabolic and inflammatory processes[4]. Interplay between these two cell types is crucial for maintaining homeostasis. However, during calcific aortic valve disease (CAVD), endothelial integrity is compromised through injury or activation[5,6], and the interstitial population becomes activated and shifts to include myofibroblast- and osteoblast-like phenotypes[7]. Heart valve leaflets that are normally thin and translucent become progressively thickened and calcified during CAVD[8]. Calcific nodules erupt from the ECM, and are often the result of a combination of dystrophic calcification (apoptosis-driven) and active remodeling and mineralization[9].

As the valve becomes increasingly calcified and the aortic orifice becomes obstructed, the mechanical environment deviates from normal tissue strain patterns[10–12]. There have been numerous studies documenting interstitial cell differentiation and calcification in 2D osteogenic environments[13–15], and a recent study revealing the strain-induced VIC formation of calcific nodules through dystrophic calcification[12]. Additional studies investigating effect of strain on endothelial phenotype and transformation have demonstrated a strong cellular response to changes in environmental mechanical forces[16,17]. However, the vast majority of studies investigating VIC phenotypic transitions due to strain analyze these cells in 2D culture conditions and in isolation from their neighboring endothelium. We have recently reported that interstitial cells require mechanical tension in 3D to calcify, but the calcific response of VIC is mitigated when co-cultured with VEC[18]. Within these 3D cultures, calcium deposition is present throughout the collagen matrix, but no nodules form as they do in 2D cultures. Cyclic strain applied in 3D has been shown to regulate cellular phenotype in smooth muscle cells[19] and human valve interstitial cells[20]. It is unclear, however, how increased mechanical tension and how prolonged exposure of cyclic strain will affect the protective nature of VEC in osteogenic environments, or if in co-culture, VIC phenotype and matrix reorganization may be altered.

Our objective, therefore, was to test how mechanical tension and cyclic strain regulate interstitial and endothelial interactions and phenotypes in 3D calcifying environments. We modified a previously reported[21] bioreactor system to apply cyclic strain over a period of 7 days and discovered that VIC+VEC co-cultures in osteogenic environments develop calcific nodules in both static and strained cultures. Differences between nodules arise between static and strained conditions, and matrix

fiber reorganization is apparent around nodule areas. VEC area and shape were analyzed on and off calcific nodules, and changes in VIC and VEC apoptosis, proliferation, and phenotype in osteogenic and strained environments were quantified. Finally, we determined that the formation of calcific nodules in 3D is dependent in part on cell contractility and the Rho-associated protein kinase (ROCK) pathway.

5.3 Materials and Methods

Valve Cell Isolation and Culture

Porcine aortic leaflets were harvested from a local abattoir (Shirk Meats, Dundee, NY), and valvular interstitial and endothelial cells were isolated immediately using collagenase digestion as described previously[22,23]. Briefly, aortic valve leaflets were partially digested in collagenase (600 U/ml, Worthington, Lakewood, NJ) solution for 3 minutes after which the endothelial layer was removed with a cotton swab, and then cultured normally. The remaining leaflet was then incubated overnight in collagenase solution and homogenized. Valve cells were cultured in Dulbecco's modified Eagle's medium (Invitrogen, Carlsbad, CA) supplemented with 10% fetal bovine serum (Gemini BioProducts, West Sacramento, CA) and 1% penicillin-streptomycin (Gibco, Grand Island, NY) at 37°C and 5% CO_2. For experiments, PAVIC were used between passages 4 and 8, while PAVEC were used between passages 3 and 5.

Preparation of Bioreactor Cassettes

Silicone membranes with 4 circular wells were created to apply strain to the collagen hydrogels as previously described[21]. Briefly, polydimethylsiloxane (Sylgard 184, Dow Corning, Midland, MI) was combined at a concentration of 15:1 and

degassed prior to use. The silicone was poured into negative polycarbonate molds and was left to solidify at 65°C overnight. The silicone molds were released from the polycarbonate, washed, mounted within the bioreactor cassettes, and autoclaved. Sterilized stainless steel compression springs (Lee Spring, Brooklyn, NY) were then inserted into each well prior to collagen hydrogel seeding.

3D Collagen Gel Formation

Three-dimensional (3D) collagen hydrogels were created using a modified procedure as previously described[18,23,24]. Porcine aortic valve interstitial cells (PAVIC) were suspended at 400,000 cells/ml in 3X DMEM with 10% FBS (Gemini Bioproducts, West Sacramento, CA), type I collagen (BD Biosciences, San Jose, CA) and 0.1M NaOH for a final gel concentration of 2 mg/ml. The collagen gel solution remained on ice while 125µl was seeded into each compression spring within the silicon mold. The collagen constructs were allowed to gel for 1 hour at 37°C before a subsequent seeding of a porcine aortic valve endothelial cell (PAVEC) monolayer at 50,000cells/gel. Collagen gels were either 1) PAVIC alone, 2) PAVEC alone (seeded on a PAVIC-free gel) or 3) the combination of PAVIC+PAVEC seeding. After 1 hour, gels were cultured with either control or osteogenic medium (OGM) (DMEM supplemented with 10mM β-glycerophosphate, 50µg/ml ascorbic acid and 10nM dexamethasone). The hydrogels were allowed to compact around the compression springs for 24 hours before being cyclically stretched.

Straining 3D Collagen Gels

An in-house bioreactor was used to apply a cyclic, equiaxial strain to the collagen constructs, as reported previously [21]. Briefly, this bioreactor applies uniform stretch

along the outer perimeter of the circular-shaped 3D hydrogel, anchored by compression springs. Aluminum cassettes containing the silicone mold, springs, and 3D hydrogels are mounted onto a stage constrained to vertical motion (Figure 5.1), controlled by a rotary stepper motor (34Y, Anaheim Automation, Anaheim, CA). Strain magnitude and frequency waveforms were applied to the motor via a controller module and custom software (DPN10601, Anaheim Automation, Anaheim, CA). After allowing gels to compact around the springs for 24 hours post-seeding, a 20% area strain was applied to all the collagen gels at 1Hz. Non-stretched hydrogels loaded into springs were used as static controls. All materials were sterilized via autoclaving

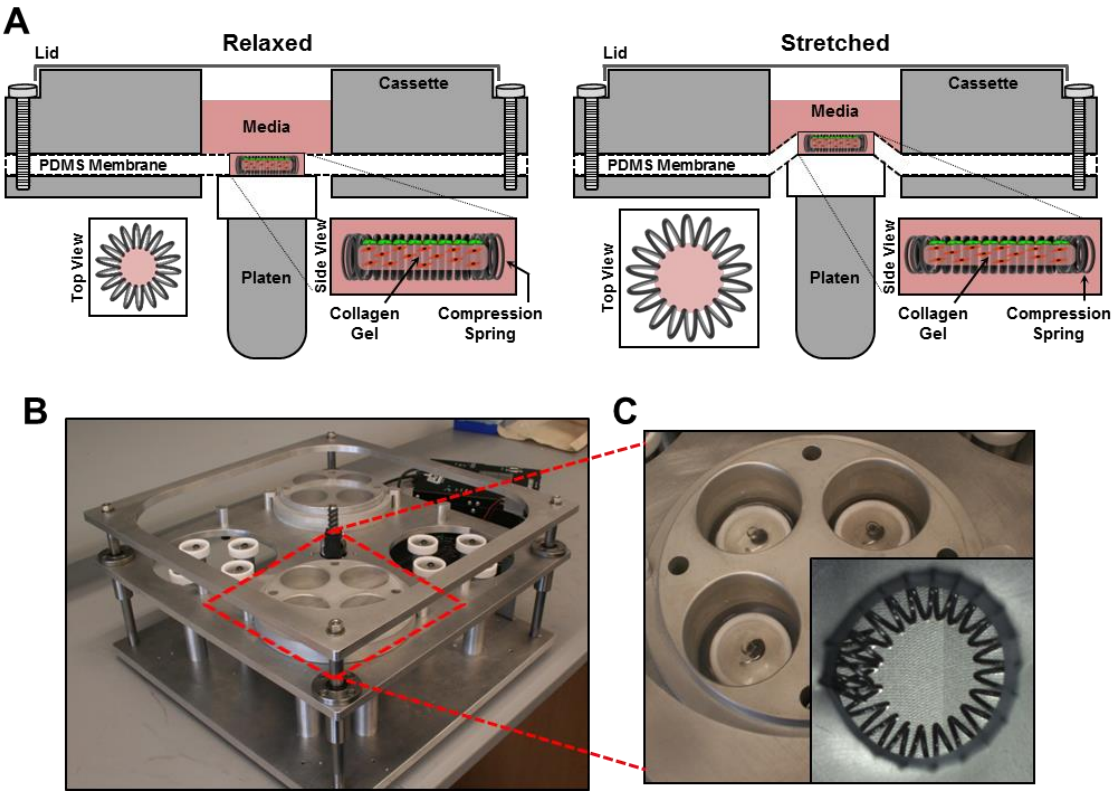

Figure 5.1: Cyclic stretch bioreactor. A) Conceptual schematic showing a cross-sectional view of collagen gel embedded within a PDMS membrane secured in an aluminum cassette in the relaxed and stretched configuration. B) Macroscopic view of the bioreactor with a total of 16 wells. C) An expanded view of the cassette and circular well within the PDMS membrane containing a stainless steel compression spring (inset).

before use, and the bioreactor system was housed in a standard tissue culture incubator, maintained at 37°C and 5% CO_2. Gels were stretched for 6 days (for a total of a 7-day culture period), with control media or OGM being changed every 2 days.

Calcium Deposition

An Alizarin Red absorbance assay was used to quantify calcium deposition within the collagen matrix, whereby the collagen hydrogels were fixed after 7 days of culture with 4% paraformaldehyde (PFA) and then stained with 40nM Alizarin Red S (ARS) dye. Calcium within the collagen matrix stained red, whereas unbound dye was removed with a series of overnight washes in PBS with gentle rocking. Gels were imaged and then incubated with 10% acetic acid to release bound ARS dye, followed by neutralization with 10% ammonium hydroxide. The concentration of dye in solution was quantified using absorbance spectroscopy at 405nm wavelength.

Nodule Analyses

Nodules formed in the collagen hydrogels were counted and their areas measured via tracing in ImageJ. To determine spatial differences, the nodules were measured as a function of radial distance from the center of the gel. These measurements were organized within a histogram to enable direct comparison between static and stretched experiments.

Quantitative qRT-PCR

Total RNA was extracted from homogenized hydrogels using the RNeasy Mini Kit (Qiagen, Valencia, CA), which was then reverse transcribed into complementary

cDNA using the iScript cDNA snythesis kit (Bio-Rad, Hercules, CA), according to the manufacturer's instructions. Quantitative real-time PCR was performed on all samples using SsoAdvanced SYBR green super mix (Bio-Rad, Hercules, CA) and a MiniOpticon or CFX96 Real-Time PCR Detection System (BioRad, Hercules, CA).

Immunohistochemistry

For cell morphology and phenotypic changes, collagen gels were fixed in 4% PFA, permeabilized with 0.2% Triton-X-100, and blocked with 10% goat serum in 1% BSA for 1 hour at 37°C. Gels were then incubated at 4°C overnight with Ki67 (proliferation), CD31 (VEC morphology), and/or αSMA (myofibroblastic activity) primary antibodies at a 1:100 concentration. Secondary antibodies at 1:100 were incubated for 2 hours following a 30 minute phalloidin (f-actin) and Draq5 (DNA) counterstain. Image z-stacks (1μm intervals) were taken with laser confocal microscopy (Leica LSM510) at fixed gain, offset, and averaging settings. Excitation lasers were sequentially activated to negate signal bleed between fluorescence channels.

Analysis of Cell Shape and Collagen Matrix Architecture

VEC and VIC were visualized via CD31 and f-actin staining, respectively. Collagen matrix fibers were visualized through reflectance confocal microscopy. Z-stacks were taken at 1μm increments through the gel. Area and circularity of VEC were quantified via ImageJ by measuring cell perimeter and shape. Circularity ranges from 0 to 1, with 1 indicating a perfect circle and 0 a straight line. Orientation of collagen fibers and VIC was achieved through the ImageJ plugin, FibrilTool. Alignment of collagen and VIC was assessed as the difference (in degrees) of fiber and cell orientation.

Apoptosis Analysis

To visualize cells undergoing apoptosis, gels were fixed with 4% PFA and stained with a terminal deoxyribonucleotidyl transferase-mediated dUTP nick end labeling (TUNEL) assay kit (Invitrogen, Grand Island, NY). Following an overnight incubation, gels were counterstained with an anti-BrdU fluorescent antibody, phalloidin (f-actin), and Draq5 (DNA). Apoptosis was measured via the percentage of TUNEL-positive cells compared to total cell nuclei, and normalized to control conditions.

Rho-kinase (ROCK) Inhibition

PAVIC+VEC co-cultures were cultured in osteogenic medium as described above, but in the presence of 10μM Y-27632 (Sigma-Aldrich, St Louis, MO) as a Rho-kinase associated protein (ROCK) inhibitor. Media was changed every other day for a total of 5 days of culture. Viability of cells within collagen hydrogels was determined via a live/dead cell viability assay (Invitrogen, Grand Island, NY), whereby percentage of live (green) cells were compared to dead (red) cells in ImageJ. Compaction of gels within the springs was measured from tracing of digital images and compared as a percentage of the original area of the gel. Measurements were normalized to control conditions. Matrix calcium deposition, apoptosis and gene expression were quantified as above.

Statistical Analysis

All data are expressed as means ± standard error, with at least 3 independent experiments per treatment. Data was analyzed statistically with JMP for Windows. Analysis of variance with Tukey's post-hoc test was used to compare differences between means (differences between means were considered significant at $P<0.05$).

5.4 Results

Nodule formation in PAVIC+VEC co-cultures

As opposed to previously reported studies where the bottom of collagen hydrogels were adhered to a cell culture dish[18], these gel constructs were seeded within a stainless steel compression spring, and either cultured statically or under cyclic strain. After 24 hours, PAVEC-only gels compacted very little around the spring, but were nonetheless adhered within the coils of the spring.

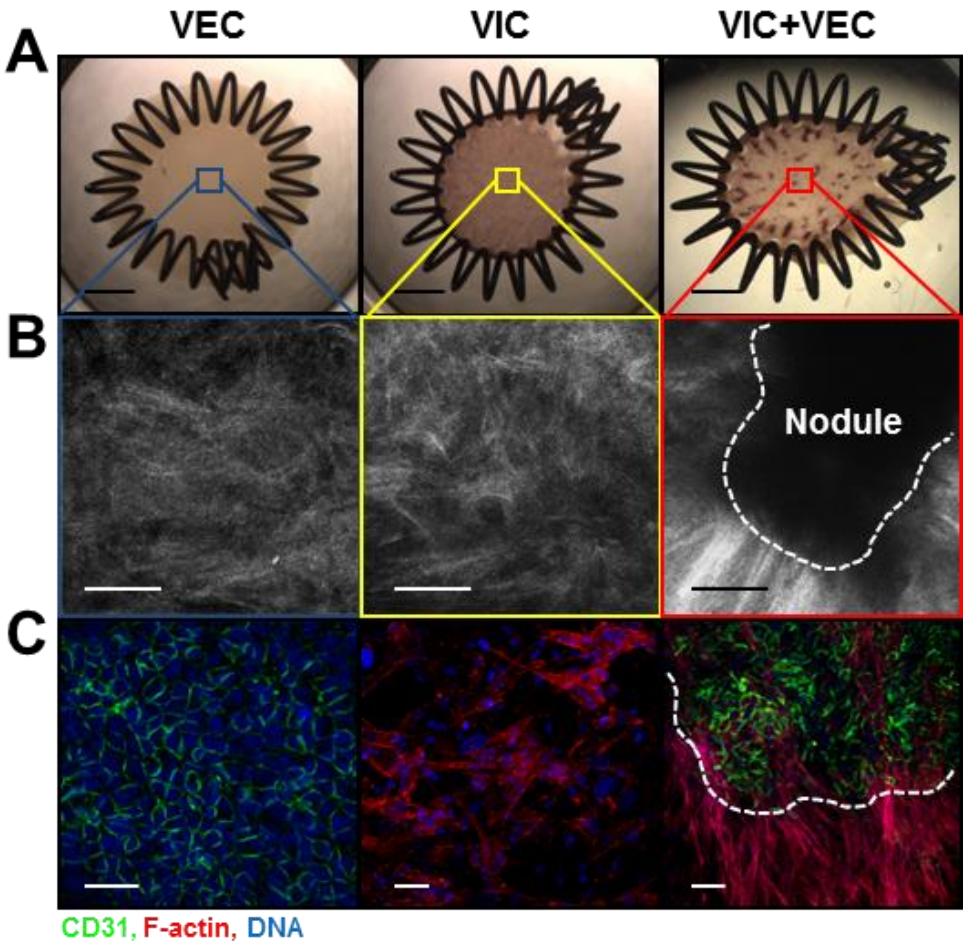

Figure 5.2: Nodule formation in VIC+VEC co-cultures. A) Representative images of VIC-only, VEC-only, and VIC+VEC co-cultures, scale bar = 2mm. B) Matrix organization of collagen visualized via confocal reflectance imaging. Nodule formation highlighted by dotted line in co-culture gels, scale bar = 20μm. C) Immunofluorescence of VIC and VEC phenotypes with 7 days of OGM culture. Co-culture nodule highlighted by dotted line, scale bar = 25 μm.

Not surprisingly, PAVIC-only gels compacted quite tightly around the coils of the spring until it was no longer able to do so freely, thus being constrained equally around the circumference of the gel. PAVIC+VEC gels cultured in osteogenic medium (OGM) compacted around the spring as well, although this condition was characterized by the formation of nodules throughout the hydrogel (Figure 5.2A).Investigation into the collagen matrix architecture via confocal reflectance imaging revealed that while the VIC- and VEC-only conditions had unorganized collagen fibers throughout the gel, the collagen fibers in the VIC+VEC OGM condition aligned radially to the nodules (Figure 5.2B). Cellular analysis shows strong CD31 expression in the endothelial cells, and spread fibroblast-like morphology of interstitial cells throughout the experimental conditions (Figure 5.2C). However, changes in the VEC shape and size arose in VIC+VEC gels near and far from nodule formations (Figure 5.3A, B). VEC covering areas away from nodules were significantly larger in area than those forming a layer around raised nodules (50.07 ± 2.12 μm^2 vs. 34.20 ± 0.89 μm^2, respectively, Figure 5.3C). Additionally, the circularity of VEC decreased in locations with nodule formations (0.70 ± 0.007 away from nodules vs. 0.65 ± 0.01 near nodules Figure 5.3D). Finally, both collagen fibers and VIC aligned in a radial direction around the nodule formations, while there was no perceptible orientation in locations away from nodules (Figure 5.3E).

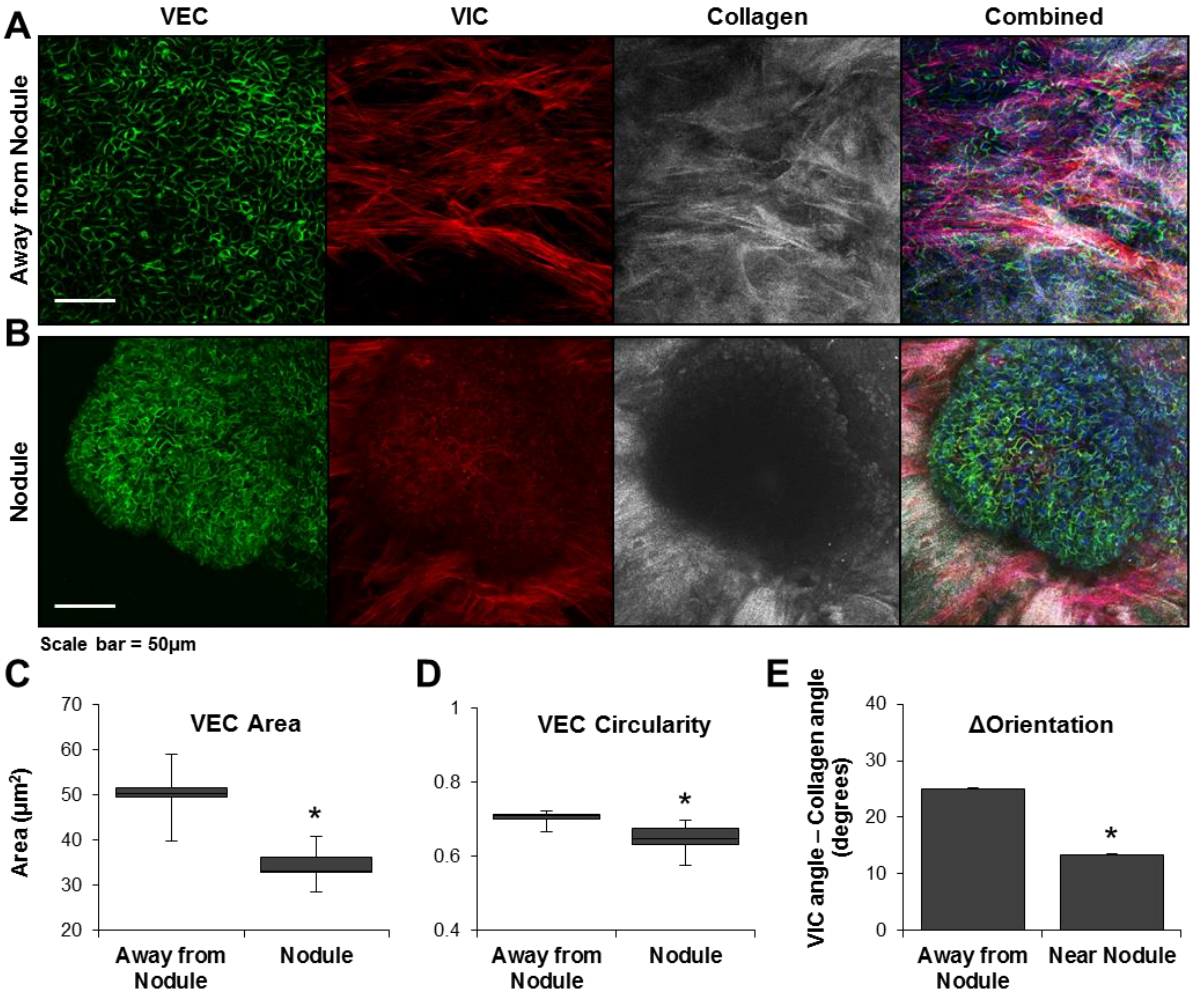

Figure 5.3: VEC shape and VIC-collagen orientation in collagen gels. A) Confocal fluorescence and reflectance of VIC+VEC collagen gels in OGM away from nodule formations. From left to right: VEC (CD31), VIC (F-actin), Collagen (reflectance), and a composite image. B) The same sequence of images of VIC+VEC collagen gels at the site of a nodule formation. Changes in C) VEC area, D) VEC circularity and E) level of collagen-VIC orientation between the nodule and non-nodule locations were quantified. n=6, *P<0.05

Cyclic strain regulate PAVIC and PAVEC gene expression and apoptosis

PAVIC-only hydrogels cultured statically in OGM for 7 days expressed significantly higher αSMA (1.55 ± 0.13 fold) vs. controls. However, both control and OGM cultures that were stretched over the 7-day period revealed significant reduction of αSMA expression (0.25 ± 0.02 fold and 0.36 ± 0.12 fold, respectively) compared to

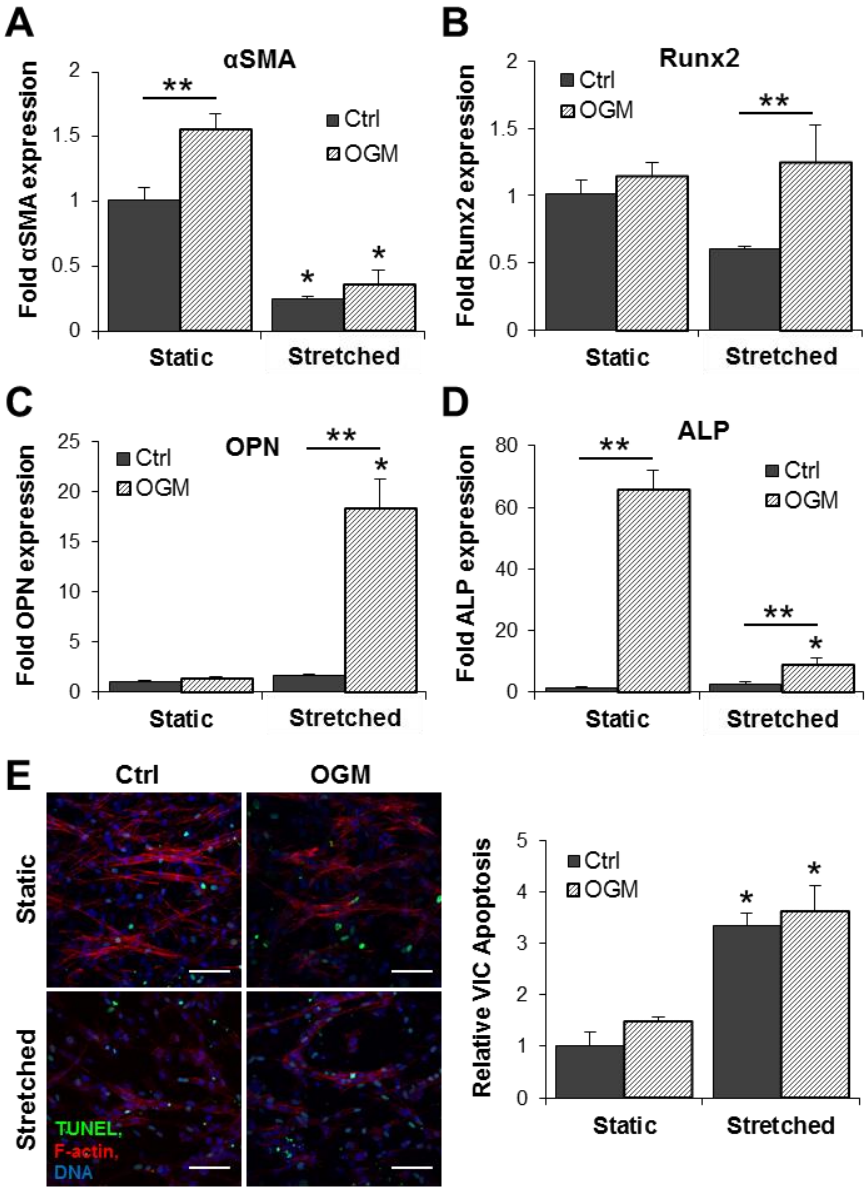

Figure 5.4: Gene expression and apoptosis of PAVIC hydrogels. Real-time PCR shows the effect of OGM and cyclic strain on myofibroblastic activation through A) αSMA expression, and osteogenic differentiation through B) Runx2, C) osteopontin (OPN), and D) alkaline phosphatase (ALP) expression. E) TUNEL immunoflourescent staining shows presence of apoptosis when cultured with OGM and strain, scale bar = 50μm. Cyclic stretch significantly increases apoptosis when compared to static cultures. Bars normalized to control condition. n=6, values are expressed as fold expression changes and are means±SEM. **P<0.05 within groups (effect of media), *P<0.05 between treatment groups (effect of strain)

the static control (Figure 5.4A). While adding OGM to PAVIC cultures in the strained conditions increased both Runx2 (0.60 ± 0.02 fold in control vs. 1.25 ± 0.28 fold in OGM) and osteopontin (1.67 ± 0.07 fold in control vs. 18.39 ± 2.88 fold in OGM) expression significantly, there was otherwise no significant change over 7 days (Figure 5.4B, C). Alkaline phosphatase (ALP) expression mimicked αSMA by increasing with OGM in both static and strained conditions (65.85 ± 6.38 fold and 9.03 ± 2.07 fold, respectively) compared to their respective controls, while overall decreasing ALP expression between static and strained conditions (Figure 5.4D). Cyclic strain also drove apoptosis in VIC-only hydrogels, increasing relative apoptosis in both control and OGM conditions (3.34 ± 0.24 and 3.62 ± 0.50, respectively) compared to static control (Figure 5.4E).

PAVEC-only hydrogels cultured statically in OGM for 7 days also expressed significantly higher αSMA (2.67 ± 0.63 fold) vs. controls. Cyclically strained control cultures revealed significant reduction of αSMA expression (0.55 ± 0.12 fold) compared to the static control, and while not significant, OGM stretched hydrogels also showed decrease αSMA expression compared to static OGM cultures (Figure 5.5A). As with PAVIC-only hydrogels, VEC-only cultures showed an increasing trend of Runx2 expression with cyclic strain (Figure 5.5B). Endothelial integrity was analyzed via VE-cadherin expression, and revealed that culture in OGM both statically and strained increased VE-cadherin expression (1.89 ± 0.37 fold and 3.01 ± 0.37 fold, respectively) compared to static controls. Cyclic stretch had a general increase of VE-cadherin expression when compared to their static counterparts (Figure 5.5C). Finally, eNOS expression was increased with OGM culture in both static and stretched conditions (2.12 ± 0.17 fold and 26.63 ± 3.24 fold, respectively) compared to static control. In addition, cyclic strain increased both control and OGM

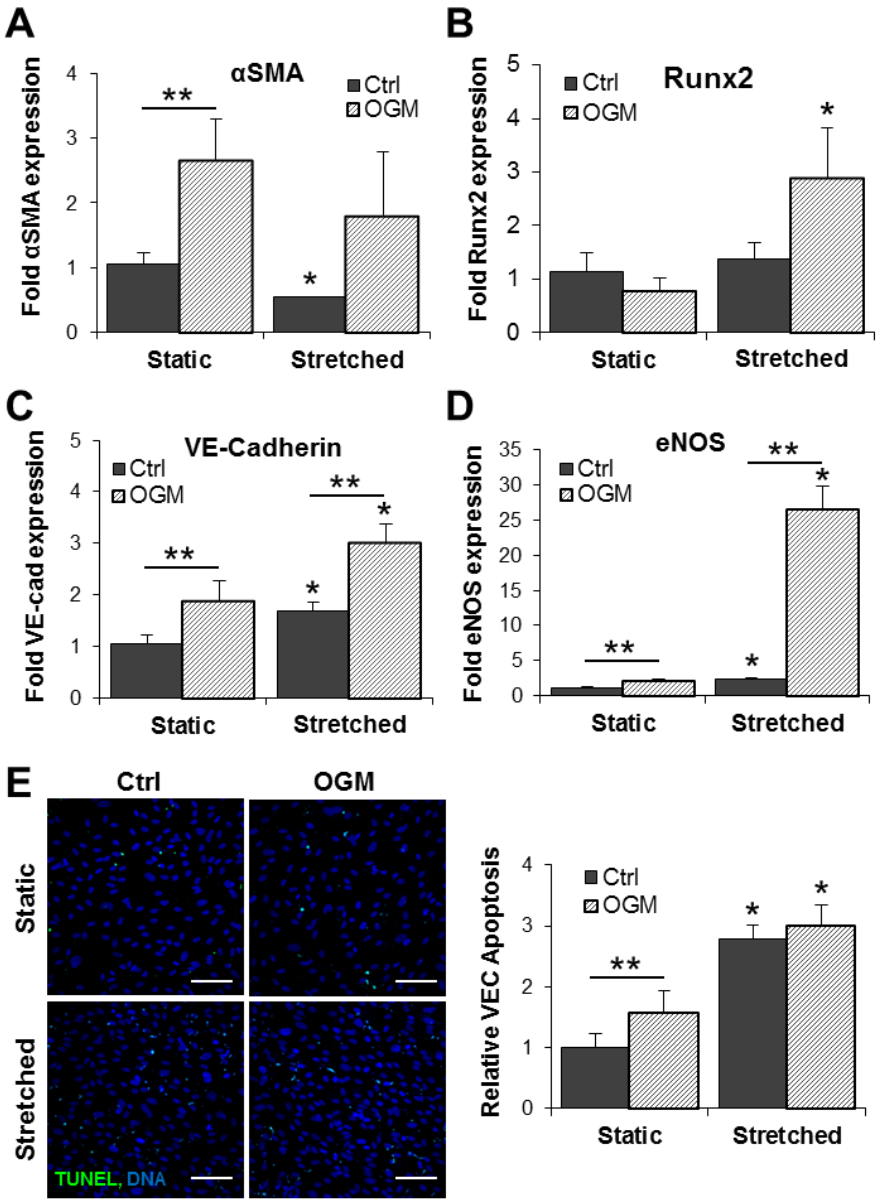

Figure 5.5: Gene expression and apoptosis of PAVEC hydrogels. Real-time PCR shows the effect of OGM and cyclic strain on myofibroblastic activation through A) αSMA expression, and osteogenic differentiation through B) Runx2 expression, and endothelial integrity via C) VE-Cadherin and D) eNOS expression. E) TUNEL immunoflourescent staining shows presence of apoptosis when cultured with OGM and strain, scale bar = 50μm. Cyclic stretch significantly increases apoptosis when compared to static cultures. Bars normalized to control condition. n=6, values are expressed as fold expression changes and are means±SEM. **P<0.05 within groups (effect of media), *P<0.05 between treatment groups (effect of strain)

levels of eNOS mRNA expression compared to their static controls (Figure 5.5D). As with PAVIC-only hydrogels, cyclic strain increased apoptosis in both control and OGM (2.79 ± 0.22 and 2.99 ± 0.35, respectively) compared to static control (Figure 5.5E). Collectively this data reveals that mechanical tension combined with an osteogenic environment drives myofibroblastic activation, osteogenic differentiation, and apoptosis in VIC and VEC. While cyclic strain appears to drive osteoblastic differentiation and apoptosis, it decreases myofibroblastic activation.

Cyclic strain regulates nodule formation and spatial heterogeneity

An Alizarin Red S (ARS) assay was used to determine whether there was calcific nodule formation in the PAVIC+VEC hydrogels in static and strained conditions. Areas with nodules stained positively (red) with ARS, indicating that nodules are indeed calcific (Figure 5.6A). Total calcium deposition within the collagen gels were analyzed, and only static OGM conditions showed significantly higher calcium deposition (1.33 ± 0.05) compared to control (Figure 5.6B). No difference was detected between static and strained conditions. However, closer analysis of the nodules themselves revealed differences in number and area between the static and strained conditions. Cyclic strain increased the total number of calcifed nodules (15.75 ± 3.53 nodules in static OGM vs. 27.1 ± 4.12 nodules in stretched OGM) within the VIC+VEC OGM gels, but significantly decreased the size of the lesions (0.07 ± 0.01mm^2 in static OGM vs. 0.02 ± 0.01mm^2 in strained OGM) (Figure 5.6C, D). Total calcium deposition remained similar between static and stretched OGM conditions due to the fact that there are fewer, but larger nodules in static conditions and more, smaller calcified nodules under strained conditions. One interesting aspect of the calcified nodules was their relative location within the collagen gels. The calcified

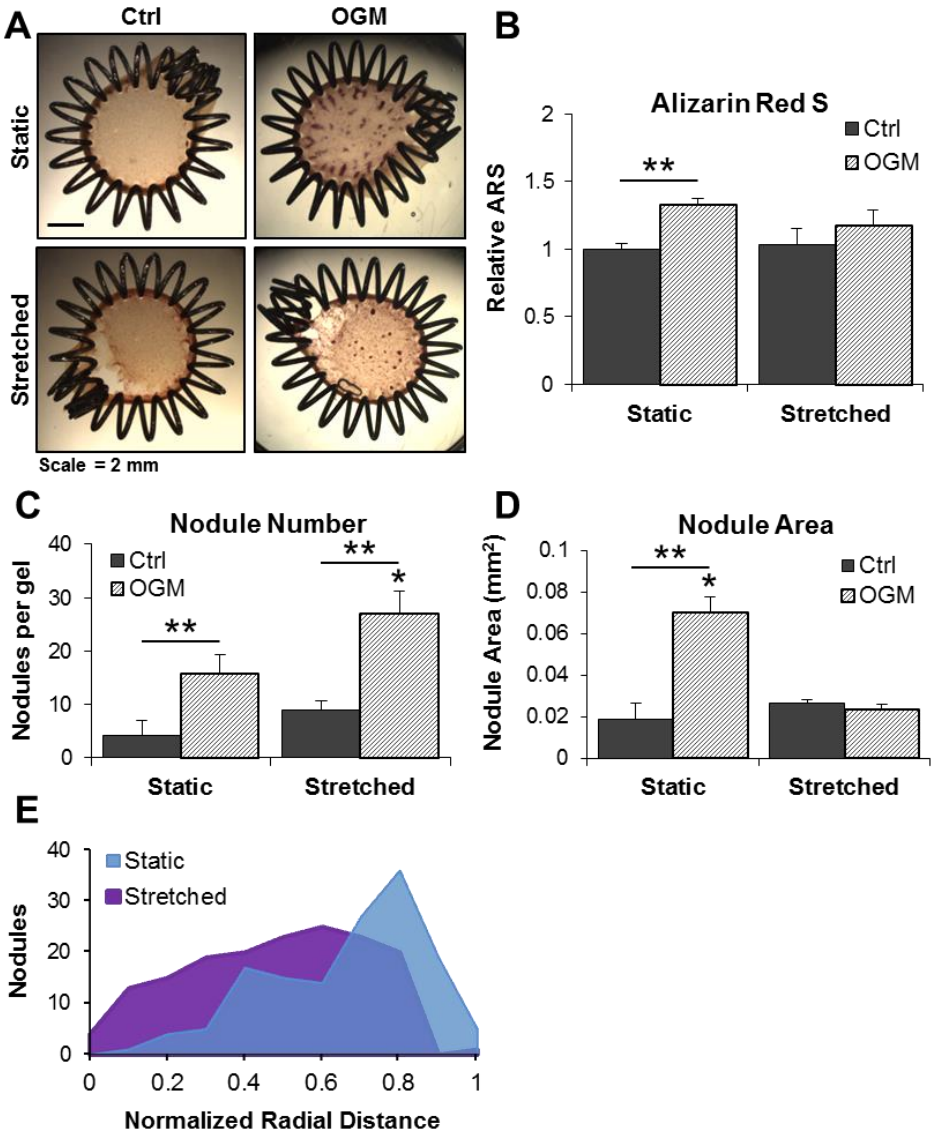

Figure 5.6: Calcific nodules in VIC+VEC co-cultures. A) Representative images of lesion formation in VIC+VEC cultured in control media and OGM, and exposed to static or stretched culture. B) Total calcium deposition within collagen gels. C) Quantification of nodule number and D) nodule size within VIC+VEC co-cultures. E) Histogram of normalized radial distance from gel center of nodules formed in co-cultures. Values are expressed as means ± SEM, *P<0.05.

nodules were measured as a function of radial distance from the center of the gel, with 0 being the midpoint of the gel, and 1 being the full radial distance from the center. The resulting histogram reveals that nodules formed in static conditions tend

to occur closer to the edge of the gel, whereas the nodules formed in stretched gels are much more evenly distributed throughout the hydrogels (Figure 5.6E). This may speak to potential stress concentrations formed in the gel during static culture that are then relieved during cyclic stretching.

Topography of nodules change with cyclic strain

Differences between nodule number and area in the static and cyclically strained conditions led us to investigate the 3-dimensional aspect of the nodule. Individual nodule height was calculated from z-stack confocal images taken from the top of the nodule to where it merged with the remaining collagen hydrogel (Figure 5.7A). Although there was some variability, cyclic strain increased average nodule height (78.55μm ± 7.06) over that of static hydrogels (50.33 μm ± 5.87) cultured in OGM

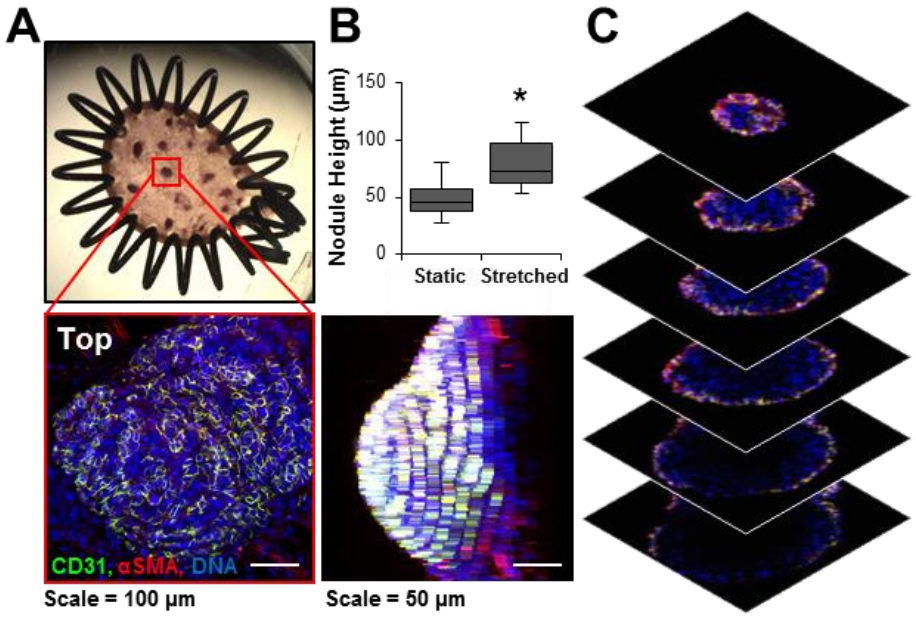

Figure 5.7: Cross-section of a nodule in VIC+VEC culture. A) Representative image of lesion formation in VIC+VEC co-culture. Zoomed immunofluorescent images of a single nodule from its top and side view highlight VIC and VEC phenotype. B) Quantification of nodule height via confocal z-stack images. Values are expressed as means ± SEM, *P<0.05. C) Exploded view of a single nodule via confocal z-stack where green = CD31, red = αSMA, and blue = DNA.

(Figure 5.7B). Projections of a z-stack through a nodule show a hypercellular lesion with a clear endothelial layer on the outer surface (Figure 5.7C). Taken together, this data suggests that while nodules forming under stretched conditions are generally smaller in area, they have a greater depth, and that there is a strong endothelial layer present at each of the nodule sites.

Strain regulates VIC+VEC apoptosis and proliferation

We next examined whether addition of OGM or cyclic strain modulated VIC+VEC apoptosis or proliferation via TUNEL assay or Ki67 immunofluorescence staining, respectively. After 7 days of culture, the number of apoptotic (green) cells in

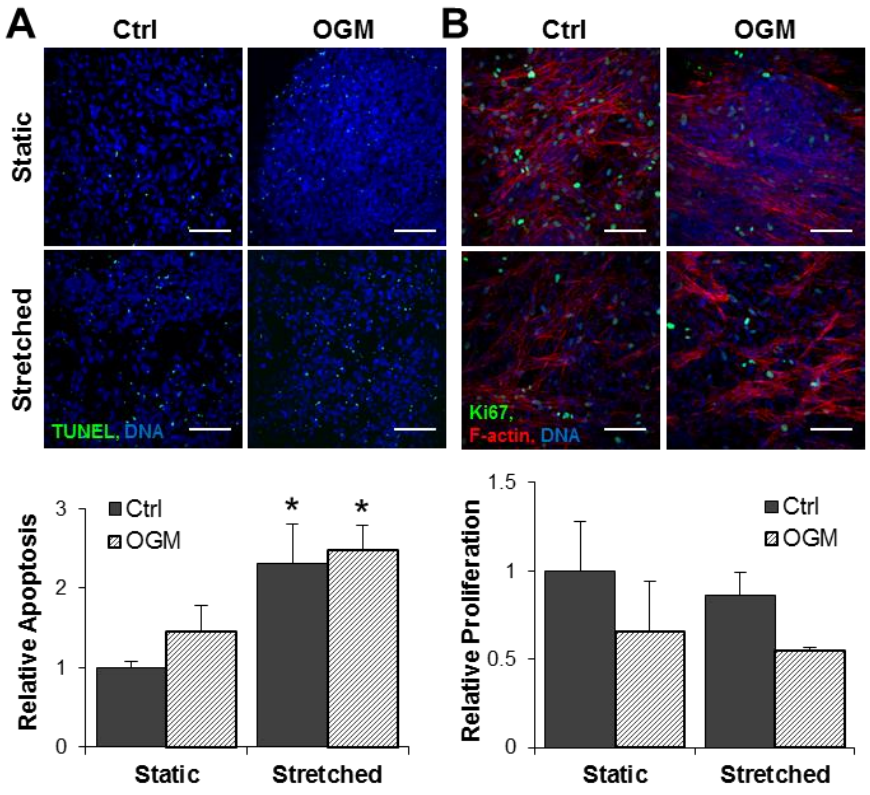

Figure 5.8: Apoptosis and proliferation of VIC+VEC co-cultures. A) TUNEL immunoflourescent staining shows presence of apoptosis when cyclically strained. B) Immunohistochemistry for Ki67 shows decreased trend of proliferation with OGM and cyclic strain. Scale bars = 50μm. Values are expressed as means ± SEM, *P<0.05.

the VIC+VEC stretched conditions increased in both the control (2.31 ± 0.49) and OGM (2.48 ± 0.30) conditions compared to the static control. However, there was no difference in apoptosis due to media in either the control or cyclically strained conditions (Figure 5.8A). This result suggests that cell death in this case is mainly driven by strain-induced apoptosis rather than osteogenic-induced apoptosis.

While there is an increase in apoptosis due to strain, there is a general downward trend of proliferation (Ki67-positive nuclei) in the strained conditions when compared to the static controls (Figure 5.8B). These findings indicate that cyclic strain enhances apoptosis while decreasing proliferation, suggesting an active remodeling of both static and strained conditions.

Myofibroblastic activation and osteogenic differentiation is modulated by strain

As in VIC- and VEC-only cultures, VIC+VEC hydrogels cultured in OGM for 7 days expressed significantly higher αSMA in static (3.47 ± 0.39 fold) and cyclically strained (2.48 ± 0.34 fold) conditions compared to the static control. However, overall αSMA expression decreased in OGM culture when the VIC+VEC gels were cyclically strained over 6 days (Figure 5.9A). This data indicates that while myofibroblastic activation increases with an osteogenic environment, it is mitigated to a certain degree with strain. Next endothelial integrity was examined through qPCR and showed an increase of VE-cadherin with OGM culture in static (4.66 ± 0.71 fold) and cyclically strained (17.34 ± 5.71 fold) conditions compared to the static control. Unlike αSMA, VE-cadherin increased significantly with strain, not only in the OGM condition, but also in the gels cultured in control medium (2.22 ± 0.433 fold) compared to static control (Figure 5.9B). Real-time PCR revealed that Runx2 was increased in the stretched OGM condition (1.97 ± 0.09 fold) compared to static control, but there was

no significant increase in the static OGM condition (Figure 5.9C). However, osteopontin significantly increased in both static OGM (7.02 ± 1.11 fold) and cyclically strained OGM (14.50 ± 5.52 fold) conditions compared to static control. Osteopontin expression was also significantly increased in the strained control condition (5.52 ± 0.39 fold) compared to its static condition (Figure 5.9D). Taken together, this data suggests that culture in osteogenic conditions increases both myofibroblastic activation and osteogenic differentiation. Myofibroblastic activation is mitigated due to strain, whereas osteogenic differentiation is enhanced when hydrogels are stretched.

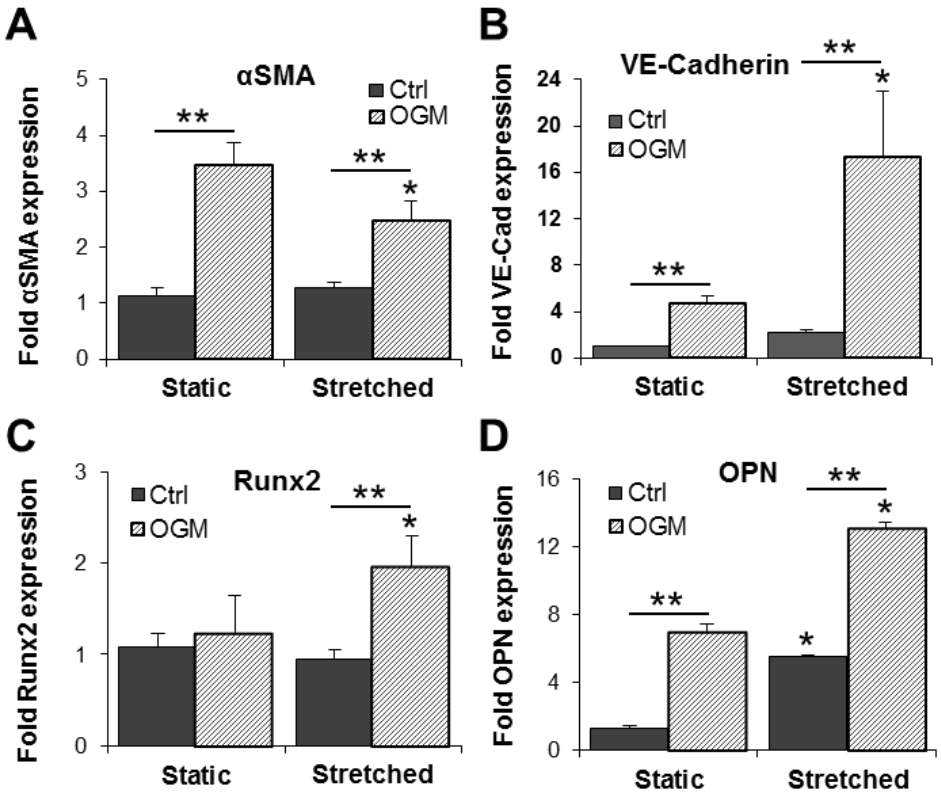

Figure 5.9: Gene expression of static and stretched PAVIC+VEC hydrogels. Real-time PCR shows the effect of OGM and cyclic strain on myofibroblastic activation through A) αSMA expression, endothelial integrity via B) VE-Cadherin and osteogenic differentiation through C) Runx2 and D) osteopontin expression. n=6, values are expressed as fold expression changes and are means±SEM. **P<0.05 within groups (effect of media), *P<0.05 between treatment groups (effect of strain).

Cell contractility is required for matrix calcification, myofibroblastic activation

PAVIC+VEC cultured for 5 days in OGM with 10μM Y-27632 failed to compact around the spring, and did not form any discernable nodules, unlike in OGM alone (Figure 5.10A). In fact, gels cultured with Y-27632 compacted significantly less than

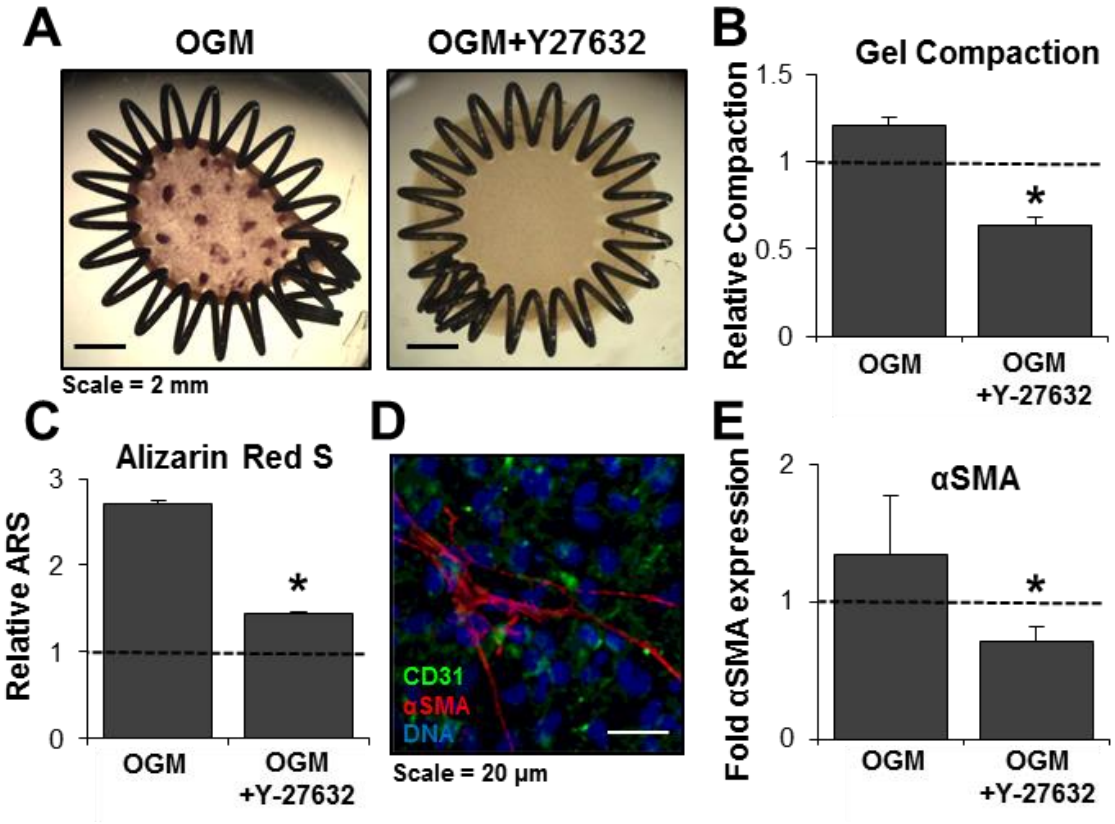

Figure 5.10: VIC+VEC static co-culture in OGM supplemented with Y-27632. A) Representative images of lesion formation (left) in PAVIC+VEC cultured in OGM, and the absence of any lesion formation when supplemented with Y-27632. B) Y-27632 decreases collagen gel compaction over 5 days and C) reduces calcium deposition within the gel. Bars normalized to control condition. D) Immunofluorescence of VIC and VEC phenotypes and E) decreased expression of αSMA in VIC+VEC OGM co-cultures with 5 day incubation of Y-27632. Bars normalized to control condition. Values are expressed as means ± SEM, *P<0.05.

PAVIC+VEC cultured in control medium (Figure 5.10B). To verify that this lack of compaction was not due to overwhelming cell death, we performed a live/dead (green/red) assay, as well as a cellular apoptosis (TUNEL) assay on the hydrogels. While there is an increase of cellular apoptosis in the hydrogels cultured in OGM+Y-27632 (4.12 ± 0.63) vs. OGM conditions (1.46 ± 0.31), the percentage of live cells in the Y-27632 cultured hydrogels were consistently above 90% viability (Figure 5.11A-D). In addition to a lack of nodule formation, the PAVIC+VEC hydrogel cultured in

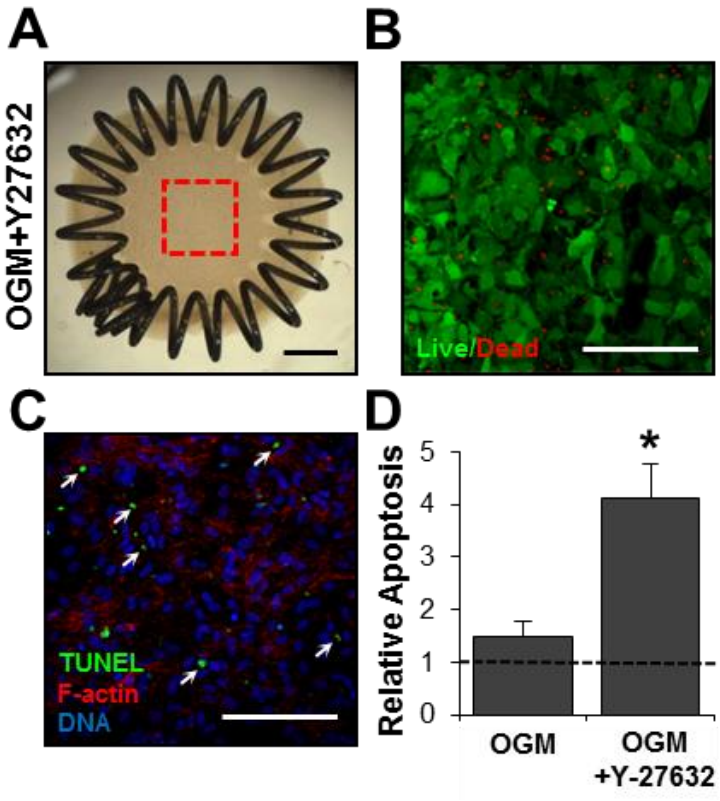

Figure 5.11: Viability of PAVIC+VEC with 5-day incubation of Y-27632. A) Representative images of PAVIC+VEC cultured in OGM when supplemented with Y-27632, red box indicating area of interest. B) Live/Dead staining reveals good cell viability with incubation with Y-27632. C) TUNEL immunoflourescent staining shows presence of apoptosis when cultured with Y27632 and D) a 5-day Y-27632 incubation significantly increases apoptosis when compared to OGM. Bars normalized to control condition. Values are expressed as means ± SEM, *P<0.05.

OGM+Y-27632 expressed significantly lower matrix calcium deposition (1.44 ± 0.03) to that of hydrogels cultured in OGM (2.70 ± 0.10). In fact, the inhibition of ROCK reduced the calcium deposition levels back to that of gels cultured in control media (Figure 5.10C). While ROCK inhibition modulated compaction and calcification, both PAVIC and PAVEC retained basic morphologies within the hydrogel, with VEC remaining in a cobblestone morphology and VIC retaining the typical spread phenotype (Figure 5.10D). However, incubation with OGM+Y-27632 decreased myofibroblastic activation of VIC as expressed by significantly reduced αSMA expression (0.71 ± 0.12 fold) as compared to hydrogels cultured in OGM alone (1.36 ± 0.42 fold) (Figure 5.10E). Collectively, these results suggest that cellular contractility through the ROCK pathway is necessary for both VIC myofibroblastic activation as well as matrix calcification.

5.5 Discussion

Calcific aortic valve disease is a serious pathology that is characterized by cellular activation and calcific nodule formation. While it is clear that the dynamic mechanical environment of the aortic valve influences both normal function and pathogenesis, it is unclear how increased tension and mechanical strain affects cellular response in a 3D environment. Prior work has focused on mechanically-driven differentiation of either VIC or VEC in isolation, and usually in a 2D setting. Here, we use a 3D collagen hydrogel construct, with the ability to be statically cultured or undergo cyclic stretch, in order to shed light on the combined cellular effects of both osteogenic and altered mechanical environments. In our static conditions, myofibroblastic and osteogenic phenotypes in VIC, as well as matrix calcium deposition, were observed after only 7 days of culture, instead of after 14 days we previously reported[18]. It has

been identified that mechanical tension is required for cellular activation and eventual pathological differentiation[25,26]. The increased mechanical tension provided by the compression springs in our 3D system may have contributed to the accelerated cellular activation processes. One of the most surprising and interesting findings during this study was the formation of calcific nodules in the VIC+VEC co-cultures in both static and strained osteogenic conditions. Not only did these nodules stain positive for calcium, but both cell types became activated and potentially contributed to this calcification. Unlike the recent 2D study where calcific nodule formation in VIC was largely driven by dystrophic calcification[12], our nodules did not have an apoptotic core, but rather were formed via cellular activity.

The loss of endothelial protection against VIC activation and calcification may be explained by our experimental conditions. Unlike our previous study where gels were only anchored on the bottom, these constructs were held around the edges, generating equal tension around the gel. It is entirely possible that the VEC experienced this anchoring in a much more dynamic way, and therefore became activated in addition to the VIC. It has been proposed that endothelial dysfunction is a key part of valve stenosis[27–29]; this may have been mimicked in this study. Cyclic strain applied in 2D has also been shown to activate VEC, affecting not only expression of endothelial markers, but also cell shape and alignment[17]. Our static culture could in fact be a model of a stenotic valve, where there is increased tension but no flexure of the valve tissue. It is interesting that in static culture, the nodules formed towards the perimeter of the gel, where stress concentrations at the spring coils could have an effect. Future studies modeling such stress concentrations in these dynamically changing constructs would be a powerful tool for predicting cell remodeling in the presence of heterogeneous strain fields. This study does show that

while cyclic strain increases osteogenic differentiation of the VIC, it decreases the myofibroblastic activation. These results mimic 2D and *ex vivo* studies showing osteoblastic differentiation of VIC due to increased cyclic strain[30,31], as well as previous reports of lowered αSMA expression in VIC after undergoing cyclic stretch for 48 hours[21].

We here demonstrate a basic mechanistic necessity of co-culture nodule formation in our 3D collagen constructs. Because the Rho/Rho kinase (ROCK) pathway is involved in cell contractility and stress fibers formation[32], we hypothesized that activation of this pathway would be necessary for cells to undergo such phenotypic changes. Indeed, when ROCK was inhibited, the cells could no longer respond or create tension in the gel, and was therefore unable to manifest the lesions within the gel, nor even calcify at all. We have shown that we can stretch a 3D co-culture dynamically for a prolonged amount of time, and that increased mechanical tension and cyclic strain does have an effect on cellular phenotype and collagen fiber organization. Calcific nodules formed in co-culture conditions under increased mechanical tension, which has been not seen in previous 3D culture conditions. Mechanical tension and strain regulates apoptosis and proliferation, as well as myofibroblastic activation, osteoblastic differentiation and calcification. These findings suggest that the behavior and interplay of VIC and VEC in valve calcification is dependent on its mechanical environment, and is a key step in understanding how the progressively increasing mechanical tension on valve leaflets during CAVD affect the pathology of both cell types within the valve.

REFERENCES

1. Arjunon S, Rathan S, Jo H, Yoganathan AP. Aortic valve: mechanical environment and mechanobiology. *Annals of biomedical engineering*. 2013;41(7):1331–46.

2. Hinton RB, Yutzey KE. Heart valve structure and function in development and disease. *Annual review of physiology*. 2011;73:29–46.

3. El-Hamamsy I, Chester AH, Yacoub MH. Cellular regulation of the structure and function of aortic valves. *Journal of Advanced Research*. 2010;1(1):5–12.

4. Leask RL, Jain N, Butany J. Endothelium and valvular diseases of the heart. *Microscopy research and technique*. 2003;60(2):129–37.

5. Mohler ER. Mechanisms of aortic valve calcification. *The American journal of cardiology*. 2004;94(11):1396–402, A6.

6. Müller AM, Cronen C, Kupferwasser LI, Oelert H, Müller K-M, Kirkpatrick CJ. Expression of endothelial cell adhesion molecules on heart valves : up-regulation in degeneration as well as acute endocarditis. *Journal of Pathology*. 2000;191:54–60.

7. Chen J-H, Simmons C a. Cell-matrix interactions in the pathobiology of calcific aortic valve disease: critical roles for matricellular, matricrine, and matrix mechanics cues. *Circulation research*. 2011;108(12):1510–24.

8. Dweck MR, Boon N a, Newby DE. Calcific aortic stenosis: a disease of the valve and the myocardium. *Journal of the American College of Cardiology*. 2012;60(19):1854–63.

9. Freeman R V, Otto CM. Spectrum of calcific aortic valve disease: pathogenesis, disease progression, and treatment strategies. *Circulation*. 2005;111(24):3316–26.

10. Balachandran K, Sucosky P, Jo H, Yoganathan AP. Elevated cyclic stretch alters matrix remodeling in aortic valve cusps: implications for degenerative aortic valve disease. *American journal of physiology. Heart and circulatory physiology*. 2009;296(3):H756–64.

11. Liu AC, Joag VR, Gotlieb AI. The emerging role of valve interstitial cell phenotypes in regulating heart valve pathobiology. *The American journal of pathology*. 2007;171(5):1407–18.

12. Fisher CI, Chen J, Merryman WD. Calcific nodule morphogenesis by heart valve interstitial cells is strain dependent. *Biomechanics and modeling in mechanobiology*. 2012;1.

13. Benton J a, Kern HB, Leinwand L a, Mariner PD, Anseth KS. Statins block calcific nodule formation of valvular interstitial cells by inhibiting alpha-smooth muscle actin expression. *Arteriosclerosis, thrombosis, and vascular biology*. 2009;29(11):1950–7.

14. Kennedy J a, Hua X, Mishra K, Murphy G a, Rosenkranz AC, Horowitz JD. Inhibition of calcifying nodule formation in cultured porcine aortic valve cells by nitric oxide donors. *European journal of pharmacology*. 2009;602(1):28–35.

15. Cloyd KL, El-Hamamsy I, Boonrungsiman S, Hedegaard M, Gentleman E, Sarathchandra P, Colazzo F, Gentleman MM, Yacoub MH, Chester AH, Stevens MM. Characterization of Porcine Aortic Valvular Interstitial Cell "Calcified" Nodules. Aikawa E, ed. *PLoS ONE*. 2012;7(10):e48154.

16. Metzler SA, Pregonero CA, Butcher JT, Burgess SC, Warnock JN. Cyclic strain regulates pro-inflammatory protein expression in porcine aortic valve endothelial cells. *The Journal of heart valve disease*. 2008;17(5):571–7; discussion 578.

17. Balachandran K, Alford PW, Wylie-Sears J, Goss J a, Grosberg A, Bischoff J, Aikawa E, Levine R a, Parker KK. Cyclic strain induces dual-mode endothelial-mesenchymal transformation of the cardiac valve. *Proceedings of the National Academy of Sciences of the United States of America*. 2011;108(50):19943–8.

18. Richards J, El-Hamamsy I, Chen S, Sarang Z, Sarathchandra P, Yacoub MH, Chester AH, Butcher JT. Side-specific endothelial-dependent regulation of aortic valve calcification: interplay of hemodynamics and nitric oxide signaling. *The American journal of pathology*. 2013;182(5):1922–31.

19. Butcher JT, Barrett BC, Nerem RM. Equibiaxial strain stimulates fibroblastic phenotype shift in smooth muscle cells in an engineered tissue model of the aortic wall. *Biomaterials*. 2006;27(30):5252–8.

20. Ferdous Z, Jo H, Nerem RM. Differences in valvular and vascular cell responses to strain in osteogenic media. *Biomaterials*. 2011;32(11):2885–93.

21. Gould RA, Chin K, Santisakultarm TP, Dropkin A, Richards JM, Schaffer CB, Butcher JT. Cyclic strain anisotropy regulates valvular interstitial cell phenotype and tissue remodeling in three-dimensional culture. *Acta biomaterialia*. 2012;8(5):1710–9.

22. Gould RA, Butcher JT. Isolation of valvular endothelial cells. *Journal of visualized experiments : JoVE*. 2010;(46):1–6.

23. Butcher JT, Nerem RM. Porcine aortic valve interstitial cells in three-dimensional culture: comparison of phenotype with aortic smooth muscle cells. *The Journal of heart valve disease*. 2004;13(3):478–85; discussion 485–6.

24. Butcher JT, Nerem RM. Valvular endothelial cells regulate the phenotype of interstitial cells in co-culture: effects of steady shear stress. *Tissue engineering*. 2006;12(4):905–15.

25. Grinnell F. Fibroblast biology in three-dimensional collagen matrices. *Trends in Cell Biology*. 2003;13(5):264–269.

26. Chen JH, Chen WLK, Sider KL, Yip CYY, Simmons C a. β-Catenin Mediates Mechanically Regulated, Transforming Growth Factor-β1-Induced Myofibroblast Differentiation of Aortic Valve Interstitial Cells. *Arteriosclerosis, Thrombosis, and Vascular Biology*. 2011;31:590–597.

27. Poggianti E, Venneri L, Chubuchny V, Jambrik Z, Baroncini LA, Picano E. Aortic valve sclerosis is associatedwith systemic endothelial dysfunction. *Journal of the American College of Cardiology*. 2003;41(1):136–141.

28. Butcher JT, Nerem RM. Valvular endothelial cells and the mechanoregulation of valvular pathology. *Philosophical transactions of the Royal Society of London. Series B, Biological sciences*. 2007;362(1484):1445–57.

29. Durbin AD, Gotlieb AI. Advances towards understanding heart valve response to injury. *Cardiovascular Pathology*. 2002;11(2):69–77.

30. Smith KE, Metzler S a, Warnock JN. Cyclic strain inhibits acute pro-inflammatory gene expression in aortic valve interstitial cells. *Biomechanics and modeling in mechanobiology*. 2010;9(1):117–25.

31. Balachandran K, Sucosky P, Jo H, Yoganathan AP. Elevated cyclic stretch induces aortic valve calcification in a bone morphogenic protein-dependent manner. *The American journal of pathology*. 2010;177(1):49–57.

32. Gu X, Masters KS. Role of the Rho pathway in regulating valvular interstitial cell phenotype and nodule formation. *American journal of physiology. Heart and circulatory physiology*. 2011;300(24):H448–H458.

CHAPTER 6

CONCLUSIONS AND FUTURE DIRECTIONS

6.1 Conclusions

Calcified aortic valve disease (CAVD) is an increasingly prevalent pathology that often manifests in the degenerative calcification of the valve tissue. Present in up to 2.5% of the total population, CAVD becomes increasingly prevalent with age, appearing in about 13% of those over the age of 75[1]. It has recently become clear that the calcific lesions that form on valve leaflets are unique from other vascular calcifications, as atherosclerotic treatments have been ineffective as a clinical therapeutic against CAVD[2]. There remains a need to clarify a mechanistic reason for the initiation of valve pathogenesis, as well as an in-depth analysis of the calcified lesions that form as a result of the disease.

Healthy aortic valves leaflets are composed of a mixed population of mainly fibroblast-like interstitial cells that are responsible for extracellular matrix maintenance and turnover[3], and monolayers of endothelial cells that are responsible for mediating signaling from the bloodstream, as well as regulating metabolic and inflammatory processes[4]. Interplay between these two cell types is crucial for maintaining homeostasis. However, during CAVD, endothelial integrity is compromised through injury or activation[5,6], and the interstitial population becomes activated and shifts to include myofibroblast- and osteoblast-like phenotypes[7]. While many have successfully mimicked disease-like cellular responses to various chemical[8–11] and mechanical stimuli[12–15], these studies are often performed in 2D environments, and the two valve cell types are studied independently.

The ultimate goal of this thesis was to develop a 3D construct in which the interplay between valve endothelial (VEC) and valve interstitial cells (VIC) could be illuminated in various calcification-prone environments. The completion of this work yielded insights into cellular response to osteogenic, physically mineralized, and altered mechanical environments, which could be used to identify potential therapeutic targets or early diagnosis strategies in the future. A 3D hydrogel construct was first developed for the co-culture of interstitial and endothelial cells, which is more physiologically relevant than current 2D models. Under osteogenic conditions, endothelial cells were found to have a protective effect against VIC activation and calcification (Chapter 2). Next, the mineralized lesions and surrounding organic tissue in calcified valves were characterized and found to have a heterogeneous composition of apatite (Chapter 3). These findings prompted the use of synthetically derived hydroxyapatite nanoparticles of two different sizes and crystallinities in order to better evaluate cellular response to a highly mineralized matrix, characteristic of later stages of valve disease (Chapter 4). Finally, the effects of an altered mechanical environment, as is typical in valve disease, were examined by increasing mechanical tension in 3D hydrogel constructs and applying cyclic mechanical strain (Chapter 5). This chapter discusses the major findings of this thesis, as well as identifying potential future directions.

Chapter 2 highlights the development of a 3D construct with which we could analyze individual and interactive cellular responses to various stimuli. We demonstrated that mechanical stress is necessary in the activation of VIC and the calcium deposition within the collagen matrix in osteogenic conditions. We established that VEC protect against the myofibroblastic activation and osteogenic differentiation in VIC, as well as mitigate calcium deposition in response to an

osteogenic stimulus. After further investigation, we identified endothelial-secreted nitric oxide (NO) as a natural antagonist of the aforementioned aspects of calcific aortic valve pathogenesis. This supports the increasing evidence of NO having beneficial effects on valve matrix stiffness[16], as well as inhibiting calcific nodule formation in 2D[9]. Due to the fact that calcified nodules in diseased human aortic valves occur almost exclusively on the aortic surface[17], we examined the side-specific nature of VEC, and their contributions to inhibiting calcification. We demonstrate that aortic-sided VEC express less eNOS protein and cGMP than ventricularis-sided VEC, both at baseline and under physiological flow conditions. We further confirmed side-specific eNOS protein expression in normal and calcific human aortic valves via immunohistochemistry. This study provides a new 3D platform to effectively incorporate endothelial and interstitial cell responses due to various external stimuli, to better understand the biological and pathobiological regulation of aortic valve function.

While we provide some mechanistic insights in Chapter 2 regarding interstitial activation due to chemical osteogenic stimuli, we sought to further investigate endothelial and interstitial responses to the mineral crystals within the tissue matrix in diseased valves. To achieve this, we first demonstrated spatial differences in mineral crystallinity and composition in both mature calcific nodules and the surrounding valve tissue. In Chapter 3, we identify the mineral in calcific nodules as crystalline apatite, and confirm the presence of poorly crystalline apatite in the surrounding matrix, in agreement with previous reports in the literature[18–21]. We incorporated a powerful imaging technique in human calcified valves in order to quantify mineral composition parameters such as the degree of tissue mineralization, carbonate substitution, crystallinity and acid phosphate. We demonstrate that more severely

calcified valves have increased mineralized tissue content, and that new mineral formation occurred on the edges of mature mineral. We identified regions of compact mineral with a higher mineral:matrix ratio than that of bone. These regions were directly adjacent to regions with lower mineral content, which demonstrates the extreme heterogeneity of the valve mineral. This work highlights the varied structure and composition of mineral lesions in calcified valves, and agree with alternate studies[22] that suggest valve calcification may in fact form by a different mechanism than that of bone.

In Chapter 4, we successfully incorporated synthetic hydroxyapatite nanoparticles into our 3D hydrogel system to evaluate cellular response to a mineral-containing matrix environment. Based on our findings of compositional differences in valve mineral in Chapter 3, we used HA particles of two different particle sizes and crystallinities. Neither particle caused significant cell death, nor induced apoptosis. However, we demonstrate myofibroblastic activation and osteoblastic differentiation in VIC due to culture with the smaller, less crystalline HA. Calcium deposition within the collagen matrix corresponded with cellular activation, as there was higher calcification due to exposure to the smaller, less crystalline HA particles. Interestingly, incubation with HA particles mitigated VEC protecting against VIC activation and calcification, as co-cultures yielded the same response to the less crystalline particles. HA nanoparticles that were larger and more crystalline did not induce an activated or osteogenic phenotype in VIC, and did not cause matrix calcium deposition within the collagen gel, most likely due to differences in specific surfaces. This study provides insight into cellular responses to a mineralized matrix, characteristic of a later stage of valve disease, whereby crystallinity or size of HA particles can drive different

responses. The mineral-containing 3D platform also highlights the susceptibility of VEC to losing the protective phenotype it displays in early valve disease models[23,24].

In Chapter 5, we highlight the importance of the mechanical environment on cellular activity by adding increased mechanical tension or cyclic strain to our 3D co-culture constructs. We demonstrate that unlike previous chapters where collagen gels adhered to a cell culture dish, gels constrained equally around the circumference of the gel and cultured in osteogenic conditions elicit nodule formation consisting of both endothelial and interstitial cells. The addition of cyclic strain further altered the nodule formation, yielding smaller, but more frequently occurring nodules throughout the gel. We confirm that the nodules formed are in fact calcific, and they form more uniformly throughout the gel when cyclic strain is applied. Unlike 2D cultures, where calcific nodules are driven by apoptosis[12], these cell-rich nodules show signs of active osteogenic activity. Osteogenic media induces myofibroblastic activation in VIC, which is then mitigated by the application of cyclic strain. However, the same is not true of osteoblastic differentiation, as it does not change between static and stretched conditions. As was seen in the previous chapter, increased tension mitigated the ability of VEC to protect against VIC activation and calcium deposition. Indeed, VEC lining calcific nodules in both static and stretched conditions had altered shape and size compared to those cells away from nodules, which could indicate an endothelial transformation. Finally, we demonstrate that nodule formation in gels is due in part to Rho kinase (ROCK) signaling, as inhibiting Rho kinase rendered the cells unable to successfully compact the gel, much less form calcific nodules. Inhibition of ROCK decreased calcium deposition within our collagen hydrogel co-cultures, as well as decreasing myofibroblastic activation even while exposed to osteogenic

environments. Our data corroborates recent studies that indicate Rho kinase pathways are essential to VIC activation and downstream calcification[25–27].

Overall, this body of work has made significant advancements in understanding individual and incorporative cellular responses to osteogenic, mineralized and mechanical 3D environments. This work has contributed to the emerging appreciation that 3-dimensional co-cultures are vital to mechanistic understanding of valve pathogenesis. To our knowledge, we are the first to show myofibroblastic activation and osteogenic differentiation of valve cells in response to 3D culture with HA mineral, as well as calcific nodule formation in anything other than in 2D valve cell culture. Our 3D platform shows great promise for the future, and could enable direct screening of molecular mechanisms of calcification and testing of potential molecular inhibitors.

6.2 Future Directions

Although the work presented in this dissertation contributed significantly to our understanding of valve cell response to various 3D calcific environments, additional work is needed to fully understand how mineral and mechanical stimuli drive valve pathogenesis. Future directions of this work include alterations to the hydrogel construct, dose responses to mineral particles, and the introduction of more physiologically relevant anisotropic strain.

Alterations of 3D collagen construct

The work presented in this dissertation reveals the importance of using valve endothelial and interstitial cells in a co-culture setting to answer questions regarding cellular behavior and interaction. However, all of the studies presented here utilize a

2mg/ml collagen gel construct, and did not explore how altering stiffness or components of the matrix might drive cell behavior. Stiffness is a key regulator in valve disease; indeed, as CAVD progresses, the valve cells are exposed to an ever stiffening environment[28]. The stiffness of collagen gels can be modulated by crosslinking the collagen modules in various ways, including ribose glycation and photo-crosslinking[29,30]. While valve interstitial cells have been shown to calcify when cultured on stiffer matrices[13], the cells were not cultured in a 3D environment, and they did not take into account interactions with an endothelial monolayer. By altering our current model, the extent to which endothelial cells can modulate interstitial activation due to increasing stiffness could be explored.

Osteogenic media with physiological concentrations of phosphate

A standard practice to induce osteogenic differentiation and calcification of cells in culture is to combine cell culture media with 10mM β-glycerophosphate (BGP), 50μg/ml ascorbic acid and 100nM dexamethasone. However, the use of such a high concentration of BGP, combined with the calcium found in the standard DMEM media, has been shown to cause the deposition of hydroxyapatite due to the over-saturation of phosphate regardless of cellular activity[31]. Lower concentrations of BGP would reveal whether calcium deposition was indeed due to differentiated cellular activity, rather than an over-saturation of phosphate within the cell culture media. Alternatively, addition of phosphatase inhibitors into the media would prevent hydrolysis of BGP[31].

Examining HA uptake as activation mechanism

Chapter 4 of this dissertation demonstrates that the uptake of aggregates of HA nanoparticles occur within interstitial cells in 3D culture. Visualization of HA particle aggregates was achieved through confocal reflectance imaging, but future studies should include a more robust method of imaging. FITC-labeled HA nanoparticles were successfully imaged via confocal microscopy, which made HA uptake into liver cells much more easily discernable[32]. Rigorous attention would have to be made that the addition of a fluorescent label does not alter the HA shape and charge. Further cellular imaging via TEM would give a greater understanding about cellular processes of HA uptake during incorporated culture. I hypothesize that cellular uptake of HA corresponds with apoptosis-driven calcification, and that this uptake is dependent on particle size, but future studies need to be conducted for verification.

Mechanistic understanding of HA-induced cell activation

Chapter 4 describes a unique phenomenon whereby crystallinity or particle size drives myofibroblastic activation, osteogenic differentiation, and calcification of valve cells by incorporating synthetically derived HA nanoparticles into 3D collagen matrices. One of the most interesting findings was the fact that the previously protective VEC no longer mitigated VIC activation, and could not inhibit matrix calcium deposition. It is currently unclear, however, by what mechanism the HA particles drive cellular activation. Osteopontin is thought to play a regulatory role in biomineralization, and is known to be an effective inhibitor of hydroxyapatite formation and growth[33]. However, dephosphorylation blocks the ability of osteopontin to inhibit hydroxyapatite formation[34]. It has been suggested that alkaline phosphatase (ALP), a key phenotypic marker of osteoblasts, may dephosphorylate osteopontin, and that

these two proteins have opposing effects on each other[35]. Our work in Chapter 4 highlights increase of osteopontin levels with HA culture, although future work is needed to identify phosphorylation states. Endothelial activation is also documented with the culture of hydroxyapatite microcrystals[36], which could account for the lack of protection against further VIC activation seen in our study. A possible connection between eNOS activation in VEC, as described in Chapter 2, with ALP and osteopontin dephosphorylation could be a future avenue of investigation.

Mineral composition correlations in mineral lesions

The work described in Chapter 3 is only the beginning of what can be accomplished with the quantification of mineral composition characteristics. One limitation of this study was the low sample size of the calcified valve leaflets. Scanning more leaflets of variable calcific severity will give us better understanding of trends in mineral composition. Also, the data presented in this study represent the means of pixel intensity values of the various mineral parameters. However, the vast majority of literature, as well as our own findings demonstrate the extreme heterogeneity of the mineral found within calcified valves. Indeed, FTIR imaging analysis revealed mineral with varying mineral:matrix ratios as well as crystallinities within areas of close proximity. Future studies could focus on more intensive individual correlations between various parameters within each imaging section, to better understand the progressive maturation of the valve mineral. Analyzing the degree of mineral:matrix relative to crystallinity or mineral:matrix relative to acid phosphate substitutions, for example, would yield information on the crystalline structure of the highly mineralized tissue and the extent of new mineral formation as a function of high or low mineral content.

Anisotropic strain

Chapter 5 describes a custom bioreactor used to apply cyclic strain to 3D constructs containing valve cell co-cultures, in order to evaluate how increased mechanical tension and cyclic stretch affects cellular interactions and responses. However, these gels were constructed in the shape of a circle, which means that equiaxial strain was applied in an isotropic manner to the cells within each gel. However, the aortic valve leaflets exhibit anisotropic strain due to the greater tensile strength exhibited by the collagen aligned in the circumferential direction[37]. By altering the shape of the gel construct, we can apply anisotropic strain to the gels. As was previously reported in our lab, by using an increasingly elliptical shape, we can evaluate biaxial 2:1 and 4:1 strain profiles[38]. By applying anisotropic strain, we could evaluate remodeling of the collagen matrix, as well as directing cellular phenotype and activity.

Pathological strain

The work in Chapter 5 describes how mechanical stretch alters calcific nodule formation and cell phenotype. We applied 20% area strain to our collagen gel constructs, which is within the range of what is thought to be “physiological”. However, exposing valve leaflets[15] and valve cells[39,40] to pathological levels of stretch has been shown in induce inflammation, transformed cell phenotypes, and calcification. By increasing the level cyclic stretch, we could evaluate changes in calcific nodule formation, calcium deposition and VIC activation, as well as endothelial response. It may be that when exposed to pathological levels of stretch, calcific nodule formation within VIC+VEC co-cultures will be similar to that of static, increased tension conditions.

Combined mechanical alterations

As has been previously stated, the aortic valve is exposed to an extremely complex mechanical environment. *In vitro* and *ex vivo* studies have explored how mechanical forces such as strain[12,14,39,40], shear stress[41,42], pressure[43], and stiffness[13] have played a role in regulating interstitial or endothelial cell behavior. However, critical knowledge can be gained from a study whereby valve cells are subjected to the combination of several mechanical stimuli, which would more closely mimic the valve's native state, and help to clarify how the interplay between mechanical stimuli drive cellular response. A recent study in valve cells combines cyclic strain and pressure, and demonstrate that the cellular response to the combined stimuli is different than that of each of the individuals[39]. A separate group attempting to create a better dynamic culture system for tissue engineered heart valves utilized a novel system that combines cyclic stretch and a fluid shear stress[44]. The benefit of a custom bioreactor system is that it can be modified to ask different mechanistic questions. Adding a fluid shear component to the current cyclic stretch bioreactor would evaluate the transformative potential of VEC due to shear stress in combination with the dynamic stretching of the whole gel construct. A combined mechanical stimuli model is a promising avenue for a better understanding of how the complex and progressively changing mechanical environment drives cellular activation and valve pathogenesis.

Human valve cells

The entirety of the *in vitro* work presented in this dissertation was done with porcine aortic valve cells, using various means to induce calcification. While there is a long history of using porcine valves due to their similar structure and composition to

that of human valves, it would be incredibly powerful to use human valve cells to answer mechanistic calcification questions. It is already clear the importance of using human valve cells to investigate mechanisms of calcification. Human valve interstitial cells have been shown in 2D cultures to be sensitive to osteogenic media whereby they expressed osteoblastic markers and increased alkaline phosphatase activity[45], while another 3D study evaluated the role of strain in activation of human VIC[14]. Whole human valve leaflets have been used in various studies investigating strain[26], and tissue engineering efforts have been made using human valve cells for a tissue engineered valve replacement[46,47]. Surprisingly few studies have focused on human endothelial cells, and there is currently no work being done involving the co-culture of human endothelial and interstitial cells. Using our 3D platform, variability in diseased valve cell phenotype could be examined from patient to patient, which could lead to an earlier diagnostic marker of valve disease. This system could also probe the question of whether or not diseased valve cells could be rescued, which could have incredible implications for screening potential therapeutic targets for the treatment of valve disease.

REFERENCES

1. Mozaffarian D, Benjamin EJ, Go a. S, Arnett DK, Blaha MJ, Cushman M, de Ferranti S, Despres J-P, Fullerton HJ, Howard VJ, Huffman MD, Judd SE, Kissela BM, Lackland DT, Lichtman JH, et al. Heart Disease and Stroke Statistics--2015 Update: A Report From the American Heart Association. *Circulation*. 2014;131:e29–e322.

2. Cowell SJ, Newby DE, Prescott RJ, Bloomfield P, Reid J, Northridge DB, Boon N a. A randomized trial of intensive lipid-lowering therapy in calcific aortic stenosis. *The New England Journal of Medicine*. 2005;352(23):2389–97.

3. El-Hamamsy I, Chester AH, Yacoub MH. Cellular regulation of the structure and function of aortic valves. *Journal of Advanced Research*. 2010;1(1):5–12.

4. Leask RL, Jain N, Butany J. Endothelium and valvular diseases of the heart. *Microscopy research and technique*. 2003;60(2):129–37.

5. Mohler ER. Mechanisms of aortic valve calcification. *The American journal of cardiology*. 2004;94(11):1396–402, A6.

6. Müller AM, Cronen C, Kupferwasser LI, Oelert H, Müller K-M, Kirkpatrick CJ. Expression of endothelial cell adhesion molecules on heart valves : up-regulation in degeneration as well as acute endocarditis. *Journal of Pathology*. 2000;191:54–60.

7. Chen J-H, Simmons C a. Cell-matrix interactions in the pathobiology of calcific aortic valve disease: critical roles for matricellular, matricrine, and matrix mechanics cues. *Circulation research*. 2011;108(12):1510–24.

8. Chen JH, Chen WLK, Sider KL, Yip CYY, Simmons C a. β-Catenin Mediates Mechanically Regulated, Transforming Growth Factor-β1-Induced Myofibroblast Differentiation of Aortic Valve Interstitial Cells. *Arteriosclerosis, Thrombosis, and Vascular Biology*. 2011;31:590–597.

9. Kennedy J a, Hua X, Mishra K, Murphy G a, Rosenkranz AC, Horowitz JD. Inhibition of calcifying nodule formation in cultured porcine aortic valve cells by nitric oxide donors. *European journal of pharmacology*. 2009;602(1):28–35.

10. Walker G a, Masters KS, Shah DN, Anseth KS, Leinwand L a. Valvular myofibroblast activation by transforming growth factor-beta: implications for pathological extracellular matrix remodeling in heart valve disease. *Circulation research*. 2004;95(3):253–60.

11. Cloyd KL, El-Hamamsy I, Boonrungsiman S, Hedegaard M, Gentleman E, Sarathchandra P, Colazzo F, Gentleman MM, Yacoub MH, Chester AH,

Stevens MM. Characterization of Porcine Aortic Valvular Interstitial Cell "Calcified" Nodules. Aikawa E, ed. *PLoS ONE*. 2012;7(10):e48154.

12. Fisher CI, Chen J, Merryman WD. Calcific nodule morphogenesis by heart valve interstitial cells is strain dependent. *Biomechanics and modeling in mechanobiology*. 2012;1.

13. Yip CYY, Chen J-H, Zhao R, Simmons C a. Calcification by valve interstitial cells is regulated by the stiffness of the extracellular matrix. *Arteriosclerosis, thrombosis, and vascular biology*. 2009;29(6):936–42.

14. Ferdous Z, Jo H, Nerem RM. Differences in valvular and vascular cell responses to strain in osteogenic media. *Biomaterials*. 2011;32(11):2885–93.

15. Balachandran K, Sucosky P, Jo H, Yoganathan AP. Elevated cyclic stretch induces aortic valve calcification in a bone morphogenic protein-dependent manner. *The American journal of pathology*. 2010;177(1):49–57.

16. El-Hamamsy I, Balachandran K, Yacoub MH, Stevens LM, Sarathchandra P, Taylor PM, Yoganathan AP, Chester AH. Endothelium-dependent regulation of the mechanical properties of aortic valve cusps. *Journal of the American College of Cardiology*. 2009;53(16):1448–55.

17. Simmons CA, Grant GR, Manduchi E, Davies PF. Spatial heterogeneity of endothelial phenotypes correlates with side-specific vulnerability to calcification in normal porcine aortic valves. *Circulation research*. 2005;96(7):792–9.

18. Mikroulis D, Mavrilas D, Kapolos J, Koutsoukos PG, Lolas C. Physicochemical and microscopical study of calcific deposits from natural and bioprosthetic heart valves. Comparison and implications for mineralization mechanism. *Journal of materials science. Materials in medicine*. 2002;13(9):885–9.

19. Prieto RM. Study on the structure and composition of aortic valve calcific deposits. etiological aspects. *Journal of Biophysical Chemistry*. 2011;02(01):19–25.

20. Tomazic BB. Physicochemical principles of cardiovascular calcification. *Zeitschrift für Kardiologie*. 2001;80:68–80.

21. Mangialardo S, Cottignoli V, Cavarretta E, Salvador L, Postorino P, Maras A. Pathological biominerals: Raman and infrared studies of bioapatite deposits in human heart valves. *Applied Spectroscopy*. 2012;66(10):1121–1127.

22. Bertazzo S, Gentleman E, Cloyd KL, Chester AH, Yacoub MH, Stevens MM. Nano-analytical electron microscopy reveals fundamental insights into human cardiovascular tissue calcification. *Nature materials*. 2013;12(6):576–83.

23. Butcher JT, Nerem RM. Valvular endothelial cells regulate the phenotype of interstitial cells in co-culture: effects of steady shear stress. *Tissue engineering*. 2006;12(4):905–15.

24. Tseng H, Balaoing LR, Grigoryan B, Raphael RM, Killian TC, Souza GR, Grande-Allen KJ. A three-dimensional co-culture model of the aortic valve using magnetic levitation. *Acta Biomaterialia*. 2014;10(1):173–182.

25. Gould ST, Matherly EE, Smith JN, Heistad DD, Anseth KS. The role of valvular endothelial cell paracrine signaling and matrix elasticity on valvular interstitial cell activation. *Biomaterials*. 2014;35(11):3596–606.

26. Bouchareb R, Boulanger MC, Fournier D, Pibarot P, Messaddeq Y, Mathieu P. Mechanical strain induces the production of spheroid mineralized microparticles in the aortic valve through a RhoA/ROCK-dependent mechanism. *Journal of Molecular and Cellular Cardiology*. 2014;67:49–59.

27. Gu X, Masters KS. Role of the Rho pathway in regulating valvular interstitial cell phenotype and nodule formation. *American journal of physiology. Heart and circulatory physiology*. 2011;300(24):H448–H458.

28. Dweck MR, Boon N a, Newby DE. Calcific aortic stenosis: a disease of the valve and the myocardium. *Journal of the American College of Cardiology*. 2012;60(19):1854–63.

29. Billiar KL. The Mechanical Environment of Cells in Collagen Gel Models Global and Local Effects in Three-dimensional Biological Hydrogels. In: *Studies in Mechanobiology, Tissue Engineering and Biomaterials*.; 2011.

30. Girton TS, Oegema TR, Tranquillo RT. Exploiting glycation to stiffen and strengthen tissue equivalents for tissue engineering. *Journal of Biomedical Materials Research*. 1999;46:87–92.

31. Boskey AL, Roy R. Cell Culture Systems for Studies of Bone and Tooth Mineralisation. *Chemical Reviews*. 2009;108(11):4716–4733.

32. Yuan Y, Liu C, Qian J, Wang J, Zhang Y. Size-mediated cytotoxicity and apoptosis of hydroxyapatite nanoparticles in human hepatoma HepG2 cells. *Biomaterials*. 2010;31(4):730–740.

33. Boskey AL, Maresca M, Ullrich W, Doty SB, Butler WT, Prince CW. Osteopontin-hydroxyapatite interactions in vitro: inhibition of hydroxyapatite formation and growth in a gelatin-gel. *Bone and mineral*. 1993;22(2):147–59.

34. Giachelli CM, Scatena M, Wada T. Osteopontin: Potential roles in vascular function and dystrophic calcificaton. *Journal of Bone and Mineral Metabolism*. 1997;15:179–183.

35. Addison WN, Azari F, Sørensen ES, Kaartinen MT, McKee MD. Pyrophosphate inhibits mineralization of osteoblast cultures by binding to mineral, up-regulating osteopontin, and inhibiting alkaline phosphatase activity. *Journal of Biological Chemistry*. 2007;282(21):15872–15883.

36. Pezzatini S, Solito R, Morbidelli L, Lamponi S, Boanini E, Bigi A, Ziche M. The effect of hydroxyapatite nanocrystals on microvascular endothelial cell viability and functions. *Journal of Biomedical Materials Research - Part A*. 2006;76:656–663.

37. Arjunon S, Rathan S, Jo H, Yoganathan AP. Aortic valve: mechanical environment and mechanobiology. *Annals of biomedical engineering*. 2013;41(7):1331–46.

38. Gould RA, Chin K, Santisakultarm TP, Dropkin A, Richards JM, Schaffer CB, Butcher JT. Cyclic strain anisotropy regulates valvular interstitial cell phenotype and tissue remodeling in three-dimensional culture. *Acta biomaterialia*. 2012;8(5):1710–9.

39. Smith KE, Metzler S a, Warnock JN. Cyclic strain inhibits acute pro-inflammatory gene expression in aortic valve interstitial cells. *Biomechanics and modeling in mechanobiology*. 2010;9(1):117–25.

40. Balachandran K, Alford PW, Wylie-Sears J, Goss J a, Grosberg A, Bischoff J, Aikawa E, Levine R a, Parker KK. Cyclic strain induces dual-mode endothelial-mesenchymal transformation of the cardiac valve. *Proceedings of the National Academy of Sciences of the United States of America*. 2011;108(50):19943–8.

41. Butcher JT, Nerem RM. Valvular Endothelial Cells Regulate the Phenotype of Interstitial Cells in Co-culture : Effects of Steady Shear Stress. *Tissue Engineering*. 2006;12(4):905–915.

42. Butcher JT, Tressel S, Johnson T, Turner D, Sorescu G, Jo H, Nerem RM. Transcriptional profiles of valvular and vascular endothelial cells reveal phenotypic differences: influence of shear stress. *Arteriosclerosis, thrombosis, and vascular biology*. 2006;26(1):69–77.

43. Warnock JN, Burgess SC, Shack A, Yoganathan AP. Differential Immediate-Early Gene Responses to Elevated Pressure in Porcine Aortic Valve Interstitial Cells. *The Journal of Heart Valve Disease*. 2006;15(1):34–42.

44. Engelmayr GC, Sales VL, Mayer JE, Sacks MS. Cyclic flexure and laminar flow synergistically accelerate mesenchymal stem cell-mediated engineered tissue formation: Implications for engineered heart valve tissues. *Biomaterials*. 2006;27:6083–6095.

45. Osman L, Yacoub MH, Latif N, Amrani M, Chester AH. Role of human valve interstitial cells in valve calcification and their response to atorvastatin. *Circulation*. 2006;114(1 Suppl):I547–52.

46. Taylor P, Allen S, Dreger S, Yacoub M. Human cardiac valve interstitial cells in collagen sponge: a biological three-dimensional matrix for tissue engineering. *The Journal of Heart Valve Disease*. 2002;11(3):298–306.

47. Duan B, Kapetanovic E, Hockaday L a., Butcher JT. Three-dimensional printed trileaflet valve conduits using biological hydrogels and human valve interstitial cells. *Acta Biomaterialia*. 2014;10(5):1836–1846.

CHAPTER 7

DISCOVERING CONGENITAL DEFECTS IN THE CLASSROOM: AN INQUIRY-BASED APPROACH TO STUDY EMBRYONIC GROWTH USING *EX-OVO* CHICKEN CULTURE

7.1 Abstract

Between 2011 and 2013, I was privileged to participate in Cornell's Learning Initiative in Medicine and Bioengineering (CLIMB) GK-12 program as a National Science Foundation STEM Fellow. This program pairs graduate students with local teachers in order to enhance science curriculum and get students more engaged in STEM activities. The program includes a 6-week summer term for the teacher, who is immersed in the scientific research outlined by the graduate student. The summer session is followed by the academic school year, where I participated in many scientific demonstrations, taught classes, and acted as a scientific mentor to young high school students. Over my two years participating in this program, I was paired with Laura Austen and Kelly Clement, both of Southside High School in Elmira, NY. During this time, I developed a novel curriculum based on research principles for local high school students. This chapter overviews my GK-12 experience, culminating in a complete curriculum with worksheets and classroom data.

7.2 Introduction

Embryonic development offers a unique perspective on the function of many biological processes and their heightened sensitivity to environmental factors. This hands-on lesson investigates the effects of various chemicals on the growth and

development of the chicken embryo. Students were given the choice of applying alcohol, nicotine, caffeine or glucose to a shell-less (ex-ovo) cultured chicken embryo, which are highly accessible and functional for a classroom setting. Throughout the activity, students were exposed to and used the scientific process that is the foundation of laboratory research, including: hypothesis formation, experimental design, interpretation of data, and drawing conclusions based on this data. This activity supports instruction on developmental biology, animal research, experimental design, and scientific ethics, and has the benefit of covering a range of clinically relevant topics.

Science Content for the Teacher

Congenital defects are health problems or physical abnormalities that are present at the time of birth. The severity of these defects can range from very mild, such as a slight discoloration of the skin, to life-threatening. Approximately 3.5% of all babies are born with some type of defect, which account for about 140,000 babies born in the United States each year. Congenital defects can be caused by both genetic and environmental factors. Genetic factors are associated with alterations and mutations within the genes, and can result in diseases such as Down syndrome, autism, or Marfan's syndrome. Environmental factors, however, are mainly caused by something in the environment that the mother is exposed to during her pregnancy. Defects caused by environmental factors can include growth deficiency, mental retardation, or craniofacial defects.

Scientists use animal models to study embryonic development and congenital defects. An animal model is a living, non-human animal that is used during the research and investigation of human disease. The use of animals in research is

highly regulated by the federal government, which has instated the Institutional Animal Care and Use Committee (IACUC) to ensure the standards of animal care during research. In this lab, chicken embryos are used to study embryonic development, and to evaluate the effect of changes in the chemical environment on the growing embryo. A chicken embryo is an ideal animal model for this particular research, because it is fast growing, can be cultured outside of the egg, and has similar features to a human embryo in the earliest stages of its development.

In this lab, students will be adding one of three chemicals (nicotine, caffeine or alcohol) to their embryos, and observing developmental changes as compared to control embryos with no chemical treatments. Each chemical is pertinent to human embryo development, which should resonate with the students once they have finished the experiment.

Chemicals added to embryos:

Nicotine is a stimulant found in tobacco, largely responsible for the addictive nature of cigarette smoking. As it enters the body, nicotine quickly enters the bloodstream and reaches the brain, where it acts as a stimulant. Nicotine is extremely toxic and can only be consumed in small dosages in a fully grown human. In a growing fetus, nicotine can cause defects in the brain as well as causing a serious dependency before birth, which can cause the newborn baby to require detoxification in the first weeks of life.

Caffeine is an addictive stimulant found in many plants, most notably the coffee bean and tea leaf. It is the world's most widely consumed legal psychoactive drug, with an estimated 90% of adults in North America consuming some kind of caffeine each day. While it is debated how much caffeine affects fetal development, scientists

agree that too much caffeine can disturb fetal blood flow and cause eventual dependency after birth.

Alcohol is a flammable, colorless liquid that is found in many beverages in the form of ethanol. Produced by fermentation, consumed alcohol has a depressant effect on the central nervous system. In large quantities, alcohol consumption can cause nausea and intoxication, as well as liver damage with long-term use. Alcohol can cause many congenital defects, with the most common affliction being fetal alcohol syndrome. This stunts fetal growth, causes distinctive facial features, and damages neurons and brain structures.

Using an *ex ovo* (outside the egg) embryo culture, students will be able to observe embryonic development in a shortened time-frame (chicken embryos develop over 21 days, rather than the 9 months of human gestation), and induce congenital defects through environmental factors. Students will be able to choose the chemical they wish to use, and make hypotheses about the effects their treatment might have on their embryos. Students will also learn valuable skills in data collection and graph plotting.

7.3 Preparation

Materials and Methods

- Fertilized chicken eggs (local poultry farm)
- Egg incubator and rocker (Little Giant Still Air Egg Incubator 9200)
- Saran wrap
- Rubber bads
- 9 oz plastic cups
- 100 mm diameter petri dish
- Thermometer
- Gloves

- Pipetter and pipet tips
- USB Microscope Veho VMS-100 (or alternative large working distance scope)
- Nicotine (E-liquid nicotine)
- Caffeine (Sigma-aldrich)
- Ethanol

Egg Incubation

Fertilized chicken eggs should be obtained from a local poultry farm. These fertilized embryos can be stored in a cooler maintained at 55°F for up to 3-4 days until ready to use. Prior to the start of the activity, clean out the incubator with soap and water to remove contaminants. Dilute bleach or 70% ethanol can be used to sterilize the incubator. Line the base of the incubator with aluminum foil for easy cleaning and place the thermometer inside. Three days prior to the lab, the teacher should put the fertilized eggs into the incubator (set to 99.5°F) on a rocker to start the incubation (Day 0). Make sure there is a cup of water in the incubator for moisture. Embryos will be at Day 3 of development on the first day of the lab.

Prepare chemicals

1. **30% Ethanol:** add 15 ml ethanol in 35 ml of water
2. **3.5 mg/egg Caffeine:** add 1.75 g caffeine in 50 ml of water
3. **Nicotine:** add 500 µl liquid nicotine to 50 ml of water

Pre-lab lecture

A day before the lab, the teacher should introduce the students to the concepts of animal models, embryonic development, and congenital defects. Students should understand why scientists use animal models to study development and disease. Students should also understand the difference between congenital defects caused

from genetic or environmental factors. Because this lab is rather elaborate, the teacher should explain the basics of the experiment beforehand, as well as giving the students time to practice some of the measurements they will be required to do during the lab.

7.4 *Ex-Ovo* Embryo Lab

Embryo Lab (Part 1)

After embryos have incubated on the rocker for 72 hours (Day 3), the lab is ready to commence. Split the students into groups of 2-3. Each group must decide what chemical (nicotine, caffeine, or alcohol) they will be treating their embryo with before the lab starts.

1. **Prepare the cups:** Fill each plastic cup about 2/3 of the way full with warm water. Place an 8x8 inch square piece of saran wrap over the cup and water so that a loose "hammock" is made for the embryo to rest on. Secure the saran wrap with a rubber band (Figure 7.1 A,B). Spray the hammock with 70% ethanol (for sterilizing) and allow to air dry.

2. **Crack the eggs:** Set aside about 6 eggs at a time for the students to crack (do not leave these out for long periods of time, as the embryo should not get much below incubation temperature). Turn each egg on its side so the embryo is able to rotate to the top (Figure 7.1 C). Carefully crack the egg and gently place it in the hammock made in the cup. Do not break the yolk. The embryo should be facing upwards, but if not, gently (with gloves!) try to stroke the yolk so the embryo moves upwards (Figure 7.1 D). It is recommended that the teacher do this if necessary.

3. Cover and label: Cover each cup with the top of a petri dish. Label each one with the group name, and either “control” or “treatment”. Place each cup in the incubator set at 99.5°F, leaving room for a cup of water to maintain humidity (Figure 7.1 E,F). It is recommended that the entire ex-ovo culture is done under the close supervision of a teacher.

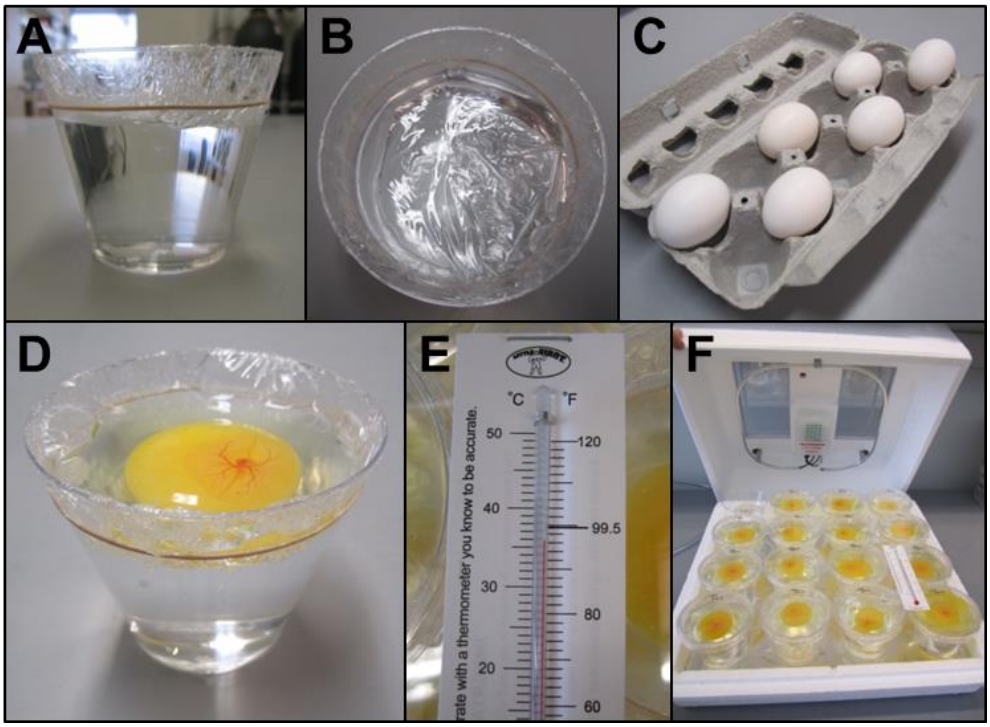

Figure 7.1: Materials and set-up of chicken embryo lab. A) Side-view of water-filled cup covered with plastic wrap and secured with a rubber band. B) Top view of plastic-wrapped cup. Plastic wrap should cover the largest surface area of water possible. C) Fertilized eggs should be placed on their side prior to cracking for correct placement of embryo. D) Cracked egg in the cup apparatus, with the embryo facing upwards. E) Embryos should be incubated at 99.5°F and placed in F) a portable heat-regulated chick incubator for the duration of the experiment.

Embryo Lab (Part 2)

1. Measure the embryo length and heartbeat: One day after cracking (Day 4), measure the embryo length from head to tail. Record in the table provided in the lab.

Also measure the heartbeat (it is recommended that one student count the heart beats while another student watches the time). Record this in the table provided (Appendix A). Students at this time can make other general observations about the embryo, including general shape and area of vasculature.

2. Treat the embryos: Each group should separate the embryos labeled "treatment" from their controls. Add 100 µl of chemical (pre-made ethanol, caffeine, or nicotine) directly onto the embryo using a pipetter. Measure the length and heart rate directly after treatment, and note any quantitative or qualitative changes.

3. Observe daily changes: Over the next few days, make the same measurements (length and heart rate), in order to gather trends of growth. Also observe any differences that the chemical-treated embryos might have over the controls (Figure 7.2).

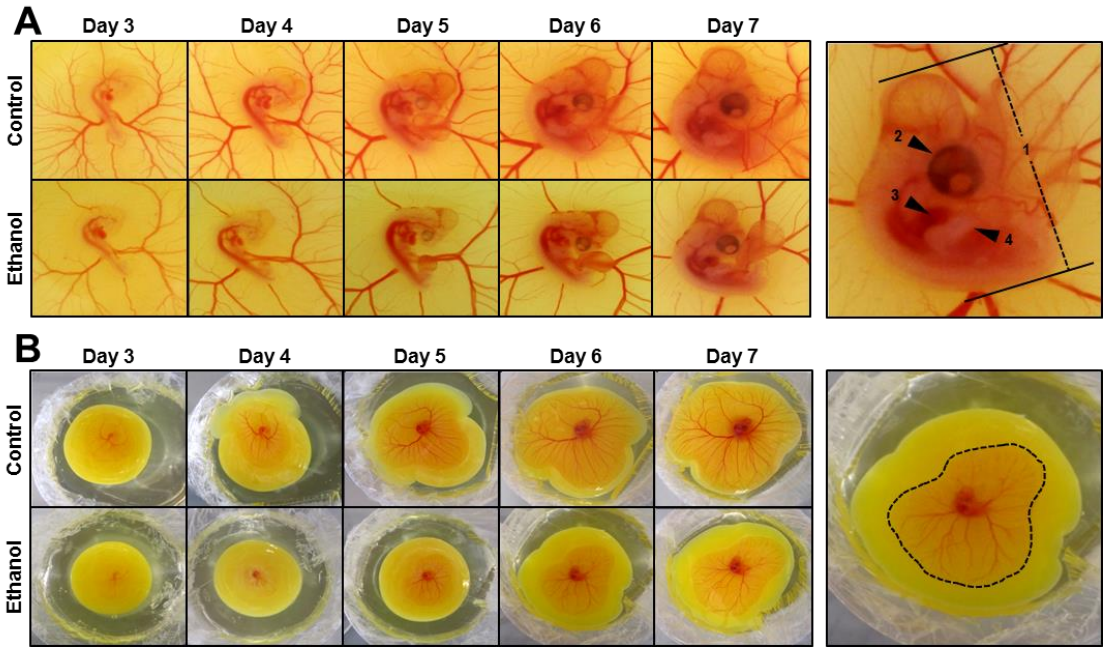

Figure 7.2: Example data from *ex-ovo* experiment. A) Progression of embryo growth with and without treatment with ethanol. Enlarged photo shows various measurements students can make including (1) tip-to-tail length, (2) eye diameter, (3) heart rate and (4) limb length. Students can also measure (B) vasculature area over time, measured via area of extending blood vessels.

7.5 Analysis and Interpretation of Results

At the end of the lab, students should graph the changes in length and heart rate. Additionally, students should pool the data from all the treatments so class data can be analyzed for any trends. Students should be discuss what they found and what it means. Did their results match the hypotheses? Make sure to discuss the class results in the context of human development and congenital defects. Discussion of the lab itself is always encouraged. Concepts of why there was a control, and what other possible treatments other than chemical could have been performed (i.e. temperature, movement). Have the students come up with alternate variables that could be measured based on their observations (i.e. eye diameter, limb development).

7.6 Discussion

The embryo is a powerful tool to study embryonic processes in biology. A chicken embryo is especially unique for classroom learning because of its plentiful availability for teachers and the ability to be grown outside of the shell. This enables students to literally watch the embryo grow through the multitudes of embryonic change, at a much faster rate than normal human gestation. This lesson answers fundamental questions of embryonic growth while highlighting the importance of staying healthy during pregnancy. Environmental changes can have huge effects on a growing embryo, and students can observe these changes first-hand. These types of experiments have additional versatility and can be used in a variety of classrooms at all levels of learning.

Using live embryos in the classroom will inevitably spark a conversation about ethics and the humane treatment of animals in scientific research. Teachers should

make it clear to their students (perhaps in an additional lecture) that animal research is highly regulated by the Institutional Animal Care and Use Committee (IACUC), and there is very little you can do with an animal in research that is not heavily monitored by Federal standards of treatment. Chicken embryos younger than embryonic day 11 have not yet fully developed a nervous system, and are therefore assumed to be unable to experience pain. All experiments presented in this lesson are well before that time, and students should be reassured of this fact. Because all experiments end on Day 7, well before any IACUC regulated euthanasia procedures are required, these eggs can be euthanized by rapid freezing (placing in a freezer). It is greatly encouraged for teachers to have an open discussion with their students about animal research, its regulations, and the vast benefits for expanding our knowledge of human health.

APPENDIX A

GK-12 MODULE TEACHING MATERIALS

Embryonic Development and Congenital Defects Pre-Test

1. What is a congenital defect?

   A health problem or physical abnormality present at the time of birth

2. The two major causes of congenital defects are ___environmental_____ and ____genetic_____ factors.

3. A mutation within the genome of an embryo can occur from (circle all that apply):

   a) Mutation of a single gene
   b) Excessive alcohol use by the mother
   c) Radiation
   d) Malnutrition or lack of vitamins
   e) Abnormal chromosomes

4. What is the difference between qualitative and quantitative?

   Qualitative: Something you can measure
   Quantitative: Something not measureable but still descriptive

5. Name the parts of an embryo, using the list provided (shown below)

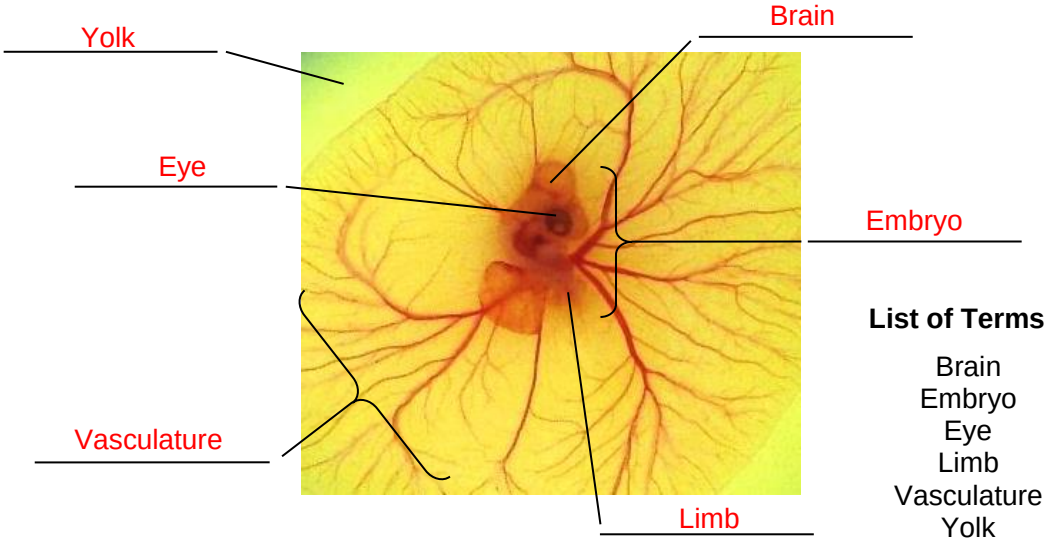

6. List two examples of animal models used in scientific research.

Mouse, rat, pig, dog, sheep, etc.…

7. The Institutional Animal Care and Use Committee (IACUC) is an organization that (circle all that apply):

a) Regulates use of animals for scientific purposes
b) Removes hazardous chemicals from a laboratory
c) Passes laws to protect lab animals' well-being
d) Checks that animals used in laboratories are being humanely treated
e) Regulates sterile techniques and the use of clean rooms in the laboratory

8. Match the question with the section in the scientific method

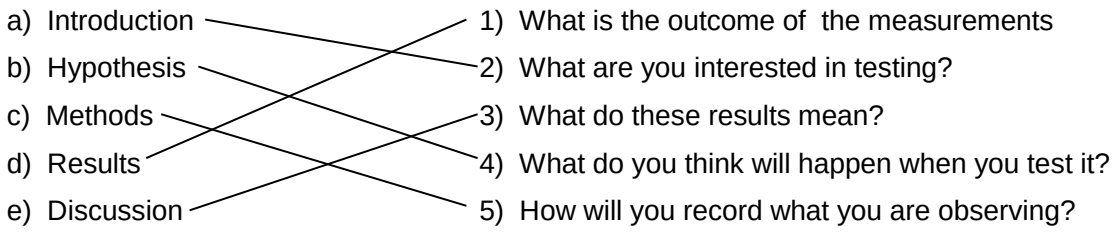

9. Can you see yourself in a future career that involves science?

Student can write anything

10. What kind of science are you most interested in?

Student can write anything

Lab Worksheet

Watch it Grow!

Embryonic Development and Congenital Defects

Introduction:

Congenital defects are health problems or physical abnormalities present at the time of birth. These can range from very mild to very severe or life-threatening. Approximately 3.5% of babies are born in the United States (about 140,000 each year!) There are two causes of congenital defects: genetic and environmental. Genetic causes of congenital defects are associated with alterations and mutations within the genes, while environmental causes are usually something in the environment that the mother is exposed to during pregnancy.

Scientists use animal models to investigate human diseases and congenital defects. In this experiment we will be using chicken embryos to investigate early embryonic development. We will also be changing the embryonic environment and making observations on how these changes in environment affect embryonic growth.

Nicotine: a stimulant found in tobacco, largely responsible for the addictive nature of cigarette smoking. As it enters the body, nicotine quickly enters the bloodstream and reaches the brain, where it acts as a stimulant. Nicotine is extremely toxic and can only be consumed in small dosages in a fully grown human. In a growing fetus, nicotine can cause defects in the brain as well as causing a serious dependency before birth, which can cause the newborn baby to undergo severe detox in the first weeks.

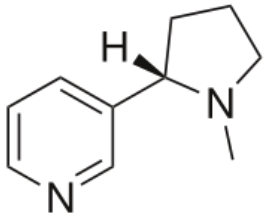

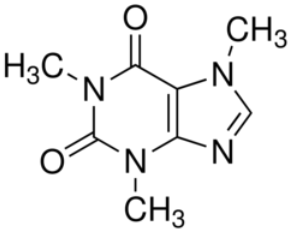

Caffeine: an addictive stimulant found in many plants, most notably the coffee bean and tea leaf. It is the world's most widely consumed legal psychoactive drug, with an estimated 90% of adults in North America consuming some kind of caffeine each day. While it is debated how much caffeine affects fetal development, scientists agree that too much caffeine can disturb fetal blood flow and cause eventual dependency after birth.

Alcohol: a flammable, colorless liquid that is found in many beverages in the form of ethanol. Produced by fermentation, consumed alcohol has a depressant effect on the central nervous system. In large quantities, alcohol consumption can cause nausea and intoxication, as well as liver damage with long-term use. Alcohol can cause many congenital defects, with the most common affliction being fetal alcohol syndrome. This stunts fetal growth, causes distinctive facial features, and damages neurons and brain structures.

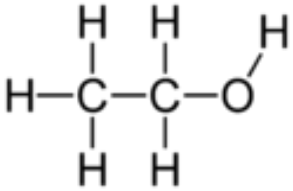

Materials:

- Fertilized eggs
- Incubators
- Plastic cups
- Saran wrap
- Rubber bands
- Water (warm)
- 70% ethanol
- Gloves
- Pipettes
- Nicotine
- Ethanol (alcohol)
- Caffeine

Understanding the Experiment

In this lab, you will be cracking 3-day old chicken eggs and observing the growth of the embryo until Day 7 of its development. In addition, you will choose one of the four chemicals listed and add it to your embryo and observe changes in overall development. In particular, you will be observing changing embryo length and heart rate as well as qualitative observations such as embryo color and movement. Some key questions to consider in this lab:

- What changes about the embryo during development?
- How do changes in the environment change embryonic development?
- How good are animal models at studying human diseases?
- Why is it important to have a control in addition to a treatment group?

Hypotheses

1. Describe how you think the embryo will change over 7 days.

2. What chemical are you adding to your embryo? _____

How do you think the addition of this chemical will change **the embryo length**?

Will this change be **instant** or seen **over time**?

3. How do you think the addition of your chemical will change the embryo **heart rate**?

Will this change be **instant** or seen **over time**?

4. Is there anything else that you think might change over time and with your treatment?

Procedure:

Prepare the cups

1. Fill each cup about 2/3 full with warm water.
2. Cut a square of saran wrap and lay it gently in the cup on the water (make a little hammock or water bed with the saran wrap)
3. Tie a rubber band around the cup to hold the saran wrap in place
4. Trim the edges of the saran wrap
5. Spray the saran wrap with 70% ethanol to sterilize. Allow the ethanol to fully evaporate before cracking the eggs.

Crack the eggs

1. Lay out the eggs in the carton sideways to settle the embryo
2. Gently crack the egg slightly on the edge of a beaker.
3. Hold the eggs in both hands, with the crack facing toward you, CAREFULLY pull the egg apart
4. Gently allow the egg yolk to drop into the cup (hold the egg right above the cup – do not let it drop far)
5. Make sure the embryo is facing upwards. Ask for help if you need to.

Cover and Label

1. Cover your cup with a petri dish cover
2. LABEL your cup with your group number and either "Control" or "Chemical Name" (alcohol, nicotine etc). This will be important to remember for later when you are collecting data.

Observations and Critical Thinking

1. Draw a picture of one of your embryos in the circle below. **Describe what you see.**

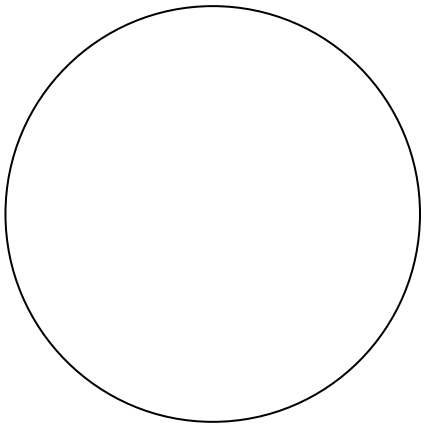

2. Why did we crack the eggs on Day 3 of their development? Why not on Day 1?

3. Based on what you have learned so far, what kind of environment is necessary to grow the embryos?

4. What is the difference between a quantitative and a qualitative measurement?

Quantitative:

Qualitative:

5. Name two qualitative and quantitative measurements you will be taking over the next few days:

Quantitative:

Qualitative:

Initial Measurements:

1. Measure the embryo from tip to tail (look at your notes as a reminder) and record your measurements in the table below in centimeters

Embryo Length (cm)	Control 1	Control 2	Treatment 1	Treatment 2
Day 3				

2. Measure the embryo heart rate and record your measurements in the table below in centimeters.
   (Hint: one person should could and the other should time. Try counting for 10 seconds and multiply by 6 to get the number of beats per minute)

Heart Rate (bpm)	Control 1	Control 2	Treatment 1	Treatment 2
Day 3				

Treating the Embryo (at Day 4)

The embryo is now at Day 4 in its development and is ready for the experiment. You will be adding your group treatment (caffeine, alcohol or nicotine), and then making the measurements discussed the day before. Remember to make qualitative observations in addition to your quantitative measurements!

Procedure:

1. Retrieve your embryos from the incubator.
2. Remove the cover of your "treatment" embryo.
3. Fill your pipette with 100 microliters of your _____ solution
4. Gently drip your liquid directly on the embryo.
5. Re-cover the cup, and observe/measure before returning to the incubator

Results

1. Measure the embryo from tip to tail (look at your notes as a reminder) and record your measurements in the table below in centimeters

Embryo Length (cm)	Control 1	Control 2	Treatment 1	Treatment 2
Day 4				

2. Measure the embryo heart rate and record your measurements in the table below in centimeters.
   (Hint: one person should could and the other should time. Try counting for 10 seconds and multiply by 6 to get the number of beats per minute)

Heart Rate (bpm)	Control 1	Control 2	Treatment 1	Treatment 2
Day 4				

3. Draw a picture of your control embryo and your treatment embryo in the circles below.

Control **Treatment**

4. Were there any immediate differences after your treatment? If so, describe them

Treating the Embryo (at Day 5)

The embryos are now at Day 5, so you should be seeing some major changes in the embryo. Measure and write down your observations.

Results

1. Measure the embryo from tip to tail (look at your notes as a reminder) and record your measurements in the table below in centimeters. Write down your measurements from the day before to remember and compare.

Embryo Length (cm)	Control 1	Control 2	Treatment 1	Treatment 2
Day 5				

2. Measure the embryo heart rate and record your measurements in the table below in centimeters.
   (Hint: one person should could and the other should time. Try counting for 10 seconds and multiply by 6 to get the number of beats per minute)

Heart Rate (bpm)	Control 1	Control 2	Treatment 1	Treatment 2
Day 3				

3. Draw a picture of your control embryo and your treatment embryo in the circles below.

Control **Treatment**

4. What kind of qualitative observations can you make about your treatment embryos?

Measuring the Embryo (at Day 6)

Results

1. Measure the embryo from tip to tail (look at your notes as a reminder) and record your measurements in the table below in centimeters.

Embryo Length (cm)	Control 1	Control 2	Treatment 1	Treatment 2
Day 6				

2. Measure the embryo heart rate and record your measurements in the table below in centimeters.
   (Hint: one person should could and the other should time. Try counting for 10 seconds and multiply by 6 to get the number of beats per minute)

Heart Rate (bpm)	Control 1	Control 2	Treatment 1	Treatment 2
Day 6				

3. Draw a picture of your control embryo and your treatment embryo in the circles below.

Control **Treatment**

4. What kind of qualitative observations can you make about your treatment embryos?

Assembling and Graphing the Data

Write down all of your numbers for both **embryo length** and **heart rate** from the previous days into one data table (below). Average your two samples for each day, and use the average for the graph

Embryo Length (cm)	Control 1	Control 2	Average	Treatment 1	Treatment 2	Average
Day 3						
Day 4						
Day 5						
Day 6						

Heart Rate (bpm)	Control 1	Control 2	Average	Treatment 1	Treatment 2	Average
Day 3						
Day 4						
Day 5						
Day 6						

3. Draw a picture of your control embryo and your treatment embryo in the circles below.

Control **Treatment**

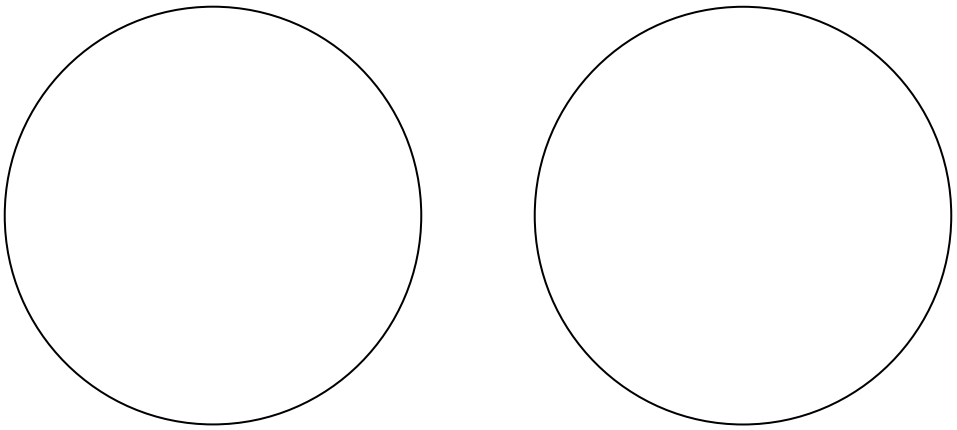

○ Control

X Treatment

Analyzing the Results

Plot the final embryo length results (average) from your complete data table from the previous page on the graph provided below:

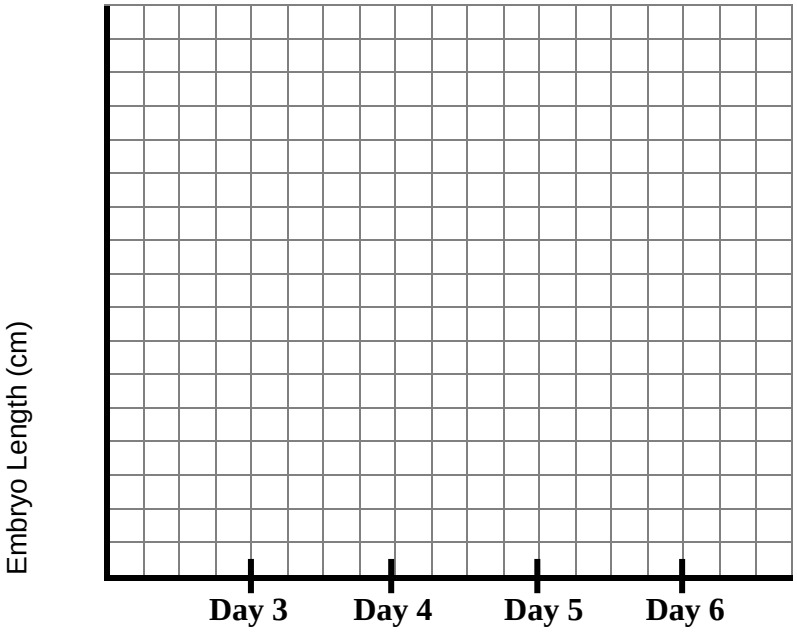

Plot the final embryo heart rate from your complete data table from the previous page on the graph below:

○ Control

X Treatment

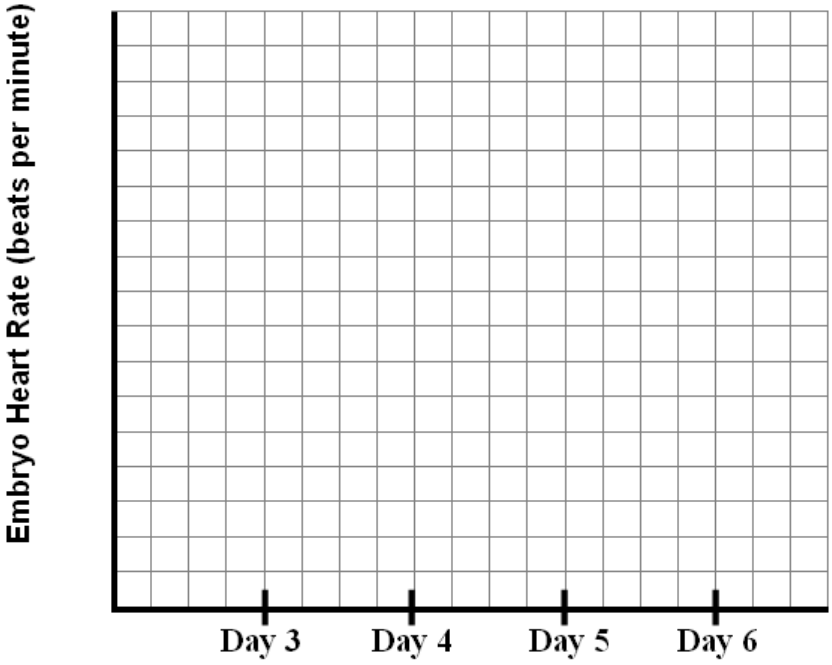

Data Analysis:

1. Compare the embryo length between the control and your treatment. Did your treatment stimulate or stunt growth?

2. Did your experiment have any embryo death? If so, what does that tell you about the toxicity of your treatment?

3. At the end of the experiment, what are some qualitative differences you can see in your control and treatment embryos?

4. What observations can you make about the vasculature (the blood vessels around the embryo) between the control and the treatment embryo? What does this tell you about the treatment?

Discussion Questions

1. What advantages and disadvantages are there to using animal models for experiments?

2. Why is it important to have a control in experiments?

3. What do these experiments tell you about congenital defects and environmental factors?

APPENDIX B

RELEVANT PROTOCOLS

Valve Endothelial and Interstitial Cell Isolation

Solutions:

- **1X Dulbecco's Phosphate Buffered Saline (DPBS) (10X, Gibco 2130-058)**
  - Make a 1X solution in 18 mΩ water
- **Dulbecco's Modified Eagle's Medium (DMEM) (Gibco 12100-046)**
  - 13.4 g DMEM
  - 3.7 g sodium bicarbonate
  - 10 ml (1%) penicillin-streptomycin
  - 100 ml (10%) FBS
  - pH to 7.0
- **Collagenase Type II (1 gm; Worthington, CLS-2)**
  - To make 600 U/ml Collagenase:
    - 0.1429 g Collagenase (210 U/mg)
    - 50 ml DMEM (with Pen-Strep, without FBS)
  - pH to 7.0
  - Sterile filter before use
  - Recommended to make the whole bottle in solution, store aliquots at -20°C
- **4% PFA**

Materials:

- **Cooler for organ transport**
- **Isolation utensils (autoclave if necessary)**
  - Forceps
  - Swabs
  - Petri dishes (sterile)
  - 15 ml centrifuge tubes

Isolation of Endothelial Cells:

1. Coat the bottom of a T25 flask with 50 µg/ml collagen type I solution (1 ml), set aside for later use.
2. Lay each valve leaflet in a sterile petri dish, rinsing once with PBS.
3. Add 5 ml of collagenase to the petri dish, ensuring all leaflets are covered.
4. Incubate at 37°C for 3 minutes.
5. Gently swab the endothelial layer by rotating the dry, sterile swab as the endothelial surface is scraped (If both surfaces isolated, flip leaflet with swabs and swipe other side). Place swab into one of the centrifuge tubes and gently

rotate to dislodge cells. Dab the swab several times in the collagenase to dislodge cells from the fibers. Repeat this procedure two more times with fresh swabs each time.

6. Collect the collagenase/cell suspension for each leaflet into one centrifuge tube.
7. Centrifuge for 5 minutes at 1000 rpm to pellet any isolated cells. Aspirate supernatant.
8. If isolating interstitial cells as well, perform that protocol while cells are centrifuged.
9. Remove remaining collagen solution from T25 flask, add 5 ml of DMEM to the flask.
10. Culture pelleted cells as normal.

Isolation of Interstitial Cells:

1. Fill one 15 ml centrifuge tube with 10 ml collagenase solution per valve. Complete this step before isolating endothelial cells if that portion of the protocol is being followed.
2. After swabbing the leaflets, immediately place the leaflets in the appropriate tube with the collagenase solution.
3. Incubate for an appropriate amount of time (12 to 18 hours). Agitate gently if desired.
4. Centrifuge the digested tissue fragments and cells for 5 minutes at 1000 rpm, and aspirate the supernatant.
5. Centrifuge the tubes at 1000 rpm for 10 minutes. Aspirate supernatant.
6. Add 5 ml of DMEM and again centrifuge tubes. Aspirate supernatant.
7. Resuspend pellet in one tube with 5 ml of DMEM and add to a T-175 filled with 35 ml DMEM.
8. Culture as normal.

3D Collagen Co-Culture Model

Materials

- ***Cell culture reagents***
  - Dulbecco's modified eagles medium (DMEM) (Invitrogen 12100-061)
  - 0.25 Trypsin-EDTA (Invitrogen 25200-072)
  - 1X Phosphate buffered saline (PBS)

- ***Collagen gel reagents (all sterile!)***
  - 3X DMEM
  - 18 mΩ H_2O
  - Fetal bovine serum (FBS)
  - Collagen type I (rat tail) (Corning 354236)
  - 0.1M NaOH

- ***Cell source***
  - Primary valve interstitial cells (use between passage 4-6)
  - Primary valve endothelial cells (use between passage 3-5)

- ***Hydrophobic barrier pen (Vector Laboratories, H-4000)***

Preparation of collagen gel reagents/cell culture plate

- ***3X DMEM (50 ml)***
  - Add 2.01g DMEM powder in 50ml of 18 mΩ H_2O. Mix thoroughly
  - Add 0.56g sodium bicarbonate to solution. Mix thoroughly.
  - pH to 7.0
  - Sterile filter with syringe filter
  - Label and store in 4°C. Keep sterile!

- ***18 mΩ H_2O (50 ml)***
  - Sterile filter water with syringe filter
  - Label and store in 4°C. Keep sterile!

- ***0.1M NaOH***
  - Add 5 ml of 1M NaOH stock to 45 ml 18 mΩ H_2O. Mix well
  - Sterile filter water with syringe filter
  - Label and store in 4°C. Keep sterile!

- ***Prepare cell culture plate***
  - With a hydrophobic pen, make a thin ring around the wells of the 24-well plate (to prevent gels from reaching the sides of the well)
  - Let dry, and UV sterilize in the biosafety cabinet at least 1 hour before seeding

Making the gels

1. Take a T75 flask of VIC out of the incubator, wash once with 10 ml of warm PBS

2. Add 4 ml of trypsin to the flask to trypsinize the cells (37°C) for 5 minutes
3. Add three times the amount of DMEM to terminate the digestion (12 ml). Transfer to a centrifuge tube. DO NOT centrifuge.
4. Count the cells using a hemocytometer.
5. Calculate the desired volume of cell suspension using *collagen only disk template* file.
   **Example: for VIC gels, use 400,000 cells/ml*
6. Transfer the desired volume of cell suspension into a 15 ml tube; centrifuge at 1000 rpm for 5 minutes
7. Prepare a bowl of ice. Put collagen, 0.1M NaOH, 18 mΩ H_2O, FBS, and 3X DMEM on ice
8. After centrifuge, aspirate the supernatant, add in order to the cell pellet

   3X DMEM
   18 mΩ H_2O
   FBS
   Collagen
   NaOH

   **Mix well with each step.*
   ***Especially** make sure the NaOH is well mixed with the collagen on the last step*

9. Dispense 200µl of gel solution into each well, taking care to dispense in the middle of the well
10. With the tip of a pipette, gently spread the gel solution so it fills up the whole center of the well, but taking care not to adhere the gel to the sides of the well
11. Incubate for 45 minutes – 1 hour

****If VIC-only gel:***

12. Add media and incubate as your experiment dictates

****If VIC+VEC gel:***

12. Take a T75 flask of VEC out of the incubator, wash once with 10 ml of warm PBS
13. Add 4 ml of trypsin to the flask to trypsinize the cells (37°C) for 5 minutes
14. Add three times the amount of DMEM to terminate the digestion (12 ml). Transfer to a centrifuge tube. DO NOT centrifuge.
15. Count the cells using a hemocytometer.
16. Calculate the desired volume of cell suspension, determined by number of gels
    **Example: use 50,000 cells/gel*
17. Transfer the desired volume of cell suspension into a 15 ml tube; centrifuge at 1000 rpm for 5 minutes

18. After centrifugation, aspirate the supernatant and add enough media to add 50µl of media+cells to each gel. Mix well
19. Carefully add cells to the top of each well (50µl each)
20. Incubate for 1-3 hours before adding media to gels (VEC will last in dropwise form for up to 3 hours before you have to worry about drying)
21. Add media and run for as long as your experiment dictates

For VEC-only gel:

1. Make the gel solution as described above, but make without any cell pellet.
   ** Note, VEC-only gels do not contract, so you can fill the well with the gel solution, and not worry about the hydrophobic pen (24 well plate: 300µl gel each well). But for best comparison between VIC, VIC+VEC gels, use the same method as described above*

Nanoparticle Incorporation into Collagen Gels

Materials

- ***Cell culture reagents***
  - Dulbecco's modified eagles medium (DMEM) (Invitrogen 12100-061)
  - 0.25 Trypsin-EDTA (Invitrogen 25200-072)
  - 1X Phosphate buffered saline (PBS)
- ***Collagen gel reagents (all sterile!)***
  - 3X DMEM
  - 18 mΩ H_2O
  - Fetal bovine serum (FBS)
  - Collagen type I (rat tail) (Corning 354236)
  - 0.1M NaOH
- ***Cell source***
  - Primary valve interstitial cells (use between passage 4-6)
  - Primary valve endothelial cells (use between passage 3-5)
- ***Hydrophobic barrier pen (Vector Laboratories, H-4000)***
- ***HA nanoparticles (A1, A3)*** *(Receive from Lara Estroff lab, Bard Hall)*

Preparation of collagen gel reagents/cell culture plate

- ***3X DMEM (50 ml)***
  - Add 2.01g DMEM powder in 50ml of 18 mΩ H_2O. Mix thoroughly
  - Add 0.56g sodium bicarbonate to solution. Mix thoroughly.
  - pH to 7.0
  - Sterile filter with syringe filter
  - Label and store in 4°C. Keep sterile!
- ***18 mΩ H_2O (50 ml)***
  - Sterile filter water with syringe filter
  - Label and store in 4°C. Keep sterile!
- ***0.1M NaOH***
  - Add 5 ml of 1M NaOH stock to 45 ml 18 mΩ H_2O. Mix well
  - Sterile filter water with syringe filter
  - Label and store in 4°C. Keep sterile!
- ***Prepare cell culture plate***
  - With a hydrophobic pen, make a thin ring around the wells of the 24-well plate (to prevent gels from reaching the sides of the well)
  - Let dry, and UV sterilize in the biosafety cabinet at least 1 hour before seeding

Making the gels

1. Take a T75 flask of VIC out of the incubator, wash once with 10 ml of warm PBS

2. Add 4 ml of trypsin to the flask to trypsinize the cells (37°C) for 5 minutes
3. Add three times the amount of DMEM to terminate the digestion (12 ml). Transfer to a centrifuge tube. DO NOT centrifuge.
4. Count the cells using a hemocytometer.
5. Calculate the desired volume of cell suspension using *collagen only disk template* file.
   **Example: for VIC gels, use 400,000 cells/ml*
6. Transfer the desired volume of cell suspension into a 15 ml tube; centrifuge at 1000 rpm for 5 minutes
7. Prepare a bowl of ice. Put collagen, 0.1M NaOH, 18 mΩ H_2O, FBS, and 3X DMEM on ice
8. Calculate the amount of HA nanoparticles to add:

   For 0.25mg/ml HA gels, calculate:

   (0.25mg/ml)*(total gel volume) = (stock HA conc.)*(x)

   Where x = amount of particles you need

   **HA particles are dialyzed in 0.1M NaOH, so you will subtract the volume of NaOH used in the making of the gel, and substitute that volume with the NaOH+particles*
9. After cell centrifugation, aspirate the supernatant, add in order to the cell pellet

   3X DMEM
   18 mΩ H_2O
   FBS
   Collagen
   NaOH – volume of NaOH+particles
   HA particles in NaOH

   Mix well with each step.* ***Especially* *make sure the NaOH is well mixed with the collagen before adding HA*

   ****Mix HA very well for a full minute for total incorporation of particles in gel solution***
10. Dispense 200µl of gel solution into each well, taking care to dispense in the middle of the well
11. With the tip of a pipette, gently spread the gel solution so it fills up the whole center of the well, but taking care not to adhere the gel to the sides of the well
12. Incubate for 45 minutes – 1 hour

****If VIC-only gel:***

13. Add media and incubate as your experiment dictates

****If VIC+VEC gel:***

13. Take a T75 flask of VEC out of the incubator, wash once with 10 ml of warm PBS
14. Add 4 ml of trypsin to the flask to trypsinize the cells (37°C) for 5 minutes

15. Add three times the amount of DMEM to terminate the digestion (12 ml). Transfer to a centrifuge tube. DO NOT centrifuge.
16. Count the cells using a hemocytometer.
17. Calculate the desired volume of cell suspension, determined by number of gels
    **Example: use 50,000 cells/gel*
18. Transfer the desired volume of cell suspension into a 15 ml tube; centrifuge at 1000 rpm for 5 minutes
19. After centrifugation, aspirate the supernatant and add enough media to add 50µl of media+cells to each gel. Mix well
20. Carefully add cells to the top of each well (50µl each)
21. Incubate for 1-3 hours before adding media to gels (VEC will last in dropwise form for up to 3 hours before you have to worry about drying)
22. Add media and run for as long as your experiment dictates

****For VEC-only gel:***

1. Make the gel solution as described above, but make without any cell pellet.
   ** Note, VEC-only gels do not contract, so you can fill the well with the gel solution, and not worry about the hydrophobic pen (24 well plate: 300µl gel each well). But for best comparison between VIC, VIC+VEC gels, use the same method as described above*

Cyclic Stretch Bioreactor

Making molds (PDMS)

1. Using the Sylgard 184 silicone elastomer kit, pour **66.5 grams** of elastomer base into a plastic cup

2. Add **3.5 grams** of elastomer curing agent into the cup, for a total of 70 grams (1:20 dilution)

3. Mix thoroughly with metal spatula (mixture should be white and bubbly)

4. Place cup in the vacuum chamber and de-gas the mixture (will take 30-45 minutes)

5. Pour one cup of mixture (70 grams) into one plastic mold. Make sure to scrape off as much of the mixture from cup as possible.

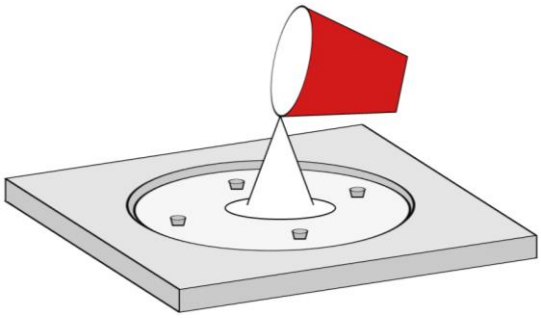

6. Use leftover PDMS to re-coat the edges of the wells on previously made silicone molds.

7. Heat in oven at 65°C for at least 6 hours (usually leave in overnight)

***Note**: to make large rectangle control mold, use two cups of PDMS mixture (70 grams each)

Cleaning cassettes and springs

1. Using tissue punch, punch out holes in PDMS mold where the screws will attach the top and bottom cassettes, with the PDMS sandwiched in between.

2. In warm water with soap, soak and scrub aluminum cassettes (especially the inner walls of the wells), bottom cassette pieces, and PDMS molds. Make sure that the wells are very clean, then rinse with DI water. Set to air dry.

3. Wash the springs by shaking in a 50ml centrifuge tube with warm water and soap. Rinse thoroughly with DI water. You may have to do this several times until completely clean. Set out to dry.

4. Preparing springs:
   For 1:1 strain: Fold one 1" spring into a circular shape (hook one end of the spring onto the other)
   For 2:1 strain: Attach two 0.625" springs at the ends to form an oval shape
   For 4:1 strain: Attach two 0.75" springs at the ends to form an oval shape

Prepping cassettes and molds

1. Place PDMS mold on top of the bottom cassette piece so the open wells are facing up, and they are in the middle of the holes in the cassette (so the platens will hit wells in the middle for an even stretch)

2. Place top cassette on top of the PDMS mold, then screw tightly into place using an Allen wrench.

3. Make up an autoclave bag for each cassette.
4. Trim off any PDMS overhanging the cassette edge with a straight edge blade, and place **one spring into each well** (to be inserted after autoclaving).
5. Seal autoclave bag, label with name and autoclave tape.

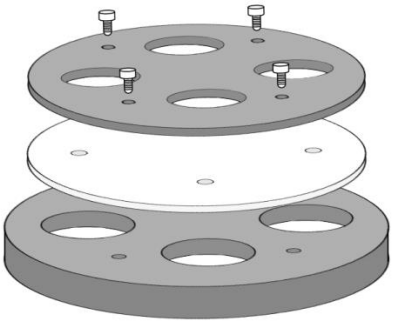

Preparing materials for experiment

1. Place extra washed springs into autoclave-appropriate boxes
2. Place gloves into a box to be autoclaved (these will be used to insert the springs)
3. Place forceps into a box to be autoclaved
4. Prepare spring controls:
   (a) Wash and dry squares of the control PDMS molds
   (b) Place washed springs into each control well (it won't matter if they crack in the autoclave because they are controls)
   (c) Put these controls in a box to be autoclaved
5. Gather cassettes (in their bags), springs, gloves, controls, and forceps and place in an autoclave bucket
6. Put cassettes on top of boxes so the bottom of the bags won't get wet
7. Autoclave setting: **GRAVITY 25:00 min sterilize, 11:00 min dry**

Pre-experiment: Checking settings on the bioreactor

Prepare bioreactor

1. Coat white plastic platens with braycote (804) rubbing on **smoothly** with finger
2. Use a small screwdriver to make sure that the small holes drilled into the sides of the platens are clear (drilled holes prevent bubbles from forming under the gel)
3. Pour lubricant into large middle screw and into all four ball bearings

Check software program

1. Plug bioreactor into the controller
2. Plug controller into the wall
3. Plug controller into the computer

This order is extremely important

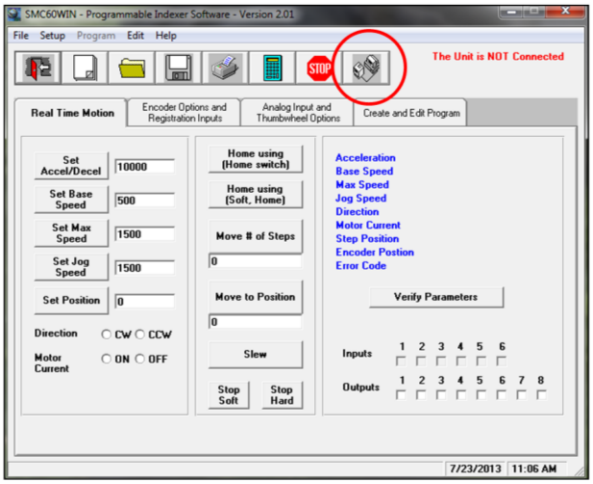

4. Open **SMC60WIN** (controller software)
5. Connect the unit (top right)
   *Note: This is **very important:** make sure unit is connected before you load any program to the controller
6. Upload program from controller
7. Send the program back to the controller (so it will know its starting point)
8. **Run** the program to see if motor and bioreactor is running smoothly

9. Set the plate manually until it is flush with the platens
10. Move plate up 200 steps (counter clockwise): this is where the cassettes will be loaded

Troubleshooting:

1. *Make sure screws are tight on the motor (or else the gears won't connect – no torque): tighten using hex screwdriver and attachment*
2. *For a tighter grip between gears, add grease to the gears*

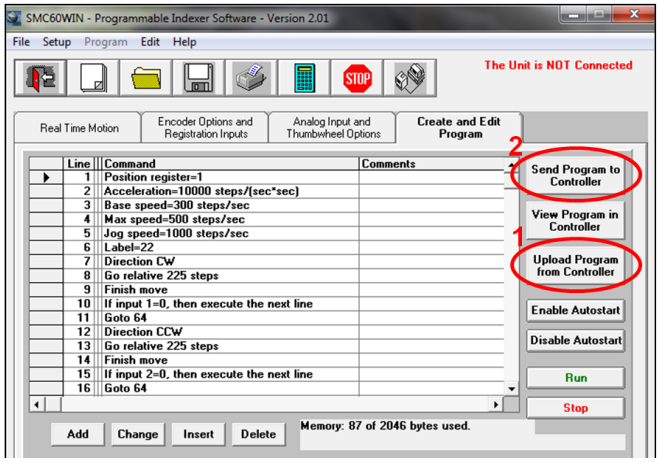

9. Set to flush position

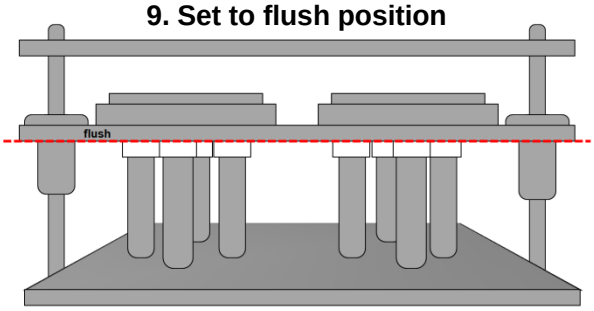

10. Up 200 steps to load cassettes

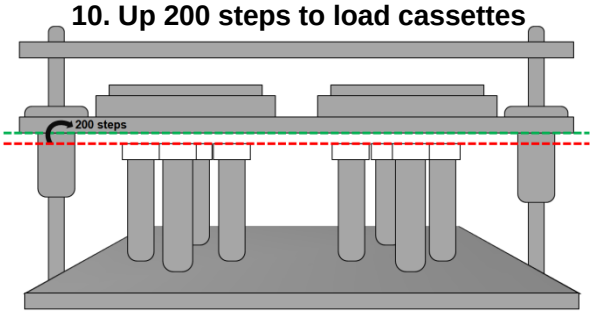

<u>Insertion of springs into wells</u>

**All of these procedures should take place in the laminar flow hood*

1. Open all autoclave bags with cassettes so you will be able to easily remove them later (do not touch cassettes yet)
2. Put on new pair of autoclaved gloves. Touch only the very edges of the gloves (do not touch the fingers). Put the right glove on first, then the left glove. The left-hand fingers and the **most important** to keep clean (they will be touching the springs)
3. Remove the cassettes with autoclaved gloves
4. Insert the springs by pushing up on mold with your right thumb from the bottom, and carefully place the spring into the well with your left thumb and fingers
5. Cover each cassette with a sterile plastic dish cover
6. Once all springs have been loaded, load each cassette into bioreactor (which should be set at 200 steps above flush)
7. Lock in cassettes with the screw-clamps
8. Place the cassettes diagonally so the loading does not unbalance the bioreactor

**Once cassettes are loaded (after springs are inserted*)

1. Go down 200 steps until flush
2. Go down 400 steps where gels will be loaded (this will be the starting point for the experiment)

1. Reset to flush position

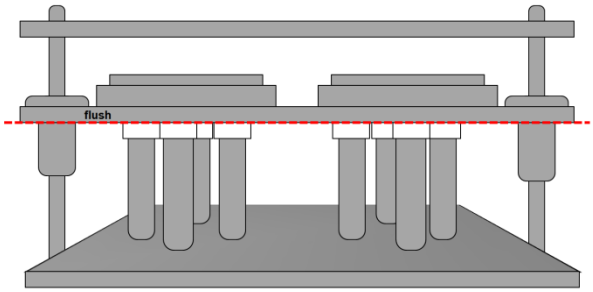

2. Go down 400 steps to load gels

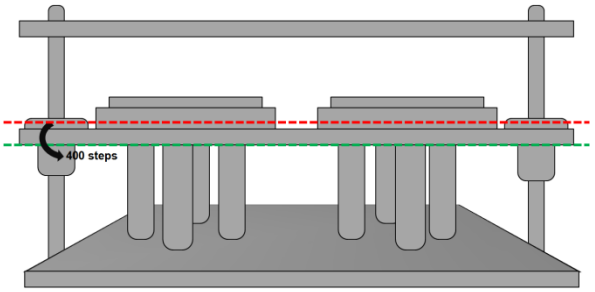

9. Turn on large incubator (37°C, around 3.6-3.7% CO_2)
10. Place bioreactor in large incubator while making collagen gels

Making collagen gels

Reagents (cell culture)	Reagents (collagen gel)	Cell Source
Dulbecco's modified eagle's medium (DMEM)	3X DMEM	Valve interstitial cells (use between passage 4-8)
0.25% Trypsin-EDTA	18 mΩ H_2O	
1X Phosphate buffered saline (PBS)	Fetal Bovine Serum (FBS)	
	Collagen type I (rat tail)	
	0.1M NaOH	

1. Take a T75 flask of VIC out of the incubator, wash once with 10 ml of warm PBS
2. Add 4 ml of trypsin to the flask to trypsinize the cells (37°C) for 5 minutes
3. Add three times the amount of DMEM to terminate the digestion (12 ml). Transfer to a centrifuge tube. **DO NOT** centrifuge.
4. Count the cells using a hemocytometer.
5. Calculate the desired volume of cell suspension using ***collagen only disk template*** file.
   **Example: for VIC gels, use 400,000 cells/ml*
6. Transfer the desired volume of cell suspension into a 15 ml tube; centrifuge at 1000 rpm for 5 minutes
7. Prepare a bowl of ice. Put collagen, 0.1M NaOH, 18 mΩ H_2O, FBS, and 3X DMEM on ice
8. After centrifuge, aspirate the supernatant, add **in order** to the cell pellet
   3X DMEM
   18 mΩ H_2O
   FBS
   Collagen
   NaOH

**Mix well with each step. Especially make sure the NaOH is well mixed with the collagen on the last step*

Seeding springs

**Best to start in back and move forward*

1. For **1:1** gels, add about 120µl
2. For **2:1** gels, add about 140µl
3. For **4:1** gels, add about 150µl

Make sure gel is completely within the coils of the springs so the gel will compact correctly. Try to suck out the air from the coils, which will bring the collagen into the spring

4. After seeding bioreactor, seed controls (and if needed, the released gels ~150 µl in a 46-well plate, released 12 hours later)
5. Set bioreactor in incubator, let gels sit for one hour
6. Add media to gels (bioreactor and controls)
7. Let gels compact around gels for 24 hours

Starting bioreactor

1. Attach water hoses to the cooling plate beneath the bioreactor
2. Plug the controller into the computer (it should already be attached to the bioreactor)
3. **Connect unit**
4. Upload program from controller, then send it back (this sets starting position)
5. **Run** the program (them remove USB connection from controller)
6. Turn on power strip where water pump in freezer is attached

   **Make sure incubator is at 37°C, around 3.6-3.7% CO_2*

Example bioreactor program (20%strain, 1 Hz)

Line	Address	SMC_Command	Command
1	0	Z1	Position register=1
2	5	A10000	Acceleration=10000 steps/(sec*sec)
3	10	B300	Base speed=300 steps/sec
4	14	M500	Max speed=500 steps/sec
5	18	J1000	Jog speed=1000 steps/sec
6	22	L22	Label=22
7	22	+	Direction CW
8	24	N225 @0G	Go relative 225 steps
9	31	F	Finish move
10	33	&10	If input 1=0, then execute the next line
11	37	X64	Goto 64
12	41	-	Direction CCW
13	43	N225 @0G	Go relative 225 steps
14	50	F	Finish move
15	52	&20	If input 2=0, then execute the next line
16	56	X64	Goto 64
17	60	X22	Goto 22
18	64	L64	Label=64
19	64	W2000	Wait 2000 msec
20	69	P1 @0G	Go to position 1
21	76	W45000	Wait 45000 msec
22	81	X22	Goto 22
23	85	Q	End of program

Materials:

Bioreactor materials

Sylgard 184 silicone elastomer kit (Dow Corning, 3097358-1004)
Castrol braycote (804) grease (SPI supplies, 05133-AB)
Lubricating oil

Compression springs

1" springs (Lee Spring Co., CI 010B 13 S316)
0.75" springs (Lee Spring Co., CI 008B 11 S316)
0.625" springs (Lee Spring Co., CI 008B 09 S316)

Collagen gel and media reagents

Dulbecco's modified eagle's medium, DMEM (Invitrogen, 12100-046)
Fetal bovine serum, FBS (GemCell 100-500)
Penicillin-streptomycin (Invitrogen, 15070-063)
Collagen Type I, Rat Tail (BD, 354236)
0.25% Trypsin-EDTA (Invitrogen, 25200072)

Collagen Gel Force Bioreactor

Making molds (PDMS)

Pouring New Molds

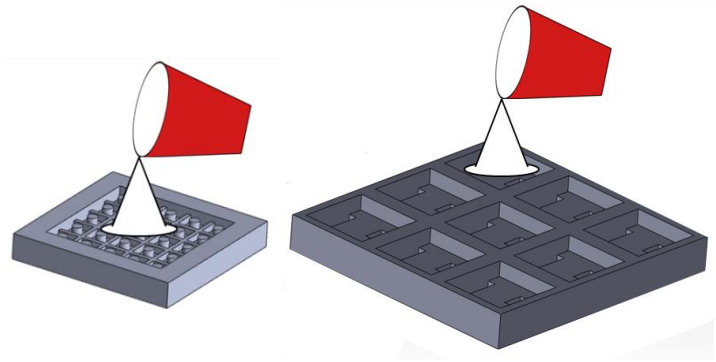

1. Using the Sylgard 184 silicone elastomer kit, pour **56 grams** of elastomer base into a plastic cup
2. Add **4 grams** of elastomer curing agent into the cup, for a total of 60 grams (1:15 dilution)
3. Mix thoroughly with metal spatula (mixture should be white and bubbly)
4. Place cup in the vacuum chamber and de-gas the mixture (will take 30-45 minutes)
5. Pour the PDMS into the two plastic molds. Divide PDMS evenly between the nine base molds, and pour the peg mold until full. Make sure to remove any bubbles, and that the molds are completely filled, but not overflowing.
6. Heat in oven at 65°C for at least 6 hours (usually leave in overnight)

Constructing and Sealing Spring Systems

1. Carefully remove cured PDMS from both molds. They will yield 9 bases and one checkered-patterned slab.
2. Using a straight razor blade, cut out each square peg, making sure to cut right along the edge of the upraised square (they have been measured to fit exactly in the mold).
   **Note: Be as straight as possible when you cut.*
3. Insert three pegs (hole opening facing the middle) into the slots in the PDMS base. They should fit snugly.
4. Thoroughly wash **1" springs** before insertion into system. Use grease remover (if necessary) and copious amounts of soap and DI water.
5. Cut springs down to size with scissors and place them into the holes in the center of the pegs. The left spring should be fixed in place, and the right spring is fixed only at the bottom.
   **Note: It is easier to use forceps for insertion. You may need to press-fit the fixed spring into place.*
6. Seal the edges of the inserted pegs by brushing on a **small** amount of extra PDMS. Also, fill in the holes with extra PDMS to hold the springs in place.
7. Heat in oven at 65°C for at least 6 hours (can leave overnight)

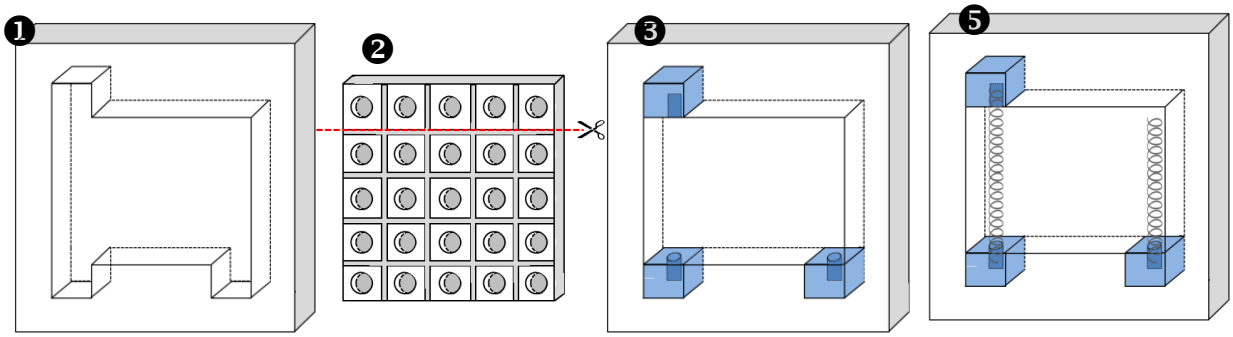

Cleaning and Prepping Spring Systems

1. After the systems have been constructed, clean by scrubbing (gently around the springs so as to not stretch them) with a sponge and Alconox solution. Rinse thoroughly with DI water.
2. Wash PDMS plugs and insert them into the base of the hollow between the two springs. Press firmly to create a good seal.
3. Place spring devices into an autoclavable tip box, tape shut and label. Place a washed pair of forceps in a separate box to autoclave. Run the **GRAVITY 30:00 min sterilize, 25:00 min dry** cycle (usually set as number 4)
4. After autoclave cycle, place each device into a well of a 6-well plate using sterile forceps. Place plates in the incubator for at least an hour before seeding (can be longer)

   **Note: the humidity of the incubator helps the collagen more easily infiltrate the coils of the spring*

Making collagen gels

Reagents (cell culture)	Reagents (collagen gel)	Cell Source
Dulbecco's modified eagle's medium (DMEM)	3X DMEM	Valve interstitial cells (use between passage 4-8)
0.25% Trypsin-EDTA	18 mΩ H_2O	
1X Phosphate buffered saline (PBS)	Fetal Bovine Serum (FBS)	
	Collagen type I (rat tail)	
	0.1M NaOH	

1. Take a T75 flask of VIC out of the incubator, wash once with 10 ml of warm PBS
2. Add 4 ml of trypsin to the flask to trypsinize the cells (37°C) for 5 minutes
3. Add three times the amount of DMEM to terminate the digestion (12 ml). Transfer to a centrifuge tube. **DO NOT** centrifuge.
4. Count the cells using a hemocytometer.
5. Calculate the desired volume of cell suspension using ***collagen only disk template*** file.

   **Example: for VIC gels, use 400,000 cells/ml*
6. Transfer the desired volume of cell suspension into a 15 ml tube; centrifuge at 1000 rpm for 5 minutes
7. Prepare a bowl of ice. Put collagen, 0.1M NaOH, 18 mΩ H_2O, FBS, and 3X DMEM on ice
8. After centrifuge, aspirate the supernatant, add **in order** to the cell pellet
   - 3X DMEM
   - 18 mΩ H_2O
   - FBS
   - Collagen
   - NaOH

**Mix well with each step. Especially make sure the NaOH is well mixed with the collagen on the last step*

Seeding Spring Device

1. Make sure the PDMS plug is still firmly in place. You can press lightly with a micropipette tip to be sure of a good seal.
2. Add **400 µl** of collagen gel solution to the hollow between the two springs. **Make sure** that the gel is completely within the coils of the springs so the gel will compact correctly
   *Note: try using a 200 µl pipettor to suck out the air from the coils, which will bring the collagen solution into the spring.
3. Set the 6-well plate into the incubator, let gels set for at least **30 minutes** (up to 1 hour).
4. Using sterile forceps, gently remove the PDMS plug, leaving only a strip of collagen gel between the two springs.
5. Add **1 ml** media to the gels, place back into the incubator.
   **Make sure incubator is at 37°C, around 3.6-3.7% CO_2*

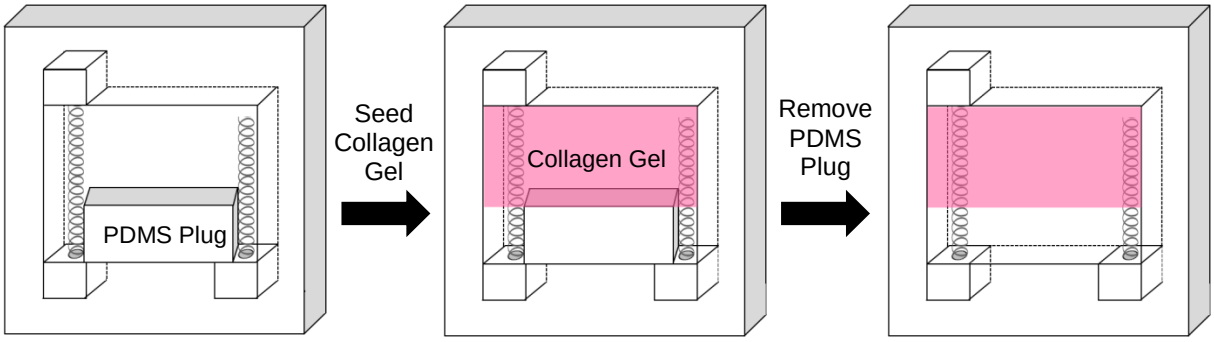

<u>Measuring and Analyzing Deflection</u>

Imaging Gels

1. Use the dissection microscope with the Infinity camera attached (found in the laminar flow hood) to image gels.
2. Turn the **fan ON** in the laminar flow hood and the **light OFF**.
3. Turn on the microscope to full brightness, and insert the microscope light into the bottom attachment under the mirrors.
4. Connect the camera to the USB on your computer. After the green light on the camera turns on, open the program **Infinity Analyze** (Lumenera).
5. Set the zoom to the smallest (0.67) and focus on the device until the springs are in full focus. Adjust the bottom mirrors until you get a clear, bright image (*I've found that an exposure of 80 gives a nice image*).
   **Note: it is important to set the zoom the same, so the measurements you are recording are always at the same scale. If you are unsure, take a picture of a hemocytometer at each zoom and convert to that scale when analyzing in ImageJ*
6. Hit **"snap"** to take the picture. Save each picture as a **.TIFF** (very important: you will not be able to open the .SIF later)

Analyzing Deflection

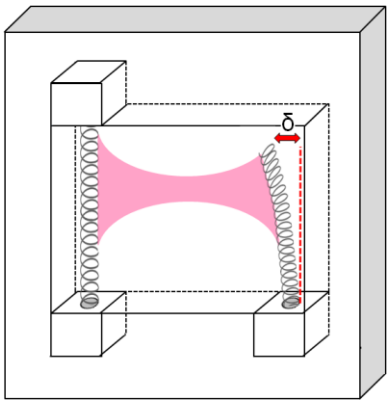

1. Import images into ImageJ. Set the scale globally to all your images based on your hemocytometer picture (a known distance).
2. Draw a straight line from the edge of the wall of the device to the edge of the spring. Be consistent as to which edge you choose each time. Hit **"ctrl+m"** to measure **or** Analyze ➞ Measure to determine deflection of the spring.
3. Compare measurements to the calibration curve (see calibration protocol) to empirically determine force generated.

Materials:

PDMS materials
Sylgard 184 silicone elastomer kit (Dow Corning, 3097358-1004)

Compression springs
1" springs (Lee Spring Co., CI 010B 13 S316)

Collagen gel and media reagents
Dulbecco's modified eagle's medium, DMEM (Invitrogen, 12100-046)
Fetal bovine serum, FBS (GemCell 100-500)
Penicillin-streptomycin (Invitrogen, 15070-063)
Collagen Type I, Rat Tail (BD, 354236)
0.25% Trypsin-EDTA (Invitrogen, 25200072)

Decalcification of Calcified Aortic Valves

Materials:

- **Solution A:** 20% Sodium Citrate
- **Solution B:** 50% Formic Acid

Protocol

1. Make solutions
    a. Solution A: **20% sodium citrate**
        500 g sodium citrate
        2500 ml dH_20
        Heat until completely dissolved

    b. Solution B: **50 % formic acid**
        1500 ml formic acid (88%)
        1500 ml dH_20

2. Mix equal parts of solutions A and B in the hood.
3. Add calcified valve to mixture, continue stirring solutions until calcification is soft (~12 hours).
4. Wash valve with running water for 30 minutes.

Immunohistochemistry (Paraffin Sections)

Melt wax by placing slides in 55C oven for ~10 minutes

*Set slides on their side, against the wall of a box, so that wax melts down, off the sample

Deparaffanization and Rehydration

1. Xylene, 3 changes for **3 minutes each**
2. 100% ethanol, 1 changes, **5 minutes**
3. 95% ethanol, 1 change, **2 minutes**
4. 70% ethanol, 1 change, **2 minutes**
5. Rinse gently in de-ionized water (gently pipette and aspirate dH_2O on sample)

Antigen Retrieval

- ***For cells on a slide:***
    - Lay slides flat in container
    - Pipet enough 2N HCl to cover samples onto each slide
    - Incubate for 70 minutes at 37°C
    - Aspirate 2N HCl
    - Pipet enough 0.1M Sodium Borate (pH 8.5) to cover samples onto each slide
    - Incubate for 12 minutes at room temperature
    - Rinse 3X in PBS for 5 minutes each

- ***For paraffin embedded sections:***
    - Tri-sodium citrate buffer:
        - Weigh out 2.94g Tri-Sodium Citrate
        - Add 1000ml distilled water
        - pH to 6.0 with 1M HCl
        - Add 0.5mL Tween-20
    - Add Sodium Citrate Buffer to tip box
    - Warm buffer by heating in microwave (Shuler lab) on High for 1 min
    - Add slides to dish
    - 5 min on “warm”, 5 min rest
    - 5 min on “warm”, 2 min rest
    - 2 min on “warm”
    - 20 min cool to RT
    - Rinse 1X in PBS

Blocking

1. Circle each sample with hydrophobic pen, let dry
2. Apply enough 10% Goat serum (in 1X PBS) to cover sample (about 75 µL per sample)
3. Incubate 60 minutes at 37°C or overnight at 4°C

Primary antibody application:

1. Make 100µL per sample of 1° antibody (1:500 in antibody dilution buffer)
   Antibody dilution buffer: 1% BSA in 1x PBS +0.3% Triton-X (Cell Signaling Tech)
   *Note: If in doubt of pipetting small volumes, err on the side of higher concentration
2. Gently aspirate 1% BSA

3. Dry slide very carefully with a kim wipe by touching a corner of the wipe to the edge of the liquid on your sample
    *Do NOT touch your samples with the kim wipe
4. Apply primary antibody
5. Incubate overnight (at least 8 hr) at 4^{o}C

Secondary antibody application:

1. Aspirate 1^{o} antibody solution
2. Place slide(s) in dish (ex: pipet box lid) with enough PBS to cover
3. Wash 3x in PBS on shaker, 5 minutes each
4. While shaking, prepare 2^{o} antibody solution:
    - Fluorescent antibody: 1:200
    - Draq 5: 1:1000
    - In solution of 1X PBS

    } Ex: 2.5µL goat anti-rabbit 568 + .5µL Draq 5 + 497µL PBS = 500µL 2^{o} antibody solution
5. Apply 100uL 2^{o} antibody solution to each sample
6. Incubate for 30 minutes at room temperature, *cover with foil*
7. 3 washes: wash 3x in PBS on shaker, 5 minutes each

Mounting

1. Remove ProLong Gold antifade reagent (Invitrogen P36934) from freezer, allow to come to room temp
    - Do not apply external heat
2. Remove excess liquid from specimen using kim wipe, as described above
3. Apply 1 drop of medium to the sample
    - Or to the slide if sample was mounted on a coverslip
4. Gently lower coverslip onto slide, avoid trapping air bubbles
5. Allow slides to cure 24 hrs at room temperature. *Protect from light!*
6. If necessary, seal the edges of the coverslip with nail polish (clear) or hot wax

Long term storage: RT, fridge, or -20 freezer

Western Blotting

Prepare Lysis Buffers

RIPA buffer (1 ml aliquots, store at -20°C)

Final concentration	Stock Concentration	20 ml
150 mM NaCl	2.5M	1.2 ml
50 mM Tris-HCl, pH 8.0	1M	1 ml
0.5% Sodium Deoxycholate	10%	1 ml
0.1% SDS	10%	0.2 ml
1% Igepal CA-630		0.2 ml
18 mΩ H_2O		16.4 ml

Protease/Phosphatase Inhibitors – *add to RIPA buffer on the day of experiment*

NaF (25 mM, 1:40 dilution from 1 M stock) – 25 µL in 1 ml RIPA
$NaVO_4$ (1 mM, 1:100 dilution from 100 mM stock) – 10 µL in 1 ml RIPA
Protease Inhibitor Cocktail (PIC) (1:500 dilution) – 2 µL in 1 ml RIPA (stored at -20°C)

Laemmli Sample Buffer (BioRad, 161-0737)

62.5 mM Tris-HCl, pH 6.8
25% glycerol
2% SDS
0.01% Bromophenol Blue

Lysing Cells

2D Cultured Cells

1. Rinse cells twice with ice cold 1X PBS
2. Add 150 µL lysis buffer (RIPA + protease/phosphotase inhibitors) to cells, incubate at room temperature for 15 minutes
3. Scrape cells and transfer to a microcentrifuge tube
4. Pipette solution several times to mix
5. Spin tubes at room temperature for 10 minutes at 15,000 rpm
6. Transfer supernatant to new microcentrifuge tubes, discard pellet
7. Flash freeze samples in liquid nitrogen
8. Store at -80°C

3D Collagen Gels

1. Remove media from gels and rinse twice with ice cold 1X PBS
2. With pipette, transfer gel into a microcentrifuge tube
3. Spin down at 15,000 rpm for 1 minute at room temperature
   **Note: You can collect supernatant for later analysis of excreted proteins*
4. Warm 150 µL Laemmli buffer (per gel) to 70°C
5. Flash freeze pellets in liquid N_2
6. Add 150 µL hot Laemmli buffer (70°C) to each gel. Vortex to mix and dislodge pellet
7. Incubate gels at 70°C for 10 minutes
8. Sonicate on ice 5-10 seconds per sample
9. Spin down at 4°C for 10 minutes at 16,000 rpm
10. Collect the supernate and store at -80°C

Protein Quantification Assay (Pierce BCA Protein Assay Kit for RIPA or 660nm assay for Laemmli buffer)

Follow protocol outlined in BCA Protein Assay Kit or 660nm assay manuals

Preparing Gel for Electrophoresis **(Can also use pre-cast gradient gels from BioRad)**

1. Prepare gel-making apparatus

   Materials: Casting frame and stand
   Two glass plates (one is larger with white runners and one is shorter with longer tips)
   Comb (thickness should match glass plate spacer thickness)
   Pipettes (with long gel loading tips, VWR 1035-960-306)
   15-50 mL conical tubes

   Solutions: 18 mΩ H_2O
   1.5 M Tris-HCl, pH 8.8
   1 M Tris-HCl, pH 6.8
   30% Acrylamide/BIS solution (stored at 4°C)
   10% SDS
   10% APS (good for about a month – freeze at -20°C for longer time periods)
   TEMED (stored in flammable cabinet)

2. Assemble 2 clean glass plates. Place them in blue casting frame **on a hard surface (benchtop)** and screw into place when glass plates are both level at the bottom.

3. Insert casting frame on stand with rubber insert, and lock into place. Ensure that the glass plates have good seal against the rubber.

4. Make the **resolving (or separating) gel**

		Amount of total gel
Ingredients:	18 mΩ H_2O	depends on gel %
	1.5 M Tris, pH 8.8	25%
	30% acrylamide/BIS	depends on gel %
	10% SDS	1%
Add just before pouring	10% APS	1%
	TEMED	0.0667%

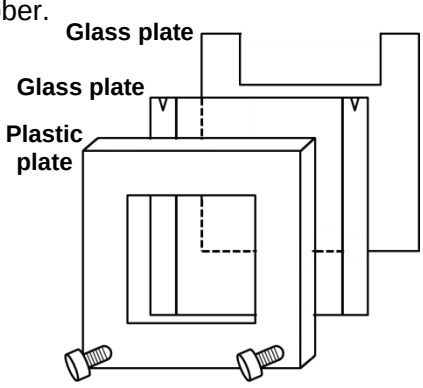

The amount of acrylamide/BIS added to the gel will depend on the desired gel percentage

Each gel requires about **7.5 mL** per gel (makes extra in case of leaking). Gently mix by inversion before adding the APS and TEMED, then add these ingredients only when everything is completely ready to go. Invert a few times more to mix.

For 1 gel:

	8%	10%	12%	15%
18 mΩ H_2O	3.47 mL	2.975 mL	2.47 mL	1.725 mL
1.5 M Tris	1.875 mL	1.875 mL	1.875 mL	1.875 mL
30% acrylamide/BIS	2.0 mL	2.5 mL	3.0 mL	3.75 mL
10% SDS	75 µL	75 µL	75 µL	75 µL
10% APS	75 µL	75 µL	75 µL	75 µL
TEMED	5 µL	5 µL	5 µL	5 µL

***Example**: How much acrylamide/BIS for 8% gel?*

Total gel % → 30 % acryl/BIS

$$100\%(0.08) = (0.3)(x)$$

Final gel % → % acryl/BIS needed

$$x = 26.667\%$$

$$7.5mL(0.26667) = \mathbf{2.0mL\ acryl/BIS\ in\ 8\%\ gel}$$

5. Load gel solution with a pipet between glass plates, leaving about an inch at the top for the stacking gel. Make sure the gel is not leaking out of the bottom. If there is some leaking, keep adding gel solution until the gel level stabilizes. Add ~500 µL methanol to the top of the gel to straighten the top surface. Let the gel polymerize for about **20 minutes**.

6. When the gel is polymerized, pour the methanol out and rinse a few times with water. Blot dry with kimwipes (may need to absorb extra water at surface with kimwipe).
7. Make the solution for the **stacking gel (5%)**
   Each gel requires **3 mL**

	5% gel
18 mΩ H_2O	2.1 mL
1.0 M Tris, pH 6.8	0.38 mL
30% acrylamide/BIS	0.5 mL
10% SDS	30 µL
Add just before pouring: 10% APS	30 µL
Add just before pouring: TEMED	3 µL

8. Transfer the solution to the top of the resolving gel between the glass plates. Make sure to suck out any bubbles that form. Fill the solution completely to the top of the glass plates. Place the comb into the space between the glass plates by sliding it in carefully. Avoid creating bubbles (note: some gel solution will spill out when inserting the comb). Let the gel polymerize for about **20 minutes**. If you are leaving the gel overnight, wrap in wet paper towels and put in plastic bag, and store at 4°C.

9. Make a 1X dilution of Running Buffer from 10X stock in a 1 L bottle (use 18 mΩ H_2O to dilute).

10. Make a 2 L of Transfer Buffer (you will need ~1.5 L, keep what you don't use today). Keep refrigerated until needed

	1 L	**2 L**
18 mΩ H_2O	700 mL	1400 mL
10X Transfer Buffer	100 mL	200 mL
Methanol	200 mL	400 mL

11. Remove casting frame from the stand (DO NOT remove glass plates). Place casting frame into the gel box. Fill the sealed area between the two gels with 1X running buffer, and then remove the combs from the gels. You should see bubbles in the wells left by the comb.

****Note: If using BioRad pre-cast gel, REMOVE GREEN TAPE from bottom of gel, and alternately screw into casting frame until tight. Place casting frame into the gel box.**

12. Wash out the wells with running buffer with a p200 pipette and a gel loading tip (be sure to wash away any remaining acrylamide/BIS).

13. Take out samples from -80°C and Odyssey® Protein Molecular Weight Marker from -20°C to thaw.

14. Prepare Laemmli Sample Buffer to mix with samples. Use 1 part Laemmli with 1 part sample. Example: For a 12 well comb, you will load about **20 µL of total sample (10 µL Laemmli, 10 µL sample)**. Adjust volume in each sample for equal mass loading. Add 50 µL β-mercaptanol for every 950 µL Laemmli buffer (as per product instructions). Mix in separate CLEAN microcentrifuge tubes.

Hint about loading in VWR gel box: The wells may be hard to see, thus making it difficult to load. Try facing the loading gel away from you, and tilting the gel box backward using a small PCR rack. Look down at a 45° angle, and the wells should be visible

15. Load 10 µL Protein Standards (ladder) to left-most well.
**Note: if possible, it is better to not load the wells at the ends (can sometimes get slanted bands)*

16. Skip one well, then load 20 µL of Laemmli-buffered samples in each well with a p20 pipete and gel loading tips. Load samples SLOWLY to ensure samples do not spill over into adjoining wells. It is best to load samples alternating controls and treatments (for later analysis)

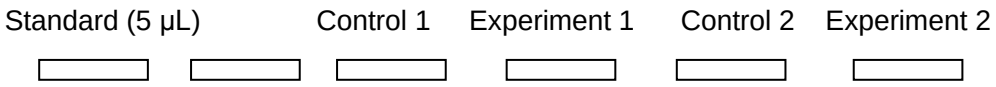

17. Fill the rest of the gel box with 1X running buffer, until buffer reaches "max fill" line on the box. **Make sure buffer completely covers the gel.** Put the lid on the box and attach the electrode assembly to the power supply. *Be sure to attach the red cord to the red electrode, and the black cord to the black electrode.*

18. **Run at 100 V constant for 2.5 hours.**
**Note: Run usually only takes 1.5-2 hours. Longer time set ensures the run does not stop and re-start.*

Gel Transfer

1. When the proteins have reached the desired separation, stop electrophoresis and remove the casting frame from gel box. Unscrew the glass plates from casting frame (gel will remain between plates).

2. Carefully separate glass plates with plastic wedge tool. Cut off most of the top layer (stacking gel). Remove gel from glass plate and place in a plastic container with transfer buffer for 15 minutes.

3. During this time, prepare transfer materials: soak blue fiber pads, filter paper, and nitrocellulose membrane in transfer buffer in plastic container

4. Layer the plates, fiber pads, filter paper, membrane and gel as depicted on the right. Keep everything soaked during layering. Remember your gel will "run to red" (charge moves from negative to positive), so have the nitrocellulose membrane between the gel and the red plate.

5. Roll the gel smooth (removing any bubbles) with small rolling pin. Lock whole sandwich together and insert into gel box.

6. Fill entire tank (until max fill) with ice-cold 1X transfer buffer. Insert an ice pack and put top on transfer tank. Attach electrode apparatus.

7. **Run 45 min, 100 V constant** (note: can also run for longer at lower voltage)

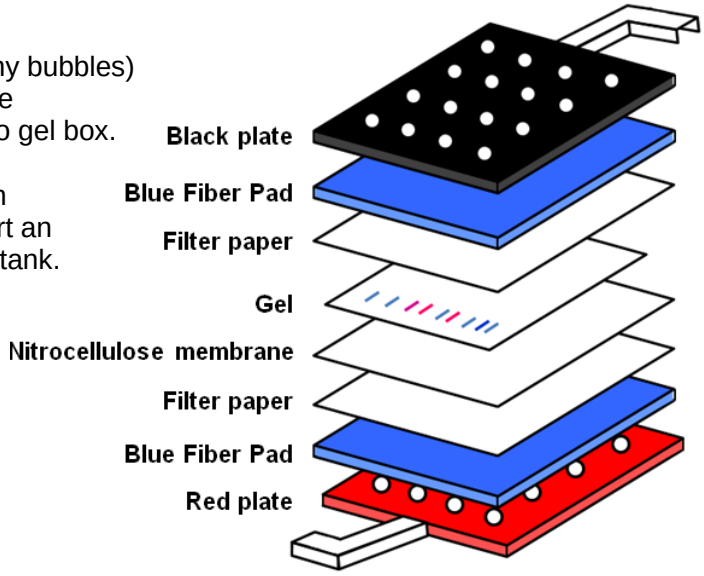

Blot Staining

1. After gel has transferred, remove cassettes and mark the data and experiment on the membrane (**DO NOT** write anywhere close to the protein) or make a notch in the corner to indicate orientation. MAKE SURE you are wearing **CLEAN** gloves. Cut around the gel and detach gel from the nitrocellulose membrane, **making sure you only touch edges of membrane** (note: it is best to handle membrane with tweezers).

2. Rinse once with PBS-Tween, then block with ~10 mL Odyssey blocking buffer. Put on rocker for **1 hour.**

3. In a 15 ml conical tube, prepare 1° antibody. Dilute in Odyssey blocking buffer+0.1%Tween-20 1:100-1:500 (check the optimal antibody dilution as indicated with antibody instructions). **Dilute in 10 mL of Odyssey blocking buffer-Tween-20.** **Note: you can add both primary antibodies (GAPDH and protein of interest) in the same solution.*

4. After blocking, rinse membrane 4 times with PBS-Tween, 5 minutes each on the rocker, then add 1° antibody. Cover and rock slowly **overnight on rocker at 4°C.**

2° Antibody and Imaging

1. Wash the membrane with PBS-Tween 4 times for 5 minutes each on the rocker, then do a final wash with 1X PBS, rocking for 5 minutes.

2. In a conical tube, prepare 2° antibody for your protein of interest. For each membrane, combine 10 mL Odyssey blocking buffer, 0.1% Tween-20 (10 μL of Tween-20), 0.02% SDS (20 μL of 10% SDS) + 0.5 μL 2° antibody for a 1:20,000 dilution. This solution can have multiple antibodies (for proteins with different molecular weights) and can be saved at 4°C in the dark for ~5 uses.

3. Add 2° antibody, cover with foil, and place on rocker at room temperature for 45 minutes.
4. Pour off antibody, then wash membrane with PBS-Tween, 4X for 5 minutes each on rocker. Do one final 5 minute wash with 1X PBS to ensure no Tween-20 remains on the membrane.

5. Walk blot to Biotech building, 3rd floor, to the Odyssey LICOR infrared imager. Image blot with Image Studio software (both red and green channels)

6. After imaging, rinse membrane a few times, then remove 1° and 2° antibodies by applying Restore Western Blot Stripping Buffer (8 mL). Rock for 15 minutes.

7. Wash the membrane with PBS-Tween 4 times for 5 minutes each on the rocker, then do a final wash with 1X PBS, rocking for 5 minutes. Re-block and repeat primary and secondary antibody application for two new proteins of interest.

Solutions and Buffers:

Stock solutions for RIPA buffer

2.5 M NaCl

7.305 g in 50 ml 18 mΩ H_2O, store at room temperature

$$(0.05\ L)\left(\frac{2.5\ moles}{L}\right)\left(\frac{58.44\ g}{mol}\right) = \mathbf{7.305\ g\ in\ 50\ ml\ H_2O}$$

1 M Tris-HCl, pH 8.0

6.057 g Tris base in 50 ml 18 mΩ H_2O

pH to 8.0 with high molar (12.1M) HCl, store at room temperature

$$(0.05\ L)\left(\frac{1\ mol}{L}\right)\left(\frac{121.14\ g}{mol}\right) = \mathbf{6.057\ g\ in\ 50\ ml\ H_2O}$$

10% Sodium Deoxycholate

5 g in 50 ml 18 mΩ H_2O, store at room temperature

10% SDS

5 g in 50 ml 18 mΩ H_2O, store at room temperature

Protease/phosphatase inhibitors stock solutions

1 M NaF

0.4199 g in 10 ml 18 mΩ H_2O, store at -20°C in 25 µl aliquots

$$(0.01\ L)\left(\frac{1\ mol}{L}\right)\left(\frac{41.99\ g}{mol}\right) = \mathbf{0.4199\ g\ in\ 10\ ml\ H_2O}$$

100 mM $NaVO_4$ (sodium orthovanadate) – *prepare under a fume hood*

$$(0.01\ L)\left(\frac{100 \times 10^{-3}\ mol}{L}\right)\left(\frac{183.91\ g}{mol}\right) = \mathbf{0.184\ g\ in\ 10\ ml\ H_2O}$$

0.184 g in <10 ml 18 mΩ H_2O

Set pH to 9.0 with HCl
Boil until colorless } Repeat this cycle until solution remains at pH 9.0 after
Cool, and set pH to 9.0 again } boiling and cooling
Bring up to 10 ml with 18 mΩ H_2O
Store at -20°C in 10 µl aliquots

Protease Inhibitor Cocktail (PIC)
Aliquot into 15 µL and store at -20°C

Gel-making solutions

30% acrylamide/BIS (37.5:1) – store at 4°C in dark **Note: Gels used for protein are commonly 37.5:1 Acrylamide:BIS or 29:1 Acrylamide:BIS*

Make ~250 ml, store at 4°C in dark
For a 37.5:1 acrylamide:bisacrylamide solution: 37.5 g Acrylamide, 1 g Bisacrylamide } in 18 mΩ H_2O

For a 30% acrylamide:bisacrylamide (37.5:1) solution: $x(0.3) = 38.5$

$$\boldsymbol{x = 128.33\ ml\ H_2O}$$

Mix 37.5 g acrylamide and 1 g bisacrylamide with 128.33 ml 18 mΩ H_2O (will need to heat solution to ~37°C to dissolve). Cover with tin foil and store at 4°C. To make ~250 ml, double all ingredients.

1.5 M Tris-HCl, pH 8.8
36.34 g Tris base in 200 ml 18 mΩ H_2O
pH to 8.8 with high molar (12.1M) HCl, store at room temperature

$$(1.5\ M)\left(\frac{121.14g}{L}\right)\left(\frac{1\ L}{1000\ ml}\right)(200\ ml) = \boldsymbol{36.34\ g\ in\ 200\ ml\ H_2O}$$

1.0 M Tris-HCl, pH 6.8
24.22 g Tris base in 200 ml 18 mΩ H_2O
pH to 6.8 with high molar (12.1M) HCl, store at room temperature

$$(1.0\ M)\left(\frac{121.14g}{L}\right)\left(\frac{1\ L}{1000\ ml}\right)(200\ ml) = \boldsymbol{24.22\ g\ in\ 200\ ml\ H_2O}$$

10% Ammonium Persulfate (APS)
APS – 0.1 g
18 mΩ H_2O – 1 ml

Buffers

10X Running Buffer (use as stock – use 1X Running Buffer in experiments)
Tris base (250 mM) – 30.3 g/L
Glycine (1.92 M) – 144.1 g/L
SDS (1%) – 10 g/L
18 mΩ H_2O – 1 L
Store at room temperature

10X Transfer Buffer (use as stock – use 1X Transfer Buffer in experiments)
Tris base (250 mM) – 30.3 g/L
Glycine (1.92 M) – 144.1 g/L
18 mΩ H_2O – 1 L
Store at 4°C

Washes

1X PBS-0.1% Tween-20
18 mΩ H_2O – 900 mL
10X PBS – 100 mL
Tween-20 – 1 mL
Store at room temperature

1X PBS
10X PBS – 100 mL
18 mΩ H_2O – 900 mL
Store at room temperature

Materials:

Chemicals
30% Acrylamide/Bis Solution, 37.5:1 (BioRad, 161-0158)
Acrylamide (Sigma A9099-25G)
Ammonium Persulfate (APS) (Sigma A9164-25G)
Bisacrylamide (N-N'-methlyenebisacrylamide) (Sigma M2022-25G)
Blotting Grade Blocker (Nonfat dry milk) (BioRad, 970-6404)
Glycine (Sigma G8898-500G)
IGEPAL CA-630 (Sigma 18896-50mL)
Methanol (Sigma 34860-1L)
Protease Inhibitor Cocktail (PIC) (Sigma P8340-1mL)
Sodium Chloride (NaCl) (Sigma S5886-500G)
Sodium Deoxycholate (Sigma D6750-10G)
SDS (Sodium Dodecyl Sulfate) (Shelton Scientific, IB07060, 100G)
Sodium Fluoride (NaF) (Sigma S7920-100G)
Sodium Orthovanadate ($NaVO_4$) (Sigma S6508-10G)
TEMED (N,N,N',N'-Tetra-methylethylenediamine) (BioRad 161-0801)
Tween-20 (Sigma P9416-100mL)

Protein Quantification
Pierce BCA Protein Assay Kit (Thermo Scientific, 23227)
Pierce 660 nm Protein Assay Kit (Thermo Scientific, 22662)

Precast Gels
4-15% Mini-PROTEAN TGX Precast Gel (BioRad, 456-1085)

Gel Loading: Protein Standards and Sample Loading Buffer
Odyssey® Protein Molecular Weight Marker (LICOR 928-40000)
Laemmli Sample Buffer (BioRad, 161-0737)
Gel Loading Pipette Tips (VWR 37001-150)

Blot Transfer
Western Blotting Filter Paper (Thermo Scientific, 88600)
Nitrocellulose Membrane (Thermo Scientific, 88018)

Blocking Buffer
Odyssey Blocking Buffer (LICOR 928-40000)

2° Antibodies
Goat anti-mouse 800 (green) (LICOR 926-32210)
Goat anti-rabbit 680 (red) (LICOR 926-68071)
Goat anti-rat 680 (red) (LICOR 926-68076)

Post-Imaging Stripping Buffer
Restore Western Blot Stripping Buffer (Thermo Scientific, 21059)

Alkaline Phosphate (ALP) Assay

Materials

- **1-Step PNPP** (Thermo Scientific 37621)
- **Alkaline Phosphatase, Calf Intestinal (CIAP)** (Promega M1821)

Media Collection and Gel Digestion

1. Collect 150 µl of media from each gel
2. Collect ~2 ml of blank gel media for standard curve
3. Wash gels with 1X PBS
4. Transfer gels into microcentrifuge tubes
5. Digest gels with papain (as outlined in PicoGreen protocol)

Standards Dilution Curve

1. Dilute calf intestinal ALP (CIAP) 1:1000 in extra media from blank gels
2. Using this solution, make a serial dilution 6 times, using water as the 7^{th} standard (zero).

ALP Quantification

Note: This is done with both media and digested gel samples

1. Equilibrate the 1-Step PNPP to room temperature, gently mix end over end.
2. Add 50 µl of standards and samples to clear 96-well plate in triplicate
3. Add 100 µl of the 1-Step PNPP to each well. Mix by gently agitating the plate.
4. Incubate plate at room temperature for 30 minutes or until sufficient color develops.
5. Add 50 µl of 2N NaOH to stope the reaction. Mix by gently agitating the plate.
6. Measure absorbance of each well at 405 nm (Protocol: “Butcher_ALP”)

Alizarin Red S (ARS) Assay for Collagen Gels

Materials:

- **40 mM Alizarin Red S (ARS) stain**
- **10% Acetic Acid** (diluted in 18 mΩ H_2O)
- **10% Ammonium Hydroxide** (diluted in 18 mΩ H_2O)
- **4% PFA**

Staining Procedure

1. Wash gels with sterile PBS, fix in 4% PFA (overnight at 4°C or 1-2 hours at room temperature)
2. Aspirate 4% PFA, store gels at 4°C in 70% ethanol (EtOH) until staining begins
3. Aspirate EtOH, wash 3X in 1X PBS on shaker for 5 minutes each
4. Add 500 µl ARS dye to each gel. Incubate on shaker for 20 minutes at room temperature
5. Aspirate ARS dye, wash 4X with 1X PBS on shaker for 15 minutes each
   Note: May need to wash longer (for gels, I have done overnight washing)
6. Aspirate the liquid
7. Take images of gel (with either Zeiss or Nikon camera)

Dye Extraction and Quantification

1. Add 400 µl of 10% acetic acid to each gel and incubate at room temperature for 30 minutes
2. Scrape the samples from each well, transferring to a 1.5 ml centrifuge tube. Vortex each sample for 30 seconds.
3. Heat samples in oven at 85°C for 10 minutes
   Note: For gels, heating for longer may be necessary
4. Cool samples on ice for 5 minutes (do not open tubes until fully cooled)
5. Centrifuge samples at 13,500 RPM for 15 minutes
6. Make ARS standards (while samples are spinning)

   High:
   - Make a **2 mM solution** by diluting ARS 1:20 with 10% acetic acid
     (50 µl ARS with 950 µl acetic acid)
   - 2-fold serial dilution:
     (2 mM, 1 mM, 500 µM, 250 µM, 125 µM, 62.5 µM, 31.3 µM)

   Low:
   - Make a **30 µM solution** by diluting the 2 mM ARS 1:66 with 10% acetic acid
     (15 µl ARS (2 mM) with 985 µl acetic acid)
   - 2-fold serial dilution:
     (30 µM, 15 µM, 7.5 µM, 3.75 µM, 1.88 µM, 0.94 µM, 0.47 µM)

7. Transfer supernatant (400 µl) from each tube to a new 1.5 ml centrifuge tube
8. Add 200 µl of 10% ammonium hydroxide to each sample (pH 4.1-4.5)
9. Add 150 µl of standards and samples in triplicate to clear 96 well plate
10. Use plate reader (Bonassar lab) to measure the dye absorbance at 405 nm (Protocol: Butcher_ARS)
11. Determine the quantity of ARS in each sample using the standard curve

Alizarin Red S (ARS) Assay for Paraffin Sections

Materials & Solutions

- **Alizarin Red Solution** (25 ml) – *Change every month!*
  - 0.5 grams Alizarin Red S
  - 25 ml distilled H_2O
  - pH to 4.1-4.3 using ammonium hydroxide
- **Acetone (100%)** (25 ml)
- **Acetone-Xylene** (25 ml)
  - 12.5 ml acetone
  - 12.5 ml xylene

Melt wax by placing slides in 55°C oven for ~10 minutes

*Set slides on their side, against the wall of a box, so that wax melts down, off the sample

Deparaffanization and Rehydration

1. Xylene, 3 changes for **3 minutes each**
2. 100% ethanol, 1 change, **5 minutes**
3. 95% ethanol, 1 change, **2 minutes**
4. 70% ethanol, 1 change, **2 minutes**
5. Rinse gently in tap water (gently pipette and aspirate H_2O on sample)

Alizarin Red S Staining:

1. Alizarin stain for **2 minutes**
2. Remove stain, lightly blot excess solution off slides
3. Acetone for **30 seconds**
   a. Note: If needed, more rinsing with acetone
4. Acetone-Xylene for **30 seconds**
   a. Note: If needed, more rinsing with acetone-xylene
5. Xylene, 2 changes for **1.5 minutes each**

Mounting:

1. Apply coverslip with Permount (mounting medium)
2. Seal edges with clear nail polish

Von Kossa Staining (Paraffin Sections)

Materials & Solutions

- **1% Aqueous Silver Nitrate Solution**
  - Silver nitrate (1 gram)
  - Distilled water (100 ml)

- **5% Sodium Thiosulfate**
  - Sodium thiosulfate (5 grams)
  - Distilled water (100 ml)

- 0.1% Nuclear Fast Red Solution
  - Nuclear fast red (0.1 grams)
  - Aluminium sulfate (5 grams)
  - Distilled water (100 ml)

    Note: Dissolve aluminum sulfate in water. Add nuclear fast red and slowly heat to boil and cool. Filter and add a grain of thymol as a preservative

Melt wax by placing slides in 55°C oven for ~10 minutes

*Set slides on their side, against the wall of a box, so that wax melts down, off the sample

Deparaffanization and Rehydration

1. Xylene, 3 changes for **3 minutes each**
2. 100% ethanol, 1 change, **5 minutes**
3. 95% ethanol, 1 change, **2 minutes**
4. 70% ethanol, 1 change, **2 minutes**
5. Rinse gently in tap water (gently pipette and aspirate H_2O on sample), 2 changes

Von Kossa Staining:

1. 1% silver nitrate solution for **20 minutes** under **ultraviolet light**

   Note: if stain was weak or rinsed off in washing steps, UV light was not strong enough. Longer staining is required for up to several hours
2. Rinse in several changes of distilled water
3. 5% sodium thiosulfate for **5 minutes** to remove un-reacted silver
4. Rinse in several changes of distilled water
5. Nuclear fast red for 5 minutes
6. Rinse in several changes of distilled water

Dehydration:

1. 70% EtOH, **1 minute**
2. 95% EtOH, **1 minute**
3. 100% EtOH, **1 minute**
4. Xylene, 3 changes, **1 minute each**

Mounting:

1. Apply coverslip with Permount (mounting medium)
2. Seal edges with clear nail polish

Osteogenic Media Protocol

Supplements

β-Glycerophosphate disodium salt hydrate (Sigma G9891-10G)
L-Ascorbic acid (vitamin C) (Sigma A4544-25G)
Dexamethasone (D4902-25MG)

Supplement Concentrations:

β-Glycerophosphate: **10 mmol/L**

$$\frac{\text{x grams}}{\text{L}} = \left(10 \times 10^{-3}\,\frac{\text{mol}}{\text{L}}\right)\left(216.04\,\underbrace{\frac{\text{mol}}{\text{L}}}_{\text{(molecular weight)}}\right) = \mathbf{2.16}\ \frac{\mathbf{g}}{\mathbf{L}}$$

Ascorbic acid (vitamin C): **50 µg/ml**

$$\left(\frac{50 \times 10^{-6}\ \text{g}}{10^{-3}\text{L}}\right)\left(\frac{1000\ \text{mg}}{1\ \text{g}}\right) = \mathbf{50}\ \frac{\mathbf{mg}}{\mathbf{L}}$$

Dexamethasone: **10^{-8} M (mol/L)**

$$\left(\frac{10^{-8}\ \text{mol}}{\text{L}}\right)\left(\frac{392.46\ \text{g}}{\text{mol}}\right)\left(\frac{1000\ \text{mg}}{1\ \text{g}}\right)\left(\frac{1\ \text{L}}{1000\ \text{ml}}\right) = \mathbf{3.92 \times 10^{-6}}\ \frac{\mathbf{mg}}{\mathbf{ml}}$$

Preparing Supplements (to be added to normal culture media):

- Supplements to be added to media: 10 ml of β-Glycerophosphate and Vitamin C solution

1 ml 1 mM Dexamethasone

β-Glycerophosphate and Ascorbic acid solution (50 X concentration)

1. Start with 50 ml of 18 MΩ water
2. Add β-Glycerophosphate:

50X concentrated

$$\left(\frac{2.16\ \text{g}}{\text{L}}\right)\left(\frac{1\ \text{L}}{1000\ \text{ml}}\right)(50\ \text{ml})(50) = \mathbf{5.4\ g\ \beta GP}$$

3. Add Vitamin C:

$$\left(\frac{50\ \text{mg}}{\text{L}}\right)\left(\frac{\text{g}}{1000\ \text{mg}}\right)\left(\frac{1\ \text{L}}{1000\ \text{ml}}\right)(50\ \text{ml})(50) = \mathbf{0.125\ g\ Ascorbic\ Acid}$$

4. Mix well until completely dissolved
5. Aliquot into five 10 ml centrifuge tubes
6. Store at -20°C

2% Dexamethasone: stored at -20°C

1. Want a 1 mM solution (dexamethasone M.W. = 392.5 mg/L)
2. 1 mM: 3.92 mg in 10 ml (dissolve in 100% ethanol)

3. Aliquot into 1 ml tubes, store at -20°C

***When making osteogenic media, make 500 ml of normal culture medium, add 10 ml of supplement solution and 1 ml of Dexamethasone to media before sterile filtering.**